P O S T G R A D O S E N O C E A N O G R A F Í A

DEPARTAMENTO DE OCEANOGRAFÍA
FACULTAD DE CIENCIAS NATURALES Y OCEANOGRÁFICAS

TESIS DE GRADO

DOCTORADO

Comité
Programa de Postgrados en Oceanografía

Diciembre 2025

UNIVERSIDAD DE CONCEPCIÓN

FACULTAD DE CIENCIAS NATURALES Y OCEANOGRÁFICAS

Programa de Postgrados en Oceanografía

VARIABILIDAD TEMPORAL DE LA CONCENTRACIÓN DE METANO DISUELTO EN EL SISTEMA DE AFLORAMIENTO COSTERO DE CHILE CENTRAL

Tesis para optar al grado de Doctor en Oceanografía

POR: SANDY ELIZABETH DEL ROCIO TENORIO SÁNCHEZ

Profesor Guía: Laura Farías
Departamento de Oceanografía
Facultad de Ciencias Naturales y Oceanográficas
Universidad de Concepción

Concepción, Chile
Diciembre, 2025

Universidad de Concepción
Dirección de Postgrado

La Tesis de "*Doctorado en Oceanografía*" titulada *"VARIABILIDAD TEMPORAL DE LA CONCENTRACIÓN DE METANO DISUELTO SUPERFICIAL Y SU INTERCAMBIO EN EL SISTEMA DE AFLORAMIENTO COSTERO DE CHILE CENTRAL"*, de la Srta. *SANDY ELIZABETH DEL ROCIO TENORIO SÁNCHEZ* y realizada bajo la Facultad de Ciencias Naturales y Oceanográficas, Universidad de Concepción, ha sido aprobada por la siguiente Comisión de Evaluación:

Dra. Laura Farías
Profesora Guía
Departamento de Oceanografía
Universidad de Concepción _____

Dra. Camila Fernández
Miembro Comité de Tesis
Departamento de Oceanografía
Universidad de Concepción _____

Dr. Diego Narváez
Miembro Comité de Tesis
Departamento de Oceanografía
Universidad de Concepción _____

Dr. Rodrigo Torres
Evaluador Externo
Centro de Investigaciones en
Ecosistemas de la Patagonia – CIEP _____

Dra. Pamela Hidalgo
Directora
Programas de Postgrados en Oceanografía
Universidad de Concepción _____

AGRADECIMIENTOS

Agradecer infinitamente a mi profesora guía Dra. Laura Farías, por su manifiesto compromiso para conmigo. Destaco de ella su entusiasmo, inteligibilidad, agudeza mental y objetividad, características que fueron necesarias en la orientación para el desarrollo de esta tesis.

Al laboratorio de biogeoquímica isotópica; donde llevé a cabo los análisis de gases y nutrientes, especialmente a Karen Sanzana, compañera del laboratorio, por su colaboración, apoyo y buena disposición en el trabajo de laboratorio.

Al Laboratorio de Oceanografía Física (LOFEC) del Dr. Diego Narváez, por el apoyo brindado, especialmente a Marcos Avendaño, Víctor Morales y Marcelo Ramírez, por la instalación y mantenimiento de los sensores oceanográficos. Su dedicación y compromiso en el trabajo realizado fueron indispensables para el desarrollo de esta tesis.

Al Dr. Diego Narváez y Dr. Luis Soto, por su tiempo y dedicación en la preparación y redacción del manuscrito. A los miembros del comité, por sus comentarios y sugerencias para la mejora de esta tesis.

Agradecer al Proyecto UCO 1866, a la Agencia Nacional de Investigación y Desarrollo (ANID), Centro de Ciencia del Clima y Resiliencia (CR)2 por financiar mis estudios en el Programa Doctorado en Oceanografía.

A mis amig@s y compañer@s: A Rosmery, Diego y Edson, por haber sido un espacio seguro y apoyo fundamental en momentos difíciles, me motivaron a seguir adelante. A Fernando y Diego, por haber creado los sábados de Sandy, llenos de risas, comida, películas y reflexión. A Milagros, Mónica, Yosvany, Maibelin, Roxana, Claudia, Marco, Iván y Flavio, por su amistad, complicidad y compañerismo, sin duda alguna, nos regalamos experiencias inolvidables. Y a todos aquell@s que, con acciones y palabras, me hicieron reflexionar, aprender y continuar. Gracias.

Índice de Contenidos

Índice de Figuras

Índice de Tablas

Curriculum Vitae

Sandy Elizabeth del Rocio Tenorio Sánchez

Nacido el 13 de septiembre de 1993, en Ferreñafe, Perú

2010-2015: Bióloga Pesquera, Licenciada en Biología-Pesquería, Universidad Nacional Pedro Ruiz Gallo, Perú.

2018-2021: Magíster en Ciencias con Mención en Oceanografía, Universidad de Concepción, Chile.

2021-2025: Doctorado en Oceanografía, Universidad de Concepción, Chile.

PUBLICACIONES

Tenorio, S., Farías, L., Narváez, D., Soto-Mardones, L. (en revisión). Short-term variability of dissolved methane in surface waters of an upwelling bay off the central Chile". Enviromental Research Journal.

Tenorio, S. E., & Farías, L. (2024). Picoplanktonic methane production in eutrophic surface waters. Biogeosciences, 21(8), 2029–2050. https://doi.org/10.5194/bg-21-2029-2024

Farías, L., Tenorio, S., Sanzana, K., & Faundez, J. (2021). Temporal methane variability in the water column of an area of seasonal coastal upwelling: A study based on a 12 year time series. Progress in Oceanography, 195. https://doi.org/10.1016/j.pocean.2021.102589

ÁREAS DE INVESTIGACIÓN

Principal: Oceanografía química

Secundaria: Biogeoquímica

CRUCEROS OCEANOGRÁFICOS

- Serie de Tiempo (Kai-Kai II), Universidad de Concepción, Chile, 2018 - 2019.
- Fjord Flux, Crucero M179, enero-febrero 2022.

RESUMEN

Variabilidad temporal de la concentración de metano disuelto en el sistema de afloramiento costero de chile central

Sandy Tenorio

Programa Doctorado en Oceanografía
Universidad de Concepción, 2025
Dra. Laura Farías, Profesora guía

El metano (CH_4) es un potente gas de efecto invernadero con un tiempo de residencia corto en la atmósfera (~10 años), por lo que cambios modestos en sus emisiones impactan el clima y los ciclos biogeoquímicos. En general, el océano actúa como fuente de CH_4, con emisiones mayores en zonas costeras; sin embargo, la dinámica variable del ecosistema, la limitada cobertura espacial y temporal, y las restricciones tecnológicas, generan grandes incertidumbres en el balance oceánico, especialmente por la subrepresentación u omisión de hot spots/moments en la superficie, que solo son capturados esporádicamente. En este contexto, teorías de metanogénesis metilotrófica se han propuesto para explicar la paradoja del CH_4, al sostener que la oxidación de sustratos metilados puede generar CH_4 y mantener sobresaturaciones en la capa superficial oxigenada.

El área de surgencia costera de Chile central (36 °S), está forzada por la intensidad y la migración del anticiclón del Pacífico Sur, quien modula un régimen de vientos de sur y con ello un marcado ciclo estacional: en primavera verano advectan las Aguas Ecuatoriales Subsuperficiales y en otoño-invierno la intrusión de Aguas Subantárticas. Pulsos y relajaciones del viento, jets costeros y bajas de presión ocurren a escala sinóptica, modificando la estratificación y la mezcla vertical. El ciclo de radiación y diferencia

termal entre el océano y la atmósfera gatillan una brisa marina que domina la variabilidad diurna del sistema. La superposición de los diferentes procesos físicos y biológicos que ocurren a diferentes escalas controla la concentración y emisiones del CH_4.

La presente tesis caracterizó la variabilidad temporal de CH_4 disuelto en la capa superficial del océano y sus flujos en la interfaz mar-atmósfera desde la escala interanual hasta la escala diurna, describiendo los procesos físicos-biogeoquímicos que modulan su dinámica, y mediante experimentos discernir sobre los procesos biológicos que permiten la formación de hot spots en la superficie de la zona de surgencia de Chile central. Para ello, se integró una serie mensual de 12 años y una serie de alta frecuencia que caracterizan la plataforma exterior (ST 18; 36° 0.802' S 73° 07.750' W) e interior (bahía Coliumo; 36°32 S 72° 56'W) de una zona costera del centro de Chile. Se aplicaron análisis de series temporales (wavelets y análisis de espectro singular, correlaciones cruzadas) y experimentos enriquecidos con sustratos metilados en diferentes fases de la productividad y sometidos a fotoperiodos de 12h luz / 12h oscuridad.

La serie mensual en la plataforma continental mostró variaciones de CH_4 entre 4,81 a 100,86 nM ($\bar{x} \pm DS = 30,65 \pm 15,44$ nM), con una fuerte variabilidad interanual asociada a eventos climáticos como el ENSO, con una débil estacionalidad posiblemente enmascarada por procesos dinámicos que escapan de la frecuencia mensual. La serie de alta frecuencia en la plataforma interior evidenció una marcada variación intraestacional, donde se desarrollan procesos de escala sinóptica como los eventos de surgencia y no surgencia (relajado y downwelling). Durante la surgencia activa, advectan las aguas frías, salinas y enriquecidas con CH_4, lo que produjo concentraciones más altas de CH_4 ($\bar{x} \pm DS = 41,2 \pm 17,6$ nM), mientras que durante la relajación, el CH_4 disminuyó casi a la mitad ($\bar{x} \pm DS = 26,7 \pm 14,7$ nM). La escala diurna (~24 h) fue débil y se relacionó negativamente con el ciclo de la brisa marina y la radiación solar.

Los resultados de experimentos evidenciaron un proceso netamente biológico en la producción de CH_4, destacando al picoplancton como el principal involucrado en este proceso, tanto en condiciones de luz como de oscuridad. En otoño-invierno (periodo no favorable a la surgencia), las bacterias heterótrofas metabolizaron ácido metilfosfónico (MPn) y formaron CH_4 como subproducto, mientras que *Synechococcus spp.*, fue responsable de la regeneración de CH_4 a través de la fotosíntesis. En primavera-verano (periodo favorable a la surgencia), los pico eucariotas metabolizaron TMA. Esto pone de manifiesto que el picoplancton es fundamentan en el reciclaje de sustratos metilados y es una potencial fuente para la formación de hot spot/moments y mantiene la capa superficial sobresaturada.

Respecto a las emisiones, se observó que la zona costera es una fuente importante de CH_4, con un gradiente costa-océano. La plataforma interior emitió el doble (1,8 y 94 μmol m^{-2} d^{-1}) de CH_4 en comparación con la plataforma continental (1,27 y 47,02 μmol m^{-2} d^{-1}), convirtiéndose un hot spot importante para la zona, sin embargo, el inventario regional de emisiones de CH_4 está dominado por la plataforma continental (1-4 Gg CH_4 $año^{-1}$), debido a una mayor superficie.

La evaluación multiescalar, refleja claramente que la serie mensual y de alta frecuencia, aun cuando ambas explican la dinámica de un ambiente similar, la capacidad de observación de procesos difiere sustantivamente, por ello, para reducir incertidumbre en ambientes dinámicos como las zonas costeras, es importante las observaciones de alta frecuencia ya que complementan y captan la dinámica real del CH_4, reduciendo las incertidumbres y contribuyen a mejorar los modelos y proyecciones climáticas..

Palabras claves: metano, bahía costera, surgencia, serie de tiempo a alta frecuencia, Chile central, Coliumo.

ABSTRACT

Temporal variability of dissolved methane concentration in the coastal upwelling system of central Chile

Sandy Tenorio

Doctoral Program in Oceanography
University of Concepción, 2025
Dr. Laura Farías, Advisor

Methane (CH_4) is a potent greenhouse gas with a short residence time in the atmosphere (~10 years), so modest changes in its emissions impact the climate and biogeochemical cycles. In general, the ocean acts as a source of CH_4, with higher emissions in coastal areas; however, the variable dynamics of the ecosystem, limited spatial and temporal coverage, and technological constraints generate great uncertainties in the ocean balance, especially due to the omission of hot spots/moments on the surface, which are only captured sporadically. In this context, theories of methylotrophic methanogenesis have been proposed to explain the CH_4 paradox, arguing that the oxidation of methylated substrates can generate CH_4 and maintain supersaturations in the oxygenated surface layer.

The coastal upwelling area of central Chile (36°S) is driven by the intensity and migration of the South Pacific anticyclone, which modulates a southerly wind regime and thus a marked seasonal cycle: in spring and summer, Subsurface Equatorial Waters advect, and in autumn and winter, Subantarctic Waters intrude. Wind pulses and relaxations, coastal jets, and low-pressure systems occur on a synoptic scale, modifying stratification and vertical mixing. The radiation cycle and thermal difference between the ocean and the

atmosphere trigger a sea breeze that dominates the system's diurnal variability. The overlap of different physical and biological processes occurring at different scales controls CH_4 concentration and emissions.

This study characterized the temporal variability of dissolved CH_4 in the ocean surface layer and its fluxes at the sea-atmosphere interface from the interannual to the diurnal scale, describing the physical-biogeochemical processes that modulate its dynamics, and using experiments to discern the biological processes that allow the formation of hot spots on the surface of the upwelling zone of central Chile. To this end, a 12-year monthly series and a high-frequency series characterizing the outer platform (ST 18; 36° 0.802' S 73° 07.750' W) and inner platform (Coliumo Bay; 36°32 S 72° 56' W) of a coastal area in central Chile were integrated. Time series analyses (wavelets and singular spectrum analysis, cross-correlations) and experiments enriched with methylated substrates at different stages of productivity and subjected to photoperiods of 12 hours of light/12 hours of darkness were applied.

Monthly series on the continental shelf showed CH_4 variations between 4.81 and 100.86 nM ($\bar{x} \pm SD = 30.65 \pm 15.44$ nM), with strong interannual variability associated with climatic events such as ENSO, with weak seasonality possibly masked by dynamic processes that escape the monthly frequency. The high-frequency series on the inner shelf showed marked intrastationary variation, where synoptic-scale processes such as upwelling and non-upwelling (relaxed and downwelling) events occur. During active upwelling, cold, saline, and CH_4-enriched waters advect, producing higher CH_4 concentrations ($\bar{x} \pm DS = 41.2 \pm 17.6$ nM), while during relaxation, CH_4 decreased by almost half ($\bar{x} \pm DS = 26.7 \pm 14.7$ nM). The diurnal scale (~24 h) was weak and negatively correlated with the sea breeze cycle and solar radiation.

Results of experiments showed a purely biological process in the production of CH_4, highlighting picoplankton as the main contributor to this process, both in light and dark conditions. In autumn-winter (a period not favorable for upwelling), heterotrophic bacteria metabolized methylphosphonic acid (MPn) and formed CH_4 as a sub product, while *Synechococcus spp*. was responsible for the regeneration of CH_4 through photosynthesis. In spring-summer (a period favorable to upwelling), picoyeucaryotes metabolized TMA. This shows that picoplankton is fundamental in the recycling of methylated substrates and is a potential source for the formation of hot spots/moments, maintaining the surface layer supersaturated.

Regard to emissions, it was observed that the coastal zone is a significant source of CH_4, with a coast-ocean gradient. The inner shelf emitted twice as much CH_4 (1.8 and 94 μmol m^{-2} d^{-1}) as the continental shelf (1.27 and 47.02 μmol m^{-2} d^{-1}), making it a significant hot spot for the area. however, the regional inventory of CH_4 emissions is dominated by the continental shelf (1-4 Gg CH_4 $year^{-1}$), due to its larger surface area.

The multiscale assessment clearly shows that the monthly and high-frequency series, even though both explain the dynamics of a similar environment, differ substantially in their ability to observe processes. Therefore, to reduce uncertainty in dynamic environments such as coastal areas, high-frequency observations are important as they complement and capture the real dynamics of CH_4, reducing uncertainties and contributing to improving climate models and projections.

Keywords: methane, coastal bay, upwelling, high-frequency time series, central Chile, Coliumo.

1. INTRODUCCIÓN

1.1. Características del metano, contexto global y ciclos biogeoquímicos

El metano (CH_4) es un gas traza orgánico cuyo potencial de calentamiento global es 28–34 veces mayor que el del CO_2, aunque su concentración atmosférica es mucho menor (1,9 ppm frente a 420 ppm del CO_2). Es el segundo gas de efecto invernadero (GEI) más importante, con un forzamiento radiativo de 0,65 W/m², en comparacion con los 2,17 W/m² del CO_2 (IPCC, 2021). El CH_4 tiene un tiempo de vida en la atmósfera de 10 a 12 años en promedio, determinado por el balance entre sus fuentes y sumideros. Dada su corta permanencia, las reducciones en sus emisiones generan una respuesta climática rápida y tangible, lo que lo convierte en un gas clave para las estrategias de mitigación a corto y mediano plazo (Denman et al., 2007; Folberth et al., 2025; Harmsen et al., 2020).

No obstante, a pesar de su relevancia climática, existen grandes incertidumbres en el presupuesto global de CH_4 (Saunois et al., 2025), especialmente en ambientes naturales como los océanos (Bakker et al., 2014; Rosentreter et al., 2021; Saunois et al., 2025), cuyos sedimentos constituyen un gran reservorio de CH_4 (Saunois et al., 2025; Wallmann et al., 2012). Las estimaciones de las emisiones oceánicas globales de CH_4 han variado ampliamente, desde 4 hasta 45 Tg CH_4 $año^{-1}$ (Bates et al., 1996; Rhee et al., 2009; Wuebbles and Hayhoe, 2002), reduciéndose a rangos más acotados, entre 6 y 20 Tg CH_4 $año^{-1}$ (Saunois et al., 2025).

Se estima que más del 75% de las emisiones oceánicas provienen de zonas costeras (Bange et al., 1994; Weber et al., 2019). Estas zonas actúan como “hotspots” debido a su alta productividad biológica, intensa remineralización de materia orgánica, los aportes continentales y la interacción dinámica entre procesos físicos y biogeoquímicos (Farías et al., 2021b; Kock et al., 2008; Rosentreter et al., 2018; Upstill-goddard et al., 2000).

Esta variabilidad se debe en parte a las metodologías utilizadas para la estimación de las emisiones: top down y bottom up (Kirschke et al., 2013; Saunois et al., 2016b, 2020, 2025), a la dinámica altamente cambiante de la atmósfera y el océano, y a los procesos biogeoquímicos de producción y consumo de este gas (Reeburgh, 2007). A ello se suma la escasa resolución temporal y espacial de los datos, ya que, a diferencia del CO_2 y el N_2O, el CH_4 es uno de los GEI menos estudiados en el océano, especialmente en el hemisferio sur (Wilson et al., 2020).

1.2. Origen y paradoja del CH_4 en la superficie del océano

En el océano, el CH_4 disuelto tiene dos orígenes: i) el CH_4 biogénico, formado por el proceso de metanogénesis, que proviene de la respiración anaeróbica de la materia orgánica y es llevada a cabo por las arqueas metanogénicas en ambientes anóxicos, como los sedimentos marinos superficiales, zona de mínimo de oxígeno y las zonas costeras eutrofizadas, y ii) el CH_4 termogénico, originado por la degradación térmica de la materia orgánica (MO) enterrada profundamente en los sedimentos, bajo condiciones de alta presión y alta temperatura. Este puede llegar a la columna de agua a través de emanaciones submarinas (seeps), márgenes continentales activos y algunas zonas costeras o fiordos (Floodgate and Juddt, 1992; Liu and Whitman, 2008; Stolper et al., 2014).

El CH_4 disuelto antes de alcanzar la interfaz océano-atmósfera, es oxidado y consumido por el proceso de metanotrofía (Reeburgh, 2007), llevado a cabo por organismos metanótrofos como arqueas y bacterias, tanto en ambientes anóxicos como óxicos, los cuales actúan como filtro natural y eficiente de CH_4 en el océano (Fenibo et al., 2023; Mao et al., 2022).

El CH_4, a pesar de tener un origen biogénico y termogénico principalmente en sedimentos, ha sido encontrado en concentraciones relativamente altas en la superficie del océano en condiciones óxicas, razón por la cual se ha descrito a este fenómeno como "paradoja del CH_4 oceánico" (Reeburgh, 2007). Primeras hipótesis surgieron en los años 70' (Fig. 1), donde se propone una producción biológica *in situ* relacionado con el fitoplancton (Scranton and Brewer, 1977), el intestino de los peces (Oremland, 1979), micro nichos del material particulado (Karl and Tilbrook, 1994) y del zooplancton (De Angelis and Lee, 1994). No obstante, estas vías son insuficientes para sostener una alta sobresaturación de CH_4 en la capa superficial y los flujos positivos hacia la atmósfera (Wäge et al., 2020). En la figura 1 se muestra una línea de tiempo sobre los principales avances de la paradoja del CH_4.

La producción óxica de CH_4 toma mayor importancia con la hipótesis fosfonato-metano (Fig. 1), la cual propone que compuestos metilados como el ácido metilfosfónico (MPn) podría estar involucrado en las vías de formación de CH_4 bajo condiciones oxigenadas (Karl et al., 2008); esto ocurre como una estrategia para los microorganismos heterotróficos que viven en ambientes limitados por fosforo (P) como fosfato (e.g. giros), degradando el compuesto fosfonatado (e.g. MPn) para adquirir el P inorgánico e incorporarlo a su crecimiento celular y liberar CH_4 como subproducto (Repeta et al., 2016). Además, la metabolización de ésteres polisacáridos de ácidos fosfónicos presentes en la fracción semilábil de la materia orgánica disuelta puede contribuir adicionalmente a la producción de CH_4 (Repeta et al., 2016).

Evidencias genómicas respaldan esta hipótesis, donde se ha evidenciado que diversos microorganismos marinos tienen la maquinaria enzimática necesaria para degradar compuestos fosfonatados y liberar CH_4 en ambientes óxicos (Metcalf et al., 2012; Sun et al., 2011). Además, Arqueas como *nitrosopumilius maritimus* puede sintetizar MPn (Metcalf et al., 2012). Este rápido recambio (turnover) de producción y

degradación de MPn podría explicar por qué sus concentraciones en el agua de mar son muy bajas o incluso indetectables (Lohrer et al., 2020).

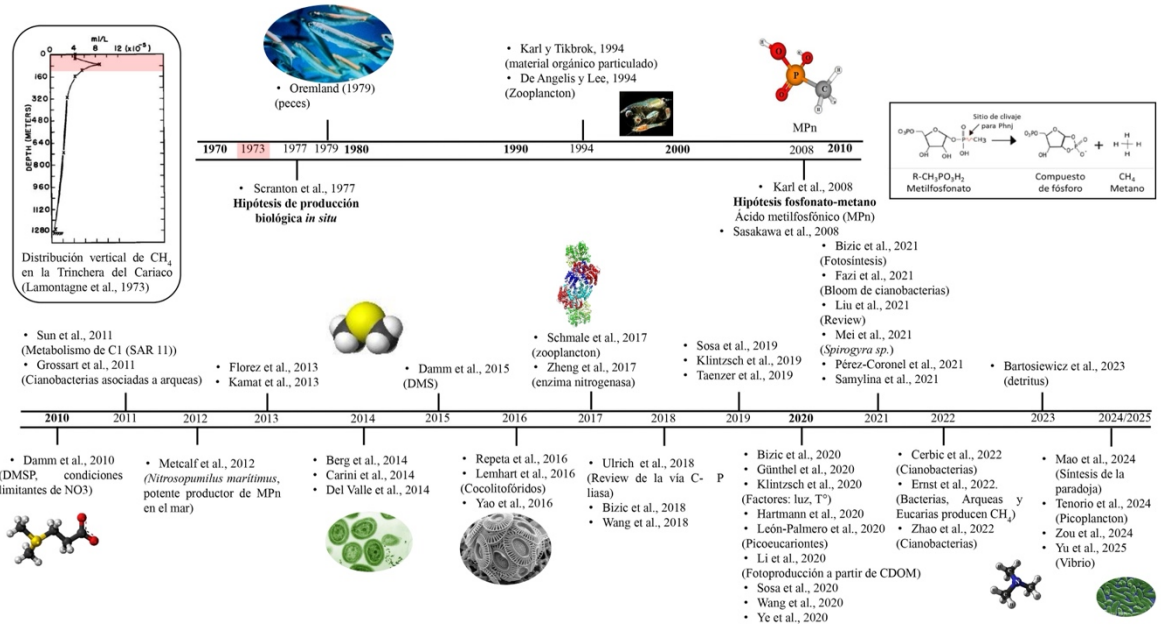

Figura 1. Línea de tiempo sobre avances de la paradoja del metano (Elaboración propia).

Otros compuestos osmolíticos producidos por la biota marina, como el dimetilsulfoniopropionato (DMSP) o las metilaminas, también están involucrados en la producción de CH_4 óxico (Fig. 1). Se ha observado que la adición de DMSP produce CH_4 (Florez-Leiva et al., 2013), aunque las vías y mecanismos de este proceso aún son poco detallados. De forma similar, también se ha evidenciado que la adición de metilaminas genera CH_4, aunque sus tasas de producción son muy bajas en ambientes ricos en nutrientes, como las zonas de surgencia, en comparación con ambientes limitantes en nutrientes, como los giros oceánicos (Bižić-Ionescu et al., 2018).

Las correlaciones entre el CH_4 y la clorofila (Lamontagne et al., 1973), encontradas en diversos ambientes (Bizic, 2021; Cerbin et al., 2022; Günthel et al., 2020; Klintzsch et al., 2023; Mao et al., 2024) sugirieron tempranamente la posibilidad de producción de CH_4 por el fitoplancton marino (Berg et al., 2014; León-Palmero et al., 2020). Experimentos en laboratorio corroboran esta hipótesis mediante el uso del ^{13}C, confirmando que algunas algas marinas (e.g. haptofitas) producen CH_4 utilizando el bicarbonato (Klintzsch et al., 2023) o compuestos de azufre metilado (Lenhart et al., 2016). Del mismo modo, cianobacterias que fijan N pueden producir CH_4 (Bižić et al., 2020) cuando expresan la enzima nitrogenasa de Fe (Zheng et al., 2017), a ello se le suma que géneros importantes como *Proclorococcus* y *Synechochoccus* convierten el carbono inorgánico fijado en CH_4 en condiciones de luz (Bižić et al., 2020; Klintzsch et al., 2020; León-Palmero et al., 2020), poniendo en relieve el papel fundamental de los fotoautótrofos en este proceso. Por otra parte, organismos del picoplancton heterótrofo han demostrado producir CH_4 en condiciones de oscuridad (Tenorio and Farías, 2024), lo que revela una compleja interacción entre procesos autotróficos y heterotróficos.

Además de la producción biológica, también existe una producción abiótica, donde el CH_4 se forma a partir de la fotooxidación de la materia orgánica disuelta cromófora o coloreada (Li et al., 2020). Reciente investigación plantea la hipótesis de la formación no enzimática de CH_4 inducido por especies reactivas del oxígeno (ROS), que es un proceso que se da en todos los organismos vivos y solo se requieren ROS, hierro libre y donantes adecuados de grupos metilo ($-CH_3$) para formar CH_4 (Ernst et al., 2022).

1.3. Escalas temporales de procesos oceanográficos y forzantes atmosféricos que controlan la capa superficial del océano.

Los procesos oceanográficos varían en el tiempo y el espacio debido a una combinación de factores atmosféricos y oceanográficos (Dickey, 1991). Del mismo modo, los procesos ecológicos en el océano son complejos y pueden implicar desfases temporales e interacciones diversas que no son fácilmente discernibles (Benway et al., 2019). En este sentido, las mediciones discretas de gases como el CH_4 han aportado información clave sobre su variabilidad en el océano (Bange et al., 2010; Farías et al., 2021b; Ma et al., 2020). No obstante, persisten grandes incertidumbres respecto a sus fluctuaciones en diferentes escalas temporales (desde días hasta años) y espaciales, que abarcan desde metros (termoclinas, oxiclinas) hasta cientos de metros (remolinos, estructuras de mesoescala). Estas brechas se deben a la escasa disponibilidad de observaciones *in situ* de largo plazo (Wilson et al., 2020), a limitaciones tecnológicas (Boulart et al., 2010) y a la complejidad del reciclaje biogeoquímico del CH_4 (Reeburgh, 2007), particularmente en la capa superficial del océano.

Programas de observación a largo plazo han aportado información clave sobre el funcionamiento de los ecosistemas marinos (Benway et al., 2019; Valdés et al., 2002, 2021). Sin embargo, existen pocas series de tiempo de larga duración para el CH_4 disuelto (Bange et al., 2010; Capelle and Tortell, 2016; Farías et al., 2021b; Ma et al., 2020; Sudheesh et al., 2020; Wilson et al., 2017). Esos estudios tienen baja frecuencia de muestreo, se centran en variaciones intra-estacionales (Atkinsont and Richards, 1967; Bange et al., 1994, 1998; Berner et al., 2003; Kock et al., 2008; Lamontagne et al., 1973; Weller et al., 2013), estacionales (Borges et al., 2017; Farías et al., 2021b; Jakobs et al., 2014; Sudheesh et al., 2020) e interanuales (Farías et al., 2021b; Wilson et al., 2017). Esta limitación dificulta la caracterización de procesos de corta duración (e.g. formación de hot

moments), los cuales pueden resolverse mediante mediciones de alta frecuencia, disminuyendo las incertidumbres en las emisiones locales, regionales y globales de CH_4.

En este contexto, procesos que ocurren a escala anual, están asociados principalmente a la estacionalidad atmosférica y oceánica. En los Sistemas de Surgencia de Borde Oriental (EBUS, por sus siglas en inglés), dominados por sistemas de alta presión (Strub et al., 1998), la circulación atmosférica y oceánica alterna entre periodos favorables (primavera-verano) y no favorables ala surgencia (otoño-invierno), que modulan la estabilidad de la columna de agua (Sobarzo et al., 2007), la oxigenación, la disponibilidad de nutrientes (Graco et al., 2017) y con ello, los procesos de producción y oxidación del CH_4 (Farías et al., 2021b; Kock et al., 2008).

La ruptura de los ciclos estacionales recurrentes da origen a una variabilidad interanual, producto del acoplamiento dinámico entre el océano y la atmósfera, dominada por procesos climáticos de gran escala como (i) El Niño – Oscilación del Sur (ENSO), que debilita la surgencia, reduce el aporte de Aguas Ecuatoriales Subsuperficiales (AESS) y por ende reduciría las concentraciones de CH_4; mientras que durante La Niña, se fortalece la surgencia, hay mayor aporte de AESS y por lo tanto podría acumular CH_4 en la superficie y potenciaría su intercambio con la atmósfera (Montecino and Lange, 2009; Shaffer et al., 1999; Strub et al., 2013). Además, se destacan eventos como precipitación extrema (Campos and Rondanelli, 2023; Montecinos et al., 2011) y descarga continental (Masotti et al., 2018; Saldías et al., 2012), que irrumpen la variabilidad anual.

Por otro lado, caracterizados por su marcada estacionalidad, alta productividad y dinámica oceanográfica, los EBUS constituyen laboratorios naturales para estudiar el CH_4. En este sentido, en el periodo favorable a la surgencia (primavera-verano), donde predominan vientos sur (hacia el ecuador) a lo largo de la costa (Garreaud et al., 2011), se genera un transporte fuera de la costa de aguas superficiales (transporte de Ekman), que

es compensada por el ascenso de Aguas Ecuatoriales Sub Superficiales (AESS) densas, con mayor salinidad, frías, ricas en nutrientes y GEI (e.g. CO_2, CH_4), pero bajas en oxígeno (Sobarzo et al., 2007). De esta manera, la capa superficial se fertiliza, lo que permite una alta productividad, la formación de zonas mínimas de oxígeno y condiciones favorables para la producción bentónica de CH_4 (Graco et al., 2007). En contraste, en el periodo no favorable a la surgencia, donde predominan vientos norte (hacia el polo) (Garreaud et al., 2011), el transporte de Ekman ocurre hacia la costa, provocando un hundimiento de las aguas superficiales y la intromisión de Aguas Subantárticas (ASA), menos densas, menos salina, más oxigenadas y con menos carga de nutrientes (Silva et al., 2009). De esta forma la columna de agua se ventila o se homogeniza (Chavez et al., 2008).

Bajo el contexto estacional, el microplancton (e.g. cadenas de diatomeas) contribuye con un ~70% a la biomasa de fitoplancton durante el periodo favorable a la surgencia (Testa et al., 2018). En este periodo, la gran cantidad de MO disponible podía favorecer la producción de CH_4. Sin embargo, la surgencia también promueve la sobresaturación de CH_4 en la capa superficial, incrementando su desgasificación, traduciéndose en altos flujos de CH_4 hacia la atmósfera (Farías et al., 2021b; Kock et al., 2008). Por otro lado, el nano (nanoflagelados heterotróficos) y picoplancton (cianobacterias) dominan en el periodo final y no favorable a la surgencia (Testa et al., 2018; Vargas et al., 2007). Durante este periodo, la capa superficial también está sobresaturada de CH_4, hecho posiblemente originado por producción de CH_4 *in situ* dado por cianobacterias (Bižić et al., 2020). A pesar de estos patrones, no se ha evidenciado una clara relación en los flujos de ambos periodos (Farías et al., 2021b), probablemente al solapamiento de procesos físicos y biológicos que no son captados mediante muestreos mensuales (Dølven et al., 2022a; Roth et al., 2022).

A escala intra-estacional, en los meses de transición entre periodos estacionales, favorables o no a la surgencia, debido al desarrollo de las condiciones atmosféricas asociada al debilitamiento o fortalecimiento de los vientos a lo largo de la costa (Ancapichun and Garcés-Vargas, 2015; Trautman and Walter, 2021); se generan condiciones biológicas importantes, como el cambio de la composición fitoplanctónica desde el microplancton al nano y picoplancton (Anabalón et al., 2007; Testa et al., 2018), que son organismos claves en la producción de CH_4 (Florez-Leiva et al., 2013; Lenhart et al., 2016).

En la escala sinóptica se destaca: (i) la variabilidad meteorológica como los pulsos de vientos y bajas de presión, que modulan estratificación y la mezcla superficial, la intensidad de la surgencia y lluvias intensas (Aguirre et al., 2021; Garreaud et al., 2011; Paduan et al., 2018; Pérez-Santos et al., 2014); (ii) mezcla vertical forzada por eventos de tormenta o ríos atmosféricos (Garcia-Santos et al., 2025; Garreaud et al., 2024; Zhu and Newell, 1998); (iii) variaciones en la oxigenación/desoxigenación de la columna de agua (Hernández-Miranda et al., 2012; Herrera-Becerril et al., 2022; Merma-Mora et al., 2024) producto del ascenso de aguas hipóxicas asociado a la surgencia, lo que intensifica el flujo de GEI hacia la superficie y favorece su emisión hacia la atmósfera (Aguirre et al., 2021); (iv) entrada de materia orgánica desde el continente debido a descargas de lluvias intensas, que estimulan la actividad microbiana y la degradación de la materia orgánica y favorecen la producción de CH_4 (Rao and Sarma, 2017); (v) floraciones fitoplantónicas (Jacques-Cooper et al., 2023), que oxigenan la superficie y de acuerdo a la sucesión fito planctónica (Lenhart et al., 2016), media la producción de CH_4 (Klintzsch et al., 2020).

Es importante destacar que durante el periodo favorable a la surgencia (primavera-verano), se presentan eventos relajados y activos de la surgencia (Send et al., 1987), debido a la alternancia de periodos activos de vientos S y periodos de calma o relajados, cuando se debilitan los vientos del S (Aguirre et al., 2021a; Bailey & Chapman, 1991). Ambos

eventos cambian la productividad biológica, la estructura y composición de la comunidad planctónica (Daneri et al., 2012), la química del agua de mar (Aguirre et al., 2021) y la dinámica de la capa superficial (Bailey and Chapman, 1991). Estos eventos se pueden ver intensificados por la presencia jet costeros que generan presión hacia el norte (Ecuador), favoreciendo los eventos de surgencia (Muñoz and Garreaud, 2005); por el contrario, se pueden ver debilitados por bajas de presión o vaguadas costeras, que debilitan los vientos del S e intensifican los vientos del N, favoreciendo los eventos relajados de la surgencia (Garreaud et al., 2002; Garreaud and Rutllant, 2003). Por lo tanto, estos eventos pueden generar pulsos de acumulación o desgasificación de CH_4 que son clave en el balance de carbono y forzamiento climático costero.

De acuerdo con lo anterior, algunas propiedades físicas y biogeoquímicas, como la temperatura, la salinidad y el pH, responden al estrés del viento favorable a la surgencia con un desfase de 12-24 horas aproximadamente (Aguirre et al., 2021); no obstante, la fluorescencia (proxy de clorofila) no depende solamente de este forzante atmosférico, sino a interacciones complejas físicas y biológicas (e.g. pastoreo, foto inhibición, etc.) que fuerzan el bloom de fitoplancton (Aguirre et al., 2021). Es decir, durante el periodo favorable a la surgencia, la productividad durante los eventos activos es menor; y durante los eventos de relajación es mayor, donde predominan periodos de calma o vientos ligeros y la columna de agua esta estratificada (Mcmanus and Peterson, 1988); habiendo cambios constantes en la dominancia de la autotrofía y la heterotrofía. Además, durante el evento relajado de la surgencia, la abundancia microbiana es un orden de magnitud mayor (1,40 $\mu g\ C\ l^{-1}\ h^{-1}$) que durante el evento activo (0,13 $\mu g\ C\ l^{-1}\ h^{-1}$), especialmente bacterias heterótrofas, favoreciendo la producción de CH_4 asociado al reciclaje de MO (Montes et al., 2020).

En la escala diaria, forzantes como la radiación solar (RS) actúa como el principal forzante, generando variaciones térmicas y dinámicas tanto en la columna de agua como

en la atmosfera. Durante el día, la absorción de calor provoca un calentamiento superficial que se traduce en una (i) estratificación vertical de la columna de agua, que crea un gradiente de densidad y una estratificación estable en la capa superficial, esto resulta en un marcado (ii) calentamiento diurno de la temperatura superficial (TS) y por lo tanto cambios diurnos en la estabilidad de la atmosfera inferior, favoreciendo el desarrollo de (iii) la brisa marina, especialmente bajo condiciones despejadas y cálidas asociadas a vientos del sur, cuando los ciclos diarios de RS y TS son más marcados. En contraste la nubosidad o los vientos del norte atenúan la RS y la TS, debilitando o suprimiendo la brisa marina. La radiación solar también influye en (iv) el ciclo diario de la fotosíntesis que es mayor durante horas de la tarde (Neveux et al., 2003), favorece la oxigenación y el consumo de nutrientes (sobre todo NO_3^- en la primera etapa del desarrollo del fitoplancton) (Zhao et al., 2022). Por la noche, la ausencia de absorción de calor produce (v) una estratificación inestable o mezcla, sumado a las mareas, donde el cizalle y las ondas internas ventilan la columna de agua (Robertson et al., 2017), modulando la estratificación, facilitando la redistribución de nutrientes, temperatura y salinidad (Deng and Zhao, 2020) y por lo tanto de gases disueltos.

No obstante, pese a estos avances, el comportamiento del CH_4 a escalas temporales cortas desde diarias a sinóptica, sigue siendo una incógnita. En particular, se desconoce cómo varía el CH_4 frente a fluctuaciones rápidas en el viento, la estratificación o los aportes continentales. Estas dinámicas de corto plazo podrían tener implicancias relevantes para la estimación de flujos en la interfaz océano-atmósfera y para la comprensión del rol de las zonas costeras de surgencia como fuentes significativas de CH_4.

Por lo tanto, considerando la importancia que tienen las zonas de surgencia costera en las emisiones de CH_4 hacia la atmósfera, esta tesis analiza la variabilidad del CH_4 a diferentes escalas temporales (estacional, sinóptica y diaria) en la zona de surgencia de Chile central, mediante datos de serie de tiempo de una estación fija (12 años), ubicada en

la plataforma continental de Chile central, así como datos de alta frecuencia en una estación ubicada en una bahía sujeta a surgencia costera. Se analiza, además, los flujos de CH_4 hacia la atmósfera y posibles vías de producción biológica en aguas superficiales oxigenadas. Esta aproximación permite explorar una dinámica más completa del CH_4 cubriendo diferentes escalas temporales, además de evaluar el impacto físico en su distribución y mejorar las estimaciones de emisiones de CH_4 en zonas costeras altamente dinámicas. Los resultados de este estudio contribuirán a reducir las incertidumbres en los presupuestos regionales de CH_4 y a comprender el rol de los ecosistemas de surgencia (incluido bahías) en el ciclo global del CH_4 en un contexto climático y presión antropogénica creciente.

2. HIPÓTESIS Y OBJETIVOS

2.1. HIPÓTESIS

1. Existe una variabilidad diaria en las concentraciones de CH_4 superficial, asociada a forzantes físicos (e.g. radiación solar, temperatura, brisa marina) que modulan la ventilación y el intercambio en la interfaz mar-atmósfera y procesos biológicos dependientes de la luz que regulan la producción y oxidación de este gas.

2. Existe una variabilidad sinóptica (2–10 días) significativa del CH_4 superficial, mayor que la estacional, impulsada por la alternancia de viento que modulan los períodos activos y relajados de surgencia.

2.2. OBJETIVO GENERAL

Caracterizar, a múltiples escalas temporales, la dinámica del CH_4 superficial y su intercambio en la interfaz mar-atmósfera, así como mecanismos físicos y biogeoquímicos que generan "hot moments" de este gas en una zona de surgencia de Chile central, integrando observaciones de alta y baja frecuencia, con el fin reducir las incertidumbres en las estimaciones de emisiones costeras.

2.3. OBJETIVOS ESPECÍFICOS

1. Determinar los modos de variabilidad de largo plazo (interanual y estacional) de la concentración de CH_4 en la zona de surgencia de Chile central.

2. Evaluar las variaciones de corto plazo (diario y sinóptico) de la concentración de CH_4 superficial en la zona costera de chile central.

3. Determinar y comparar estimaciones flujos de CH_4 derivadas de series de alta (horarias) y baja frecuencia (mensuales) para cuantificar el sesgo por submuestreos y la reducción de incertidumbre en emisiones costeras**.**

4. Identificar los procesos/interacciones microbianas y condiciones oceanográficas que favorecen eventos de acumulación de CH_4 ("*hot moments*") en la capa superficial, mediante experimentos controlados de laboratorio.

3. MATERIAL Y MÉTODOS

3.1. Área de estudio

En la región del Pacífico Sur Oriental (PSO), la posición e intensidad del Anticiclón Subtropical del Pacífico Sudeste (ASPS) regulan la circulación atmosférica regional, generando vientos hacia el Ecuador que favorecen la surgencia costera. Estos vientos modulan estacionalmente las condiciones oceanográficas frente a Chile central, con periodos favorables a la surgencia en primavera-verano y periodos no favorables a la surgencia en otoño-invierno (Strub et al., 1998).

Este estudio se realizó en la zona costera de Chile central (36°S), caracterizada por una plataforma continental extensa (~40 km de extensión) delimitada por los cañones submarinos de los ríos Itata y Biobío (Sobarzo et al., 2001). Esta área presenta un régimen estacional de surgencia costera forzado por vientos del sur (S) y suroeste (SO); predominantes en primavera-verano (Sobarzo et al., 2007; Sobarzo and Djurfeldt, 2004). Dicho proceso induce al afloramiento de Aguas Ecuatoriales Sub-Superficiales (AESS), ricas en nutrientes y pobres en oxígeno. Por el contrario, durante otoño-invierno, el debilitamiento de los vientos del S y SO, y el predominio de los vientos del norte (N) generan condiciones de hundimiento o downwelling, favoreciendo la presencia de Aguas SubAntárticas (ASAA) (Ahumada and Chuecas, 1979), caracterizadas por su alto contenido de oxígeno y baja concentración de nutrientes.

Estas características confieren a la zona una alta productividad (1,1 kg C m^{-2} $año^{-1}$), debido al ascenso de aguas AESS que fertiliza la capa superficial, durante primavera-verano. No obstante, durante otoño-invierno se pueden detectar pulsos de productividad debido al ingreso de nutrientes por medio de las aguas continentales, especialmente de río Itata y eventualmente del Biobío coincidentes con la época de precipitaciones que hacen

variar la salinidad, permitiendo una productividad basal relativamente alta todo el año (Testa et al., 2018).

A lo largo de la costa de Chile central, debido a la forma irregular de la línea de costa, destacan algunas bahías cuya característica particular es que están sujetas a la surgencia costera (Largier, 2020a). Entre ellas se encuentra la Bahía de Coliumo, una bahía pequeña (4,6 km^2), poco profunda, orientada hacia el ecuador. Debido a su ubicación, la surgencia dada en la plataforma costera impacta dentro de la bahía, generando características similares a las descritas anteriormente. Sin embargo, su morfología atenúa la intensidad de los vientos incidentes y modula la ventilación y el intercambio con el océano adyacente (Calliari and Alfaro, 1997).

3.2. Estaciones y frecuencias de muestreo

Se contaron con dos estaciones de muestreo, la Estación 18 (36° 0.802’ S 73° 07.750’ W) y la estación de la boya costera (36°32 S 72° 56’W), ambas pertenecientes al Departamento de Oceanografía de la Universidad de Concepción (ex COPAS) (Fig. 2). La Estación 18 (ST18), es un punto fijo que cuenta con una serie temporal larga (desde 2002). Ubicada sobre la plataforma continental de Chile central a 28,4 km de la costa, frente a Dichato y tiene una profundidad de ~90 m. Esta estación fue creada en 1994 en el marco Expedición Thioploca-Chile 1994 y luego establecida como estación fija de serie de tiempo en el año 2002 por el centro COPAS, sin embargo, muestras de CH_4 se empezaron a colectar a partir del 2007 y se mantiene hasta la actualidad. El periodo estudiado comprende desde abril 2007 hasta abril 2019 (muestreos mensuales). Los cruceros se realizaron a bordo de la embarcación oceanográfica Kay-Kay II de la misma universidad. Los muestreos de invierno, generalmente se caracterizaron por fuertes tormentas y mezcla vertical, homogeneizando y oxigenando la columna de agua, además

de una disminución marcada en la salinidad superficial debido a la influencia de mayores descargas del río Itata, producto de las precipitaciones durante este periodo.

La boya está localizada en el interior de la bahía de Coliumo frente al sector Villarrica donde se encuentra la Estación de Biología Marina de Dichato (36° 32’ 26’’ S 72° 55 ’60’’ O). Tiene una profundidad de 10 m aproximadamente. Esta boya cuenta con sensores oceanográficos que registran temperatura, salinidad y metano. En la estación de Biología Marina se cuenta con una estación meteorológica, donde se registran variables atmosféricas (temperatura del aire, dirección e intensidad del viento, humedad, radiación). También se contaron con registros atmosféricos (dirección e intensidad del viento, presión atmosférica, precipitación) de la estación meteorológica de Carriel Sur (Fig. 2).

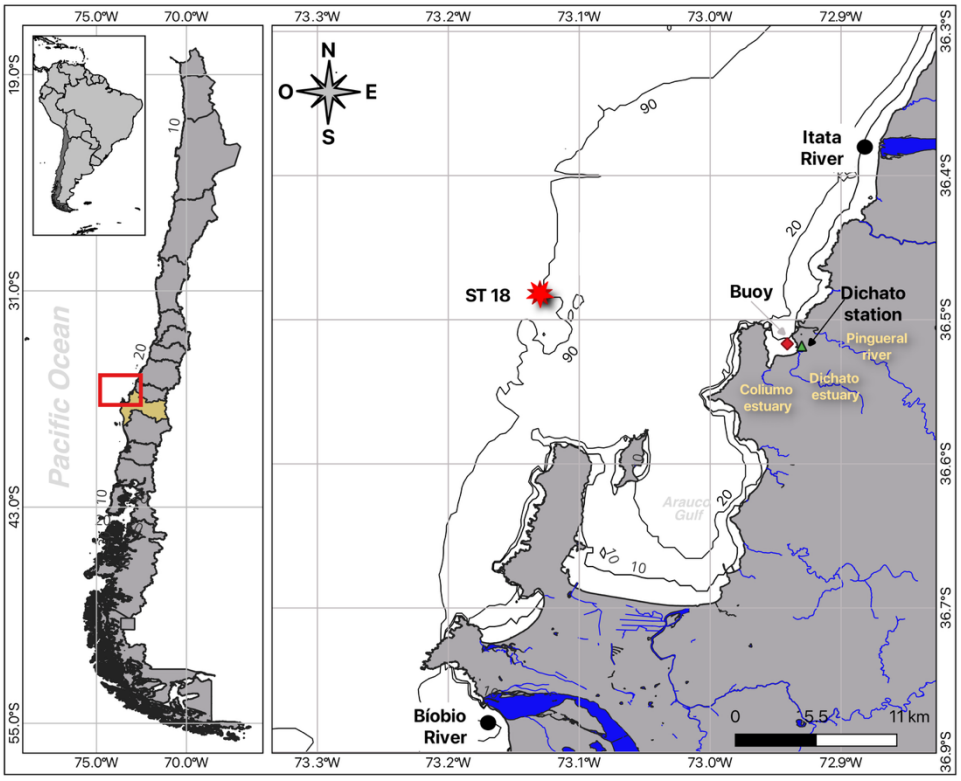

Figura 2. Localización geográfica de la estación 18 (ST18) y la boya oceanográfica costera, situada sobre la plataforma continental de Chile central y en el interior de la Bahía de Coliumo, respectivamente, influenciados por los ríos Itata y Bíobio.

3.3. CAPÍTULO 1. Determinar los modos de variabilidad de largo plazo (interanual y estacional) de la concentración de CH_4 en la zona de surgencia de Chile central

Para este este objetivo, se utilizaron datos disponibles de la serie de tiempo de CH_4 y otras variables oceanográficas desde abril 2007 hasta abril 2019. Se realizó un análisis estadístico descriptivo de las diferentes variables oceanográficas. Pruebas estadísticas para verificar una igualdad de varianza y si se ajustan a una distribución normal fueron realizadas a través de la prueba de Levene y la prueba de Kolmogorov-Smirnov, respectivamente. Para evaluar el grado de asociación o interdependencias entre las variables discretas de la columna de agua y sus respectivos inventarios, así como variables atmosféricas como velocidad y estrés del viento se usó el Coeficiente de Correlación de Spearman.

3.3.1. Variables oceanográficas y biogeoquímicas.

Las variables oceanográficas de la columna de agua se obtuvieron mediante un perfilador CTD (Sea-Bird 19 PLUS). Se registró temperatura, salinidad, presión y oxígeno disuelto. Ocho profundidades que cubrieron toda la columna de agua fueron establecidas cada 5 m entre los 0 y 20 (capa superficial) y cada 10-20 m entre los 30, 50, 65 y 80 m (capa subsuperficial).

Se recolectaron muestras discretas en las profundidades mencionadas para determinar variables biogeoquímicas como la concentración de gases (CH_4 y O_2 disuelto), nutrientes (nitritos, nitratos, fosfatos y silicatos), Carbono Orgánico Disuelto (COD) y clorofila-a. Todas fueron preservadas de acuerdo con sus respectivos protocolos.

Las muestras para Oxígeno disuelto (OD) se recolectaron en frascos de vidrio de 125 mL (triplicado) y fueron fijadas a bordo de la embarcación Kay-kay II y

posteriormente analizadas mediante el método de Winkler (Carpenter, 1965), usando un Dosimat 665 con detector de punto final fotométrico automático, con un límite de detección de 2 μm L^{-1}.

Para medir la concentración de CH_4 se recolectó agua de mar en viales cromatográficos de 20 mL (triplicado), obtenidos directamente de la botella Niskin a través de una manguera Tygon que llegó hasta el fondo del vial de manera que se desbordara tres veces su volumen; impidiendo la presencia de burbujas. Inmediatamente después se inoculó 50 μL de cloruro de mercurio ($HgCl_2$) concentrado para detener la actividad biológica y se selló con septas de goma y tapas de aluminio para evitar contaminación con gases de la atmósfera. El CH_4 fue analizado por el método del equilibrio de fases; para ello se tomó cada vial y se añadió 5 mL de helio (gas inerte) para crear un espacio de cabeza o "headspace", permitiendo un equilibrio entre la fase acuosa y gaseosa. Posteriormente, la fase gaseosa se analizó por cromatografía gaseosa en un cromatógrafo de gas (Shimadzu 17) con detector de ionización de llama (FID) con una columna Restek RT QS-Bond (de 30 metros 0,53 mm ID, 20 μm Film) con una temperatura de 30 ºC y flujo de la columna de 3,5 mL min^{-1}.

Las muestras de nutrientes (por triplicado) se recolectaron con una jeringa de 60 mL y fueron filtradas con un filtro de acetato de celulosa de 0.45 μm, el filtrado se almacenó en frascos de polietileno Falcon de 15 mL. Las muestras fueron analizadas mediante técnicas colorimétricas estándares (Grasshoff et al., 1983) en un auto analizador Seal AA3 de flujo segmentado, el cual consta de cuatro canales con módulos específicos para cada nutriente. Para obtener las muestras de clorofila-a (triplicado) se filtró 100 mL (GF/F) de agua de mar y se analizó por el método de (Holm-Hansen et al., 1965) utilizando el fluorómetro Turner desings 10AU.

3.4. CAPÍTULO 2. Evaluar las variaciones de corto plazo (diario y sinóptico) de la concentración de CH_4 superficial en la zona costera de chile central.

Para este este objetivo, se utilizaron datos de alta frecuencia de la boya Docencia desde septiembre 2024 hasta febrero 2025 en primavera-verano, un periodo de surgencia costera. Se realizaron análisis de correlación cruzada para evaluar la relación entre las concentraciones de metano y variables ambientales como la temperatura, la salinidad, la velocidad del viento y el flujo de CH_4.

3.4.1. Observación continua de variables oceanográficas y biogeoquímicas.

Las variables oceanográficas y biogeoquímicas se obtuvieron a partir de sensores oceanográficos ubicados a 1,5 m de profundidad. Las concentraciones de CH_4 se midieron utilizando un sensor HydroC CH_4 (4H Jena Engineering), mientras que la temperatura y la salinidad se registraron con un RBR CTD (Duo 3). Los daros fueron almacenados cada minuto desde el inicio de la surgencia (septiembre) hasta su total desarrollo (febrero de 2025). Se contaron con datos atmosféricos de la Estación Meteorológica de Dichato, estos fueron magnitud y dirección del viento, radiación solar y temperatura superficial de mar.

Para validar los datos del sensor de CH_4; semanalmente se realizaron muestreos discretos de agua de mar para CH_4 utilizando una botella Niskin de 10 L. Las muestras de CH_4 (por triplicado) se recogieron directamente del Niskin a través de una manguera impermeable a los gases en viales de cromatografía de gases (GC) de 20 mL y se conservaron mediante la adición de 50 µL de cloruro mercúrico saturado (Karl and Tilbrook, 1994) e inmediatamente se sellaron con un septo de caucho butílico gris y un tapón de aluminio y se almacenaron en la oscuridad. El análisis de las muestras se llevó a cabo de manera similar como se describió en la sección anterior.

3.4.2. Post procesamiento del Raw data de metano.

Debido a que el tiempo de respuesta del sensor de CH_4 (τ63) es de unos 50 a 55 minutos (según las especificaciones del fabricante) debido al proceso de difusión y posterior equilibrio dentro del sensor, se utilizó el método de deconvolución basado en problemas estadísticos inversos para corregir el tiempo de respuesta de los sensores basados en membrana propuesto por Dølven et al. (2022). El algoritmo estima la verdadera concentración ambiental a partir de los datos convolutivos del sensor, considerando las características del tiempo de respuesta de este (Dølven et al., 2022a). Este método resuelve la ley de la ecuación de crecimiento, expresada como una ecuación diferencial ordinaria de primer orden (Ecuación 1), que describe la difusión:

$$\frac{du_m}{dt} = k(u_a - u_m) \qquad \text{(Ecuación 1)}$$

Donde u_m es la presión parcial ambiente de interés (real), u_a es la presión parcial dentro de la cámara de medición del sensor (µatm), k es el coeficiente de crecimiento, definido por $k = \frac{1}{\tau_{63}}$, donde τ_{63} es el tiempo de respuesta del sensor. Esta ecuación se resolvió utilizando la función *deconv_master* en MATLAB, disponible online, desarrollada por Dolven et al 2022 (https://github.com/KnutOlaD/Deconv_code_data/blob/main/deconv.py). Esta función implementa la regularización de Tikhonov para estimar la verdadera concentración ambiental a partir de la señal medida del sensor, teniendo en cuenta el tiempo de respuesta del sensor. El parámetro óptimo de regularización se determinó mediante el análisis de la curva L, que equilibra la precisión del modelo con la suavidad de la solución, evitando que exagere ante pequeñas variaciones o ruido en los datos. Este método garantiza que las series temporales deconvolucionadas reflejen con exactitud la variabilidad de alta frecuencia en la concentración de CH_4 ambiental, evitando al mismo tiempo el sobreajuste al ruido.

3.4.3. Metano disuelto y conversión de ppm a nM

La concentración de metano disuelto en nM se calculó a partir de su presión parcial (ρ CH_4, en µatm), aplicando la ley de Henry (ecuación 2):

$$C_{CH_4} = K_H * \rho CH_4 \quad \text{(Ecuación 2)}$$

El coeficiente de solubilidad (K_H; mol L^{-1} atm^{-1}) se calculó mediante la ecuación empírica propuesta por Wiesenburg & Guinasso (1979), basada en la temperatura y la salinidad *in situ*.

3.4.4. Validación del sensor de metano

Para validar los datos del sensor de CH_4 se utilizó muestras discretas de CH_4 disuelto in situ. Se aplicó un modelo de regresión lineal simple utilizando la función *fitlm* de MATLAB. La variable independiente (X) fue la concentración de CH_4 medida por el sensor y la variable dependiente (Y) fue la concentración de CH_4 in situ. La bondad de ajuste (R^2), el error cuadrático medio (RMSE) y el valor *p* se tuvieron en cuenta para verificar la calidad de la validación y el rendimiento del sensor. Además, para complementar el análisis de validación del sensor, se utilizó un diagrama de Taylor, usando la función *STaylorDiag* (Versión 1.5.2) en MATLAB (Liu, 2025) (Zhaoxu, 2025), donde se evaluaron la desviación estándar, la Diferencia Cuadrática Media (RMSD) y la correlación entre ambas series.

3.4.5. Espectro de Wavelet

Para identificar y comparar las frecuencias dominantes de las variables a lo largo del periodo estudiado, se realizó un análisis wavelet de las series temporales horarias normalizando los datos. Se utilizó el paquete *wavelet* disponible online para MATLAB (Torrence and Compo, 1998).

3.4.6. Componentes del viento y estrés del viento (t)

Las componentes del viento se calcularon a partir de la magnitud del viento (çV,ç en m s^{-1}). u representa la componente zonal del viento (m s^{-1}) y v representa la componente meridional del viento (m s^{-1}), q es la dirección del viento (grados convertidos a radianes), como se indica en las siguientes ecuaciones.

$$u = \vec{V} * cos\,(\theta) \qquad \text{(Ecuación 3)}$$

$$v = \vec{V} * sin\,(\theta) \qquad \text{(Ecuación 4)}$$

Ambas componentes del viento se utilizaron para calcular el estrés del viento según (Nelson, 1977).

$$\mathbf{t}_x = C_d * r_{air} * ½V½ * v \qquad \text{(Ecuación 5)}$$

Donde Cd es el coeficiente de arrastre, en este caso utilizamos 0,0013 (Kraus, 1972), ρ_{air} es la densidad del aire (0,00122 g cm^{-3} o 1,22 kg m^{-3}), | V| es la magnitud del viento y v es la componente meridional de los vientos.

Los eventos de afloramiento se calcularon según el índice de afloramiento (UI, m^3 s^{-1}), que se obtuvo a partir del transporte zonal de Ekman por 1000 m de línea de costa (Bakun, 1973).

$$UI = \left(\frac{\mathbf{t}_x}{r * f}\right) * 1000\ m \qquad \text{(Ecuación 6)}$$

Donde $\mathbf{t}_x$ (N m^{-2}) es la tensión meridional del viento, que representa la densidad media de la columna de agua (1026,21 kg m^{-3}) y f es el parámetro de Coriolis, correspondiente a la latitud donde se encuentra la boya de entrenamiento (8,6829 x 10-05 s^{-1}).

3.5. CAPÍTULO 3. Determinar y comparar estimaciones flujos de CH_4 derivadas de series de alta (horarias) y baja frecuencia (mensuales) para cuantificar el sesgo por submuestreos y la reducción de incertidumbre en emisiones costeras.

Para este objetivo se usaron los datos mensuales de la serie de tiempo de la ST18 y las series horarias de la boya costera.

3.5.1. Flujos de metano en la interfaz océano-atmósfera

Los flujos de CH_4 fueron estimados con la ecuación de flujos de Wanninkhof (1992):

$$F = Kw*(Cw - C*) * 0.24 \quad \text{(Ecuación 7)}$$

Donde, F es el flujo del gas que se desea calcular (μmol $m^{-2}d^{-1}$); kw (cm h^{-1}) es la velocidad de transferencia del gas; Cw (nmol L^{-1}) es la concentración promedio de CH_4 en la capa de mezcla (10m); C* (μmol m^{-3}) es la concentración de CH_4 en equilibrio con la atmósfera.

La velocidad de transferencia del gas (K_w) se calculó de acuerdo a Wanninkhof (1992), siguiendo la ecuación 8.

$$K_w = 0.31 * U^2 * \left(\frac{Sc}{660}\right)^{-0.5} \quad \text{(Ecuación 8)}$$

Donde U es la velocidad del viento (m s^{-1}) correspondiente al promedio de una semana previa al día de muestreo (incluyendo el día muestreado). Magnitud y dirección del viento (por horas), se obtuvieron a partir de la estación meteorológica Carriel Sur (http://www.meteochile.gob.cl/). Sc es el número de Schmidt en función de la temperatura (Sarmiento and Gruber, 2006) y se calculó de la siguiente manera

$$Sc = 2039.2 - 120.31\,x\,T + 3.4209\,x\,T^2 - 0.040437\,x\,T^3 \qquad \text{(Ecuación 9)}$$

La concentración de CH_4 en equilibrio con la atmósfera, se calculó a partir de Wiesenburg and Guinasso (1979), como se muestra en la ecuación 10.

$$\mathrm{C} * = \beta * (1 - \mathrm{P_{vP}}) * \mathrm{f_G} \qquad \text{(Ecuación 10)}$$

β = Coeficiente de solubilidad de Bunsen, calculado a partir de la ecuación 11.

$$\beta = Exp\left[-68.8862 + 101.4956\left(\frac{100}{T}\right) + 28.7314 * ln\left(\frac{T}{100}\right) + S\left(-0.076146 + 0.043970\left(\frac{T}{100}\right) + 0.0068672\left(\frac{T}{100}\right)^2\right)\right] \qquad \text{(Ecuación 11)}$$

Pvp = corresponde la presión del vapor de agua (atm), en función de la temperatura (K) y la salinidad (Ecuación 12)

$$\mathrm{Pvp} = \mathrm{Exp}\left(24.4543 - 67.4509\left(\frac{100}{\mathrm{T}}\right) - 4.8489\ln\left(\frac{\mathrm{T}}{100}\right) - 0.000544\mathrm{S}\right)$$

fG = fracción molar de gases atmosféricos, obtenidos a partir de promedios mensuales de las concentraciones de CH_4 del ESRL de la NOAA (http://www.esrl.noaa.gov).

3.5.2. Análisis de incertidumbre de las series temporales.

La incertidumbre de los flujos de CH_4 se estimó mediante un enfoque no paramétrico basado en bootstrap (re-muestreo) por bloques móviles (Vogel and Shallcross, 1996), con la finalidad de cuantificar la variabilidad de los estimadores (media de los flujos de CH_4). Se hicieron bloques de diferente longitud de acuerdo con lo permitido por la serie de tiempo mensual y de alta frecuencia (Tabla 1).

Tabla 1. Longitudes de las series mensuales y de alta frecuencia de flujos de metano hacia la atmósfera.

Serie	Periodo	Bloques: días (d) y meses (m)
Mensual	Abril 2007 – Abril 2019	3, 6, 12 m
Alta frecuencia (diaria)	Septiembre 2024 – Febrero 2025	1, 3, 7, 15, 30 d

Los datos se dividieron en bloques de acuerdo con la Tabla 1 y se seleccionaron aleatoriamente para construir la serie bootstrap de igual longitud que la serie original, cada réplica b genera una media bootstrap: $\bar{x}^*(b)$, donde $\bar{x}^*(b)$: es el valor i-ésimo de la serie reconstruida a partir de los bloques seleccionados aleatoriamente. Tras las B réplicas (en este caso usamos B=5000), se obtiene una distribución bootstrap ($\bar{x}^*(1), \bar{x}^*(2)\ldots, \bar{x}^*(B)$), de la cual se estimó la media, el error estándar bootstrap y los intervalos de confianza. El IC95 se calculó usando los percentiles empíricos 2.5% y 97.5% de la distribución bootstrap:

$$IC_{95\%} = 0.95\ [P_{2.5}, P_{97.5}]$$

El semi-ancho del intervalo se calculó:

$$h = \frac{P_{97,5} - P_{2,5}}{2} \qquad \text{(Ecuación } \textit{13}\text{)}$$

3.6. CAPÍTULO 4. Identificar los procesos/interacciones microbianas y condiciones oceanográficas que favorecen eventos de acumulación de CH_4 ("hot moments") en la capa superficial, mediante experimentos controlados de laboratorio.

Para desarrollar este este objetivo, se utilizaron datos disponibles de la serie de tiempo de CH_4 y otras variables oceanográficas, desde enero 2018 hasta diciembre 2021. Pruebas estadísticas para evaluar las variables oceanográficas fueron similares al capítulo anterior.

3.6.1. Anomalías y hot moments de CH_4

Anomalías de CH_4 fueron estimados mensualmente sólo en la capa superficial, siguiendo la siguiente ecuación

$$Anomalía = \frac{xCH_4 - \bar{x}CH_4}{\sigma CH_4} \quad \text{(Ecuación 14)}$$

Donde x CH_4 es el valor discreto a una determinada profundidad (superficie) y $\bar{x}CH_4$ es el valor medio para todo el período (2018-2021) en superficie, y σCH_4 es la variación estándar de este conjunto de datos. Los hot moments de CH_4 se definieron como un valor 3 veces superior al valor medio mensual de la anomalía ($\bar{x}$ DCH_4) a cada profundidad dentro de la capa superficial (Ecuación 3):

$$\frac{\Delta CH_4}{X_{\Delta CH_4}} > 3 \quad \text{(Ecuación 15)}$$

Donde ΔCH_4 es la anomalía mensual estimada este gas a cada profundidad.

3.6.2. Experimentos de reciclaje de CH_4 en viales GC a partir de comunidad planctónica fraccionada por tamaño y enriquecida con sustratos orgánicos

Con la finalidad de evaluar la capacidad que tienen los microorganismos del plancton en producir CH_4 y ver cómo estos responden a diferentes tratamientos con sustratos metilados, diversos experimentos fueron realizados en diferentes fases de la productividad (Tabla 2).

Tabla 2. Resumen de la configuración de los experimentos en viales GC y microcosmos con diferentes tratamientos. NC: agua de mar con plancton natural (control); <3 µm: picoplancton; <0,2 µm: femtoplancton (control +); <0,2 µm + $HgCl_2$: femtoplancton con $HgCl_2$ (control +); CC: concentrado de picoplancton; y la adición de sustratos metilados (MPn: ácido metilfosfónico; TMA:trimetilaminas). Las diferentes fases del período de productividad son las siguientes: PI - Fase I; PII - Fase II; y PIII - Fase III.

Fecha	Tipo	Setup	Fracción (µm)	Lugar	Tiempo (h)	Periodo de productividad
Diciembre 2018	Vial GC	Plancton fraccionado	CN, < 3 and < 0,2	Incubador	24	Alto (PI)
Enero 2019	Vial GC	Plancton fraccionado	CN, < 3 and < 0,2	Incubador	24	Alto (PI)
Marzo 2019	Vial GC	Adición de MPn	<3	Incubador	24	Intermedio (PII)
Mayo 2019	Vial GC	Adición de MPn y TMA	<3	Incubador	24	Basal (PIII)
Abril 2019	Microcosmos	Adición de MPn y TMA	CC	Cámara de frío	~60	Intermedio (PII)
Septiembre 2019	Microcosmos	Adición de MPn y TMA	CC	Cámara de frío	~60	Alto (PI)

Para los experimentos de corto plazo, se filtraron 5 L de agua de mar de forma secuencial a través de filtros de diferentes filtros, obteniéndose tres comunidades: 150 µm (microplancton), 3 µm (pico o bacterioplancton) y 0,22 µm (fentoplancton). Esta última comunidad se usó como controles negativos. También se consideró un tratamiento sin filtrar como control positivo. Antes de iniciar las incubaciones se tomaron muestras de oxígeno, clorofila-a y nutrientes.

Una vez obtenidas las diferentes comunidades, fueron puestas en viales cromatográficos de 20 ml (108 en total). Las incubaciones se realizaron a 13°C con un fotoperiodo se 12h de luz (11 – 11,5 µmol $m^{-1}s^{-1}$). Cada 4 horas se eliminaron tres viales por tratamiento y se preservaron con $HgCl_2$ hasta ser analizados en un cromatógrafo de gases.

En otro set de experimentos, se estudió la capacidad del picoplancton para metabolizar sustratos metilados y producir CH_4. Se realizaron experimentos similares, donde se añadieron sustratos metilados a una concentración final de 1 µM: MPn (ácido metil fosfónico) y TMA (trimetilamina). Las condiciones de incubación y la forma de eliminar viales fueron las mismas que los experimentos anteriores.

3.6.3. Experimentos de reciclaje de CH_4 en microcosmos a partir de la comunidad planctónica fraccionada por tamaño y enriquecida con sustratos orgánicos.

Estos experimentos se realizaron en dos periodos importantes de productividad (Tabla 1). Se utilizaron sólo tres tratamientos: la comunidad natural (CN), el picoplancton (3 µm) y el picoplancton concentrado (CC) (ver Tabla 2).

Para los experimentos de largo plazo, se utilizaron botellas de policarbonato de 13L con 10L de agua de mar y 3L de espacio libre (headspace). Cada botella fue un sistema

cerrado, conectado a un espectrómetro de gases (Picarro G-2308), capaz de medir gases continuamente. Cada botella tenía una tapa con cuatro capilares de vidrio conectados a mangueras impermeable a los gases: (1) manguera conectad al espectrómetro para medir gases en equilibrio con el agua; (2) manguera conectada a una bolsa Tedlar con N, esto fue para compensar la presión cuando se extraían muestras de agua; (3) manguera que permitía recircular el aire desde el espectrómetro al headspace; (4) manguera sumergida en el agua, esta fue usada para extraer muestras discretas.

Inicialmente, los tratamientos fueron aclimatados en oscuridad por 6h. Las incubaciones tuvieron una duración de 60 horas, y fueron realizadas en una cámara fría a una temperatura controlada (12-13°C) con ciclos de fotoperiodo de 12 horas. Se extrajeron muestras de CH_4, DOC, nutrientes y clorofila-a diariamente. Los tratamientos enriquecidos con sustratos metilados tuvieron una concentración final de 1 µM.

3.6.4. Análisis biológico y químico

El CH_4 disuelto, oxígeno, nutrientes y clorofila, se analizaron de la misma forma que en la sección anterior. Para la evaluación del DOC, se recolectaron 60 mL de agua de mar por triplicado utilizando botellas de polietileno. Cada muestra fue filtrada a través de un filtro GF/F previamente muflada a 450 °C durante 4 h. Una vez filtradas las muestras, se acidificaron (pH de 2-3) y se almacenaron a -20 °C. Para el análisis de estas muestras se utilizó el método de combustión infrarroja utilizando un analizador de carbono orgánico Shimadzu (TOC-LCPH).

Muestras de citometría fueron para determinar la abundancia de picoplancton. Se fijaron 3 ml de agua con una solución de glutaraldehído (1 %) y se congelaron rápidamente (-80 °C) en nitrógeno líquido para su almacenamiento. Las muestras se analizaron con

citometría de flujo utilizando un Cytopeia de Influx equipado con cinco láseres (355, 457, 488, 532, 638nm). Las bandas de clasificación se optimizaron en función de la autofluorescencia de cada grupo. *Synechococcus sp*. se identificó por su fluorescencia naranja (530/40 nm) con láser azul de 488 nm y verde de 532 nm, los picoeucariotas se identificaron por su fluorescencia roja (692/40 nm) con un láser azul de 488 nm, y el bacterioplancton se detectaron con una combinación de láser azul de dispersión lateral (SSC) (relacionada con el tamaño celular) y fluorescencia verde (530/40 nm).

3.6.5. Tasas de reciclaje de metano

La tasa neta de reciclaje de CH_4 (acumulación neta de CH_4 menos consumo de CH_4) en diferentes fracciones de la comunidad fitoplancton se calculó mediante una regresión lineal de las concentraciones de CH_4 (Farías et al., 2009) durante el tiempo de incubación (24 h), separando los ciclos de luz y oscuridad (12 horas cada uno).

4. RESULTADOS

4.1 CAPÍTULO 1: DETERMINAR LOS MODOS DE VARIABILIDAD Y ESTACIONAL E INTERANUAL DE LA CONCENTRACIÓN DE METANO Y SU INTERCAMBIO CON LA ATMÓSFERA EN LA ZONA DE SURGENCIA DE CHILE CENTRAL

En este capítulo se presentan los resultados de la variabilidad estacional de CH_4 en la columna de agua. Como resultado se publicó el siguiente manuscrito: Farías, L., Tenorio, S., Sanzana, K., & Faundez, J. (2021). Temporal methane variability in the water column of an area of seasonal coastal upwelling: A study based on a 12 year time series. *Progress in Oceanography*, *195*. https://doi.org/10.1016/j.pocean.2021.102589

RESUMEN

Se analizó la distribución temporal del CH_4 disuelto en una zona de fuerte afloramiento costero estacional frente a Chile central (36,5◦S,73◦W). Las observaciones se tomaron de una serie temporal de doce años que incluía muestreos mensuales del agua a ocho profundidades. La concentración de CH_4 fluctuó entre 1,75 y 100,9 nmol L-1 (o 67,11% y 3965% de la saturación), con los niveles más altos en las aguas del fondo, que aumentan a medida que evoluciona el afloramiento. Se identificaron tres tipos de perfiles de CH_4; una distribución clásica de difusión-advección, con una relación de concentración de CH_4 fondo/superficie > 2, se observó predominantemente en ~ 54% de todos los perfiles y se atribuyó a la alta producción de CH_4 en los sedimentos durante la estación de afloramiento costero (primavera-verano austral); un período de mayor productividad

biológica, así como en condiciones hipóxicas/anóxicas. Por el contrario, se observaron perfiles relativamente homogéneos (relación de nivel de CH_4 entre la profundidad del fondo y la superficie < 2) en aproximadamente ~ 46% de todos los perfiles durante periodos de mezcla vertical extrema (como las tormentas de invierno).

Además, se observó un perfil irregular de CH_4 con máximos superficiales entre la superficie y los 15-30 m de profundidad. Estos picos indicaban que las tasas de producción local superan las tasas de mezcla turbulenta, lo que sugiere un rápido ciclo del CH_4 debido a procesos microbianos en la superficie. A pesar de que se observó una fuerte estacionalidad en la mayoría de las variables oceanográficas, según los periodos favorables y no favorables de afloramiento, sólo se observó una débil estacionalidad en el contenido de CH_4 y en su flujo aire-mar, oscilando este último entre 1,27 y 47,02 µmol m^{-2} d^{-1} ($\bar{x} \pm DS = 10,94 \pm 7,48$). La media anual ponderada de los flujos de CH_4 durante los periodos de afloramiento (64%) y no afloramiento (36%) fluctuó entre 1,66 y 6,22 mmol m^{-2} ($\bar{x} \pm DS = 3,40 \pm 1,43$), destacando la importancia de la plataforma continental bajo la influencia del afloramiento costero como fuente significativa de CH_4 hacia la atmósfera.

Progress in Oceanography 195 (2021) 102589

Contents lists available at ScienceDirect

Progress in Oceanography

journal homepage: www.elsevier.com/locate/pocean

Temporal methane variability in the water column of an area of seasonal coastal upwelling: A study based on a 12 year time series

L. Farías [a,b,c,*], S. Tenorio [b,d], K. Sanzana [a], J. Faundez [b,e,f]

[a] Departmento de Oceanografía, Facultad de Ciencias Naturales y Oceanográficas, Universidad de Concepción, Concepción, Chile
[b] Centro de Ciencia del Clima y la Resiliencia (CR^2), Chile
[c] Instituto Milenio en Socio-ecología Costera (SECOS), Chile
[d] Programa de Graduados en Oceanografía, Departamento de Oceanografía, Universidad of Concepción, Concepción, Chile
[e] Facultad de Biología, Pontificia Universidad Católica de Chile
[f] Estación Costera de Investigaciones Marinas (ECIM), Chile

A B S T R A C T

Temporal distribution of dissolved CH_4 was analysed in a zone of strong seasonal coastal upwelling off central Chile (36.5°S,73°W). Observations were taken from a twelve-year time series that included monthly sampling of the water at eight depths. CH_4 concentration fluctuated between 1.75 and 100.9 nmol L^{-1} (or 67.11% and 3965% of saturation), with the highest levels at bottom waters, which increase as upwelling evolved. Three kind of CH_4 profiles were identified; a classical diffusion–advection distribution, with bottom/surface CH_4 concentration ratio > 2, was predominantly observed in ~ 54% of the all profiles and attributed to high CH_4 production in the sediments during coastal upwelling season (austral spring-summer); a period of higher biological productivity, as well as in hypoxic/anoxic condition. In contrast, relatively homogeneous profiles (CH_4 level ratio between bottom and surface depth < 2) was observed about ~ 46% of all profiles during periods of extreme vertical mixing (such as winter storms). Furthermore, irregular CH_4 profile with superficial peaks occurring between the surface and 15–30 m depth was likely observed. These peaks indicated that local production rates exceed turbulent mixing rates, suggesting a rapid CH_4 cycling due to microbial processes on the surface. Despite the fact that strong seasonality was observed in most oceanographic variables, according to favourable and non-favourable upwelling periods, only a weak seasonality was observed in CH_4 content and its air-sea flux, the latter ranged from 1.27 to 47.02 μmol m^{-2} d^{-1} (mean ± SD: 10.94 ± 7.48). The annual weighted mean CH_4 effluxes during upwelling (64%) and non-upwelling (36%) periods fluctuated from 1.66 to 6.22 mmol m^{-2} (mean ± SD: 3.40 ± 1.43), highlighting the importance of the continental shelf under the influence of coastal upwelling as a significant CH_4 source toward the atmosphere.

1. Introduction

Methane (CH_4) is the most abundant organic trace gas in the atmosphere and, also the second most important anthropogenically emitted greenhouse gas. On a per molecule basis, it is 20 times more potent in terms of being a climatically active gas than CO_2 (Etminan et al., 2016). Currently, atmospheric CH_4 concentration increases 2.5 over its pre-industrial baseline (from 700 to 1750 ppm; Houweling et al., 2000) and this trend continues to increase in response to greater anthropogenic forcing upon Earth Systems (Saunois et al., 2020). There are concerns around how increasing CH_4 concentrations may affect atmospheric chemistry and climate (Wuebbles and Hayhoe, 2002). Increased CH_4 in the atmosphere depends on the equilibrium between anthropogenic and natural CH_4 sources and sinks from major reservoirs within the Earth's systems, such as atmospheric, terrestrial and oceanic systems.

Current knowledge on oceanic CH_4 distributions is based on relatively recent investigations, that are focused on technical constrains to effectively measure dissolved CH_4 (Wilson et al., 2017). Since the mid-1950's it has been reported that CH_4 concentrations reach millimolar levels in the sediments, whereas in oceanic waters CH_4 levels rarely exceed nanomolar levels (Lamontagne et al., 1973). Despite significant efforts in recent decades to quantify marine-derived CH_4, the global oceanic CH_4 dataset remains limited and indicates a concerning ambiguity around the global estimates of CH_4 emissions, that are reported to widely vary from 5 to 25 Tg yr^{-1} (Bates et al., 1996; Rhee et al., 2009; Saunois et al., 2020; Wuebbles and Hayhoe, 2002). Recently, Weber et al. (2019) using ΔCH_4 database of ~ 120,000 observations compiled into a monthly climatology, reduce by a factor of three the range of oceanic CH_4 emission (6–12 Tg CH_4 yr^{-1}).

Some studies have driven important efforts to obtain more accurate CH_4 measurements, from diurnal to decadal time scales, as well as from different spatial scales ranging from decameters up to much larger size scales; such as estuaries, coastal upwelling zones, continental shelves, subtropical gyres, and even global scales (Bates et al., 1996; Shindell

* Corresponding author at: Departmento de Oceanografía, Facultad de Ciencias Naturales y Oceanográficas, Universidad de Concepción, Concepción, Chile.
E-mail address: laura.farias@udec.cl (L. Farías).

https://doi.org/10.1016/j.pocean.2021.102589
Received 29 July 2020; Received in revised form 22 March 2021; Accepted 17 April 2021
Available online 27 April 2021

et al., 2005). Relatively few studies exist on the temporal distribution of CH_4 in coastal areas, such as salt marshes, estuaries and coastal upwelling (Borges et al., 2016; Weber et al., 2019). Including the present study, there seems to be only five studies on CH_4 time series in oceanic waters (Bange et al., 2010; Capelle and Tortell, 2016; Ma et al., 2020; Sudheesh et al., 2020; Wilson et al., 2017).

Furthermore, there are still unresolved aspects of the biogeochemical processes that lead to CH_4 recycling. This gas is produced through a process known as methanogenesis that involves microorganisms known as methanogens (including bacteria and archaea). Whereas CH_4 consumption occurs through processes called methanotrophy involving microorganisms known as methanotrophs (Reeburgh, 2007). Microorganisms use various substrates to generate CH_4 during the anaerobic respiration of organic matter (OM), including CO_2, formate and acetate; thus, it is widely accepted that methanogenesis only occurs in anoxic environments, such as in sediments and oxygen deficient waters (Reeburgh, 2007). These types of pathways (anaerobic digestion) have also been identified in zooplankton and fish (Oremland's hypothesis in 1979), and within the pycnocline during CH_4 production in suspended particles (micro-niches), according to Karl and Tilbrook's hypothesis in 1994.

However, despite current knowledge indicating that methanogenesis is a strictly anaerobic process, it is clear that CH_4 is partially produced *in situ* within oxygenated waters; a phenomena known as aerobic methanogenesis. For this reason, this phenomenon has been termed the 'oceanic CH_4 paradox'. This has been mentioned in earlier studies by Wolfe (1971), suggesting that methylotrophs can utilize one-carbon (C1) or non C-C bond compounds, such as methylphosphonate (MPn), dimethylsulphoniopropionate (DMSP), dimethylsulphide (DMS), and methylamines (MAs), among others (Damm et al., 2010; Florez-Leiva

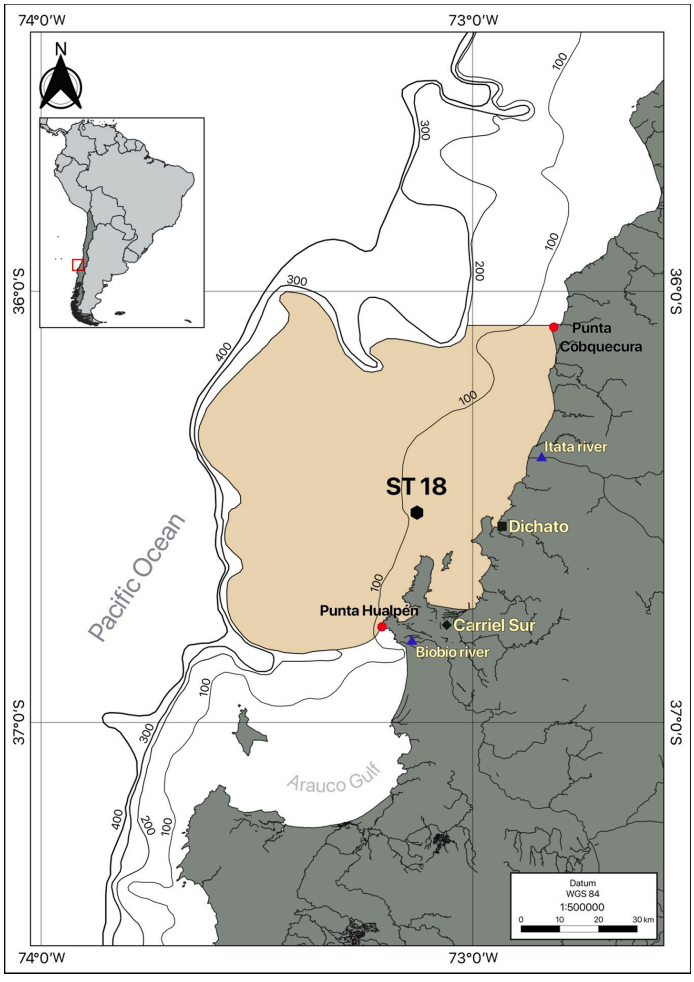

Fig. 1. Bathymetry and geographic location of time series station, Station 18 (ST18); Carriel Sur weather station, Itata (IT) and Biobío (BB) rivers are indicated. The shaded area represents the integrated shelf area off Concepcion and comprises as far offshore as the 200 m depth contour between Cobquecura and Punta Hualpén.

et al., 2013; Karl et al., 2008; Neufeld et al., 2008). This pathway may be referred as 'methylotrophic methanogenesis', which seems to involve varying poorly understood biochemical routes (Repeta et al., 2016); where CH_4 is produced as a by-product (cleavage) of metabolic processes involving dissolved organic carbon (DOC). Additionally, marine bacteria are involved in these pathways, coupled with phytoplankton, which provide alternative organic substrates (Lenhart et al., 2016). In addition to CH_4 production associated with the degradation of OM mediated directly or indirectly by phytoplankton biomass, there are recent evidences that Cyanobacteria (Bizic et al., 2020) and widespread marine (Klintzsch et al., 2019) and fresh water (Morana et al., 2020) phytoplankton are able to release a substantial amount of CH_4 during photosynthesis.

This study aims to report the temporal CH_4 distribution in a coastal area off central Chile. Excluding Patagonia, this area comprises the widest section of the continental shelf off the Chilean coast, and is subjected to seasonal coastal upwelling. During the austral spring-summer, the intensification of south and southwest winds drives coastal upwelling, carrying Equatorial Subsurface Water (ESSW) with high levels of preformed NO_3^- but low dissolved oxygen (DO) concentrations toward the surface (Sobarzo and Djurfeldt, 2004). This upwelling system results in high rates of primary and secondary production (Daneri et al., 2000; Montero et al., 2007; Testa et al., 2018), which subsequently influence DO consumption and rapid OM mineralization (Farías et al., 2009). During late autumn and early winter, Sub-Antarctic Water (SAAW) dominates at the surface layer, which is rich in DO and relatively low in nutrients compared to ESSW.

2. Material and methods

2.1. Sampling

Monthly cruises were carried out as a part of an ongoing time series program at the University of Concepción. This program includes the monitoring of one fixed time series station situated at 92 m depth on the mid-continental shelf (known as ST 18; see Fig. 1). This station has been regularly sampled on a monthly basis since 2002 to date (University of Concepción on board the R.V Kay-Kay II). CH_4 measurements were initiated in 2007 and continue to date. In this study, data came from April 2007 to April 2019 were analysed.

Continuous profiles of temperature, salinity and DO were collected using a conductivity, temperature and depth apparatus (CTD-O model SBE-25 from 2007 to 2015 or SBE-19 from 2016 to date). Fluorescence (Wet Labs) measurements were taken using sensors attached to the CTD-O_2 probe. Seawater samples were taken using 10-L Niskin bottles. Eight depth measurements of DO, CH_4, nutrients and pigments sampled consecutively in this order were obtained between the surface and 80 m depth (sup (>2 m), 5, 10, 20, 30, 50, 65 and 80 m depth). Triplicate samples were taken for measuring DO using iodometric bottles and fixed immediately. CH_4 samples (triplicate) were collected in 20 mL gas chromatography (GC) vials and preserved through the addition of 50 μL of saturated mercuric chloride (Karl and Tilbrook, 1994) and immediately sealed with a grey butyl-rubber septum and aluminium cap, and stored in darkness until analysis. To obtain nutrient samples (NO_3^-, NO_2^- and PO_4^{3-}), syringes were directly connected to the spigot of the Niskin bottle and samples were filtered through a 0.45 μm Uptidisc adapted to the syringe, then stored at −20 °C. Chl-a was filtered (in triplicate) through a glass-fibre filter (GF/F) and the filters were immediately frozen at −20 °C.

2.2. Chemical analyses.

DO (125 mL, triplicate samples) was analysed following the Winkler method with an automatic procedure based on a photometric end point with a Dosimat 665 (Williams and Jenkinson, 1982). Dissolved CH_4 was analysed through static-headspace equilibration (McAuliffe, 1963) for GC; to achieve this, 5 mL of ultrapure Helium was added into GC vials, generating a headspace for the equilibration between both phases. Once the equilibrium was reached, gas injection was carried out both automatically (2007–2018, Agilent 7697A autosampler) and manually (2018 to date) on a Schimadzu 17A GC with a Flame ionization detector and capillary column (Restek RT QS, 0.53 mm 3 × 30 m), operated at 30 °C temperature with a flow of 2.6 mL min^{-1}, using N_2 as an ultra-pure gas carrier.

Four point calibration curves were made for each sample set from 2007 to 2015, following certified standards (Mathison gas mixture) and from 2016 to date using primary standard with a composition and concentration similar to that of the current atmosphere from NOAA (1863.4 ± 0.3 ppbv for CH_4) (Bullister et al., 2016), two standard gas mixtures (Air Liquide, USA) and zero air (synthetic air without CH_4 tracers). Each day two standards were used to assess the performance of GC. The detector has a linear response to different used CH_4 concentration from 0.5 to 5 ppmv. The analytical error for CH_4 measurements was approximately 5%. Measurement uncertainty was calculated using the standard deviation taken from triplicate measurements by depth. Depth CH_4 measurements (triplicates) with a variation coefficient higher than 10% were not integrated into the CH_4 database.

Nutrients were analysed using a standard manual techniques (from 2007 to 2009), or automated techniques (with an autoanalyzer, SEAL Analytical, from 2009 to present), based on colorimetric methods (Grasshoff et al., 1983). Chlorophyll *a* was measured with a Turner Designs Fluorometer (10AU), following the standard technique described in Holm-Hansen et al. (1965), using the appropriate pigment standard (Sigma-Aldrich C6144-1MG).

2.3. Data analysis

Dissolved CH_4 concentration was calculated in accordance with the solubility coefficient from Wiesenburg and Guinasso (1979). In order to interpret the vertical and temporal variation of CH_4, the water column was divided into two layers, according to density gradient (pycnocline) and light penetration (euphotic layer) (more details in Farías et al., 2015); i.e., 1) the layer from surface down to 25 m depth, which was continually well mixed and illuminated, in accordance with previous estimates of the photic layer depth (mean ± SD: 23.9 ± 11 m) and mixing layer depth (MLD) (mean ± SD: 9 ± 10 m), based on climatology data from the time series station (Aguirre et al., 2018; Testa et al., 2018); 2) a subsurface layer that extend from 26 m to 80 m depth, overlaying the sediments (~92 m depth). Inventories of gases, nutrients and Chl-a (only in the surface layer) were calculated through the trapezoidal integration of measurements taken over several depths (minimum of 3–5 depths) within each layer.

The daily CH_4 flux (F = μmol m^{-2} d^{-1}) across air-sea interface was determined using the equation from Broecker and Peng (1974), modified by Wanninkhof (1992) or W92:

$$F = K_w{}^*(C_w - C^*)$$

where, kw (cm h^{-1}) is the gas transfer velocity; Cw (nmol L^{-1}) is the mean CH_4 concentration in the MLD, according to ML climatology based on 15 years of CTD measurements using a potential Kara's density-based criterion (García, 2017). C* is the gas concentration at equilibrium with the atmosphere, determined by the solubility equation for CH_4 (Wiesenburg and Guinasso, 1979) according to the last contact with the atmosphere. Historical atmospheric values were obtained from registers of gas hemispheric and global monthly means from the NOAA/ESRL program at NOAA (http://www.esrl.noaa.gov).

The gas transfer velocity or *Kw* was calculated according to W92, which is estimated to be the best available parametrization of wind regime within the study area according to previous studies (Farías et al., 2015). A comparison was made with the parametrization from Nightingale et al. (2000) and Wanninkhof (2014) or W14.

$$K_w = 0.31 * U^2 * \left(\frac{Sc}{660}\right)^{-0.5}$$

where U is the wind speed (m s^{-1}) and Sc is the Schimdt number for CH_4; this indicated the relationship between viscosity and the diffusion coefficient of CH_4 in the water column, which was dependent on the temperature and salinity of the seawater. For CH_4, the Schmidt number was a function of temperature (°C) updated by Sarmiento and Gruber (2006).

$$Sc = 2039.2 - 120.31xT + 3.4209xT^2 - 0.040437xT^3$$

Wind speed and direction based on an hourly register, were obtained from a permanent meteorological station located at Carriel Sur (http://www.meteochile.gob.cl/), the station meets international standards and it is established as a coastal station. These data were compared with daily wind fields recorded via satellite, averaged every 6 h and interpolated linearly for this study area, from 0.25° to 0.05°. Two products related to satellite observations were obtained from Copernicus marine service (https://resources.marine.copernicus.eu/) sources. Data for both periods are derived from scatterometers and radiometers (2007 to 2018) (WIND_GLO_WIND_L4_NRT_OBSERVATIONS_012_006) and during 2019 (WIND_GLO_WIND_L4_NRT_OBSERVATIONS_012_004).

Alongshore wind (v = m s^{-1}) was derived from meridional component which generates upwelling in the area, calculated from the wind magnitude (|V| = m s^{-1}) and direction (converted to radians), as follows.

$$v = -|V| * \cos\left(\frac{dd * \pi}{180}\right)$$

Daily stress (τ_y; N m^{-2}) was calculated following Nelson (1977):

$$\tau_y = C_d \hat{A} \cdot \rho_{air} \hat{A} \cdot |V| \hat{A} \cdot v$$

where C_d is the empirical drag coefficient, coinciding with the 10 m above sea level, corresponding to 0.0013 (Kraus, 1972), ρ_{air} is the air density that corresponds to 0.00122 g cm^{-3} or 1.22 kg m^{-3}, |V| is the wind magnitude in m s^{-1}, and v is the southern component of the wind in m s^{-1}. To evaluate the cumulative alongshore wind stress, a 5-day running mean was used, according Barth et al. (2007).

The upwelling index (UI; m^{-3} s^{-1}) from 2007 to 2019 was obtained through Ekman zonal transport per 1000 m of coastline (Bakun, 1973), as:

$$UI = \left(\frac{\tau_y}{\rho f}\right) * 1000m$$

Where τ_y (Pa; kg m^{-1} s^{-2}) is the mean wind stress meridional component within the box 73-74°W, 36-39°S, ρ represents the mean density of the water column at ST18 (1026.21 kg m^{-3}), and f indicates the Coriolis parameter corresponding to the latitude of ST18 (8.67 $*10^{-5}$ s^{-1}).

Regarding El Niño–Southern Oscillation (ENSO), oceanic episodes of El Niño (EN) and La Niña (LN) were detected using values of standardized Southern Oscillation Index (SOI), along the Tropical Pacific Ocean. Anomalous low negative values in pressure indicate an EN episode, and high positive values are related with LN (Trenberth, 1984). The data were obtained from the UCAR-NCAR climate data guide (https://climatedataguide.ucar.edu/).

2.4. Statistical analysis

Spearman correlations (Rho) were calculated between oceanographic variables (T°C, S, DO, Chl-a, nutrients) along with CH_4 efflux, alongshore wind (ASW) and cumulative wind stress and, estimated inventories (CH_4, DO, Chl-a, and nutrients) for two layers (except for Chl-a), in order to determine which physical and biogeochemical variables closely explained the temporal variation of CH_4. The threshold value for statistical significance was set at $p < 0.05$ and $p < 0.01$. Procedures for several pairwise comparisons between average values were carried out using a Kruskal-Wallis test, with the prior application of a Shapiro–Wilks test to confirm normal distribution.

In order to classify the occurrence of types of CH_4 vertical distributions (119 total profiles), the vertical profiles were analyzed qualitatively, and the CH_4 concentration difference between the surface and the bottom was taken into account as a vertical distribution type criterion. In general, all the profiles showed an increase with depth, but when the ratio of CH_4 concentration between the bottom and the surface depths exceed 2, the profiles were classified as diffusion–advection profiles (type I) and when the mentioned ratio was close or<2, they were a profiles almost constant (type II). On certain occasions, the type I or II profiles presented several surface peaks, so they were classified as type III profiles.

To determine the similarity between monthly profiles according to our classification (type I, II and II), we compared each vertical profile against each type of vertical distribution throughout a normalized cross correlation (NCC) at lag zero. Firstly, all vertical profiles were interpolated to fill the data gap of sampling depths. Secondarily, the 3 vertical distribution types were theoretically created using absolute values between 1 (minimum as the surface) and 10 (maximum as the bottom) instead of concentration values with the aim to reproduce profile type. Finally, each of 118 profiles were compared with each type using the NCC and R = 0.95 as a threshold.

3. Results

3.1. Time series of oceanographic variables including dissolved methane

Time-series plots from April 2007 to April 2019, for variables as Chl-a, DO, NO_3^-, HPO_3^2, inorganic dissolved N.P ratio and CH_4, are presented in Fig. 2; while the temperature and salinity time series are included in the Supplementary Material (Fig. A.1). All these variables, except CH_4, have been previously analysed in Farías et al. (2015) and other studies, describing the variation of physical variables, such as temperature and salinity. The present study continues time series analysis and includes by first time CH_4 covering the period from 2007 to 2019.

There was generally a wide fluctuation of Chl-a within the photic layer, between 0.11 and 47.70 μg L^{-1} (mean ± SD: 3.91 ± 6.16), with maximum values in the spring-summer period (upwelling period), and minimum values (<1.00 μg L^{-1}) in the winter (non-upwelling period) and revealed a marked seasonal cycle (Fig. 2a). Although the surface layer remained well oxygenated, the subsurface layer presented hypoxic levels during the austral winter, followed by a gradual deoxygenation during September to April, reaching values of DO close to zero (Fig. 2b). That distribution revealed a marked seasonality and indicated the presence of an oxygen minimum zone (OMZ) with a marked oxycline occurring at depths as shallow as 20–30 m during the upwelling season. Remarkably, an oxygenation event (also accompanied by subsurface waters with warming and higher salinity) was observed during fall-winter of 2017 (Fig. 2 b).

Nutrients, such as NO_3^- (Fig. 2c) and PO_4^{3-} (Fig. 2d), also showed a seasonal variability mainly in subsurface waters, with increased levels during upwelling-favourable periods that diminished during non-upwelling periods. This was owed to the dominance of different water masses (ESSW vs. SAAW) and differential nutrient uptake rates by phytoplankton, which increase during upwelling periods. However, NO_3^- and PO_4^{3-} concentrations were never depleted in surface waters, despite periods of high photoautotrophic production. Aside from some exceptional high values of PO_4^{3-}, during Dec 2016 and Feb 2017, whose cause has not been determined; the inorganic $NO_3^- + NO_2^-/PO_4^{3-}$ ratio averaged 9.09 ± 3.13 (ranging from 1.06 to 19.1) (Fig. 2e), being lower than expected ratio of 16: 1 (Redfield et al., 1963). These ratios indicated a NO_3^- deficit due to N loss process in subsurface waters associated with very low DO.

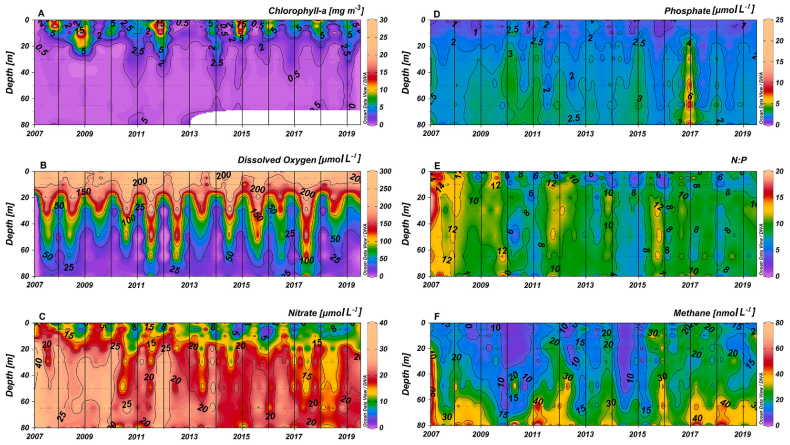

Fig. 2. Time series vertical distributions at ST18 based on data collected from April 2007 to April 2019 of: (A) Chlorophyll-a levels (µg L^{-1}); (B) Dissolved Oxygen (DO) concentrations (µmol L^{-1}); (C) Nitrate concentrations (µmol L^{-1}); (D) Phosphate concentrations (µmol L^{-1}); (E) Inorganic dissolved N/P ratio and (F) Dissolved CH_4 concentrations (nmol L^{-1}). Vertical lines represent every year (January).

Dissolved CH_4 levels varied widely from 1.74 to 100.9 nmol L^{-1}, equivalent to 67.11 and 3965% of saturation (mean ± SD: 762.79 ± 496.43%) (Fig. 2f). In the surface layer, CH_4 levels varied from 1.74 to 54.63 nmol L^{-1}, whereas in subsurface waters CH_4 levels reached values as high as 100 nmol L^{-1}. Thus, CH_4 level ratio between the surface and the bottom water fluctuated from 0.57 to 18.71 folds. The highest CH_4 levels were always found in bottom waters at ~ 80 m depth (close to the sediments), with suboxic/anoxic conditions, high NO_3^- concentration and the lowest inorganic dissolved N:P ratio (Fig. 2e).

When comparing the CH_4 levels during favourable vs. non-favourable upwelling periods, significant differences were observed in subsurface layer ($p = 0.011$), however no significant differences of CH_4 levels were observed in the surface layer ($p = 0.272$). Regarding temperature T°C ($p < 0.000$), salinity S ($p < 0.000$), DO ($p < 0.000$) and Chl-a ($p < 0.000$), they showed a marked significance between both periods. On the other hand, non-differences were observed in both periods for NO_3^- ($p = 0.764$), however, when separating the surface ($p = 0.003$) and subsurface ($p < 0.000$) layer, a statistical significance in NO_3^- was evidenced. In the case of PO_4^{3-} the difference was only given by the subsurface layer ($p < 0.000$).

3.2. Annual cycles of methane and other variables

Fig. 3 presents the annual cycles of CH_4 (Fig. 3a), Chl-a (Fig. 3b) and DO (Fig. 3c), based on 12 years of sampling at each sampled depth. The annual CH_4 cycle indicated that the bottom layer (80 m depth) is the depth with the highest mean values, ranging from 23.81 ± 11.62 and 45.05 ± 7.16 nmol L^{-1} and reaching maxima values in the summer months (February). Subsequently, CH_4 levels decreased towards the surface with mean values fluctuating from 7.22 ± 6.43 to 21.92 ± 11.64 nmol L^{-1}. In additions the surface layer presented a weak CH_4 variation that appeared to be unassociated with upwelling cycles, contrary to the observed patterns for Chl-a and DO (Fig. 3b and 3c). Besides, the difference in mean CH_4 concentration between the surface and bottom waters reached maximum and minimum values in summer and winter months, respectively (Fig. 3a). Chlorophyll-a and DO, in contrast to CH_4, showed a marked seasonal variation (Fig. 3b, Fig. 3c), Chl-a had high mean values during the austral spring-summer; for example, mean ± SD value taken at 5 m depth in December showed Chl-a levels up to 16.58 ± 11.17 µg L^{-1}, however mean levels of 0.38 ± 0.31 µg L^{-1} were observed during in June and July (austral winter) (Fig. 3b).

In contrast with CH_4 pattern, DO presented mean ± SD values during annual cycle between 64.16 ± 52.98 and up to 249.45 ± 42.82 µmol L^{-1} throughout the year at surface depth; whereas mean ± SD values at 5 and 10 m depth remained similar (Fig. 3c), but below 20 m depth, DO presented marked vertical and seasonal fluctuations from hypoxic to suboxic/anoxic levels. This distribution clearly marked the existence of the OMZ and indicated marked vertical gradients (oxycline) in the spring-summer (Fig. 3c), which diminished in fall-winter with slight increase in DO at 80 m depth. However, DO values at 80 m remained persistently low (4.48 ± 3.21 µmol L^{-1}) and these values may be zero given the sensitivity of the DO measurement methodology.

To demonstrate differences in the vertical CH_4 distribution between upwelling and non-upwelling favorable periods, the CH_4 inventories over layers and seasonal periods were calculated. Table 1 shows the inventories (mean ± SD) of different variables separated into favourable and non-favourable (Table 1) periods and into surface and subsurface layers. When comparing the Chl-a and DO inventories or pool sizes between both periods, a significant differences ($p < 0.000$) were observed, however these were not the case of mean inventories for NO_3^-, NO_2^- and HPO_4^{3-} and CH_4 with p values, respectively, of $p = 0.799$, $p = 0.215$, $p = 0.302$ and $p = 0.570$.

Fig. 4a, 4c and 4e showed box-and-whisker plot of CH_4, Chl-a and DO inventories over both layers throughout an annual cycle (month values based on a 12 year time series). Theses CH_4 inventories throughout the subsurface layer fluctuated between 268.95 and 3102.02 µmol m^{-2}, and when they were compared with those estimated into the surface layer (73.58 to 871.28 µmol m^{-2}), revealed that the majority of CH_4 was accumulated in the subsurface water. The highest CH_4 inventories were observed in both December and April (Fig. 4a), and the former month coincided with maximum Chl-a biomass (December). Chl-a inventories were highly variable (ranging from 3.02 to 585.4 mg m^{-2}) with an abrupt increase in early spring, coinciding with an increase in upwelling favorable winds (Fig. 6) and showing a maximum Chl-a value in December (Fig. 4c). The DO inventories throughout the surface water column fluctuated between 2,356 and 19,058 mol m^{-2}, continually showing increased values in winter-spring and a weak seasonality, which contrasted with a marked variation in the subsurface layers (142.76 and 12675.47 mol m^{-2}) with extreme low values during February (Fig. 4e).

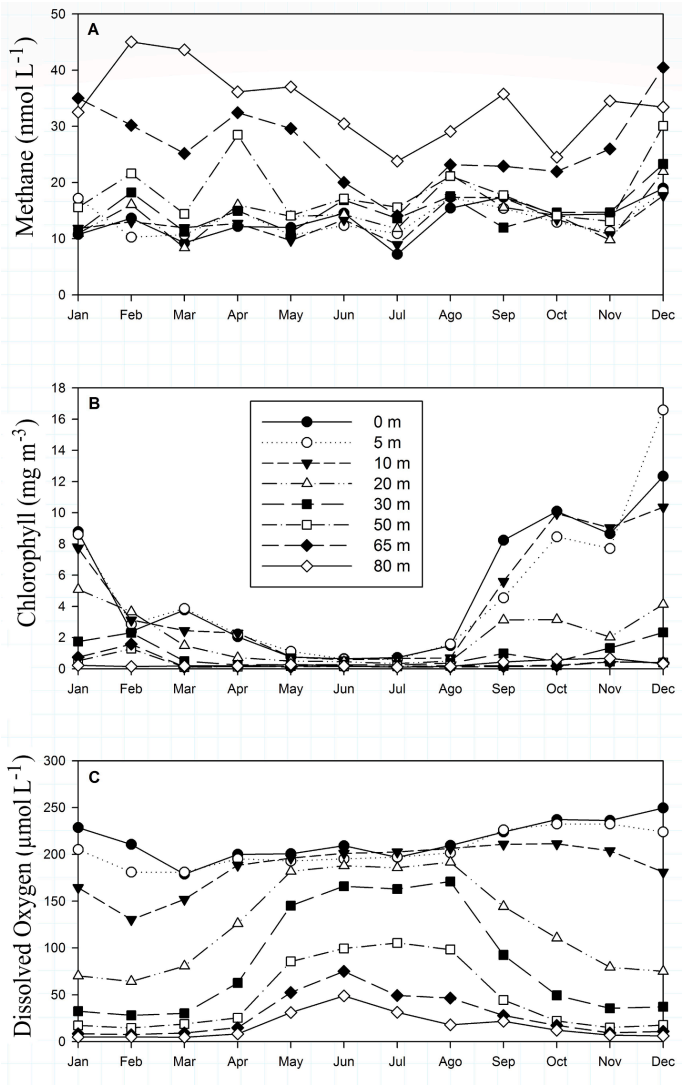

Fig. 3. Mean annual climatology for variables measured at different depths throughout the water column (A) CH_4 (B) Chlorophyll-a, and (C) Dissolved Oxygen (DO) concentrations.

3.3. Inter-annual variability among variables (including dissolved methane)

When interannual CH_4 variability was analysed (Fig. 2f), there was a significant difference between years ($p = 0.000$), and the austral summer of 2009/10 and 2014/15 and 2016/17, showing anomalous behaviour. For example, during 2009–10 and 2014–15 no CH_4 accumulation in the bottom water was registered and, but during 2016/17 a CH_4 accumulation in the whole water column was observed. The latter also coincided with the occurrence of more saline, warmer and oxygenated waters, suggesting a change in normal hydrographic conditions (Fig. A.1 and Fig. 2b). Respect to Chl-a, differences among years were found ($p = 0.032$) and values above 0.68 µg L^{-1} were recorded especially in 2007, 2011, 2014. Regarding to DO, besides highly oxygenated waters (Fig. 2b) observed in the entire water column in winter 2017, there was another in winter 2011; however, non-statistical differences among years were observed ($p = 0.937$).

Fig. 4b, 4d and 4f showed box-and-whisker plot of CH_4, Chl-a and DO

Table 1
Seasonal averages (mean ± SD) of methane, chlorophyll-a, dissolved oxygen, nitrate, phosphate inventories during the upwelling (spring-summer) and non– upwelling (fall-winter) season and in both the surface (SL) and subsurface (SSL) layers.

Years	Upwelling Season	CH_4 μmol/m^2	Chl-a mg/m^2	DO mol/m^2	NO_3^- μmol/m^2	PO_4^{3-} μmol/m^2	Non upwelling season CH_4 μmol/m^2	Chl-a mg/m^2	DO mol/m^2	NO_3^- μmol/m^2	PO_4^{3-} μmol/m^2
2007–2008	SL	418.29 ± 131.47	165.81 ± 117.62	4937.76 ± 1480.74	426.05 ± 112.97	35.10 ± 8.38	344.68 ± 140.47	35.61 ± 24.51	5355.61 ± 760.87	507.90 ± 117.37	36.60 ± 4.38
	SSL	1518.52 ± 769.60		1972.60 ± 1487.72	1441.50 ± 219.47	132.13 ± 12.33	1248.01 ± 623.43		4043.00 ± 682.56	1366.26 ± 293.63	110.08 ± 4.68
2008–2009	SL	274.92 ± 80.47	210.62 ± 210.88	4931.34 ± 784.95	334.80 ± 133.76	35.52 ± 10.07	249.83 ± 6.11	15.09 ± 11.69	5652.47 ± 832.26	425.85 ± 22.55	38.63 ± 2.22
	SSL	1310.23 ± 276.24		1312.36 ± 701.32	1361.56 ± 171.53	146.40 ± 9.86	1770.66 ± 869.11		5136.89 ± 2287.42	1234.70 ± 177.23	124.72 ± 36.64
2009–2010	SL	144.38 ± 21.29	96.49 ± 68.01	4738.24 ± 669.76	383.55 ± 152.27	51.37 ± 22.14	301.76 ± 118.94	17.38 ± 9.82	5156.74 ± 624.15	500.95 ± 77.00	41.62 ± 6.42
	SSL	1133.17 ± 1280.58		1036.52 ± 724.20	1386.09 ± 357.01	159.06 ± 26.65	977.64 ± 347.70		2984.07 ± 1326.69	1352.94 ± 141.69	139.60 ± 12.66
2010–2011	SL	275.05 ± 106.15	138.54 ± 91.70	5543.53 ± 1513.94	249.04 ± 167.64	35.47 ± 22.96	160.02 ± 21.50	22.51 ± 3.13	5532.84 ± 1006.05	378.50 ± 117.32	51.29 ± 14.78
	SSL	1368.50 ± 526.80		1276.78 ± 993.43	1055.20 ± 192.86	154.84 ± 22.58	612.32 ± 148.87		4515.52 ± 1707.42	1009.61 ± 311.19	151.79 ± 43.86
2011–2012	SL	398.77 ± 178.96	222.30 ± 209.88	4821.62 ± 554.12	433.16 ± 130.10	43.05 ± 10.46	473.77 ± 65.87	11.69 ± 7.10	6296.12 ± 470.70	369.42 ± 109.57	39.27 ± 18.90
	SSL	1635.86 ± 546.63		725.84 ± 226.96	1536.52 ± 272.37	149.96 ± 11.77	1385.18 ± 449.76		7454.21 ± 3824.17	1008.50 ± 239.85	108.11 ± 40.46
2012–2013	SL	404.50 ± 172.48	28.79 ± 21.18	5496.32 ± 429.47	402.39 ± 45.95	48.86 ± 9.44	299.02 ± 65.09	17.95 ± 5.55	6489.89 ± 323.64	325.44 ± 80.77	32.08 ± 10.35
	SSL	1059.51 ± 119.18		1458.39 ± 805.03	1195.11 ± 32.15	140.33 ± 7.23	1163.22 ± 440.53		8182.87 ± 4161.85	1077.67 ± 265.33	108.62 ± 16.78
2013–2014	SL	419.52 ± 114.86	110.28 ± 92.08	5101.43 ± 1422.49	305.46 ± 124.31	41.57 ± 14.43	388.84 ± 190.44	13.80 ± 3.15	4369.16 ± 1649.86	400.61 ± 166.74	48.33 ± 2.26
	SSL	1408.85 ± 293.51		831.57 ± 771.57	1249.08 ± 259.35	135.24 ± 17.25	1324.67 ± 486.06		3093.39 ± 860.55	938.29 ± 269.92	119.46 ± 11.01
2014–2015	SL	258.63 ± 146.60	231.68 ± 234.14	5063.85 ± 1648.61	228.18 ± 63.52	37.81 ± 12.15	128.85 ± 82.91	16.88 ± 5.27	6019.82 ± 208.76	302.01 ± 47.64	40.16 ± 5.95
	SSL	1030.32 ± 424.20		1384.67 ± 908.90	1000.08 ± 208.42	157.54 ± 14.31	534.30 ± 235.09		5422.46 ± 1103.75	944.96 ± 38.62	132.52 ± 8.38
2015–2016	SL	536.77 ± 199.86	121.62 ± 116.81	4516.74 ± 124.94	198.14 ± 99.64	25.53 ± 8.33	725.56 ± 5.82	11.83 ± 7.86	5880.22 ± 741.41	406.48 ± 102.51	40.94 ± 4.08
	SSL	1455.69 ± 631.33		1878.77 ± 1340.29	1101.74 ± 186.48	115.92 ± 24.24	1342.86 ± 311.20		4645.37 ± 2033.98	1180.86 ± 236.72	123.53 ± 10.97
2016–2017	SL	588.09 ± 226.12	99.87 ± 68.32	4870.77 ± 862.09	276.36 ± 189.66	47.84 ± 37.43	566.92 ± 267.52	20.34	4818.54 ± 89.70	379.28 ± 66.52	45.50 ± 4.57
	SSL	1733.38 ± 587.30		1357.53 ± 1183.16	1015.75 ± 462.83	248.85 ± 345.48	1179.03 ± 389.40		5277.15 ± 1480.23	1223.98 ± 111.62	135.24 ± 50.75
2017–2018	SL	558.50 ± 66.03	155.64 ± 96.25	4660.19 ± 1039.46	306.08 ± 70.93	41.44 ± 2.81	458.34 ± 83.51	20.58 ± 8.35	5776.91 ± 309.23	240.38 ± 59.26	28.00 ± 6.14
	SSL	1487.66 ± 591.60		1377.05 ± 1652.70	978.75 ± 337.24	137.23 ± 20.61	1568.68 ± 235.98		8305.43 ± 3344.72	854.01 ± 122.77	93.63 ± 9.18
2018–2019	SL	373.51 ± 108.94	121.07 ± 140.34	4713.87 ± 1142.76	277.88 ± 49.16	37.49 ± 3.76	366.96 ± 162.97	24.79 ± 26.35	5283.49 ± 723.20	254.51 ± 59.37	31.19 ± 5.01
	SSL	1372.38 ± 330.90		1525.02 ± 1195.83	1108.90 ± 151.05	130.70 ± 15.92	1657.53 ± 665.92		2903.48 ± 1035.39	801.84 ± 161.49	93.49 ± 16.66

inventories over both layers (except Chl-a) for each year sampled (from 2007 to 2019). When the estimated annual CH_4 inventories in both surface and subsurface layers are compared (Fig. 4b), a clear interannual variability was observed in subsurface water ($p < 0.000$), and in surface layer ($p = 0.006$). Specifically, the years 2009/10 and 2014/15 showed the lowest records in Chl-a pool size whereas the 2008, 2011 and 2017 years had the highest pool sizes, but there was no inter-annual variability ($p = 0.768$), likewise DO did not reveal significant differences among years ($p = 0.460$; Fig. 4f), but winter of 2017 was a season of an extreme higher oxygenation in the entire water column.

3.4. Vertical distribution of dissolved methane

Fig. 5 shows averaged vertical profiles calculated by monthly means of CH_4, DO and NO_3^- for each sampled depth based on data from 2007 to 2019. All obtained profiles in this study (119 in total) were included in Supplementary Material (Fig. A.2). It was possible to identify a transition of CH_4 profiles throughout the seasonal cycle. As the upwelling developed (Oct., Nov., Dec., Jan., Feb., March and April), a type I vertical distribution dominated in 54% of all profiles. This was a diffusion–advection profile, with a high CH_4 concentration in the bottom layer that gradually decreases towards surface (Fig. 5) and with a mean CH_4 level ratio between surface/bottom depth up to 4.5 (e.g., February). This pattern coincided with a sharp decline in DO towards the sediment and a marked increase in nutrients below the surface water. Both distributions were observed during the upwelling season and triggered by the dominance of the ESSW and highest rate of OM mineralization. Towards the end of summer and early fall (Feb., March and April), the accumulation of CH_4 in bottom waters reached a maximum value and DO was extremely low reaching values near anoxia (Fig. 5, Feb. and March). Although NO_3^- levels had a gradual increase with depth, which is more pronounced in summer, this nutrient showed sometime a relative decrease at 80 m depth due to their consumption through the anaerobic mineralization processes of OM (denitrification); sometime a relative

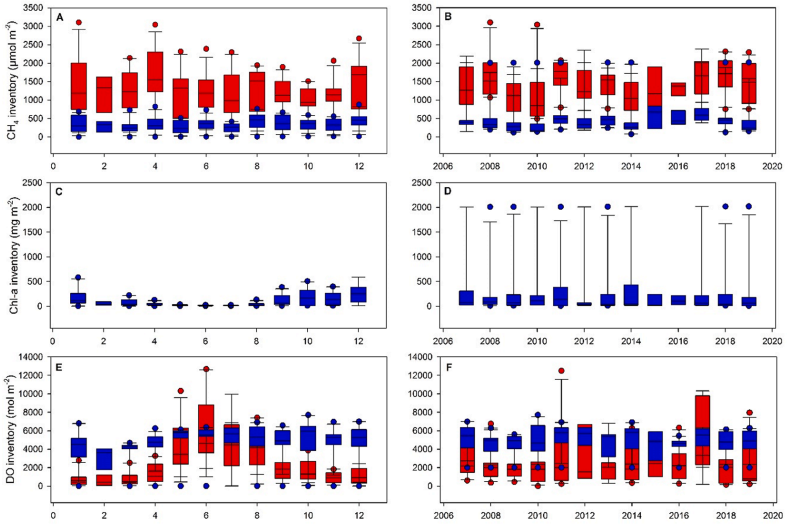

Fig. 4. Box-and-whisker plot of monthly and annually inventories, respectively, of CH_4 (A and B); Chlorophyll-a (D and E) and Dissolved Oxygen (G and H) throughout the water column separated by surface (blue box) and subsurface (red box) layer. The box represents the interquartile range (first and third quartile) containing 25 to 75% of the values of each variable. The line on the box represents the median. The whiskers represent the range of non-typical values. The filled circles represent outliers.

CH_4 decrease in 80 m depth was also registered (Fig. A.2) probably associated with consumption by anaerobic CH_4 oxidation in the sediment.

The type II profiles presented a relatively homogeneous CH_4 distribution with a mean ratio of CH_4 bottom/surface concentration around or<2. This type of profile was observed 46% of the all profiles mainly during May, June, July and August, September (austral fall-winter), and could be related to intense mixing processes throughout the entire water column, which coincided with periods of higher oxygenation and low NO_3^- content, owing to the dominance of the SAAW.

A type III vertical distribution of CH_4 was also described and included cases of irregular vertical CH_4 distribution or CH_4 peaks in surface water ~ 15–30 m depth (Fig. 5 and Fig. A.2). These peaks were observed in both type I and II profiles and found in 40% of all profiles, being more frequent in transition months between favourable or non-favourable upwelling periods such as April and May (fall) and August-September (winter to spring) (Fig. A.2).

3.5. Air-sea CH_4 exchange and relationships between environmental variables

The daily wind speed taken from the weather station and satellite data ranged from 0.64 to 13.38 (means ± SD: 3.53 ± 1.44) and 0.06 to 14.91 m s^{-1} (means ± SD: 5.03 ± 2.60), respectively. Wind speeds obtained from the satellite were 30% higher than those obtained by the weather station. Thus, both data sources were used to estimate gas exchange, considering that the range includes both a conservative (weather station) and maximum (satellite) values. The alongshore wind speeds fluctuated from −13.16 to 5.75 and −14.05 to 12.50 m s^{-1} from weather station and satellite data, respectively. These winds, that provoke favourable upwelling events (positive values), occurred more frequently during spring-summer, and overall during about 64.20% (weather station) and 73.90% (satellite) of the whole year; whereas non-favourable upwelling events (negative values) took place in part of fall and winter (around 27–34% of the year).

Alongshore wind stress (Fig. 6a) and upwelling index (Fig. 6b) (only using winds from weather station) varied from −0.27 to 0.18 N m^{-2} (mean ± SD: 0.01 ± 0.02) and from −3009.01 to 2053.31 m^3 s^{-1} (mean ± SD: 147.37 ± 236.40), respectively, and clearly showed a cumulative upwelling-favourable wind stress during spring-summer (Table 2). Sea surface temperature (SST) measured at 10 m depth (to avoid the effect of solar radiation), displayed a similar pattern to the cumulated wind stress, indicating the upwelling of cold, rich-nutrient and low DO subsurface water to the surface through vertical advection (data not shown).

Using W92 parametrization, along with the speed wind measurements from the weather station, CH_4 air-sea fluxes were always positive (toward the atmosphere) and varied from 1.27 to 47.02 μmol m^{-2} d^{-1} (mean ± SD = 10.94 ± 7.48; Fig. 6c). Maximum CH_4 efflux was registered during December 2015 was 47.01 μmol m^{-2} d^{-1} followed by 30.36 (January 2008) and 29.00 μmol m^{-2} d^{-1} (October 2017), as well as other similar values during the summer periods. Using the same parametrization (W92) with satellite wind data, air-sea CH_4 efflux was on average 2.3 fold higher (data not shown). Furthermore, when W92 parametrization was compared with Nightingale (2000) parametrization, the latter overestimated the air-sea gas exchange by only 4.64 ± 7.58%, while no differences were found between W92 and W14, indicating that W92 is a suitable parametrization for the existing local wind regime.

Table 2 presents daily CH_4 effluxes (mean ± SD) and cumulative wind stress (mean ± SD) averaged by upwelling and non-upwelling periods from 2007 to 2019. Air-sea CH_4 exchange did not show a marked seasonal difference between upwelling and non-upwelling ($p = 0.513$; Table 2), being lightly lower (mean ± SD: 8.51 ± 5.99 μmol m^{-2} d^{-1}) during non-favourable upwelling periods and higher (mean ± SD: 12.29 ± 7.91 μmol m^{-2} d^{-1}) during favourable upwelling periods. A comparison among years (Table 2) indicated that maxima effluxes were registered during upwelling season of 2015–2016 and 2017–2018 (19.18 ± 12.93 and 20.41 ± 10.27 μmol m^{-2} d^{-1}, respectively); whereas 2009–2010 presented the lowest seasonal upwelling CH_4 efflux of about 4.69 ± 2.62 μmol m^{-2} d^{-1} (Table 2). Notably, during fall-winter of 2015

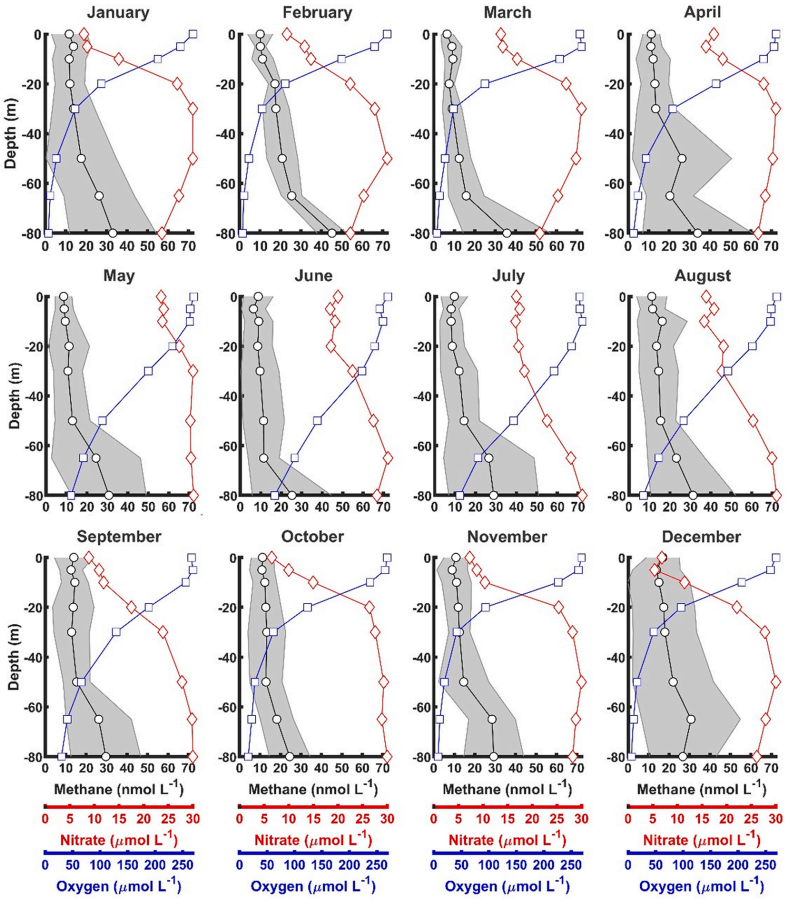

Fig. 5. Mean CH_4 profile (black line) and its standard deviation (shown as a shadow) with corresponding dissolved oxygen (blue line) and nitrate (red line) vertical distributions for each months (based on 12 years of monthly frequency).

and 2017, CH_4 efflux equal or greater than those estimated in spring-summer periods were recorded. Cumulative wind stress was always significantly higher ($p = 0.00$) in upwelling periods (cumulated of 242 days) compared to non-upwelling periods (cumulate of 123 days); also significant differences ($p = 0.05$) among years were observed in any of both mentioned periods.

Fig. 7 shows a Spearman correlations matrix for CH_4, T, S, DO, Chl-a, and nutrient variables along with ASW (Fig. 7a) and also among their inventories in the whole water columns, as well as ASW, cumulative wind stress and CH_4 effluxes (Fig. 7b). The results indicated that CH_4 levels were significantly correlated with variables such as temperature, DO and Chl-a (negative correlation) and salinity and nutrients (positive correlation). These implied that more CH_4 was accumulated or produced in saltier, cooler, rich-nutrients and less oxygenated bottom waters (mainly associated with ESSW); but the negative correlation was observed among CH_4 and Chl-a (Fig. 7a) would indicate at least a lag between Chl-a and the amount of CH_4 accumulated. Correlation matrix among the inventories in the whole water column and CH_4 fluxes are presented in Fig. 7b. CH_4 efflux revealed significant negative correlations with NO_3^- and positive correlations with Chl-a and wind stress, suggesting that more CH_4 was accumulated in surface water as NO_3^- was consumed in favourable upwelling period (coinciding with favourable upwelling wind stress).

4. Discussion

4.1. Temporal variability in oceanographic conditions including methane distribution

Despite a widely recognised lack of information around oceanic CH_4 distribution and its exchange with the atmosphere, it is well established that coastal systems are important in terms of CH_4 production and emissions (IPCC, 2013, Weber et al., 2019). The seawater overlaying continental shelves are significantly more enriched with CH_4 in comparison to the open ocean, with reductions of up to one order of magnitude as the sea floor deepens. For example, recent studies by

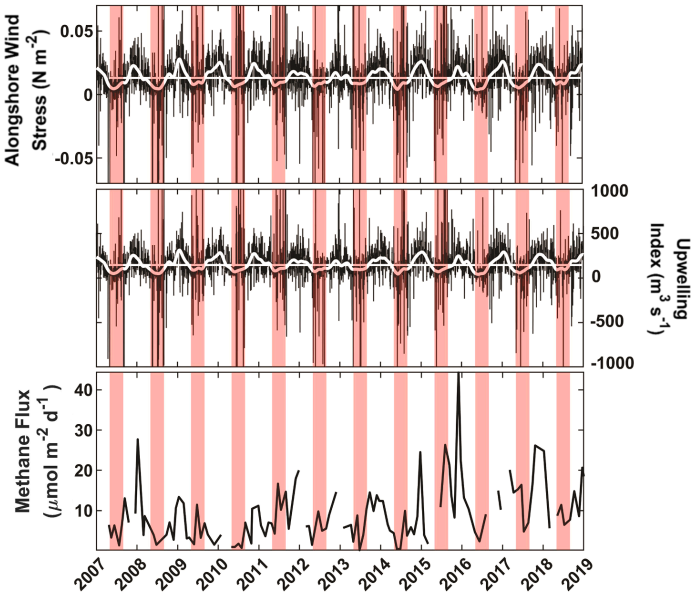

Fig. 6. (a) Alongshore wind Stress (N m^{-2}) (b) Upwelling Index (m^3 s^{-1}), (c) Daily CH_4 fluxes (μmol m^{-2} d^{-1}) estimated from weather wind from April 2007 to April 2019. Red shadow shows non-favorable upwelling periods (mid-April to the first week of September). The solid white line shows the smoothed values through a timespan (3% of total samples), solved by a local quadratic polynomial function resistant to outliers. While the thin white line represent the average.

Table 2
Seasonal effluxes of CH_4 along with cumulative wind stress during upwelling (spring summer) and non-upwelling season (late autumn–winter).

Year	CH_4 Flux μmol/m^2 day	Wind Stress N/m^2	CH_4 Flux mmol/m^2 day	Wind Stress N/m^2
	Non Upwelling period (123 days) (May, Jun, Jul, Aug)		Upwelling period (242 days) (Sep, Oct, Nov, Dec, Jan, Feb, Mar, Apr)	
2007–2008	5.58 ± 2.62	0.88 ± 0.01	12.56 ± 8.54	3.49 ± 0.01
2008–2009	3.64 ± 2.11	−0.90 ± 0.03	8.97 ± 5.03	4.04 ± 0.01
2009–2010	7.34 ± 4.97	1.30 ± 0.01	4.69 ± 2.62	4.40 ± 0.01
2010–2011	3.92 ± 3.87	1.10 ± 0.02	8.77 ± 3.54	4.14 ± 0.01
2011–2012	13.41 ± 6.29	1.46 ± 0.01	11.57 ± 7.36	3.70 ± 0.01
2012–2013	8.52 ± 3.85	0.18 ± 0.02	9.12 ± 5.41	3.37 ± 0.01
2013–2014	7.20 ± 4.94	0.86 ± 0.01	11.63 ± 4.26	4.04 ± 0.01
2014–2015	5.53 ± 5.60	0.83 ± 0.01	10.31 ± 8.98	4.21 ± 0.01
2015–2016	20.27 ± 11.92	1.39 ± 0.01	19.18 ± 12.93	3.96 ± 0.01
2016–2017	6.12 ± 3.52	0.70 ± 0.00	16.83 ± 3.91	4.35 ± 0.01
2017–2018	12.62 ± 6.82	0.29 ± 0.01	20.41 ± 10.27	4.06 ± 0.01
2018–2019	10.84 ± 1.87	0.80 ± 0.01	15.60 ± 5.41	4.56 ± 0.01

Sudheesh et al. (2020) off the South-Eastern Arabian Sea, and Sierra et al. (2020) in the SE Spain report a reduction from ~ 20–40 nmol L^{-1} on the inner shelves to ~ 2–4 nmol L^{-1} on the outer shelf.

High CH_4 content in coastal zones is predominantly linked to areas of high biological productivity, which in turn is exported to the sediment, where OM sedimentation occurs. The input of OM stimulates the metabolisms of benthic organisms, and if OM input is sufficient, an increased flux of CH_4 from the sediments to the overlying water column could occur (Jayakumar et al., 2001; Martens and Klump, 1980). The correlation between CH_4 and Chl-a has been explored in several studies over different spatial scales; however, similar to the results of this study, a clear positive correlation is not always observed (see Fig. 7a) (Bange et al., 2010; Borges et al., 2017; Ma et al., 2020; Weber et al., 2019). This could be due to a time gap that takes for the OM to settle and mineralize as it sinks into the water column or/and, due to other processes are taking place, such as cold seeps, especially on continental margins (Johnson et al., 2019), as well as other forms of physical CH_4 transport (e.g., continental runoff) and superficial CH_4 production (discussed in the following).

Coastal upwelling is identified to occur at sites with enhanced CH_4 concentrations and emissions; such as in the NW and SW Arabian Sea, the Oregon coast off the west coast USA, and off Canarias Islands and Namibia (SW Africa) (Kock et al., 2008; Monteiro et al., 2006; Owens et al., 1991; Rehder et al., 2002; Sudheesh et al., 2020). This is also the case in the upwelling region off central Chile, which shows a marked seasonality in biological productivity (Fig. 2a) and DO (Fig. 2b), i.e., during periods of wind driven stress on surface waters occurring ~ 64% of the year (Fig. 6a), which provokes the upwelling of subsurface water with particular features. This regime reintroduces bio-available NO_3^- (Fig. 2c) and PO_4^{3-} (Fig. 2d) to the euphotic layer, enhancing primary production (Testa et al., 2018). This process is also triggered by the vertical advection of cold and more saline water (Sobarzo et al., 2007),

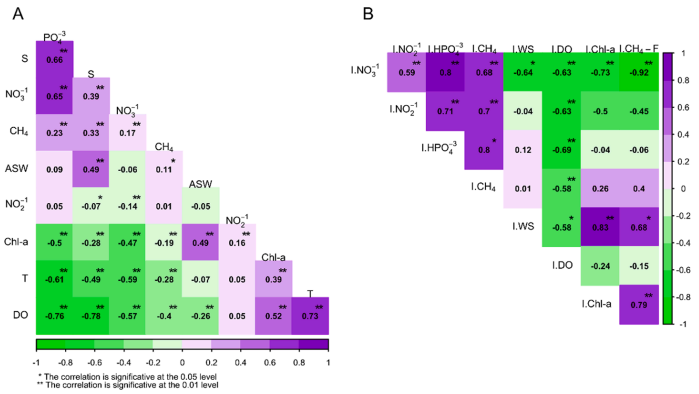

Fig. 7. Correlations matrix among (A) variables and (B) parameters (inventories in the whole water column, CH_4 efflux and cumulative wind stress). Values in violet shades (green) represent, respectively, positive (negative) values of the Spearman correlations (Rho). Variables correspond to the T°C: temperature, S: salinity, DO: dissolved oxygen; Chl-a, chlorophyll-a; CH_4: methane; NO_3^-; nitrate; PO_4^{3-}: phosphate; air-sea CH_4 exchange: CH_4F.; ASW: along shore wind and WS: wind stress. * and ** mean significant correlation at the 0.05 and 0.01 level, respectively. I denotes inventory.

which in turn has low DO (Fig. 2b), creating a well-established OMZ.

The intensity and vertical presence of the OMZ varies according to upwelling evolves over time with upwelling strength (Fig. 2b), leading to the development of hypoxic/suboxic conditions at intermediate and bottom depths, that coincide with low N:P ratios as low as 6 (Fig. 2e). This nitrogen deficit is partially caused through substantial nitrogen loss in subsurface water (Galán et al., 2017) as well as the consumption of NO_3^- through denitrification in the sediments, particularly during the spring-summer (Farías et al., 2004). These variations are also related with the increase in biomass (Chl-a) and the typical succession of phytoplankton; that initiates with large diatoms and terminates with small flagellates (Anabalón et al., 2007).

In contrast with DO (Fig. 3c) and Chl-a (Fig. 3b), it is not possible to clearly define a seasonality within the annual CH_4 cycle (Fig. 3a). Indeed, when comparing the CH_4 inventories during non– and upwelling favourable periods, there are no significant differences observed in surface waters (see Table 1). It is important to note that CH_4 levels increase in the surface layer towards the end of winter (Fig. 3a; Fig. 4a), a transitional period that coincides with the largest discharge of fresh water from rivers (Testa et al., 2018) and the lowest salinities in the surface waters (Fig. A.1), indicating the potential impact of continental ecosystems. It is notable in winter 2009, 2011 2015 (Table 1 and 2). Rivers and wetlands have been recognized for their CH_4 inputs during seasonal runoff, as recorded in estuarine waters (Rao and Sarma, 2017; Upstill-Goddard et al., 2000; Upstill-Goddard and Barnes, 2016). Only a few studies in central-south Chile report high CH_4 levels in estuarine systems which increase during periods of enhanced continental freshwater runoff (Bello, 2016; Daniel et al., 2013; Farías et al., 2018).

The oceanographic time series off central Chile constitutes an excellent tool to study seasonal processes, as has been described, however with 12 years of monthly sampling interannual variability in CH_4 contents (regarding both depth concentrations and inventories) can be analysed (Fig. 2f, Fig. 4b). CH_4 time series indicates that *in situ* CH_4 production and/or input are not necessarily associated with seasonal cycles as those associated with coastal upwelling or that there is another source of variability. In fact, part of the variability could be associated with the ENSO cycle. That is the case with four warm events in the past 12 years, the 2006/07, 2009/2010, the failed 2014 event, 2015/16 Godzilla EN and the intense coastal EN during summer-fall 2017 (Cai et al., 2020).

For example, during 2009/10, 2011/12 and 2015/16 EN, CH_4 inventories in the surface layer are similar or even higher in non-upwelling period, compared to upwelling, losing the expected seasonality. This is not accompanied by changes in the phytoplankton biomass, but in the case of 2009/10 and 2015/16 coincides with the occurrence of more saline and warming waters, suggesting a change in normal hydrographic conditions (Fig. A.1). Besides, notable oxygenation and anomalous PO_4^{3-} concentrations (Fig. 2d) are only registered during the 2017 coastal EN.

It is known that ENSO, especially to its warm phase (EN) changes completely the physical, chemical, and biological dynamics of eastern South Pacific (Escribano et al., 2004; Graco et al., 2017; Gutiérrez et al., 2008). For example, coastal waters off Peru under EN conditions, (i) increase of sea surface temperature and 15 °C isotherm progressive deepens in the water column, (ii) change of water mass distribution, dominating in surface Surface Subtropical Water (SSW), (iii) decrease of primary production mainly associated with a decreasing in nutrient supply to surface waters and, iv) the upper boundary limit of the OMZ, usually shallower, deepens to>100 m depth.

However, a few time series of the whole water column reveal a rich spectrum of variability of different oceanographic distributions that includes frequencies ranging from seasonal to interannual scales (Escribano et al., 2004; Farías et al., 2015; Graco et al., 2017). Differences in the response of the ocean could be depended on the genesis (region in the equatorial Pacific) and the diversity of the EN events taking place during in the 21st century (Cai et al., 2020; Capotondi et al., 2015); different types of responses or manifestations in vertical distribution of biogeochemical variables could depend on if EN or LN events have strong, moderate or weak signals through the eastern South Pacific, but that observed as the 2017 coastal EN clearly differs from the others registered and could be similar to that observed 1997–98 EN (Escribano et al., 2004; Graco et al., 2017).

It is possible that coastal waters off central Chile respond differently to those off Peru and northern Chile due to the efficient oceanic teleconnection respect to central-southern Chile; the latter can be considered as the southernmost region where the Kelvin wave signal can arrive more altered and the oceanographic and hydrographic conditions are also different. In additions, central-south Chilean region is experiencing an intensification of coastal upwelling mainly associated with changes Southeast Pacific Subtropical Anticyclone (SPSA), which in turn are partially controlled by ENSO like process (Aguirre et al., 2018; Pinochet et al., 2019; Winckler et al., 2020).

4.2. Vertical methane distribution in coastal upwelling water

The shape of vertical profiles are determined by a number of factors; inputs from the sediment, vertical diffusion and advection transport, removal through gas exchange with the atmosphere, as well as *in situ* biological production and consumption in the pelagic zone. In contrast to CH_4 profiles in the coastal ocean (Fig. 5), CH_4 concentration in the open ocean decreases with depth, or peaks at the surface or within the

pycnocline (Forster et al., 2009; Kelley and Jeffrey, 2002). There is a coincidence between CH_4 and Chl-a maxima at the subsurface that may be a product of phytoplankton metabolism (Scranton and Brewer, 1977) or from CH_4 production in the guts of zooplankton (Alldredge and Cohen, 1987; Paerl and Prufert, 1987; Scranton and Brewer, 1977), which are likely to be grazing in increased concentrations within this layer. In this sense, the superficial CH_4 peak coincides with the maximum stratification of the water column inferred through Brunt Väisälä frequency; this index shows its maximum values between 10 and 25 m. depth (data not shown), depths that match with the thermocline and oxycline along with the base of the photic layer; therefore, many metabolisms involved in the CH_4 production could meet in this layer.

In the coastal ocean, vertical CH_4 distributions are similar to those observed in marine systems dominated by intense benthic production, as the findings in this study (Fig. 5). A clear increase in CH_4 concentrations is continually observed in the bottom layer, and it is particularly marked during the summer (February and March). There is a clear variation in differences in CH_4 levels between the surface and deeper waters throughout the whole study with up to an 18 fold difference between the surface and bottom waters in the summer period. This is also evident in annual CH_4 inventories, which always maintain higher levels in the subsurface layer; being higher in upwelling compared to no upwelling periods (Table 1).

The consistently elevated concentrations of CH_4 in bottom waters over the continental shelf implies the benthic origin of CH_4 through diagenesis in the sediments, which then act as a source to the water column (Capelle and Tortell, 2016; Martens and Klump, 1980). It is widely accepted that the sediments beneath upwelling zones receive a higher input of OM through sedimentation (Hebbeln et al., 2000) and accumulate large reservoirs of C and N (Summerhayes, 1983), thus they play a role in global C and nutrient cycles (Walsh, 1991). The majority of biogenic CH_4 is generated through the fermentation of acetate and by the reduction of CO_2 with H_2 (Whiticar et al., 1986), pathways that require completely anoxic conditions, as well as a sequential use of electron acceptors, such as O_2, Fe, NO_3^- and $SO_4^=$. High rates of OM remineralization through anaerobic pathways have been observed in the continental shelf sediments off central Chile (Farías et al., 2004; Ferderlman et al., 1997; Glud et al., 1999; Gutierrez et al., 2000; Thamdrup and Canfield, 1996). Indeed, local NO_3^- depletion was observed in bottom waters (Fig. 2c), indicating NO_3^- consumption in bottom waters and/or within the sediments by dissimilative NO_3^- reduction and denitrification, as previously observed by Farías et al. (2004) and Galán et al. (2014, 2017). In turn, these processes coincide with local NH_4^+ and NO_2^-accumulation (data non shown), which is partially associated with benthic OM matter remineralization (Farías et al., 2004). In addition to denitrification and anammox, also sulphate reduction and methanogenesis has been reported within the sediment of the study area (Ferderlman et al., 1997; Glud et al., 1999; Gutiérrez et al., 2000) confirming the prevalence of anoxic conditions and sufficient OM availability in the sediments. However, this study was unable to determine if the CH_4 accumulated in bottom water originates from anaerobic methanogenesis in the sediment or it is partially formed in the bottom water.

On another hand, our findings frequently show a shallower CH_4 maximum (Fig. 5 and Fig. A.2). It is possible that a depth with an elevated CH_4 concentration may be positioned in between two adjacent depths with a higher rates of CH_4 loss, either through aerobic CH_4 oxidation or sea–air exchange. Thus, the observed CH_4 peaks in the surface layer would be a result of local CH_4 production and consumption, or both processes are occurring simultaneously and operating at faster rates compared to vertical mixing, and/or advection. Regarding advection, piston or gas transfer velocities (*Kw*) can be used to calculate the duration for gaseous equilibration to be reached with the atmosphere. Considering that the mixed layer is typically positioned at about 10–20 m depth, the length of required time to push all of the gas through this layer is at minimum between half-day and one day, considering that the wind velocity exceeds 7 m h^{-1}. It suggests that surface CH_4 production rate may be fast enough to lead to local accumulation. Similarly, the CH_4 maximum in surface waters observed in numerous other studies suggest that the timescales for biological CH_4 production/consumption processes are relatively short compared with those of physical mixing (Burke et al., 1983; Conrad and Wolfgang, 1988; Karl and Tilbrook, 1994).

CH_4 production in anoxic environments is predominantly produced by archaea methanogens, however CH_4 production in oxic water requires further investigation and new insights in terms of CH_4 cycling (Damm et al., 2010; Florez-Leiva et al., 2013; Holmes et al., 2000; Karl et al., 2008; Repeta et al., 2016). The previously mentioned authors found that some methylated substrates, such as methylphosphonate, methylamines and even DMSP and DMS (the most abundant methylated compounds) could be cycled through methylotrophic methanogenesis pathways facilitated by microorganisms (Levipan et al., 2007; Neufeld et al., 2008). CH_4 microbial production in surface water could be directly related to the use of compounds by bacterioplankton in oligotrophic regions as established by Karl et al. (2008) or through DOC substrates generated by phytoplankton growth as DMSP (Damm et al., 2010) or via the production of exudates through extracellular release, which are directly coupled with heterotrophic bacteria (Dinasquet et al., 2018; Lenhart et al., 2016; Neufeld et al., 2008). These processes are particularly active in coastal upwelling zones off central Chile, where a direct coupling between both communities has been identified, leading to rapid DOC cycling (Cuevas et al., 2004; Vargas et al., 2007). Additionally, this also generates substrate for methylotrophic bacteria which have been detected within the study area (Levipan et al., 2007).

Ample evidence exists on the subject of microbial production; indeed, Sun et al. (2011) found that SAR11 Alphaproteobacteria, the most abundant heterotrophs in the ocean, are likely to play a major role in mineralizing marine dissolved organic carbon. Additionally, analyses of metagenomic data indicate that the genes involved in C1 metabolism frequently occur in natural SAR11 populations, as observed by Carini et al. (2014). The microorganisms produce enzymes that are able to break down compounds, thus liberating phosphorus for growth, and producing CH_4 as a by-product (Metcalf et al., 2012). Thus, SAR11′s ability to cleave off CH_4 is noteworthy, as it is can partially explain the increased in CH_4 abundance in mid-oceanic waters with elevated DO. This goes hand in hand with our finding in the study area, where Bacteroidetes (orders Sphingo bacteriales and Flavobacteriales), SAR11 (subclades Ia–Candidatus Pelagibacter ubiquea nd II) dominated in surface waters containing DO levels $\geq$ 70 μM (Aldunate et al., 2018).

Finally, studies by Ward and Kilpatrick (1993) at a limited number of oceanic sites that focus on aerobic CH_4 oxidation and consumption (MOx), or methanotrophy, observe that the highest CH_4 oxidation rates in the California Bight are associated with the pycnocline, with a maximum concentration in the subsurface. A further occurrence of MOx processes are observed in the northern Gulf of Mexico (Kelley and Jeffrey, 2002). It appears that CH_4 production and oxidation may be coupled at this density interface, generating a transient CH_4 accumulation and/or depletion. Recently, Steinle et al. (2017) found that MOx is a ubiquitous process that acts as pelagic microbial filter and is able to adapt rapidly within changing environments; furthermore MOx rates can reach levels up to 11.6 nmol L^{-1} d^{-1} in coastal waters and MOx effectively proceeds at sub-micromolar DO levels (Steinle et al., 2017).

4.3. Air sea exchange of methane in the coastal ocean

Marine coastal areas are an important CH_4 source that must be considered in the global methane balance. Bange et al. (1998) indicated annual oceanic emissions ranging from 10.9 to 17.8 Tg CH_4; furthermore these values have been re-evaluated and may reach from 5 to 50 Tg yr^{-1} (Bates et al., 1996; Rhee et al., 2009). This inconsistency of up to one order of magnitude is due to a potential multiplying effect caused by several factors, such as gas transfer coefficient (kw) (Sweeney et al., 2007) and estimates of wind speed (weather station vs. satellite) as is the

case in this study.

The estimates for CH_4 fluxes in the study area indicate that those based on the winds recorded by satellite were more elevated than those efflux based on Carriel Sur winds (Fig. 6); thus, this discrepancy would have a considerable effect on the calculations of air-sea CH_4 exchange, whereas effluxes based on satellite wind are from 0.01 up to 14.07 times greater than these based on weather station (Carriel Sur station). This could be due the location of the Carriel Sur station, on the border continent and may be exposed to some physical barriers, whereas the satellite wind is frequently overestimated with respect to the actual wind velocity over the sea surface (Lebedev et al., 2019; Salvacao and Guedes, 2015). In order to take a more conservative approach, this study discusses the CH_4 fluxes obtained with wind from the Carriel Sur weather station.

In addition, several gas exchange parametrizations are used in the literature in order to estimate gas exchange across the air-sea interface. This study makes several comparisons among the most used parameterizations, but all of them get similar results (<5% difference). CH_4 air-sea fluxes in our study area range from 1.27 to 47.02 with a mean ± SD values of 10.94 ± 7.48 μmol m^{-2} d^{-1}, there are no significant difference in daily fluxes between upwelling (mean ± SD: 12.29 ± 7.91 μmol m^{-2}) and non-upwelling periods (mean ± SD: 8.51 ± 5.99 μmol m^{-2}), suggesting a continuous CH_4 production throughout the year, but coastal upwelling exerts an overall role of outgassing; indeed CH_4 efflux are correlated with wind stress.

Regarding interannual variability in CH_4 efflux (Table 2), the lowest and highest CH_4 efflux are observed during the 2009/10 and the 2015/16 EN, respectively; also higher CH_4 efflux is found during the 2017 coastal EN. These differences seem to be associated with the type of the EN-ENSO events. CH_4 efflux variability seems not associated with changes in favorable upwelling wind stress (Table 2); so these may be due to some biogeochemical and hydrographical conditions in the water column remotely advected.

Remarkably, during fall-winter of 2009, 2011, 2012 and 2015, CH_4 effluxes are greater or similar than those estimated in spring-summer (Table 2). This is a different pattern from that usually observed where the weighted average CH_4 efflux in spring summer always exceed between 1.4 and 2.7 time that estimated in fall-winter. In addition, these periods coincide with lower CH_4 inventories in the surface layer (Table 1) during upwelling with respect to non-upwelling and, with inverted vertical CH_4 distributions (decreasing from surface to bottom water) (Fig. A.2). Even though, interannual variability of CH_4 efflux remains unresolved and it is more likely to be associated with oceanographic conditions and variations in advected water masses and/or continental runoff. Knowing that the EN events increase rainfall, CH_4 levels could come from the rivers discharge and continental runoff. But further efforts are necessary to better understand the related biogeochemical and physical mechanisms (e.g., ENSO, Pacific Decadal Oscillation PDO, and other climate teleconnections).

Considering i) annual CH_4 effluxes, calculated through the weighted averages for during upwelling (64%) and non-upwelling (36%) periods (which fluctuate from 1.66 to 6.22 mmol m^{-2}, mean ± SD: 3.40 ± 1.43) and, ii) a representative continental shelf area equivalent to 41 150 km^2 (*sensu* Farías et al., 2015), that is located between the coastline and the 200 m isobath, and 36°10′52.07″ and 36° 47′20.03″ latitudes (Cobquecura and Punta Hualpen, respectively, Fig. 1), the areal CH_4 efflux ranges from ~ 1 to 4 Gg y^{-1} is estimated in this study. As continental shelf off Concepción represents only 3.5% of the global area of coastal upwelling (EPA, 2010), this area becomes a true hot spot for CH_4 emission, accounting from 1.7 to 13% of global emission for upwelling regions, which vary from 0.02 to 1.5 Tg C $year^{-1}$ (Bakker et al., 2014). This could be the case of other coastal upwelling areas underlying continental shelves. These estimations align with those values from Berner et al. (2003), Jayakumar et al. (2001) and Rhee et al. (2009), and reiterate that coastal upwelling regions are a major CH_4 source (Bakker et al., 2014; Denman et al., 2007; Hamdan and Wickland, 2016).

5. Conclusions

Based on a 12 year time series with monthly frequency, this study reported different temporal variability scale of dissolved CH_4 in the water column subjected to coastal upwelling. CH_4 widely fluctuated between 67.11% and 3965% (or 1.75 and 100.86 nmol L^{-1}), with greatest concentration in bottom waters during the upwelling season, indicating that most of CH_4 came from benthic OM remineralization under suboxic/anoxic conditions. In fact, classical diffusion–advection distribution dominated over 54% of the all obtained profiles.

Despite the fact that strong seasonality was observed in most oceanographic variables such as physical (temperature, salinity wind-driven stress), DO and even Chl-a, according to favorable and non-favorable upwelling periods, only a weak seasonality was observed in CH_4 and nutrient contents, these suggested an intense local recycling (production/consumption) at a high frequency that we could not be captured with a monthly sampling.

Continental shelf off central Chile behaved as a permanent source of CH_4 into the atmosphere with effluxes ranged from 1.27 to 47.02 μmol m^{-2} d^{-1} (mean ± SD: 10.94 ± 7.48), highlighting the importance of coastal upwelling as the major outgassing regions. Indeed, this area became a true hot spot for CH_4 emission, accounting from 1.7 to 13% of global emission for upwelling regions.

Although a weak seasonality was also found in air-sea CH_4 efflux, the annual weighted mean CH_4 effluxes during upwelling (64%) and non-upwelling (36%) periods fluctuated from 1.66 to 6.22 mmol m^{-2} (mean ± SD: 3.40 ± 1.43). That revealed a strong inter-annual variability, which was not associated with changes in along shore wind or favorable wind stress to coastal upwelling, but rather reflected variations in CH_4 content and other physical variables in the water column, that could be associated with EN events like the one observed in 2009–10 or those occurs in 2015/16 and 2017 .

6. Data availability

The dataset will be availiable in Pangaea if the manuscritp were published, meanwhile the research data can be accessed by contacting the corresponding author.

Declaration of Competing Interest

The authors declare that they have no known competing financial interests or personal relationships that could have appeared to influence the work reported in this paper.

Acknowledgements

The authors thank the biogeochemistry group of the Universidad de Concepción for their help and support. Both the crew of R/V *Kay Kay* (*II*) and the Dichato Marine Station of the University of Concepción provided valuable help during fieldwork, as well as all participating colleagues in the Station 18 time series (COPAS program from 2001 to 2015 and FONDECYT projects and CR^2 from 2016 to date), who provided the core measurements. Special thanks to Dr. Renato Quiñones for joining us to the effort to continue the time series of Station 18. This research was funded by FONDECYT N° 1161138 and 1200861 (LF), the Center of Excellence FONDAP CONICYT N° 15110009 and Millennium Science Initiative Program ICN2019_015.

References

Aguirre, C., García-Loyola, S., Testa, G., Silva, D.i., Farías, L., 2018. Insight into anthropogenic forcing on coastal upwelling off south-central Chile. Elementa 6. https://doi.org/10.1525/elementa.314.

Aldunate, M., De la Iglesia, R., Bertagnolli, A.D., Ulloa, O., 2018. Oxygen modulates bacterial community composition in the coastal upwelling waters off central Chile.

Deep Sea Res. Part II Top. Stud. Oceanogr. 156, 68–79. https://doi.org/10.1016/j.dsr2.2018.02.001.
Alldredge, A.L., Cohen, Y., 1987. Can microscale chemical patches persist in the sea? Microelectrode study of marine snow, fecal pellets. Science (80-.). 235, 689–691. https://doi.org/10.1126/science.235.4789.689.
Anabalón, V., Morales, C.E., Escribano, R., Varas, A.M., Varas, M.A., 2007. The contribution of nano- and micro-planktonic assemblages in the surface layer (0–30 m) under different hydrographic conditions in the upwelling area off Concepción, central Chile. Prog. Oceanogr. 75, 396–414. https://doi.org/10.1016/j.pocean.2007.08.023.
Bakker, D., Bange, H., Gruber, N., Johannessen, T., Upstill-Goddard, R.C., Borges, A., Delille, B., Löscher, C., Naqvi, S., Omar, A., Santana-Casiano, J., 2014. Air–sea interactions of natural long-lived greenhouse gases (CO_2, N_2O, CH_4) in a changing climate. In: Liss, P.S., Johnson, M.T. (Eds.), Ocean-Atmosphere Interactions of Gases and Particles. Springer, pp. 113–169.
Bakun, A., 1973. Coastal upwelling indices, west coast of North America, 1946-71. NOAA Tech. Rep. NMFS SSRF-671.
Bange, H.W., Bergmann, K., Hansen, H.P., Kock, A., Koppe, R., Malien, F., Ostrau, C., 2010. Dissolved methane during hypoxic events at the Boknis Eck Time Series Station (Eckernförde Bay, SW Baltic Sea). Biogeosciences 7, 1279–1284. https://doi.org/10.5194/bg-7-1279-2010.
Bange, H.W., Ramesh, R., Rapsomanikis, S., Andreae, M., 1998. Methane in surface waters of the Arabian Sea. Geophys. Res. Lett. 25, 3547–3550.
Barth, J.A., Menge, B.A., Lubchenco, J., Chan, F., Bane, J.M., Kirincich, A.R., McManus, M.A., Nielsen, K.J., Pierce, S.D., Washburn, L., 2007. Delayed upwelling alters nearshore coastal ocean ecosystems in the northern California current. Proc. Natl. Acad. Sci. U. S. A. 104, 3719–3724. https://doi.org/10.1073/pnas.0700462104.
Bates, T.S., Kelly, K.C., Johnson, J.E., Gammon, R.H., 1996. A reevaluation of the open ocean source of methane to the atmosphere. J. Geophys. Res. [Atmos.] 101, 6953–6961. https://doi.org/10.1029/95JD03348.
Bello, E., 2016. Variabilidad estacional en la descarga de metano disuelto desde un sistema estuarino a la zona marina adyacente, el caso de ríos de la zona central de chile (río Itata). Universidad de Concepción.
Berner, U., Poggenburg, J., Faber, E., Quadfasel, D., Frische, A., 2003. Methane in ocean waters of the Bay of Bengal: Its sources and exchange with the atmosphere. Deep. Res. Part II Top. Stud. Oceanogr. 50, 925–950. https://doi.org/10.1016/S0967-0645(02)00613-6.
Borges, A.V., Champenois, W., Gypens, N., Delille, B., Harlay, J., 2016. Massive marine methane emissions from near-shore shallow coastal areas. Sci. Rep. 6, 1–8. https://doi.org/10.1038/srep27908.
Borges, A.V., Speeckaert, G., Champenois, W., Scranton, M.I., Gypens, N., 2017. Productivity and temperature as drivers of seasonal and spatial variations of dissolved methane in the Southern Bight of the North Sea. Ecosystems 21, 583–599. https://doi.org/10.1007/s10021-017-0171-7.
Broecker, W.S., Peng, T.H., 1974. Gas exchange rates between air and sea. Tellus XXVI 1, 21–35. https://doi.org/10.1111/j.2153-3490.1974.tb01640.x.
Bullister, J.L., Wisegarver, D.P., Wilson, S.T., 2016. The production of methane and nitrous oxide gas standards for Scientific Committee on Ocean Research (SCOR) Working Group #143.
Burke, R.A., Reid, D.F., Brooks, J.M., Lavoie, D.M., 1983. Upper water column methane geochemistry in the eastern tropical North Pacific. Am. Soc. Limnol. Oceanogr. 28, 19–32. https://doi.org/10.4319/lo.1983.28.1.0019.
Cai, W., McPhaden, M.J., Grimm, A.M., Rodrigues, R.R., Taschetto, A.S., Garreaud, R.D., Dewitte, B., Poveda, G., Ham, Y.-G., Santoso, A., Ng, B., Anderson, W., Wang, G., Geng, T., Jo, H.-S., Marengo, J.A., Alves, L.M., Osman, M., Li, S., Wu, L., Karamperidou, C., Takahashi, K., Vera, C., 2020. Climate impacts of the El Niño-Southern Oscillation on South America. Nat. Rev. Earth Environ. 1, 215–231. https://doi.org/10.1038/s43017-020-0040-3.
Capelle, D.W., Tortell, P.D., 2016. Factors controlling methane and nitrous-oxide variability in the southern British Columbia coastal upwelling system. Mar. Chem. 179, 56–67. https://doi.org/10.1016/j.marchem.2016.01.011.
Capotondi, A., Wittenberg, A.T., Newman, M., Di Lorenzo, E., Yu, J.-Y., Braconnot, P., Cole, J., Dewitte, B., Giese, B., Guilyardi, E., Jin, F.-F., Karnauskas, K., Kirtman, B., Lee, T., Schneider, N., Xue, Y., Yeh, S.-W., 2015. Understanding enso diversity. Bull. Am. Meteorol. Soc. 96, 921–938. https://doi.org/10.1175/BAMS-D-13-00117.1.
Carini, P., White, A.E., Campbell, E.O., Giovannoni, S.J., 2014. Methane production by phosphate-starved SAR11 chemoheterotrophic marine bacteria. Nat. Commun. 5, 1–7. https://doi.org/10.1038/ncomms5346.
Conrad, R., Wolfgang, S., 1988. Methane and hydrogen in seawater (Atlantic Ocean). Deep Sea Res. Part A. Oceanogr. Res. Pap. 35, 1903–1917. https://doi.org/10.1016/0198-0149(88)90116-1.
Damm, E., Helmke, E., Thoms, S., Schauer, U., Nöthig, E., Bakker, K., Kiene, R.P., 2010. Methane production in aerobic oligotrophic surface water in the central Arctic Ocean. Biogeosciences 7, 1099–1108. https://doi.org/10.5194/bgd-6-10355-2009.
Daneri, G., Dellarossa, V., Quiñones, R., Jacob, B., Montero, P., Ulloa, O., 2000. Primary production and community respiration in the Humboldt Current System off Chile and associated oceanic areas. Mar. Ecol. Prog. Ser. 197, 41–49. https://doi.org/10.3354/meps197041.
Daniel, I., DeGrandpre, M., Farías, L., 2013. Greenhouse gas emissions from the Tubul-Raqui estuary (central Chile 36°S). Estuar. Coast. Shelf Sci. 134, 31–44. https://doi.org/10.1016/j.ecss.2013.09.019.
Denman, K., Brasseur, G., Chidthaisong, A., Ciais, P., Cox, P., Dickinson, R., Hauglustaine, D., Heinze, C., Holland, E., Jacob, D., Lohman, U., Ramachandran, S., Da Silva Dias, P., Wofsy, S., Zhang, X., 2007. Couplings between changes in the climate system and biogeochemistry. In: Solomon, S., Qin, D., Manning, M., Chen, Z., Marquis, M., Averyt, K., Tignor, M., Miller, H. (Eds.), Climate Change 2007: The physical science basis. Contribution of Working Group I to the fourth assessment report of the Intergovermental Panel on Climate Change. Cambridge University Press, Cambridge/ New York, pp. 499–587, 10.1021/acs.bioconjchem.6b00417.
Dinasquet, J., Tiirola, M., Azam, F., 2018. Enrichment of bacterioplankton able to utilize one-carbon and methylated compounds in the Coastal Pacific Ocean. Front. Mar. Sci. 5, 1–13. https://doi.org/10.3389/fmars.2018.00307.
EPA, 2010. Methane and nitrous oxide emissions from natural sources. U.S. Environmental Protection Agency, Washington D.C. USA.
Escribano, R., Daneri, G., Farías, L., Gallardo, V.A., González, H.E., Gutiérrez, D., Lange, C.B., Morales, C.E., Pizarro, O., Ulloa, O., Braun, M., 2004. Biological and chemical consequences of the 1997–1998 El Niño in the Chilean coastal upwelling system: A synthesis. Deep. Res. Part II Top. Stud. Oceanogr. 51, 2389–2411. https://doi.org/10.1016/j.dsr2.2004.08.011.
Etminan, M., Myhre, G., Highwood, E.J., Shine, K.P., 2016. Radiative forcing of carbon dioxide, methane, and nitrous oxide: A significant revision of the methane radiative forcing. Geophys. Res. Lett. 43, 12614–12623. https://doi.org/10.1002/2016GL071930.
Farías, L., Bello, E., Arancibia, G., Fernandez, J., 2018. Distribution of dissolved methane and nitrous oxide in Chilean coastal systems of the Magellanic Sub-Antarctic region (50°–55°S). Estuar. Coast. Shelf Sci. 215, 229–240. https://doi.org/10.1016/j.ecss.2018.10.020.
Farías, L., Besoain, V., García-Loyola, S., 2015a. Presence of nitrous oxide hotspots in the coastal upwelling area off central Chile: An analysis of temporal variability based on ten years of a biogeochemical time series. Environ. Res. Lett. 10, 1–13. https://doi.org/10.1088/1748-9326/10/4/044017.
Farías, L., Fernández, C., Faúndez, J., Cornejo, M., Alcaman, M.E., 2009. Chemolithoautotrophic production mediating the cycling of the greenhouse gases N_2O and CH_4 in an upwelling ecosystem. Biogeosciences 6, 3053–3069.
Farías, L., Florez-Leiva, L., Besoain, V., Sarthou, G., Fernández, C., 2015b. Dissolved greenhouse gases (nitrous oxide and methane) associated with the naturally iron-fertilized Kerguelen region (KEOPS 2 cruise) in the Southern Ocean. Biogeosciences 12, 1925–1940. https://doi.org/10.5194/bg-12-1925-2015.
Farías, L., Graco, M., Ulloa, O., 2004. Temporal variability of nitrogen cycling in continental-shelf sediments of the upwelling ecosystem off central Chile. Deep. Res. Part II Top. Stud. Oceanogr. 51, 2491–2505. https://doi.org/10.1016/j.dsr2.2004.07.029.
Ferderlman, T.G., Lee, C., Pantoja, S., Harder, J., Bebout, B.M., Fossing, H., 1997. Sulfate reduction and methanogenesis in a *Thioploca*-dominates sediment off tha coast of Chile. Geochim. Cosmochim. Acta 61, 3065–3079.
Florez-Leiva, L., Damm, E., Farías, L., Farias, L., 2013. Methane production induced by dimethylsulfide in surface water of an upwelling ecosystem. Prog. Oceanogr. 112–113, 38–48. https://doi.org/10.1016/j.pocean.2013.03.005.
Forster, G., Upstill-Goddard, R.C., Gist, N., Robinson, C., Uher, G., Woodward, E.M.S., 2009. Nitrous oxide and methane in the Atlantic Ocean between 50°N and 52°S: Latitudinal distribution and sea-to-air flux. Deep. Res. Part II Top. Stud. Oceanogr. 56, 964–976. https://doi.org/10.1016/j.dsr2.2008.12.002.
Galán, A., Faúndez, J., Thamdrup, B., Santibáñez, J.F., Farías, L., 2014. Temporal dynamics of nitrogen loss in the coastal upwelling ecosystem off central Chile: Evidence of autotrophic denitrification through sulfide oxidation. Limnol. Oceanogr. 59, 1865–1878. https://doi.org/10.4319/lo.2014.59.6.1865.
Galán, A., Thamdrup, B., Saldías, G.S., Farías, L., 2017. Vertical segregation among pathways mediating nitrogen loss (N_2 and N_2O production) across the oxygen gradient in a coastal upwelling ecosystem. Biogeosciences 14, 4795–4813. https://doi.org/10.5194/bg-14-4795-2017.
García, S.A., 2017. Variaciones temporales de los parámetros físicos y biogeoquímicos en un sistema costero de Chile central bajo distintos forzantes atmosféricos : Un estudio basado en observaciones y modelación unidimensional. University of Concepción.
Glud, R.N., Gundersen, J.K., Holby, O., 1999. Benthic in situ respiration in the upwelling area off central Chile. Mar. Ecol. Prog. Ser. 186, 9–18. https://doi.org/10.3354/meps186009.
Graco, M.I., Purca, S., Dewitte, B., Castro, C.G., Morón, O., Ledesma, J., Flores, G., Gutiérrez, D., 2017. The OMZ and nutrient features as a signature of interannual and low-frequency variability in the Peruvian upwelling system. Biogeosciences 14, 4601–4617. https://doi.org/10.5194/bg-14-4601-2017.
Grasshoff, K., Ehrhardt, M., Kremling, K., 1983. Methods of Seawater Analysis. Second, Second, Re. ed. John Wiley & Sons, Ltd, Deerfield Beach, Florida: Verlag Chemie. Doi: 10.1002/iroh.19850700232.
Gutiérrez, D., Enríquez, E., Purca, S., Quipúzcoa, L., Marquina, R., Flores, G., Graco, M., 2008. Oxygenation episodes on the continental shelf of central Peru: Remote forcing and benthic ecosystem response. Prog. Oceanogr. 79, 177–189. https://doi.org/10.1016/j.pocean.2008.10.025.
Gutierrez, D., Gallardo, V.A., Mayor, S., Neira, C., Vasquez, C., Sellanes, J., Rivas, M., Soto, A., Carrasco, F., Baltazar, M., 2000. Effects of dissolved oxygen and fresh organic matter on the bioturbation potential of macrofauna in sublittoral sediments off Central Chile during the 1997/1998 El Nino. Mar. Ecol. Prog. Ser. 202, 81–99. https://doi.org/10.3354/meps202081.
Hamdan, L.J., Wickland, K.P., 2016. Methane emissions from oceans, coasts, and freshwater habitats: New perspectives and feedbacks on climate. Limnol. Oceanogr. 61, S3–S12. https://doi.org/10.1002/lno.10449.
Hebbeln, D., Marchant, M., Freudenthal, T., Wefer, G., 2000. Surface sediment distribution along the Chilean continental slope related to upwelling and productivity. Mar. Geol. 164, 119–137. https://doi.org/10.1016/S0025-3227(99)00129-2.

Holm-Hansen, O., Lorenzen, C.J., Holmes, R.W., Strickland, J.D.H., 1965. Fluorometric determination of chlorophyll. J. du Cons. Int. pour L'Exploration la Mer 30, 3–15. https://doi.org/10.1093/icesjms/30.1.3.

Holmes, E.M., Sansone, F.J., Rust, T.M., Popp, B.N., 2000. Methane production, consumption, and air-sea exchange in the open ocean: An evaluation based on carbon isotopic ratios. Global Biogeochem. Cycles 14, 1–10. https://doi.org/10.1029/1999GB001209.

Houweling, S., Dentener, F., Lelieveld, J., Walter, B., Dlugokencky, E., 2000. The modeling of tropospheric methane: How well can point measurements be reproduced by a global model? J. Geophys. Res. [Atmos.] 105, 8981–9002. https://doi.org/10.1029/1999JD901149.

IPCC, 2013. Climate Change 2013: The physical science basis. Contribution of Working Group I to the fifth assessment report of the Intergovernmental Panel on Climate Change. Cambridge University Press, Cambridge, United Kingdom and New York, NY, USA.

Jayakumar, D.A., Naqvi, S.W.A., Narvekar, P.V., George, M.D., 2001. Methane in coastal and offshore waters of the Arabian Sea. Mar. Chem. 74, 1–13. https://doi.org/10.1016/S0304-4203(00)00089-X.

Johnson, H.P., Merle, S., Salmi, M., Embley, R., Sampaga, E., Lee, M., 2019. Anomalous concentration of methane emissions at the continental shelf edge of the northern Cascadia Margin. J. Geophys. Res. Solid Earth 124, 2829–2843. https://doi.org/10.1029/2018JB016453.

Karl, D., Beversdorf, L., Björkman, K., Church, M., Martinez, A., DeLong, E., 2008. Aerobic production of methane in the sea. Nat. Geosci. 1, 473–478. https://doi.org/10.1038/ngeo234.

Karl, D., Tilbrook, B., 1994. Production and transport of methane in oceanic particulate organic matter. Nature 368, 732–734.

Kelley, C.A., Jeffrey, W.H., 2002. Dissolved methane concentration profiles and air-sea fluxes from 41°S to 27°N. Global Biogeochem. Cycles 16. https://doi.org/10.1029/2001gb001809.

Kock, A., Gebhardt, S., Bange, H.W., 2008. Methane emissions from the upwelling area o ff Mauritania (NW Africa). Biogeosciences 5, 1119–1125.

Kraus, E.B., 1972. Atmosphere-ocean interaction, in: Libes, S. 1992 (Ed.), An Introduction to Marine Biogeochemistry. Oxford Univ. Press, New York, p. 734.

Lamontagne, R.A., Swinnerton, J.W., Linnenbom, V.J., Smith, W.D., 1973. Methane concentrations in various marine environments. J. Geophys. Res. 78, 5317–5324. https://doi.org/10.1029/JC078i024p05317.

Lebedev, S.A., Sorokin, A.S., Kluev, P.V., Kravchenko, P.N., 2019. Validation of wind speed calculated on satellite altimetry data by measurements on weather stations located along the White Sea Coast. Ecol. Montenegrina 25, 36–43. https://doi.org/10.37828/em.2019.25.4.

Lenhart, K., Klintzsch, T., Langer, G., Nehrke, G., Bunge, M., Schnell, S., Keppler, F., 2016. Evidence for methane production by the marine algae *Emiliania huxleyi*. Biogeosciences 13, 3163–3174. https://doi.org/10.5194/bg-13-3163-2016.

Levipan, H.A., Quiñones, R.A., Johansson, H.E., Urrutia, H., 2007. Methylotrophic methanogens in the water column of an upwelling zone with a strong oxygen gradient off central Chile. Microbes Environ. 22, 268–278. https://doi.org/10.1264/jsme2.22.268.

Ma, X., Sun, M., Lennartz, S.T., Bange, H.W., 2020. A decade of methane measurements at the Boknis Eck Time-series Station in the Eckernförde Bay (Southwestern Baltic Sea). Biogeosciences Discuss. 2020, 1–22. https://doi.org/10.5194/bg-2020-107.

Martens, C.S., Klump, V.J., 1980. Biogeochemical cycling in an organic-rich coastal marine basin-I. Methane sediment-water exchange processes. Geochim. Cosmochim. Acta 44, 471–490. https://doi.org/10.1016/0016-7037(80)90045-9.

McAuliffe, C., 1963. Solubility on water of C1–C9 hydrocarbons. Nature 200, 1092–1093.

Metcalf, W.W., Griffin, B.M., Cicchillo, R., Gao, J., Janga, S., Cooke, H., Circello, B., Evans, B., Martens-Habbena, W., Stahl, D., Van Der Donk, W., 2012. Synthesis of methylphosphonic acid by marine microbes: A source for methane in the aerobic ocean. Science 80-.). 337, 1104–1107. https://doi.org/10.1126/science.1219875.

Monteiro, P.M.S., Van Der Plas, A., Mohrholz, V., Mabille, E., Pascall, A., Joubert, W., 2006. Variability of natural hypoxia and methane in a coastal upwelling system: Oceanic physics or shelf biology? Geophys. Res. Lett. 33, 1–5. https://doi.org/10.1029/2006GL026234.

Montero, P., Daneri, G., Cuevas, A., González, H.E., Jacob, B., Lizárraga, L., Menschel, E., 2007. Productivity cycles in the coastal upwelling area off Concepción: The importance of diatoms and bacterioplankton in the organic carbon flux. Prog. Oceanogr. 75, 518–530. https://doi.org/10.1016/j.pocean.2007.08.013.

Nelson, C.S., 1977. Wind stress and wind stress curl over the California current 1–87. Doi: 10.5962/bhl.title.60783.

Neufeld, J.D., Boden, R., Moussard, H., Schäfer, H., Murrell, J.C., 2008. Substrate-specific clades of active marine methylotrophs associated with a phytoplankton bloom in a temperate coastal environment. Appl. Environ. Microbiol. 74, 7321–7328. https://doi.org/10.1128/AEM.01266-08.

Nightingale, D., Malin, G., Law, C.S., Watson, A.J., Liss, P.S., Liddicoat, M.I., Boutin, J., Upstill-Goddard, R.C., 2000. In situ evaluation of air-sea gas exchange parameterizations using novel conservative and volatile tracer. Global Biogeochem. Cycles 14, 373–387.

Oremland, R.S., 1979. Methanogenic activity in plankton samples and fish intestines: A mechanism for in situ methanogenesis in oceanic surface waters. Limnol. Ocean. 24, 1136–1141.

Owens, N.J.P., Law, C.S., Mantoura, P.H., Burkill, P.H., Llewellyn, C.A., 1991. Methane flux to the atmosphere from the Arabian Sea. Nature 354, 293–296.

Paerl, H.W., Prufert, L.E., 1987. Oxygen-poor microzones as potential sites of microbial N_2 fixation in nitrogen-depleted aerobic marine waters. Appl. Environ. Microbiol. 53, 1078–1087. https://doi.org/10.1128/aem.53.5.1078-1087.1987.

Pinochet, A., Garcés-Vargas, J., Lara, C., Olguín, F., 2019. Seasonal variability of upwelling off Central-Southern Chile. Remote Sens. 11 https://doi.org/10.3390/rs11151737.

Rao, G.D., Sarma, V.V.S.S., 2017. Influence of river discharge on the distribution and flux of methane in the coastal Bay of Bengal. Mar. Chem. 197 https://doi.org/10.1016/j.marchem.2017.11.002.

Reeburgh, W.S., 2007. Oceanic methane biogeochemistry. Am. Chem. Soc. 107, 486–513. https://doi.org/10.1021/cr050362v.

Rehder, G., Collier, R.W., Heeschen, K., Kosro, P.M., Barth, J., Suess, E., 2002. Enhanced marine CH_4 emissions to the atmosphere off Oregon caused by coastal upwelling. Global Biogeochem. Cycles 16. https://doi.org/10.1029/2000gb001391.

Repeta, D.J., Ferrón, S., Sosa, O.A., Johnson, C.G., Repeta, L.D., Acker, M., DeLong, E.F., Karl, D.M., 2016. Marine methane paradox explained by bacterial degradation of dissolved organic matter. Nat. Geosci. 9, 1–7. https://doi.org/10.1038/ngeo2837.

Rhee, T.S., Kettle, A.J., Andreae, M.O., 2009. Methane and nitrous oxide emissions from the ocean: A reassessment using basin-wide observations in the Atlantic. J. Geophys. Res. [Atmos.] 114, 1–20. https://doi.org/10.1029/2008JD011662.

Salvacao, N., Guedes, C., 2015. Offshore wind energy assessment for the Iberian coasts using remotely sensed data, in: Guedes Soares, C. (Ed.), Renewable Energies Offshore. Taylor & Franci Group, London, pp. 237–244. Doi: 10.1201/b18973-35.

Sarmiento, J.L., Gruber, N., 2006. Air-Sea Interface. In: Ocean Biogeochemical Dynamics. Princeton University Press, Princeton, New Jersey, p. 503, 10.2307/j.ctt3fgxqx.

Saunois, Marielle, Stavert, Ann, Poulter, Ben, Bousquet, Philippe, Canadell, Josep, Jackson, Robert, Raymond, Peter, Dlugokencky, Edward, Houweling, Josep, et al., 2020. The Global Methane Budget 2000 – 2017. Earth System Science Data 12 (3), 1561–1623. https://doi.org/10.5194/essd-12-1561-2020.

Scranton, M.I., Brewer, P.G., 1977. Occurrence of methane in the near-surface waters of the western subtropical North-Atlantic. Deep. Res. 24, 127–138. https://doi.org/10.1016/0146-6291(77)90548-3.

Shindell, D.T., Faluvegi, G., Bell, N., Schmidt, G.A., 2005. An emissions-based view of climate forcing by methane and tropospheric ozone. Geophys. Res. Lett. 32, 1–4. https://doi.org/10.1029/2004GL021900.

Sierra, A., Jiménez-López, D., Ortega, T., Fernández-Puga, M.C., Delgado-Huertas, A., Forja, J., 2020. Methane dynamics in the coastal – Continental shelf transition zone of the Gulf of Cadiz. Estuar. Coast. Shelf Sci. 236, 1–18. https://doi.org/10.1016/j.ecss.2020.106653.

Sobarzo, M., Bravo, L., Donoso, D., Garcés-Vargas, J., Schneider, W., 2007. Coastal upwelling and seasonal cycles that influence the water column over the continental shelf off central Chile. Prog. Oceanogr. 75, 363–382. https://doi.org/10.1016/j.pocean.2007.08.022.

Sobarzo, M., Djurfeldt, L., 2004. Coastal upwelling process on a continental shelf limited by submarine canyons, Concepción, central Chile. J. Geophys. Res. 109, 1–20. https://doi.org/10.1029/2004JC002350.

Steinle, L., Maltby, J., Treude, T., Kock, A., Bange, H.W., Engbersen, N., Zopfi, J., Lehmann, M.F., Niemann, H., 2017. Effects of low oxygen concentrations on aerobic methane oxidation in seasonally hypoxic coastal waters. Biogeosciences 14, 1631–1645. https://doi.org/10.5194/bg-14-1631-2017.

Sudheesh, V., Gupta, G.V.M., Naqvi, W.A., 2020. Massive methane loss during seasonal hypoxia/anoxia in the nearshore massive methane loss during seasonal hypoxia/anoxia in the nearshore waters of Southeastern Arabian Sea. Front. Mar. Sci. 7, 1–13. https://doi.org/10.3389/fmars.2020.00324.

Summerhayes, C.., 1983. Sedimentation of organic matter in upwelling regimes, in: Thiede, J., Suess, E. (Eds.), Coastal upwelling, its sediment record. Part B: Sedimentary Records of Ancient Coastal Upwelling. Plenum, New York, pp. 29–72.

Sun, J., Steindler, L., Thrash, J.C., Halsey, K.H., Smith, D.P., Carter, A.E., Landry, Z.C., Giovannoni, S.J., 2011. One carbon metabolism in SAR11 pelagic marine bacteria. PLoS ONE 6, 1–12. https://doi.org/10.1371/journal.pone.0023973.

Sweeney, C., Gloor, E., Jacobson, A.R., Key, R.M., McKinley, G., Sarmiento, J.L., Wanninkhof, R., 2007. Constraining global air-sea gas exchange for CO_2 with recent bomb ^{14}C measurements. Global Biogeochem. Cycles 21, 1–10. https://doi.org/10.1029/2006GB002784.

Testa, G., Masotti, I., Farías, L., 2018. Temporal variability in net primary production in an upwelling area off central Chile (36°S). Front. Mar. Sci. 5, 1–17. https://doi.org/10.3389/fmars.2018.00179.

Thamdrup, B., Canfield, D.E., 1996. Pathways of carbon oxidation in continental margin sediments off central Chile. Limnol. Oceanogr. 41, 1629–1650. https://doi.org/10.4319/lo.1996.41.8.1629.

Trenberth, K.E., 1984. Signal versus noise in the Southern Oscillation. Am. Meteorol. Soc. 112, 326–332. https://doi.org/10.1175/1520-0493(1984)112<0326:SVNITS>2.0.CO;2.

Upstill-goddard, R.C., Barnes, J., 2016. Methane emissions from UK estuaries : Re-evaluating the estuarine source of tropospheric methane from. Europe 180, 14–23. https://doi.org/10.1016/j.marchem.2016.01.010.

Upstill-goddard, R.C., Barnes, J., Frost, T., Punshon, S., Owens, N.J.P., 2000. Methane in the southern North Sea : Low-salinity inputs , estuarine removal , and atmospheric flux 14, 1205–1217.

Vargas, C.A., Martínez, R.A., Cuevas, L.A., Pavez, M.A., Cartes, C., González, H.E., Escribano, R., Daneri, G., 2007. The relative importance of microbial and classical food webs in a highly productive coastal upwelling area. Limnol. Oceanogr. 52, 1495–1510. https://doi.org/10.4319/lo.2007.52.4.1495.

Walsh, J.J., 1991. Importance of continental margins in the marine biogeochemical cycling of carbon and nitrogen. Nature 350, 53–55.

Wanninkhof, R., 2014. Relationship between wind speed and gas exchange over the ocean revisited. Limnol. Oceanogr. Methods 12, 351–362. https://doi.org/10.4319/lom.2014.12.351.

Wanninkhof, R., 1992. Relationship between wind speed and gas exchange. J. Geophys. Res. 97, 7373–7382.

Ward, B.B., Kilpatrick, K.A., 1993. Methane oxidation associated with mid-depth methane maxima in the Southern California Bight. Cont. Shelf Res. 13, 1111–1122. https://doi.org/10.1016/0278-4343(93)90044-X.

Weber, T., Wiseman, N.A., Kock, A., 2019. Global ocean methane emissions dominated by shallow coastal waters. Nat. Commun. 10, 1–10. https://doi.org/10.1038/s41467-019-12541-7.

Whiticar, M.J., Faber, E., Schoell, M., 1986. Biogenic methane formation in marine and freshwater environments: CO_2 reduction vs. acetate fermentation-Isotope evidence. Geochim. Cosmochim. Acta 50, 693–709. https://doi.org/10.1016/0016-7037(86)90346-7.

Wiesenburg, D.A., Guinasso, N.L., 1979. Equilibrium solubilities of methane, carbon monoxide, and hydrogen in water and sea water. Am. Chem. Soc. 24, 356–360.

Williams, P.J.l.B., Jenkinson, N.W., 1982. A transportable microprocessor-controlled precise Winkler titration suitable for field station and shipboard use. Limnol. Oceanogr. 27, 576–584. https://doi.org/10.4319/lo.1982.27.3.0576.

Wilson, S.T., Ferrón, S., Karl, D.M., 2017. Interannual variability of methane and nitrous oxide in the North Pacific Subtropical Gyre. Geophys. Res. Lett. 44, 9885–9892. https://doi.org/10.1002/2017GL074458.

Winckler, P., Aguirre, C., Farías, L., Contreras, M., Masotti, I., 2020. Evidence of climate-driven changes on atmospheric, hydrological, and oceanographic variables along the Chilean coastal zone. Clim. Change 163 (2), 1–20. https://doi.org/10.1007/s10584-020-02805-3.

Wolfe, R.S., 1971. Microbial formation of methane, 6th ed. Advances in microbial physiology. Academic press, London and New York.

Wuebbles, D.J., Hayhoe, K., 2002. Atmospheric methane and global change. Elsevier Sci. 57, 177–210. https://doi.org/10.1016/S0012-8252(01)00062-9.

Progress in Oceanography 195 (2021) 102589

Contents lists available at ScienceDirect

Progress in Oceanography

journal homepage: www.elsevier.com/locate/pocean

Temporal methane variability in the water column of an area of seasonal coastal upwelling: A study based on a 12 year time series

L. Farías [a,b,c,*], S. Tenorio [b,d], K. Sanzana [a], J. Faundez [b,e,f]

[a] Departmento de Oceanografía, Facultad de Ciencias Naturales y Oceanográficas, Universidad de Concepción, Concepción, Chile
[b] Centro de Ciencia del Clima y la Resiliencia (CR^2), Chile
[c] Instituto Milenio en Socio-ecología Costera (SECOS), Chile
[d] Programa de Graduados en Oceanografía, Departamento de Oceanografía, Universidad of Concepción, Concepción, Chile
[e] Facultad de Biología, Pontificia Universidad Católica de Chile
[f] Estación Costera de Investigaciones Marinas (ECIM), Chile

A B S T R A C T

Temporal distribution of dissolved CH_4 was analysed in a zone of strong seasonal coastal upwelling off central Chile (36.5°S,73°W). Observations were taken from a twelve-year time series that included monthly sampling of the water at eight depths. CH_4 concentration fluctuated between 1.75 and 100.9 nmol L^{-1} (or 67.11% and 3965% of saturation), with the highest levels at bottom waters, which increase as upwelling evolved. Three kind of CH_4 profiles were identified; a classical diffusion–advection distribution, with bottom/surface CH_4 concentration ratio > 2, was predominantly observed in ~ 54% of the all profiles and attributed to high CH_4 production in the sediments during coastal upwelling season (austral spring-summer); a period of higher biological productivity, as well as in hypoxic/anoxic condition. In contrast, relatively homogeneous profiles (CH_4 level ratio between bottom and surface depth < 2) was observed about ~ 46% of all profiles during periods of extreme vertical mixing (such as winter storms). Furthermore, irregular CH_4 profile with superficial peaks occurring between the surface and 15–30 m depth was likely observed. These peaks indicated that local production rates exceed turbulent mixing rates, suggesting a rapid CH_4 cycling due to microbial processes on the surface. Despite the fact that strong seasonality was observed in most oceanographic variables, according to favourable and non-favourable upwelling periods, only a weak seasonality was observed in CH_4 content and its air-sea flux, the latter ranged from 1.27 to 47.02 μmol m^{-2} d^{-1} (mean ± SD: 10.94 ± 7.48). The annual weighted mean CH_4 effluxes during upwelling (64%) and non-upwelling (36%) periods fluctuated from 1.66 to 6.22 mmol m^{-2} (mean ± SD: 3.40 ± 1.43), highlighting the importance of the continental shelf under the influence of coastal upwelling as a significant CH_4 source toward the atmosphere.

1. Introduction

Methane (CH_4) is the most abundant organic trace gas in the atmosphere and, also the second most important anthropogenically emitted greenhouse gas. On a per molecule basis, it is 20 times more potent in terms of being a climatically active gas than CO_2 (Etminan et al., 2016). Currently, atmospheric CH_4 concentration increases 2.5 over its pre-industrial baseline (from 700 to 1750 ppm; Houweling et al., 2000) and this trend continues to increase in response to greater anthropogenic forcing upon Earth Systems (Saunois et al., 2020). There are concerns around how increasing CH_4 concentrations may affect atmospheric chemistry and climate (Wuebbles and Hayhoe, 2002). Increased CH_4 in the atmosphere depends on the equilibrium between anthropogenic and natural CH_4 sources and sinks from major reservoirs within the Earth's systems, such as atmospheric, terrestrial and oceanic systems.

Current knowledge on oceanic CH_4 distributions is based on relatively recent investigations, that are focused on technical constrains to effectively measure dissolved CH_4 (Wilson et al., 2017). Since the mid-1950's it has been reported that CH_4 concentrations reach millimolar levels in the sediments, whereas in oceanic waters CH_4 levels rarely exceed nanomolar levels (Lamontagne et al., 1973). Despite significant efforts in recent decades to quantify marine-derived CH_4, the global oceanic CH_4 dataset remains limited and indicates a concerning ambiguity around the global estimates of CH_4 emissions, that are reported to widely vary from 5 to 25 Tg yr^{-1} (Bates et al., 1996; Rhee et al., 2009; Saunois et al., 2020; Wuebbles and Hayhoe, 2002). Recently, Weber et al. (2019) using ΔCH_4 database of ~ 120,000 observations compiled into a monthly climatology, reduce by a factor of three the range of oceanic CH_4 emission (6–12 Tg CH_4 yr^{-1}).

Some studies have driven important efforts to obtain more accurate CH_4 measurements, from diurnal to decadal time scales, as well as from different spatial scales ranging from decameters up to much larger size scales; such as estuaries, coastal upwelling zones, continental shelves, subtropical gyres, and even global scales (Bates et al., 1996; Shindell

* Corresponding author at: Departmento de Oceanografía, Facultad de Ciencias Naturales y Oceanográficas, Universidad de Concepción, Concepción, Chile.
E-mail address: laura.farias@udec.cl (L. Farías).

https://doi.org/10.1016/j.pocean.2021.102589
Received 29 July 2020; Received in revised form 22 March 2021; Accepted 17 April 2021
Available online 27 April 2021

4.2 CAPÍTULO 2: EVALUAR LAS VARIACIONES DE CORTO PLAZO (DIARIO Y SINÓPTICO) DE LA CONCENTRACIÓN DE CH_4 SUPERFICIAL EN LA ZONA COSTERA DE CHILE CENTRAL.

En este capítulo se presentan los resultados de interpretar la variabilidad sinóptica y diurna de las concentraciones de CH_4 disuelto en la Bahía de Coliumo, una bahía sujeta a surgencia costera. Como resultado se envió el manuscrito "Short-term variability of dissolved methane in surface waters of an upwelling bay off the central Chile" (Tenorio, S., Farías, L., Narváez, D., y Soto-Mardones., L.) a la revista Geophysical Research Letters.

RESUMEN

Short-term variability in dissolved methane (CH_4) is critical in coastal systems. Hourly dissolved CH_4 time series in an upwelling bay (Coliumo, 36.5°S, Chile) was register using a buoy-based system during the upwelling season (September 2024–February 2025). Spectral and wavelet analyses revealed a multiscale structure with variance dominated by a >10 d low-frequency (52.1%), followed by synoptic (3–10 d; 40.3%) and a weak diurnal mode (2.5%). Intraseasonal (>10 d) variability provided the background over which synoptic events modulated CH_4 via alternating active upwelling and relaxation/downwelling events. During active upwelling, cold, saline, and CH_4-enriched waters upwelled, yielding higher CH_4 concentrations (mean 41.2±17.6 nM), whereas during relaxation, CH_4 decreased by almost half (mean 26.7±14.7 nM). The diurnal band (~24 h) was weak and negatively related to the land–sea breeze cycle and solar heating. High-frequency observations capture CH_4 dynamics previously missed, reducing bias in coastal emission estimates.

Short-term variability of dissolved methane in surface waters of an upwelling bay off the central Chile

Sandy E. Tenorio[1,2], Diego Narváez[2,3], Luis Soto-Mardones[4] and Laura Farías[2,3,5,6,*]

[1] Programa de Graduados en Oceanografía, Departamento de Oceanografía, Universidad de Concepción, Concepción, 4070043, Chile.
[2] Departamento de Oceanografía, Facultad de Ciencias Naturales y Oceanográficas, Universidad de Concepción, Concepción, 4070043, Chile.
[3] COPAS COASTAL, Chile
[4] Departamento de Física, Facultad de Ciencias, Universidad del Bío-Bío, Av. Collao 1202, Casilla 5-C, Concepción, Chile
[5] Centro de Ciencia del Clima y la Resiliencia (CR2), Chile.
[6] Instituto Milenio en Socio-ecología Costera (SECOS), Chile.

*Corresponding author: Laura Farías (laura.farias@udec.cl)

Key Points:

- Intraseasonal (>10 d) variability shapes CH_4 background (~52% variance), while synoptic (3–10 d; ~40%) drives short-term variability.
- At synoptic scale, active upwelling events double surface CH_4 concentration relative to relaxation upwelling or downwelling event.
- CH_4 shows a weak diurnal cycle, negatively correlated with sea breeze intensity and solar radiation.

Abstract

Short-term variability in dissolved methane (CH_4) is critical in coastal systems. Hourly dissolved CH_4 time series in an upwelling bay (Coliumo, 36.5°S, Chile) was register using a buoy-based system during the upwelling season (September 2024–February 2025). Spectral and wavelet analyses revealed a multiscale structure with variance dominated by a >10 d low-frequency (52.1%), followed by synoptic (3–10 d; 40.3%) and a weak diurnal mode (2.5%). Intraseasonal (>10 d) variability provided the background over which synoptic events modulated CH_4 via alternating active upwelling and relaxation/downwelling events. During active upwelling, cold, saline, and CH_4-enriched waters upwelled, yielding higher CH_4 concentrations (mean 41.2±17.6 nM), whereas during relaxation, CH_4 decreased by almost half (mean 26.7±14.7 nM). The diurnal band (~24 h) was weak and negatively related to the land–sea breeze cycle and solar heating. High-frequency observations capture CH_4 dynamics previously missed, reducing bias in coastal emission estimates.

Plain Language Summary

Dissolved methane in coastal bays can change quickly, affecting how much reaches the atmosphere. We measured methane hourly in Coliumo Bay (Chile) through an upwelling season to see how it responds to physical forcing (e.g., wind). Multi-day swings tied to alternating upwelling and relaxation/downwelling explained most variability: when cold, salty subsurface water reached the surface, methane averaged ~41 nM; during relaxation it fell to ~27 nM. Daily cycles were smaller and linked to the land–sea breeze and daytime heating. High-frequency observations reveal short-lived peaks missed by occasional sampling, improving coastal methane emission estimates and informing near-term mitigation.

1 Introduction

Methane (CH_4), the second most important greenhouse gas after CO_2, has increased 2.6-fold since the pre-industrial era (Saunois et al., 2025). Its ~10-year atmospheric lifetime makes it an attractive target for near-term climate mitigation (IPCC, 2021). Oceanic CH_4 emissions range widely from 4 to 45.9 Tg CH_4 yr^{-1} (Bakker et al., 2014; Rosentreter et al., 2021), with >75% emitted from coastal areas (Weber et al., 2019). Part of the wide range come from limited spatiotemporal coverage, best addressed by combining satellite and *in situ* observations, and from biogeochemical recycling pathways still under study (Wilson et al., 2020). Although decades of CH_4 measurements have advanced our understanding of the marine CH_4 cycle, with long-term datasets revealing interannual (Farías et al., 2021a; Wilson et al., 2017) and seasonal patterns (Borges et al., 2017; Jakobs et al., 2014), major knowledge gaps remain in short-term variability (daily to intraseasonal scales) (Brown et al., 2023). It is particularly important in highly dynamic coastal zones (Lachkar et al., 2024; Resplandy et al., 2024), but it is still poorly resolved, limiting our ability to produce accurate flux estimates.

Recent studies show that CH_4 concentrations and their air–sea fluxes can fluctuate significantly from subdaily to synoptic scales, driven by short-term hydrodynamic variability (Brown et al., 2023; Roth et al., 2022). These highlight the multiscale nature of CH_4 dynamics in coastal and estuarine environments and the need of high-frequency observations to capture transient biogeochemical events and to improve flux models.

The distribution of dissolved CH_4 in coastal environments is shaped not only by physical processes such as wind and tidal forcing, which influence stratification, vertical mixing, and ventilation, but also by biogeochemical processes in bottom waters and sediments, primarily via methanogenesis (Reeburgh, 2007) and oxidation/consumption through methanotrophy (Mao et al., 2022). Recent studies further highlight the role of microalgae and microbial communities in CH_4 production via methylotrophic methanogenesis in the surface layer (Bizic, 2021; Thomas Klintzsch et al., 2019).

The central Chile coast has a broad continental shelf shaped by seasonal upwelling (Sobarzo et al., 2007), affecting numerous bays and gulfs and generating highly dynamic and heterogeneous ecosystems (Largier, 2020). In upwelling bays, physical dynamics are modulated by local topography, bay orientation, and interactions with the open coast via wind forcing, river discharge, and shelf–ocean gradients (Largier, 2020). These conditions stimulate high primary productivity (Broullón et al., 2023), enhancing organic matter export to sediments and promoting greenhouse-gas production and recycling. We employ a state-of-the-art buoy system to resolve high frequency dissolved CH_4 variability in Coliumo Bay, an upwelling bay. We characterize short term variability and its physical drivers, improving understanding of CH_4 dynamics in coastal upwelling systems as they respond to anthropogenic impacts.

2 Methods and Data

Coliumo Bay (central Chile) is a small, shallow, north-facing semi-enclosed embayment (4.76 km^2; <5–20 m depth; Fig. S1) with minor freshwater input from the small Coliumo, Dichato, and Pingueral creeks. Alongshore-wind upwelling brings Equatorial Subsurface Water (ESSW) in spring–summer, whereas late-fall/winter downwelling favors Subantarctic Surface Water (SAAW) with increased precipitation and runoff (Sobarzo et al., 2007). These alternating regimes drive strong seasonal shifts in salinity, temperature, dissolved oxygen, and primary production (Testa et al., 2018). The water residence time is short (2–5 d), making the bay highly responsive to environmental forcing.

2.1 Data collection

Seawater data were collected near an oceanographic buoy deployed in Coliumo Bay (36°32.301′ S, 72°56.462′ W). The buoy belongs to the Coastal Observation Program of the Department of Oceanography, University of Concepción, and is located near the middle of the bay with sensors mounted on a fixed frame at 1.5 m depth. Dissolved CH_4 concentrations were measured with a CONTROS HydroC™ CH4 sensor (Gen. III, compact with 5P pump; 4H Jena Engineering). Temperature and salinity were recorded with an RBR Duo^3 CTD. Data were acquired every minute during upwelling season (September 2024-February 2025). Meteorological data were obtained from Dichato Marine Station and Carriel Sur Airport. Instrumentation details and data-processing for salinity (UNESCO, 1981) are summarized in supporting information (Table S1). All datasets were averaged to hourly resolution for consistency. Anomalies were computed by subtracting the series average from each original time series. The mean diurnal-cycle anomaly was calculated by subtracting, for each day, the daily mean from the hourly values and then computing the mean and standard deviation for each hour across the study period (Aguirre et al., 2021).

To validate the CH_4 sensor data, weekly discrete seawater samples were collected using a 10-L Niskin bottle. CH_4 samples (in triplicate) were drawn directly from the Niskin through a gas-tight hose into 20mL GC vials and preserved with 50 µL saturated mercuric chloride in the dark (Karl & Tilbrook, 1994) Dissolved CH_4 was analyzed by static headspace equilibration (McAuliffe, 1963) and quantified by GC with a flame ionization detector (Agilent Technologies 6850), following (Farías, Tenorio, et al., 2021).

2.2 Post-processing of raw methane data sensor

The CH_4 sensor responds slowly ($\tau_{63} \approx 50–55$ min), diffusion across the membrane and internal equilibration introduce a lag. To correct it, the deconvolution method based on statistical inverse problems was applied using the *deconv_master* python function (Dølven et al., 2022). It estimates the true ambient concentration from the measured sensor signal, accounting for the sensor's response time. The optimal regularization parameter (Δt) was determined through L-curve analysis (in this case, 900 seconds), balancing fidelity and smoothness to avoid noise amplification. The corrected series preserves overall structure ($R^2 = 0.98$; MAE = 0.72 µatm) (Fig. S2a and b), and enhance peaks (Fig. S2a), indicating that accounting for the sensor's response time improves recovery of the system's natural variability.

Dissolved methane concentration in nM was calculated from its partial pressure (ρ CH_4, in µatm), applying Henry's law (Eq. 1) from the corrected series.

$$C_{CH_4} = K_H * \rho CH_4 \quad \text{(Eq. 1)}$$

The solubility coefficient (K_H; mol L^{-1} atm^{-1}) was calculated according Wiesenburg & Guinasso (1979), using *in situ* temperature and salinity.

Sensor data agreed well with discrete CH_4 measurements (R = 0.91; RMSD = 9.3 nM; Fig. S2c and d), indicating good performance despite the highly dynamic environment and sensor response time (τ = 50 min). Removing the apparent outlier reduce agreement (R = 0.83; RMSD = 7.8 nM; Fig. S2d), implying it reflects real variability rather that error. The regression of discrete samples fell below the 1:1 line, suggesting slight underestimation by discrete samples relative to the sensor (Fig. S2e). Interception in both fits indicated a small systematic bias, particularly evident at low concentrations (Fig. S2e).

2.3 Wind components, wind stress (τ_x and τ_y) and upwelling index (UI)

The wind components (u and v; m s^{-1}) were determined from the magnitude and direction of the wind, the zonal and meridional wind stress (τ_x and τ_y; N m^{-2}) was calculated using the u and v component of the wind (Nelson, 1977). To characterize upwelling phases, upwelling index (UI, m^3 s^{-1}) was used, according to Aguirre et al., (2021), which was obtained from Ekman's zonal transport by 1000 m of coastline (Bakun, 1973). In this case, the Coriolis parameter (ƒ) used was 8.6829 x 10^{-5} s^{-1}. Active upwelling events were defined where a minimum of 2 days of positive duration of UI was over 80 m^3 s^{-1} (UI>80). Due to the short period studied, in this study inactive upwelling (0<UI< 80) and downwelling (UI<0) periods (Aguirre et al., 2021) were grouped in relaxed upwelling events, ultimately retaining only active and relaxed upwelling events. Finally,

a composite analysis of detected active upwelling events was performed using only the anomalies to summarize the average effect of upwelling into the bay.

2.4 Statistical data analysis

To validate CH_4 sensor data, a simple linear regression model and a Taylor diagram (MATLAB function STaylorDiag v1.5.2; Liu, 2025) was used. To test statistically significant differences in CH_4 levels between active and relaxed upwelling periods, we used the Mann–Whitney U test. All statistical tests were conducted at a significant level of $\alpha = 0.05$.

To identify and compare the dominant frequencies of atmospheric and oceanographic variables, we performed spectral analysis on Lanczos-filtered time series, retaining variability with periods shorter than 15 days, using wavelet analysis (Torrence & Compo, 1998). Additionally, to quantify the relative contribution of modes of variability during the upwelling period, we used Singular Spectrum Analysis (Vautard et al., 1992) to decompose the time series into principal components (2–10 days), facilitating the identification of patterns associated with different physical and biogeochemical processes.

3 Results and Discussion

3.1 Time series and variability modes of methane and other hydrographic and atmospheric variables

Figure 1 shows hourly time series of meteorological forcing (wind stress), the upwelling index (UI), and temperature, salinity and surface-water dissolved CH_4 anomalies. Wind stress ranged from −0.60 to +0.32 N m^{-2}; positive values (southerlies) denoted upwelling-favorable conditions, negative values (northerlies) indicated downwelling (Fig. 1a). The wind rose (Fig. S3) shows southerly-sector winds (SE–SW) prevailed ~70.95%, consistent with predominantly upwelling-favorable winds during the study period; while intermittent weakening of southerlies and/or strengthening of northerly–northeasterly winds were ~24.54%; the remainder were calm conditions or missing data. The upwelling index (UI) ranged from -2.1×10^3 to 748.4 $m^3\ s^{-1}$ (Fig. 1b), reflecting alongshore-wind variability at synoptic (3–10 d) and intraseasonal (>10 d) scales. Synoptic disturbances modulated the anticyclonic regime: coastal jets promoted upwelling, whereas coastal low-pressure systems suppressed it (Garreaud et al., 2002; Ricardo C Muñoz & Garreaud, 2005). Using the criterion UI > 80 for >2 days (Aguirre et al., 2021), 20 active upwelling events lasting 2.4–9 days (total 104 days) were identified. The longest, most intense occurred in spring (UI> 200), lasting 6–9 days (e.g., events 12, 13, 17, 18; Fig. 1b). Conversely, 21 relaxation periods, driven by weakened southerlies lasted 1–7 days (total 77 days); blank intervals in Fig. 1b mark these periods. Negative UI occurred mainly in spring and early summer; the strongest (R3, 18–24 September 2024) coincided with a coastal low and heavy precipitation (Fig. S4a–b) and a marked salinity decrease (Fig. 1d). Alternation among upwelling-favorable (UI > 0), inactive (0 < UI < 80), and downwelling (UI < 0) conditions were most frequent in spring (e.g., R5, R6, R7, R10; Fig. 1b), consistent with episodic disruption of equatorward winds by coastal jets and lows (Garreaud et al., 2002).

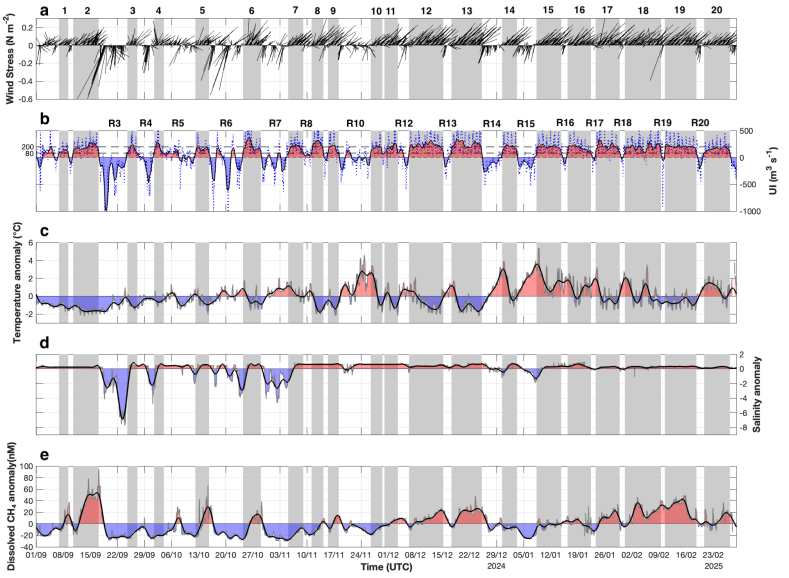

Figure 1. Hourly time series of **a.** stick diagram of wind stress (N m^{-2}), arrow length and direction indicate magnitude and flow direction, respectively; **b.** upwelling index (m^3 s^{-1}); (**c-e**) anomalies of temperature (°C); salinity (psu); and dissolved methane (nM) Coliumo Bay (September 2024-February 2025). Vertical gray bars indicate active upwelling. Black lines in **c-e** represent high-pass (<15 d) Lanczos-filtered. Numbers with R denotes relaxed (relaxation/downwelling).

Temperature and salinity anomalies responded coherently to wind forcing. In situ temperature ranged from 10.5 to 18.2 °C. Negative temperature anomalies (down to −2 °C, Fig. 1c) coincided with positive wind stress (Fig. 1a) and positive UI (Fig. 1b), indicating intrusion of cold, nutrient-rich ESSW into inner Coliumo Bay . Conversely, positive anomalies (up to +5 °C) occurred under negative wind stress and negative UI (relaxed upwelling or downwelling; Fig. 1a–b). As the upwelling season progressed, warming episodes became more pronounced due to strong solar heating, which strengthened near-surface stratification (Aguirre et al., 2021). Salinity varied markedly (26.2–34.9). Positive salinity anomalies generally marked ESSW upwelling, whereas several low-salinity events (negative anomalies; Fig. 1d) coincided with coastal low-pressure systems and precipitation (Fig. S4a and b), consistent with small freshwater inputs from local creeks and nearby rivers (Sobarzo et al., 2022). For example, during 18–23 September 2024, heavy rainfall (~25.6 mm) freshened the surface layer (Fig. S4b).

Finally, during the upwelling season, hourly surface CH_4 concentrations exhibited high temporal variability (Fig. 1e), ranging from 4.8 to 129 nM and corresponding to saturations of

181–4552%. Peaks in CH_4 anomalies (>40 nM) occurred immediately after active upwelling, coinciding with low temperature and high salinity. This pattern indicates ventilation and vertical advection of ESSW, which is oxygen-poor and CH_4-enriched, likely reinforced by diffusive CH_4 fluxes from sediments. In contrast, abrupt decreases or negative anomalies (down to −20 nM) were associated with upwelling relaxation ($0 < UI < 80$) or downwelling ($UI < 0$) and with enhanced surface ventilation linked to low-pressure systems that break down water-column stratification. Together, these changes underscore strong biogeochemical control: mean CH_4 was significantly higher during active upwelling (41.2 ± 17.6 nM) than during relaxation (26.7 ± 14.7 nM) and downwelling (27.7 ± 15.4 nM). The high CH_4 concentrations in Coliumo Bay, relative to the adjacent shelf, likely result from local hydrography and benthic–pelagic coupling (Largier, 2020). The bay's semi-enclosed morphology, short residence time, and shallow depth (~10 m) favor accumulation of sediment-produced CH_4, while upwelling episodes inject CH_4-enriched subsurface water into the coastal zone. These two sources, sedimentary diffusion and advective input, increase CH_4 availability in the water column. Similar mechanisms have been observed on the adjacent continental shelf and in other major upwelling systems (Naqvi et al., 2010).

3.2 Multiscale variability in physical and biogeochemical variables

Wavelet analyses (Fig. 2) show a multiscale temporal structure with energy in the diurnal and synoptic bands. The zonal (τx) and meridional (τy) wind-stress components exhibit power in the diurnal band associated with the sea-breeze dominance (Fig. 2f; (Lerczak et al., 2001) and in the 3–10-day band (Fig. 2g), respectively, revealing recurrent alternation between southerly and northerly winds forced by passing mid-latitude cyclones and coastal lows (Garreaud et al., 2002). Temperature shows significant diurnal power (Fig. 2h), especially in summer (Fig. 2c), reflecting solar forcing (Aguirre et al., 2021). During summer, temperature also exhibits non-significant power in the synoptic band, consistent with repeated cooling–warming cycles associated with upwelling events (Aguirre et al., 2021). Salinity (Fig. 2d) displays high energy in the 3–8-day band (Fig. 2i) during early spring, coincident with freshwater inputs and rainfall that modulate the surface layer. Methane variability (Fig. 2e) concentrates energy in the ~3–10-day range, though not significantly (Fig. 2j), reflecting close coupling to physical forcing and the advection of CH_4-enriched subsurface waters during active upwelling. The pervasive synoptic-band (3–10 d) power across variables suggests modulation by alternating active/relaxed upwelling, well documented for the area (Aguirre et al., 2021; Sobarzo et al., 2022). Other synoptic processes such as frontal passages (storms), coastal lows (Garreaud et al., 2002; Sobarzo et al., 2022), atmospheric rivers (Garreaud et al., 2024), and high river discharge, should imprint signals as well, but their episodic nature calls for longer, high-frequency time series.

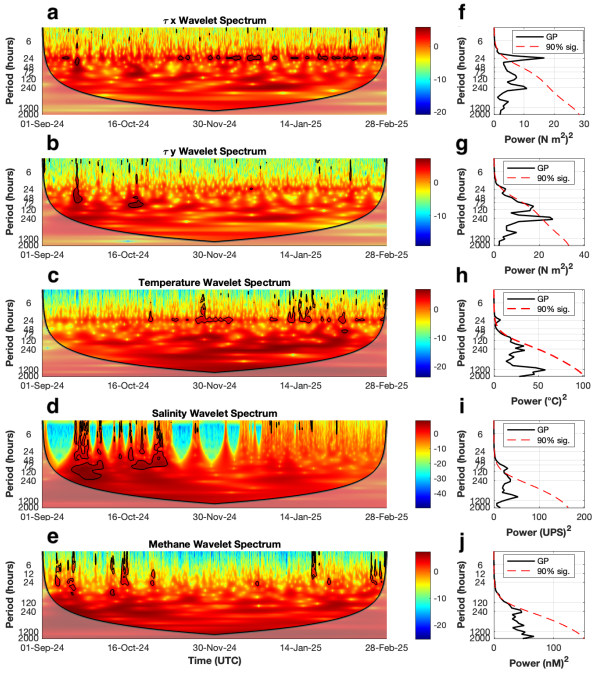

Figure 2. Wavelet power spectra of **a.** zonal wind stress (τx), **b.** meridional wind stress (τy), **c.** temperature, **d.** salinity, and **e.** dissolved methane in Coliumo Bay (September 2024-February 2025). The color scale indicates normalized power. Thick black contours denote 90% confidence level. Shading indicates the cone of influence (edge effects). Time series were Lanczos high-pass filtered (<15 d).

Singular Spectrum Analysis, for wind speed, temperature, salinity, CH_4, is summarized in Table 1. A dominant low-frequency (>10 d; Mode 1) component was present in all variables, representing the background trend/intraseasonal regime. Synoptic variability (3–10 d) also contributes substantially to the variance, 31.1% (wind), 39.3% (temperature), 26.5% (salinity), and 40.3% (CH_4), whereas the diurnal band is negligible for salinity (0.6%), modest for CH_4 (2.5%), and more pronounced for temperature (8.9%) and wind (19.6%).

Table 1. Variance (%) from SSA (Singular Spectrum Analysis) modes and frequency bands for methane, temperature, and wind. Mode 1 (*) represents the low-frequency trend (>10 days). "Diurnal" and "synoptic" sum SSA eigenpairs whose reconstructed components show dominant

252 spectral peaks at 20–24 h and 3–10 d, respectively. Percentages do not sum 100% because only
253 a subset of modes is reported; the remainder is considered noise.
254

Modes	Winds	Temperature	Salinity	CH4
Mode 1 (*)	20.5	40.0	33.2	52.1
Synoptical	31.1	39.3	26.5	40.3
Diurnal	19.6	8.9	0.6	2.5

255 3.3 Intraseasonal variability

256 During the upwelling season (September–February), intraseasonal modulation captured
257 by SSA Mode 1 (>10 d) is evident. The progression of the season is apparent in wind-stress and
258 temperature anomalies and in the concomitant dissolved CH_4 responses (Fig. 1), as well as in
259 gradual changes in the amplitude of synoptic (3–10 d) variability and in the duration of active
260 upwelling events (Figs. 2–3). This evolution is driven by the poleward migration of the Southeast
261 Pacific Anticyclone (SPA) beginning in spring (September), which strengthens equatorward
262 (southerly) alongshore winds favorable for upwelling; intermittent coastal lows modulate these
263 winds until the SPA stabilizes in summer (Strub et al., 2013). Wind stress exhibited a clear
264 transition from a stormy phase with strong northerlies (Sep–Oct; Fig. 1a), associated with low-
265 pressure systems and rainfall (Fig. S4), to a phase dominated by upwelling-favorable southerlies,
266 as previously reported for the area (Garreaud et al., 2002). Aligned with the seasonal progression,
267 biogeochemical conditions also shifted (Testa et al., 2018), regulating CH_4 cycling (Fig. 1e). In
268 spring, intermittent upwelling, high photosynthetically active radiation, and shallow stratification
269 yielded peak net primary production (NPP ≈ 18–26 g C m^{-2} d^{-1}) dominated by microphytoplankton
270 (diatoms). By late summer (Jan–Mar), NPP declined (~1–2 g C m^{-2} d^{-1}) owing to changes in water-
271 column structure and community composition, with a relative increase in nano- and
272 picophytoplankton (Testa et al., 2018). These conditions are critical for CH_4 cycling, because
273 methylated substrates can fuel CH_4 production via picoplankton-mediated methylotrophic
274 methanogenesis (Karl et al., 2008; Tenorio & Farías, 2024). Altogether, these processes indicate
275 that Coliumo Bay acts as a dynamic biogeochemical hotspot, where physical forcing and microbial
276 processes jointly sustain locally elevated dissolved CH_4 relative to the adjacent shelf. Thus,
277 intraseasonal variability establishes the background, and synoptic (3–10 d) and diel (~24 h)
278 variability further modulate CH_4 concentrations and the processes that control its cycling.

279 3.4 Synoptic variability and influence of the upwelling area on the bay

280 Twenty active upwelling events were identified during the six-month period, spanning a
281 range of intensities and durations (Fig. 1b). To compare events, we constructed composites
282 aligned to onset and demise (t = 0) based on regional wind forcing, characterizing upwelling
283 phenology and its impacts inside Coliumo Bay (Fig. 3). At onset, strengthening southerlies (Fig.
284 3a, left panels) generated positive meridional wind stress ($\tau_y > 0$) and offshore Ekman transport
285 over the shelf. The composite response showed surface salinity increased within <12 h, sea-
286 surface temperature cooled after ~23 h, and dissolved CH_4 rose after ~32 h. The longer CH_4 lag

likely reflects accumulation in bottom waters and subsequent vertical advection/ventilation into the surface layer (Farías, Tenorio, et al., 2021).

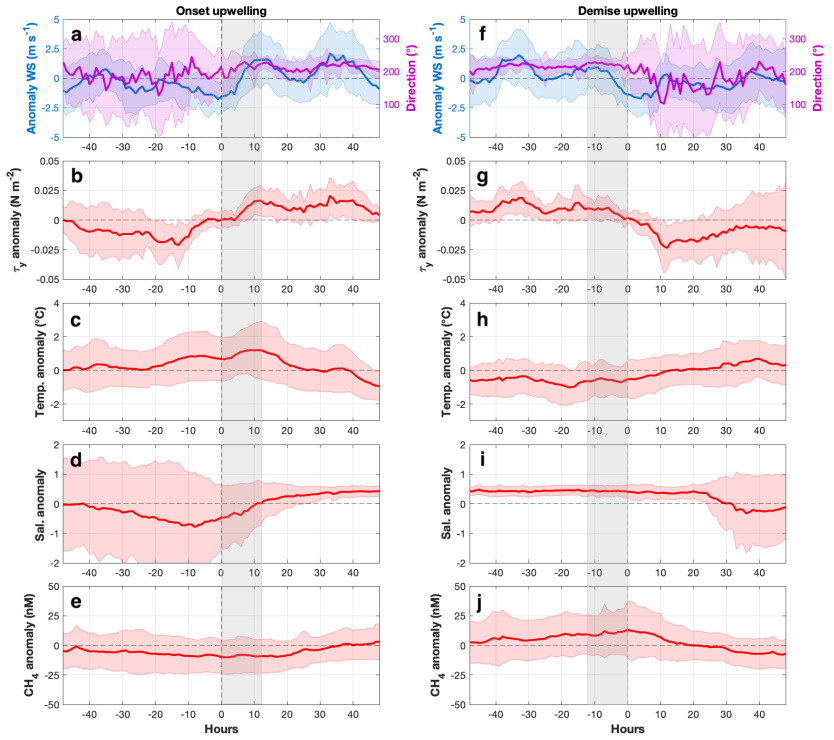

Figure 3. Composite analysis at upwelling onset (left column) and demise (right). (**a**, **f**) wind-speed anomaly (m s^{-1}) and wind direction (°); (**b**, **g**) alongshore wind-stress (τy; N m^{-2}); (**c**, **h**) temperature (°C); (**d**, **i**) salinity; (**e, j**) dissolved CH_4 (nM) anomalies. Shaded area represents the standard deviation. Vertical gray bar denotes the 12 h after onset and before demise.

Consistent with this, leading salinity and temperature anomalies originated from water just below the mixed layer, first, a near-surface salinity increase as intruding ESSW reached the surface, followed by slower cooling because daytime heating and stratification delayed the full thermal adjustment. In eastern boundary upwelling systems, equatorward (southerly) alongshore winds drive offshore surface Ekman transport lowering coastal sea level and inducing compensating onshore flow at depth. This return flow advected cold, saline ESSW into semi-enclosed bays through their mouths and along the bed (Largier, 2020; Valle-Levinson et al., 2003). In our events, intensified southerlies and the associated pressure gradients favored shelf–bay

intrusions of colder, saltier water (Sobarzo et al., 2007). Upwelling thus ventilates CH_4-enriched, O2-poor subsurface waters and sedimentary sources, elevating surface CH_4 patterns also documented in other coastal upwelling systems (Kock et al., 2008; Morgan et al., 2019; Naqvi et al., 2010).

By contrast, during relaxation or northerlies (Fig. 3, right panels), τ_y turned negative, surface Ekman transport became onshore, surface waters warmed within ~10 h, and dissolved CH_4 decreased. These conditions are often associated with the passage of mid-latitude cyclones, low-pressure systems, and rainfall (Garreaud et al., 2002). The reduction in surface CH_4 to ~10 nM is consistent with the onshore advection of Subantarctic Surface Water (SAAW), which is CH_4-poor (5–7 nM; Farías, Troncoso, et al., 2021). Although creeks can deliver CH_4-rich freshwater (Rocher-Ros et al., 2023) as those measured by Dichato creek (45-1089 nM, unpublished data); no clear event-scale relationship was found in this study, suggesting that downwelling dominates the bay's dynamics (Sobarzo et al., 2022). Rapid warming reflects intrusion of warmer surface waters plus diurnal heating, while salinity decreases after ~30 h indicates an internal-circulation response within the bay (Largier, 2020). Therefore, the synoptic coherence among CH_4, wind, temperature, and salinity indicate strong coupling to vertical advection of CH_4-rich O_2-poor waters, during different phases and intensity of upwelling events in Coliumo Bay (Fig. 1 and 3).

3.5 Diel variability

The mean diurnal cycles of atmospheric (radiation, air temperature, wind) and surface oceanic (e.g., temperature) variables (Fig. S5) revealed a well-defined pattern in the study area (Aguirre et al., 2021; R. C. Muñoz, 2008; Sobarzo et al., 2010), with coherent atmospheric–oceanic responses to solar forcing and a canonical land–sea breeze driven by differential land–ocean heating (Garreaud & Muñoz, 2005). CH_4 time series showed a minor but non-significant diurnal cycle, hourly anomalies exhibited slight nighttime–early-morning accumulation (~2 nM; 20:00–09:00; Fig. S5e) covarying with temperature and wind (Fig. S5c, d), consistent with higher solubility at lower temperatures and weaker winds that reduce ventilation, whereas daytime heating and stronger winds enhanced outgassing and mixing/ventilation, lowering surface CH_4. Nighttime standard deviations were larger, indicating greater short-term variability under calmer conditions, this suggest a biogeochemistry contributes. At night, heterotrophic activity can stimulate methylotrophic methanogenesis and diel zooplankton migration enhances micro-anoxic niches and substrates, while CH_4 oxidation intensifies, offsetting accumulation (Van Grinsven et al., 2021; T. Klintzsch et al., 2020; Wäge et al., 2020).

4 Conclusions

During the upwelling season, CH_4 variability was dominated by low-frequency (>10 d; 52.1%), followed by synoptic (3–10 d; 40.3%) and a weak diurnal band (2.5%). The intraseasonal mode set the background against which synoptic events modulated CH_4, via alternation and duration of active/relaxed upwelling and downwelling that drove advection of cold, saline, CH_4-enriched, low-O_2 ESSW into the bay, yielding significantly higher CH_4 during active upwelling than during relaxation/downwelling. Composite analyses support the observed CH_4-anomaly patterns and their physical forcing. Although wind and temperature (but not salinity) showed strong diurnal signals, CH_4 exhibited only a modest diel cycle reflecting the land–sea breeze and solar

heating. High-frequency observations are essential to resolve short-term CH_4 drivers and reduce bias in coastal emission estimates. Intensifying alongshore winds and more frequent synoptic extremes—together with shelf warming/deoxygenation, continental inputs, and local eutrophication—may enhance CH_4-rich intrusions and ventilation, widening variability, amplifying peaks, and increasing net fluxes; this underscore upwelling margins role in the global CH_4 budget and the need for sustained high-frequency monitoring to inform climate models.

Acknowledgments

Thanks to Agencia Nacional de Investigación y Desarrollo (ANID) for grand 21220537 (ST), FONDECYT 1250210 (LF and DN). Marcos Avendaño, Víctor Mora and Marcelo Ramirez, technician's LOFEC COPAS, PROGRAMA DE OBSERVACION COSTERA from Department of Oceanography (DOCE) from University of Concepcion and Crew members of the Kay Kay II.

Open Research

Data Availability Statement

The data sets presented in this study are accessible at

Pangaea (https://issues.pangaea.de/browse/PDI-42498) **e-mail:** stenorio@udec.cl **PW:** Datos123+

Conflict of Interest Disclosure

The authors declare there are no conflicts of interest for this manuscript.

Figure 1. Hourly time series of **a.** stick diagram of wind stress (N m^{-2}), arrow length and direction indicate magnitude and flow direction, respectively; **b.** upwelling index (m^3 s^{-1}); (**c**-**e**) anomalies of temperature (°C); salinity (psu); and dissolved methane (nM) Coliumo Bay (September 2024-February 2025). Vertical gray bars indicate active upwelling. Black lines in **c**-**e** represent high-pass (<15 d) Lanczos-filtered. Numbers with R denotes relaxed (relaxation/downwelling).

Figure 2. Wavelet power spectra of **a.** zonal wind stress (τx), **b.** meridional wind stress (τy), **c.** temperature, **d.** salinity, and **e.** dissolved methane in Coliumo Bay (September 2024-February 2025). The color scale indicates normalized power. Thick black contours denote 90% confidence level. Shading indicates the cone of influence (edge effects). Time series were Lanczos high-pass filtered (<15 d).

Figure 3. Composite analysis at upwelling onset (left column) and demise (right). (**a**, **f**) wind-speed anomaly (m s^{-1}) and wind direction (°); (**b**, **g**) alongshore wind-stress (τy; N m^{-2}); (**c**, **h**) temperature (°C); (**d**, **i**) salinity; (**e, j**) dissolved CH_4 (nM) anomalies. Shaded area represents the standard deviation. Vertical gray bar denotes the 12 h after onset and before demise.

Table 1. Variance (%) from SSA (Singular Spectrum Analysis) modes and frequency bands for methane, temperature, and wind. Mode 1 (*) represents the low-frequency trend (>10 days). "Diurnal" and "synoptic" sum SSA eigenpairs whose reconstructed components show dominant spectral peaks at 20–24 h and 3–10 d, respectively. Percentages do not sum 100% because only a subset of modes is reported; the remainder is considered noise.

References

Aguirre, C., Garreaud, R., Belmar, L., Farías, L., Ramajo, L., & Barrera, F. (2021). High-frequency variability of the surface ocean properties off central Chile during the upwelling season. *Frontiers in Marine Science*, *8*(702051), 1–19. https://doi.org/10.3389/fmars.2021.702051

Bakker, D., Bange, H., Gruber, N., Johannessen, T., Upstill-Goddard, R. C., Borges, A., et al. (2014). Air–sea interactions of natural long-lived greenhouse gases (CO2, N2O, CH4) in a changing climate. In P. S. Liss & M. T. Johnson (Eds.), *Ocean-Atmosphere Interactions of Gases and Particles* (pp. 113–169). Springer. https://doi.org/https://doi.org/10.1007/978-3-642-25643-1_3

Bakun, A. (1973). Coastal upwelling indices, west coast of North America, 1946-71. *NOAA Technical Report NMFS SSRF-671*. Retrieved from https://repository.library.noaa.gov/view/noaa/9041

Bizic, M. (2021). Phytoplankton photosynthesis: An unexplored source of biogenic methane emission from oxic environments. *Journal of Plankton Research*, *43*(6), 822–830. https://doi.org/10.1093/plankt/fbab069

Borges, A. V., Speeckaert, G., Champenois, W., Scranton, M. I., & Gypens, N. (2017). Productivity and Temperature as Drivers of Seasonal and Spatial Variations of Dissolved Methane in the Southern Bight of the North Sea. *Ecosystems*, *21*(4), 583–599. https://doi.org/10.1007/s10021-017-0171-7

Broullón, E., Franks, P. J. S., Fernández Castro, B., Gilcoto, M., Fuentes-Lema, A., Pérez-Lorenzo, M., et al. (2023, June 1). Rapid phytoplankton response to wind forcing influences productivity in upwelling bays. *Limnology And Oceanography Letters*. John Wiley and Sons Inc. https://doi.org/10.1002/lol2.10309

Brown, I. J., Kitidis, V., & Rees, A. P. (2023). Simultaneous high-precision, high-frequency measurements of methane and nitrous oxide in surface seawater by cavity ring-down spectroscopy. *Frontiers in Marine Science*, *10*. https://doi.org/10.3389/fmars.2023.1197727

Dølven, K. O., Vierinen, J., Grilli, R., Triest, J., & Ferré, B. (2022). Response time correction of slow-response sensor data by deconvolution of the growth-law equation. *Geoscientific Instrumentation, Methods and Data Systems*, *11*(2), 293–306. https://doi.org/10.5194/gi-11-293-2022

Farías, L., Troncoso, M., Sanzana, K., Verdugo, J., & Masotti, I. (2021). Spatial distribution of dissolved methane over extreme oceanographic gradients in the Subtropical Eastern South Pacific (17° to 37°S). *Journal of Geophysical Research: Oceans*, *126*(5). https://doi.org/10.1029/2020JC016925

Farías, L., Tenorio, S., Sanzana, K., & Faundez, J. (2021). Temporal methane variability in the water column of an area of seasonal coastal upwelling: A study based on a 12 year time series. *Progress in Oceanography*, *195*. https://doi.org/10.1016/j.pocean.2021.102589

Garreaud, R. D., & Muñoz, R. C. (2005). The Low-Level Jet off the West Coast of Subtropical South America: Structure and Variability. *American Meteorological Society*, (133), 2247–2261. https://doi.org/https://doi.org/10.1175/MWR2972.1

Garreaud, R. D., Rutllant, J. A., & Fuenzalida, H. (2002). Coastal Lows along the Subtropical West Coast of South America: Mean Structure and Evolution. *American Meteorological Society*, *130*, 75–88. https://doi.org/https://doi.org/10.1175/1520-0493(2002)130<0075:CLATSW>2.0.CO;2

Garreaud, R. D., Jacques-Coper, M., Marín, J. C., & Narváez, D. A. (2024). Atmospheric Rivers in South-Central Chile: Zonal and Tilted Events. *Atmosphere*, *15*(4). https://doi.org/10.3390/atmos15040406

Van Grinsven, S., Oswald, K., Wehrli, B., Jegge, C., Zopfi, J., Lehmann, M. F., & Schubert, C. J. (2021). Methane oxidation in the waters of a humic-rich boreal lake stimulated by photosynthesis, nitrite, Fe(III) and humics. *Biogeosciences*, *18*(10), 3087–3101. https://doi.org/10.5194/bg-18-3087-2021

IPCC. (2021). *Climate change 2021: the physical science basis. Working Group I contribution to the IPCC sixth assessment report*. Cambridge University Press. https://doi.org/https://doi.org/10.1017/9781009157896

Jakobs, G., Holtermann, P., Berndmeyer, C., Rehder, G., Blumenberg, M., Jost, G., et al. (2014). Seasonal and spatial methane dynamics in the water column of the central Baltic Sea (Gotland Sea). *Continental Shelf Research*, *91*, 12–25. https://doi.org/10.1016/j.csr.2014.07.005

Karl, D., & Tilbrook, B. (1994). Production and transport of methane in oceanic particulate organic matter. *Nature*, *368*, 732–734. https://doi.org/https://doi.org/10.1038/368732a0

Karl, D., Beversdorf, L., Björkman, K., Church, M., Martinez, A., & DeLong, E. (2008). Aerobic production of methane in the sea. *Nature Geoscience*, *1*, 473–478. https://doi.org/10.1038/ngeo234

Klintzsch, T., Langer, G., Wieland, A., Geisinger, H., Lenhart, K., Nehrke, G., & Keppler, F. (2020). Effects of temperature and light on methane production of widespread marine phytoplankton. *Journal of Geophysical Research: Biogeosciences*, *125*(9), 1–16. https://doi.org/10.1029/2020JG005793

435 Klintzsch, Thomas, Langer, G., Nehrke, G., Wieland, A., Lenhart, K., & Keppler, F. (2019). Methane production by
436 three widespread marine phytoplankton species: release rates, precursor compounds, and relevance for the
437 environment. *Biogeosciences*, *16*, 4129–4144. https://doi.org/https://doi.org/10.5194/bg-16-4129-2019
438 Kock, A., Gebhardt, S., & Bange, H. W. W. (2008). Methane emissions from the upwelling area off Mauritania (NW
439 Africa). *Biogeosciences*, *5*(4), 1119–1125. https://doi.org/10.5194/bg-5-1119-2008
440 Lachkar, Z., Cornejo-D'Ottone, M., Singh, A., Arístegui, J., Dewitte, B., Fawcett, S., et al. (2024, March 7).
441 Biogeochemistry of greenhouse gases in coastal upwelling systems: Processes and sensitivity to global change.
442 *Elementa*. University of California Press. https://doi.org/10.1525/elementa.2023.00088
443 Largier, J. L. (2020). Upwelling Bays: How Coastal Upwelling Controls Circulation, Habitat, and Productivity in
444 Bays. *Annual Review of Marine Science*. https://doi.org/https://doi.org/10.1146/annurev-marine-010419-
445 011020
446 Lerczak, J. A., Hendershott, M. C., & Winant, C. D. (2001). Observations and modeling of coastal internal waves
447 driven by a diurnal sea breeze. *Journal of Geophysical Research: Oceans*, *106*(C9), 19715–19729.
448 https://doi.org/10.1029/2001jc000811
449 Liu, Z. (2025). Taylor diagram class . *MATLAB Central File Exchange*. Retrieved from
450 https://la.mathworks.com/matlabcentral/fileexchange/130889-taylor-diagram-class
451 Mao, S. H., Zhang, H. H., Zhuang, G. C., Li, X. J., Liu, Q., Zhou, Z., et al. (2022). Aerobic oxidation of methane
452 significantly reduces global diffusive methane emissions from shallow marine waters. *Nature Communications*,
453 *13*(1). https://doi.org/10.1038/s41467-022-35082-y
454 McAuliffe, C. (1963). Solubility in water of C1-C9 hydrocarbons. *Nature*, *200*(4911), 1092–1093.
455 https://doi.org/https://doi.org/10.1038/2001092a0
456 Morgan, E. J., Lavric, J. V., Arévalo-Martínez, D. L., Bange, H. W., Steinhoff, T., Seifert, T., & Heimann, M. (2019).
457 Air-sea fluxes of greenhouse gases and oxygen in the northern Benguela Current region during upwelling events.
458 *Biogeosciences*, *16*(20), 4065–4084. https://doi.org/10.5194/bg-16-4065-2019
459 Muñoz, R. C. (2008). Diurnal cycle of surface winds over the subtropical southeast Pacific. *Journal of Geophysical*
460 *Research Atmospheres*, *113*(13). https://doi.org/10.1029/2008JD009957
461 Muñoz, Ricardo C, & Garreaud, R. D. (2005). Dynamics of the Low-Level Jet off the West Coast of Subtropical South
462 America. *American Meteorological Society*, 3661–3677. https://doi.org/https://doi.org/10.1175/MWR3074.1
463 Naqvi, S. W. A., Bange, H. W., Farías, L., Monteiro, P. M. S., Scranton, M. I., & Zhang, J. (2010). Marine
464 hypoxia/anoxia as a source of CH4and N2O. *Biogeosciences*, *7*, 2159–2190. https://doi.org/10.5194/bg-7-2159-
465 2010
466 Nelson, C. Scott. (1977). Wind stress and wind stress curl over the California current, 1–87.
467 https://doi.org/10.5962/bhl.title.60783
468 Reeburgh, W. S. (2007). Oceanic methane biogeochemistry. *American Chemical Society*, *107*, 486–513.
469 https://doi.org/10.1021/cr050362v
470 Resplandy, L., Hogikyan, A., Müller, J. D., Najjar, R. G., Bange, H. W., Bianchi, D., et al. (2024). A Synthesis of
471 Global Coastal Ocean Greenhouse Gas Fluxes. *Global Biogeochemical Cycles*, *38*(1).
472 https://doi.org/10.1029/2023GB007803
473 Rocher-Ros, G., Stanley, E. H., Loken, L. C., Casson, N. J., Raymond, P. A., Liu, S., et al. (2023). Global methane
474 emissions from rivers and streams. *Nature*, *621*(7979), 530–535. https://doi.org/10.1038/s41586-023-06344-6
475 Rosentreter, J. A., Borges, A. V., Deemer, B. R., Holgerson, M. A., Liu, S., Song, C., et al. (2021). Half of global
476 methane emissions come from highly variable aquatic ecosystem sources. *Nature Geoscience*, *14*(4), 225–230.
477 https://doi.org/10.1038/s41561-021-00715-2
478 Roth, F., Sun, X., Geibel, M. C., Prytherch, J., Brüchert, V., Bonaglia, S., et al. (2022). High spatiotemporal variability
479 of methane concentrations challenges estimates of emissions across vegetated coastal ecosystems. *Global*
480 *Change Biology*. https://doi.org/10.1111/gcb.16177
481 Saunois, M., Martinez, A., Poulter, B., Zhang, Z., Raymond, P. A., Regnier, P., et al. (2025). Global Methane Budget
482 2000–2020. *Earth System Science Data*, *17*(5), 1873–1958. https://doi.org/10.5194/essd-17-1873-2025
483 Sobarzo, M., Bravo, L., Donoso, D., Garcés-Vargas, J., & Schneider, W. (2007). Coastal upwelling and seasonal
484 cycles that influence the water column over the continental shelf off central Chile. *Progress in Oceanography*,
485 *75*(3), 363–382. https://doi.org/10.1016/j.pocean.2007.08.022
486 Sobarzo, M., Bravo, L., & Moffat, C. (2010). Diurnal-period, wind-forced ocean variability on the inner shelf off
487 Concepción, Chile. *Continental Shelf Research*, *30*(20), 2043–2056. https://doi.org/10.1016/j.csr.2010.10.004
488 Sobarzo, M., Soto-Riquelme, C., Flores, R. P., & Saldías, G. S. (2022). Synoptic Flow Variability in a River-
489 Influenced Inner Shelf off Central Chile. *Journal of Marine Science and Engineering*, *10*(4).
490 https://doi.org/10.3390/jmse10040501

Strub, T., Combes, V., Shillington, F. A., & Pizarro, O. (2013). Currents and processes along the eastern boundaries. In *International Geophysics* (Vol. 103, pp. 339–384). Academic Press. https://doi.org/10.1016/B978-0-12-391851-2.00014-3

Tenorio, S. E., & Farías, L. (2024). Picoplanktonic methane production in eutrophic surface waters. *Biogeosciences*, *21*(8), 2029–2050. https://doi.org/10.5194/bg-21-2029-2024

Testa, G., Masotti, I., & Farías, L. (2018). Temporal variability in net primary production in an upwelling area off central Chile (36°S). *Frontiers in Marine Science*, *5*(179), 1–17. https://doi.org/10.3389/fmars.2018.00179

Torrence, C., & Compo, G. P. (1998). A Practical Guide to Wavelet Analysis. *Bulletin of the American Meteorological Society*, *79*(1), 61–78. https://doi.org/https://doi.org/10.1175/1520-0477(1998)079<0061:APGTWA>2.0.CO;2

UNESCO. (1981). Background Papers and Supporting Data on the International Equation of State of Seawater 1980. *UNESCO Technical Papers in Marine Science*, (38), 1. Retrieved from https://fermi.jhuapl.edu/denscalc/unesco1981.pdf#:~:text=The%20International%20Equation%20of%20State%2C%201980%20has,the%20Ocean%20(IAPSO)%20in%20December%201979%2C%20the

Valle-Levinson, A., Atkinson, L. P., Figueroa, D., & Castro, L. (2003). Flow induced by upwelling winds in an equatorward facing bay: Gulf of Arauco, Chile. *Journal of Geophysical Research: Oceans*, *108*(2). https://doi.org/10.1029/2001jc001272

Vautard, R., Yiou, P., & Ghil, M. (1992). Singular-spectrum analysis: A toolkit for short, noisy chaotic signals. *Physica D*, *58*(58), 95–126. https://doi.org/https://doi.org/10.1016/0167-2789(92)90103-T

Wäge, J., Schmale, O., & Labrenz, M. (2020). Quantification of methanogenic Archaea within Baltic Sea copepod faecal pellets. *Marine Biology*, *167*(10). https://doi.org/10.1007/s00227-020-03759-x

Weber, T., Wiseman, N. A., & Kock, A. (2019). Global ocean methane emissions dominated by shallow coastal waters. *Nature Communications*, *10*(1), 1–10. https://doi.org/10.1038/s41467-019-12541-7

Wiesenburg, D. A., & Guinasso, N. L. (1979). Equilibrium solubilities of methane, carbon monoxide, and hydrogen in water and sea water. *American Chemical Society*, *24*(4), 356–360. https://doi.org/https://doi.org/10.1021/je60083a006

Wilson, S. T., Ferrón, S., & Karl, D. M. (2017). Interannual Variability of Methane and Nitrous Oxide in the North Pacific Subtropical Gyre. *Geophysical Research Letters*, *44*(19), 9885–9892. https://doi.org/10.1002/2017GL074458

Wilson, S. T., Al-Haj, A. N., Bourbonnais, A., Frey, C., Fulweiler, R. W., Kessler, J. D., et al. (2020). Ideas and perspectives: A strategic assessment of methane and nitrous oxide measurements in the marine environment. *Biogeosciences*, *17*(22), 5809–5828. https://doi.org/10.5194/bg-17-5809-2020

4.3 CAPÍTULO 3: DETERMINAR Y COMPARAR ESTIMACIONES FLUJOS DE CH4 DERIVADAS DE SERIES DE ALTA (HORARIAS) Y BAJA FRECUENCIA (MENSUALES) PARA CUANTIFICAR EL SESGO POR SUBMUESTREOS Y LA REDUCCIÓN DE INCERTIDUMBRE EN EMISIONES COSTERAS.

Intercambio de metano con la atmosfera medido con series de baja frecuencia

Basado en muestreos mensuales realizados durante 12 años, la estimación de flujos de CH_4 fueron siempre positivos (hacia la atmósfera), fluctuando entre 1,27 y 47,02 µmol m^{-2} d^{-1} con máximos estacionales durante primavera-verano (Tabla 3). Cuando los flujos se agrupan entre estaciones del año definidas como favorable y no favorable a la surgencia, el intercambio de CH_4 con la atmosfera fue de 8,1 µmol m^{-2} d^{-1} y 3,6 µmol m^{-2} d^{-1}, respectivamente. Sin embargo, ambos periodos no mostraron diferencias estadísticamente significativas ($p > 0.05$), lo que sugiere que el control físico-biogeoquímico sobre la emisión atmosférica es más complejo y no responde de forma lineal al patrón de surgencia. Un análisis de incertidumbre para cada régimen estacional (surgencia vs. no-surgencia), indica que la mayor variabilidad estacional se observa en el periodo de no surgencia (CV: 55 %, Tabla 2), indicando una mayor consistencia y predictibilidad en los flujos durante los meses de surgencia (Sep-Abr) y una mayor variabilidad en el periodo de no surgencia, posiblemente asociada a aspectos biogeoquímicos (ver Cap. 4) o mayor inestabilidad física debido a paso de frentes de mal tiempo, o procesos transitorios de corto tiempo como eventos de fuerte mezcla vertical, lluvias extremas o ríos atmosféricos.

Tabla 3. Resumen estadístico de las incertidumbres del flujo aire-mar de CH_4 estimadas para la serie mensual. IC95%: Intervalo de confianza del 90% (semi-ancho), es la incertidumbre del promedio en término de porcentaje.

Escala / meses	Escala/año	N° bloques	Min por grupo (µmol m^{-2} d^{-1})	Max por grupo (µmol m^{-2} d^{-1})	Media por grupo	SD	CV (%)	Error estándar (µmol m^{-2} d^{-1})	IC95 (%)
Serie total	12 años	1	1,27	47,01	10,94	7,48	68,32	1,05	18,78
Régimen	Surgencia	13	8,10	21,19	12,60	4,04	32,04	1,09	16,91
Régimen	No-surgencia	12	3,64	20,27	8,75	4,81	55,02	1,33	29,35
Estacional	Dic, Ene, Feb	12	7,09	28,86	15,17	5,90	38,88	1,63	21,03
Estacional	Mar, Abr, May	13	1,63	18,25	7,26	4,33	59,66	1,13	30,33
Estacional	Jun, Jul, Ago	12	2,15	20,27	9,09	5,02	55,21	1,37	29,40
Estacional	Sep, Oct, Nov	12	4,83	23,61	12,72	5,19	40,83	1,44	22,17
Interanual	12 m	13	6,42	18,90	11,22	3,76	33,55	1,00	17,56
	6 m	25	3,55	24,80	10,76	4,73	44,02	0,93	16,95
	3 m	49	1,63	28,99	11,22	5,94	52,96	0,84	14,45

En este periodo estudiado (2007–2019), se detectó una variabilidad interanual significativa en las concentraciones e inventarios de CH_4, tanto en la subsuperficial ($p<0,000$), como en la superficie ($p=0,006$). Años como 2009/10 y 2014/15, coincidentes con eventos El Niño moderados mostraron una ausencia de acumulación de CH_4 en el fondo, asociada a condiciones hidrográficas anómalas (mayor oxigenación, salinidad y temperatura). Esto sugiere un debilitamiento de la surgencia y una alteración en la eficiencia de acumulación de CH_4. En contraste, el año 2016/17 mostró una acumulación anómala de CH_4 en toda la columna de agua, coincidiendo con un evento de transición post-El Niño. Cabe destacar que la productividad (Chl-a) y el oxígeno disuelto no mostraron variaciones interanuales significativas como las del CH_4, lo que reafirma su mayor sensibilidad a forzamientos climáticos interanuales y condiciones locales

subóxicas. Estas condiciones se ven reflejadas en los flujos de CH_4, que también presentaron una variabilidad interanual (Figura 3), donde valores más altos se registraron durante periodos frío de 2016–2017 y 2017–2018 (~20 µmol m^{-2} d^{-1}), mientras que los más bajos ocurrieron en 2009–2010 (~4,7 µmol m^{-2} d^{-1}), confirmando el impacto directo de los eventos ENSO en el forzamiento y ventilación de CH_4 en sistemas de surgencia.

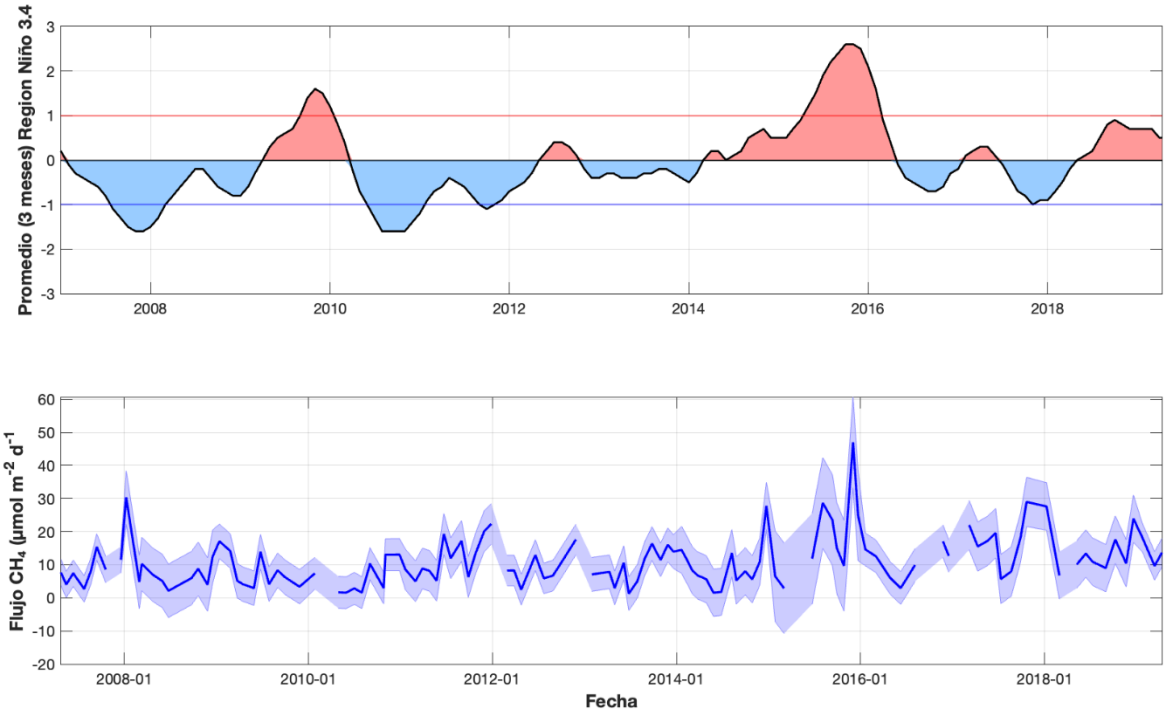

Figura 3. Índice de El Niño en la región 3.4 y flujos de metano hacia la atmósfera durante 2007 – 2019.

Estacionalmente, los mayores flujos medios se registraron en verano (15,2 µmol m^{-2} d^{-1}) y primavera (12,7µmol m^{-2} d^{-1}), coherentes con la intensificación del viento. Por el contrario, los mínimos se observaron en otoño e invierno con 7,3 µmol m^{-2} d^{-1} y 9,3 µmol m^{-2} d^{-1}, respectivamente. Las incertidumbres siguieron el mismo patrón del regimen

estacional (Tabla 2), lo que refuerza la mayor estabilidad del régimen de surgencia frente a la variabilidad de los meses de otoño e invierno.

A escala interanual, la incertidumbre fue menor (17 %), en comparación con las escalas estacionales, esto indicaría perturbaciones significativas dadas por las estaciones en el promedio climatológico del CH_4 y sus flujos.

Por otro lado, al analizar las incertidumbres inter anuales y sub anuales (6 y 3 meses) con re muestreos por grupos, se observaron que las incertidumbres disminuyeron (de 17 a 14%) con el aumento de la escala temporal (Tabla 1), lo que indica que al integrar un mayor número de observaciones, las fluctuaciones de corto plazo tienden a compensarse, reduciendo la incertidumbre; a diferencia de las agrupaciones estacionales climáticas, donde los datos se agrupan por procesos similares, no obstante presentan una mayor variabilidad (CV38-59%), debido a las condiciones climáticas dada por los diferentes años (e.g. ENOS).

Intercambio de metano medido con datos de alta frecuencia en un periodo de surgencia costera

Las emisiones de CH_4 diarias durante un periodo de surgencia fueron positivas hacia la atmósfera, variaron ampliamente entre 1,6 y 94 μmol m^{-2} d^{-1}, con máximos registrado durante los eventos activos de la surgencia (Fig. 4), como los observados el 14 de septiembre de 2024, entre el 19 y 23 de diciembre de 2024 y el 24 de enero al 10 de febrero de 2025 (Fig. 4). En este estudio 103 y 50 días representaron eventos activos e inactivos de la surgencia, respectivamente. Cuando comparamos el flujo diario promedio entre ambos periodos, los eventos activos fueron 2,8 veces mayores, lo que indica el efecto

del viento en la desgasificación y el alto contenido de CH_4 en las aguas superficiales debido al evento activo de la surgencia.

Eventos extremos (>40 µmol m^{-2} d^{-1}, considerando el doble del promedio total: ~18,8 µmol m^{-2} d^{-1}) abarcaron el 11% (20 días) del periodo estudiado y tuvieron mayor incidencia en periodos activos de la surgencia (eventos A2, A11, A12, A16 y A17), asociado a vientos mayores a 2,6 m s^{-1} (Fig. 4B) En el periodo inactivo de la surgencia también se observaron outlayers, asociados principalmente a ráfagas o cambios en el viento (eventos I5, I6), aunque no lo suficientemente persistente como para producir un evento de surgencia activa (evento I3 en Fig. 4B).

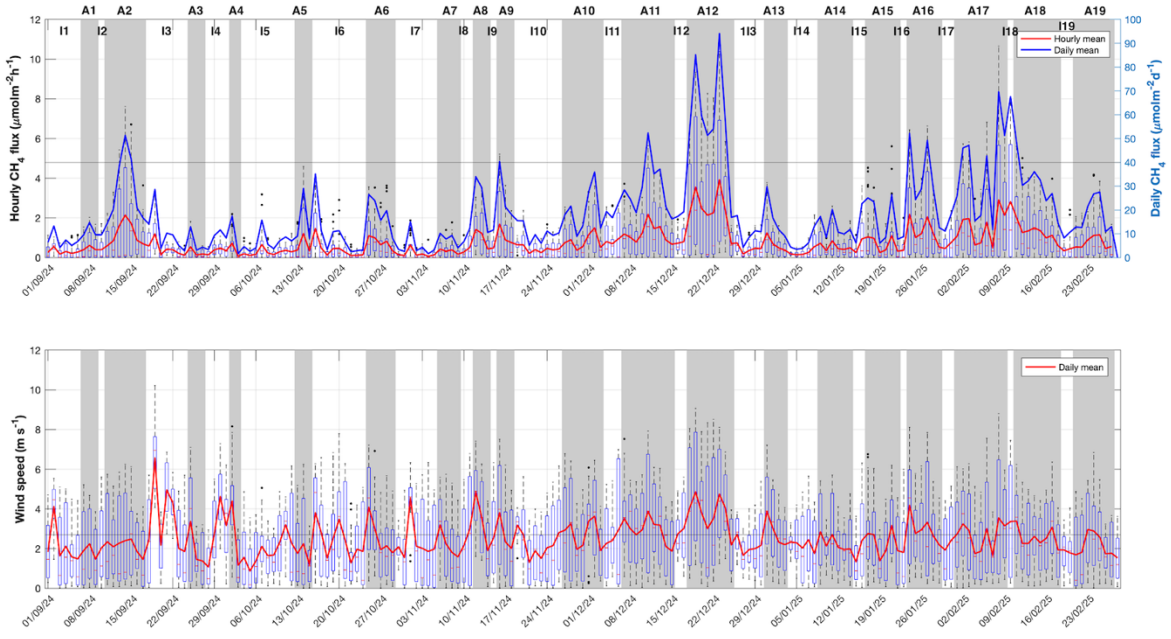

Figura 4. A. Histograma diario de los flujos horarios y acumulación diaria de los flujos de CH_4 en la Bahía de Coliumo durante un periodo de surgencia costera (Sept 2024 - Feb 2025). La línea roja representa el promedio horario de los flujos de CH_4 y la línea azul representa la acumulación diaria de los flujos de CH_4. B. Velocidad del viento (m s-1) durante un periodo de surgencia costera tomado de la estación meteorológica de Dichato del Departamento de Oceanografía de la UdeC. La línea roja representa el promedio diario de los vientos.

La figura 5 muestra el ciclo diario promedio de algunas variables atmosféricas y oceanográficas con sus respectivas desviaciones estándar. En general, las variables atmosféricas presentaron una clara señal diurna, con máximos valores durante las horas de mayor radiación. Los vientos variaron en promedio de 0,9 a 4,5 m s^{-1}, con predominancia de los vientos del sur durante la noche y vientos del oeste durante el día (Fig. 5D). Los flujos de CH_4 también mostraron una clara variabilidad diurna con valores más bajos entre las 2 y las 7 horas, con medias entre 0,9 y 1,2 μmol m^{-2} h^{-1}. Los valores más altos se registraron entre las 15 y las 18 horas, con medias que oscilaron entre 1,3 y 4,5 μmol m^{-2} h^{-1}. Los valores más bajos de flujos coincidieron con valores de vientos calmos (media ~1 m s^{-1}) con dirección hacia el N y bajas temperaturas durante la noche (Fig. 5). Se observaron flujos de CH_4 más altos después de la máxima radiación durante las horas de la tarde, con el aumento de la velocidad del viento (~4,5 m s^{-1}) y el cambio de dirección del viento hacia el este, coincidente con la predominancia de la componente U del viento (Fig. 5B).

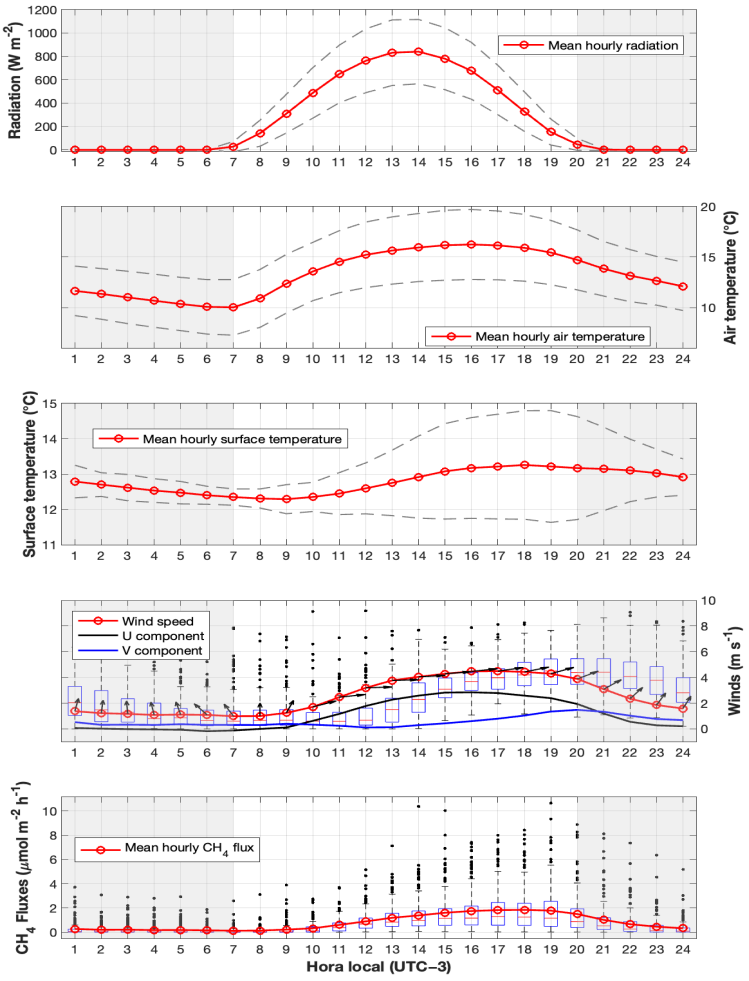

Figura 5. Climatología horaria de la A. Radiación (W/m2), B. Temperatura del aire (°C), C. Temperatura sueprficial de la bahía de Coliumo, D. Vientos de la estación meteorológica de la estación de Dichato, las flechas en negro representan la dirección del viento (de donde viene) y E. flujos CH_4 en la Bahía de Coliumo durante un periodo de surgencia costera (Sept 2024 - Feb 2025). La línea roja representa el promedio horario de las variables.

En la tabla 4 se muestra un resumen estadístico de la variabilidad de los flujos de CH_4 a diferentes escalas temporales para evaluar la incertidumbre de los flujos calculados. En general el promedio suavizó todos los peaks de emisiones de CH_4, observándose el mismo valor en todas las escalas temporales, esto es debido al método utilizado, ya que

los bloques se forman a partir de la misma serie completa. Sin embargo, estadísticos como los mínimos y máximos variaron ampliamente, con un rango mucho mayor en la escala temporal más corta del orden de un día, acotándose hacia la escala mensual (30d). Además, se observó una varianza (CV) más alta a una escala temporal corta (por ejemplo, CV ∼86.38 % a los 1 d), pero con menor porcentaje de incertidumbre (12.5%), lo que indica que los intervalos cortos capturan mucha variabilidad y la verdadera dinámica de los flujos de CH_4.

Tabla 4. Resumen estadístico de las incertidumbres del flujo aire-mar de CH_4 estimadas para la serie temporal de alta frecuencia.

Serie	Días	N de bloques (n)	Min (µmol m^{-2} d^{-1})	Max (µmol m^{-2} d^{-1})	Prom (µmol m^{-2} d^{-1})	DS (µmol m^{-2} d^{-1})	CV (%)	ES (µmol m^{-2} d^{-1})	IC95 (%)
HF	1	181	1,63	94,08	18,87	16,30	86,38	1.20	12,50
HF	3	60	2,85	66,47	18,86	14,08	74,66	1,80	18,94
HF	7	25	5,79	43,20	18,83	11,25	59,75	2,13	21,94
HF	15	12	8,84	37,75	18,86	9,67	51,27	2,71	27,75
HF	30	6	10,56	32,04	18,86	8,83	46,81	3,43	34,37

A escala sinóptica, las correlaciones cruzadas mostraron que los flujos de CH_4 tenían una buena correlación con los vientos (R=0,77) y están en fase (lag = 0 h), lo que significa que la respuesta del flujo de CH_4 al viento es prácticamente instantánea. Por otro lado, cuando se analizó el ciclo horario, el flujo de CH_4 también mostró una buena correlación con los vientos (R=0,99; Lag 0h), pero se observó una mayor dominancia de la componente U del viento (R = 0,99; Lag -1h), frente a la componente V (Lag = -3h). Esto significa que la brisa marina influye en la variabilidad a lo largo del día.

4.4 CAPÍTULO 4: IDENTIFICAR LOS PROCESOS/INTERACCIONES MICROBIANAS Y CONDICIONES OCEANOGRÁFICAS QUE FAVORECEN EVENTOS DE ACUMULACIÓN DE CH_4 ("HOT MOMENTS") EN LA CAPA SUPERFICIAL, MEDIANTE EXPERIMENTOS CONTROLADOS DE LABORATORIO.

En este capítulo se presentan los resultados de interpretar las principales interacciones microbianas responsables de la acumulación de CH_4 en la capa superficial. Como resultado se publicó el manuscrito: Tenorio, S. E., & Farías, L. (2024). Picoplanktonic methane production in eutrophic surface waters. *Biogeosciences*, *21*(8), 2029–2050. https://doi.org/10.5194/bg-21-2029-2024

RESUMEN

Durante la última década, se han realizado numerosas investigaciones sobre la paradoja del metano (CH_4), que implica la producción aeróbica de CH_4. Presentamos notables observaciones de sobresaturación de CH_4 dentro de la capa superficial de la zona de surgencia de Chile central (36° S, 73° W) durante dos ciclos estacionales consecutivos (2018-2021). Complementando estas observaciones, se realizaron experimentos de ciclado de CH_4, utilizando distintas fracciones de plancton (abarcando la comunidad planctónica natural, fracciones <150, <3 y <0,2 μm), en diferentes períodos de productividad de la producción y composición fitoplanctónica a lo largo del año. Nuestros hallazgos subrayan el papel fundamental del picoplancton (<3 μm) en la producción de CH_4 en la superficie del océano, que contrasta con la contribución limitada de los microorganismos de mayor tamaño (<150 μm). Notablemente, las incubaciones con

sustratos metilados, como el ácido metilfosfónico (MPn) y la trimetilamina (TMA), inducen una mayor producción de CH_4 dentro de la fracción picoplanctónica. Este fenómeno se observa consistentemente durante las temporadas de surgencia (primavera-verano austral) y de no surgencia (invierno), con significancia en el último período, cuando *Synechococcus sp*. exhibe una abundancia relativa notablemente alta. Los experimentos de microcosmos a largo plazo resaltan los roles cruciales que desempeñan las bacterias heterotróficas y las cianobacterias en la metanogénesis metilotrófica. Este proceso mejora la producción de CH_4, facilitado por el reciclaje de carbono orgánico disuelto (DOC). El picoplancton emerge como un factor fundamental que influye en el reciclaje de sustratos metilados y es responsable de mantener la sobresaturación de CH_4. Estos hallazgos proporcionan información valiosa sobre los procesos biogeoquímicos que impulsan la dinámica de CH_4, particularmente en áreas de surgencia altamente productivas.

Biogeosciences, 21, 2029–2050, 2024
https://doi.org/10.5194/bg-21-2029-2024

Biogeosciences Open Access EGU

Picoplanktonic methane production in eutrophic surface waters

Sandy E. Tenorio[1,2,4] **and Laura Farías**[1,2,3]

[1]Departamento de Oceanografía, Facultad de Ciencias Naturales y Oceanográficas, Universidad de Concepción, Concepción, 4070043, Chile
[2]Centro de Ciencia del Clima y la Resiliencia (CR2), Santiago, Chile
[3]Instituto Milenio en Socio-ecología Costera (SECOS), Santiago, Chile
[4]Programa de Graduados en Oceanografía, Departamento de Oceanografía, Universidad de Concepción, Concepción, 4070043, Chile

Correspondence: Laura Farías (laura.farias@udec.cl)

Received: 3 October 2023 – Discussion started: 9 October 2023
Revised: 27 February 2024 – Accepted: 28 February 2024 – Published: 25 April 2024

Abstract. Over the past decade, extensive research has delved into the methane (CH_4) paradox, which involves aerobic CH_4 production. We present noteworthy observations of CH_4 oversaturation within the surface layer of the central Chile upwelling zone (36° S, 73° W) over two consecutive seasonal cycles (2018–2021). Complementing these observations, CH_4 cycling experiments were conducted, utilizing distinct plankton fractions (encompassing the natural planktonic community, fractions < 150, < 3 and $< 0.2\,\mu m$), in different productivity periods of phytoplanktonic production and composition throughout the year. Our findings underscore the pivotal role of picoplankton ($< 3\,\mu m$) in CH_4 production on the ocean surface, contrasting with the limited contribution of larger microorganisms ($< 150\,\mu m$). Notably, incubations with methylated substrates, such as methylphosphonic acid (MPn) and trimethylamine (TMA), induce heightened CH_4 production within the picoplanktonic fraction. This phenomenon is consistently observed during both upwelling (austral spring–summer) and non-upwelling (winter) seasons, with significance in the latter period, when *Synechococcus sp.* exhibits notably high relative abundance. Long-term microcosm experiments highlight the crucial roles played by heterotrophic bacteria and cyanobacteria in methylotrophic methanogenesis. This process enhances CH_4 production, facilitated by the recycling of dissolved organic carbon (DOC). Picoplankton emerges as a pivotal factor influencing the recycling of methylated substrates, and it is responsible for maintaining CH_4 supersaturation. These findings provide valuable insights into the biogeochemical processes driving CH_4 dynamics, particularly in highly productive upwelling areas.

Key points.

1. Picoplankton plays a crucial role in maintaining CH_4 supersaturation in the surface layer under different oceanographic conditions, influencing its exchange with the atmosphere.
2. Methylated substrates, such as methylphosphonic acid (MPn) and trimethylamine (TMA), notably stimulate CH_4 production through picoplankton-mediated methylotrophic methanogenesis.
3. *Synechococcus sp.*, utilizing the MPn substrate during the non-upwelling season, and picoeukaryotes, utilizing the TMA substrate during the onset of upwelling, could emerge as crucial microorganisms involved in CH_4 generation.

1 Introduction

Methane (CH_4) is a short-lived yet potent greenhouse gas, exhibiting a significantly higher heat-trapping capacity than CO_2 over a century. Its importance lies in its substantial influence on global climate dynamics and the necessity for robust mitigation strategies (IPCC, 2021; Harmsen et al., 2020). The ocean holds considerable amounts of dissolved and hydrate CH_4, rendering its thorough study crucial for precise climate change modeling and comprehending its ecological diversification within oceanic ecosystems (IPCC, 2021; Xu et al., 2022).

Published by Copernicus Publications on behalf of the European Geosciences Union.

The distribution of CH_4 is intricate and influenced by both complex physical (transport) and biogeochemical (production and consumption rates) processes (Reeburgh, 2007). In the open ocean, surface waters generally display slight oversaturation, whereas deeper waters tend toward equilibrium or undersaturation with respect to the atmosphere. However, there is often CH_4 accumulation within the pycnocline (Lamontagne et al., 1973; Cicerone and Oremland, 1988; Holmes et al., 2000). These distribution patterns led to the identification of the CH_4 paradox (see review in Reeburgh, 2007). Early hypotheses have suggested various sources for CH_4 oversaturation in the surface layer, including organic matter respiration within anoxic niches of particulate organic material (Karl and Tilbrook, 1994), within fish (Oremland, 1979) and in zooplankton guts (De Angelis and Lee, 1994). However, these classical methanogenesis pathways remain obscured in the surface and oxic zone of aquatic systems. Subsequent advancements in this field highlighted biochemical processes, such as methylotrophic methanogenesis, now understood as the production of CH_4 from methylated compounds under diverse biogeochemical conditions (Karl et al., 2008; Damm et al., 2010, 2015; Repeta et al., 2016).

Methylated compounds are synthesized or degraded by diverse autotrophic and heterotrophic microorganisms; for example, *Nitrosopumilus maritimus* produces phosphonates like methylphosphonic acid (MPn) (Metcalf et al., 2012), whereas different species of phytoplankton, in turn, contribute to sulfur derivates such as methionine (Lenhart et al., 2016), dimethylsulfoniopropionate (DMSP), dimethyl sulfide (DMS) (Belviso et al., 1990; Stefels and Van Boekel, 1993) and trimethylamines (TMA) (Sun et al., 2019), serving as potential carbon sources for microorganisms and thereby contributing to CH_4 generation via methylotrophic methanogenesis. Furthermore, there is a suggestion that photosynthesis plays a role in direct CH_4 production (Berg et al., 2014; León-Palmero et al., 2020; Klintzsch et al., 2023). Several studies have shown associations between CH_4 anomalies in surface waters and specific phytoplanktonic groups, such as coccolithophores (Lenhart et al., 2016) and cyanobacteria (Bižić et al., 2020). Hence, recognizing phytoplankton in various size fractions as direct links to CH_4 production in diverse marine ecosystems (Bizic, 2021) becomes imperative, especially through pathways involving demethylation from methylated compounds (Damm et al., 2010; Florez-Leiva et al., 2013; Lenhart et al., 2016; Karl et al., 2008; Sun et al., 2011; Repeta et al., 2016).

Coastal upwellings, due to their high productivity, represent an emblematic site for the study of CH_4 production, but the proximity to anoxic sediments and prevalent anaerobic methanogenesis in sediments or in the oxygen minimum zones (OMZs) often obscures the study of CH_4 generation within oxygen-rich surface waters. Indeed, CH_4 profiles predominantly exhibit significant increases towards anoxic sediments (Farías et al., 2021; Ma et al., 2020; Kock et al., 2008). Coastal regions serve as intensive CH_4 sources, facilitating lateral transport to open waters (Borges and Abril, 2012; Upstill-Goddard and Barnes, 2016) and/or the atmosphere due to vertical advection linked to coastal upwelling (Farías et al., 2021; Kock et al., 2008). Current global CH_4 balances exhibit high uncertainly (Saunois et al., 2020; Roth et al., 2022; Lu et al., 2021) and considerable spatial and temporal variability, particularly in coastal environments, where fluxes represent over 40 % of total atmospheric fluxes (Weber et al., 2019; Bange et al., 1994).

Given the upwelling systems are expected to integrate all above-mentioned mechanisms, investigating CH_4 dynamics becomes pivotal. Upwelling processes dynamically transport nutrient-rich water onto continental shelves and the surface, significantly enhancing biological productivity to eutrophic levels. This surge in high microbial productivity, biomass and organic matter decomposition establishes these areas as pivotal hubs for carbon cycling, particularly in CH_4 (Capone and Hutchins, 2013). Indeed, in upwelling systems a large part of the primary production is channeled to dissolved organic carbon (DOC) through the microbial food web and a smaller percentage directly to copepods via the herbivore food chain (Vargas et al., 2007). In addition, coastal areas receive large amounts of DOC from rivers (Bianchi, 2011), and this is also the case of upwelling systems off central Chile (Vargas et al., 2013). These microbial food web and riverine pathways not only transport and remineralize nutrients and DOC but also foster the generation of greenhouse gases like CH_4 (Dinasquet et al., 2018; Sun et al., 2019).

Crucially, specific microbial groups such as *Pelagibacter*, SAR11, considered key players in DOC recycling, have been identified as potential contributors to CH_4 regeneration from diverse C1 compounds (Carpenter et al., 2012; Repeta et al., 2016; Sun et al., 2019). The synergy between autotrophic (e.g., picoeukaryotes, cyanobacteria) and heterotrophic picoplankton ($< 3\,\mu m$) could represent pathways for CH_4 production in coastal regions. Therefore, the main aim of this study is to investigate the dynamics of CH_4 oversaturation within the surface layer of the central Chile upwelling zone using observational and experimental approaches. Among objectives are to discern the contributions of different plankton fractions, particularly picoplankton, and to unravel the involvement of methylated substrates like MPn and TMA in stimulating CH_4 production. Ultimately, this research will provide comprehensive insights into the biogeochemical mechanisms that drive CH_4 dynamics within highly productive upwelling water, emphasizing the role of picoplankton in maintaining CH_4 oversaturation in the surface ocean.

2 Material and methods

2.1 Regional setting

The continental shelf off central Chile undergoes wind-driven coastal upwelling, seasonally controlled by the migration of the South Pacific anticyclone (Strub et al., 1998). This process leads to alongshore equatorward winds during the summer–spring period, producing coastal upwelling (Sobarzo and Djurfeldt, 2004; Sobarzo et al., 2007). The area is influenced by Equatorial Subsurface Water (ESSW), which is nutrient-rich and has low dissolved O_2 levels (less than 44 µM). The ESSW interacts with sediments and serves as a nutrient source during coastal upwelling, delivering low O_2 concentrations and high organic matter content to the bottom water and sediments, fostering anaerobic organic matter mineralization supporting denitrification, sulfate reduction and methanogenesis (Ferderlman et al., 1997; Farías et al., 2004).

2.2 Water collection

Seawater was collected from the upwelling zone of central Chile (36°0.802′ S; 73°07.750′ W) at the University of Concepción's time series station (ST18), situated at a depth of 90 m (Fig. 1). Monthly samplings have been conducted on board the RV *Kay–Kay II* since 2002. Continuous sampling with a CTD-O (conductivity, temperature and depth including oxygen; SBE 19) instrument was performed to obtain temperature, salinity and dissolved oxygen (DO) profiles, whereas seawater samples using 10 L Niskin bottles at various depths (0, 5, 10, 20, 30, 50, 65 and 80 m) were obtained in triplicate for dissolved gas (DO and CH_4), nutrient and chlorophyll-*a* (chl-*a*) analysis. Detailed methodologies can be found in Farías et al. (2021). From March 2019 to June 2020, DOC samples were specifically procured from depths of 5, 20, 50 and 80 m.

To investigate the role of differently sized planktonic communities in CH_4 cycling, seawater was gathered at a depth of 10 m, a depth commonly associated with the chl-*a* peak (Testa et al., 2018). Large zooplankton (150 µm mesh sieve) were excluded using the methodologies outlined by Sieburth et al. (1978). The experimental setup is outlined in Table 1 and includes two negative controls: (1) sterile filtration using a 0.2 µm filter, an often-used method for the removal of microorganisms (Hahn, 2004), and (2) poisoning with the addition of $HgCl_2$ to ensure total inactivation of the few bacterial species which can pass through 0.2 µm filters (Hahn, 2004). The positive control was the natural community (NC) without any filtration.

Another set of experiments enriched with the organic methylated substrates MPn and TMA were performed using only the fractioned picoplanktonic community. To maintain the integrity of the samples, seawater was transported in dark and refrigerated drums placed inside expanded polystyrene boxes surrounded by ice packs to preserve the natural temperature of the seawater (∼ 13 °C) and minimize microbial activity. The average time for transportation to the Marine Station Biology Laboratory at Dichato was approximately 4 h. However, it is important to note that there were delays of 8 to 12 h between arrival at the laboratory and the onset of short- and long-term experiments, respectively. These delays were due to filtering and a short acclimatization process (6 h) required before initiating the experiments, but these procedures were done in a cool room (13 °C).

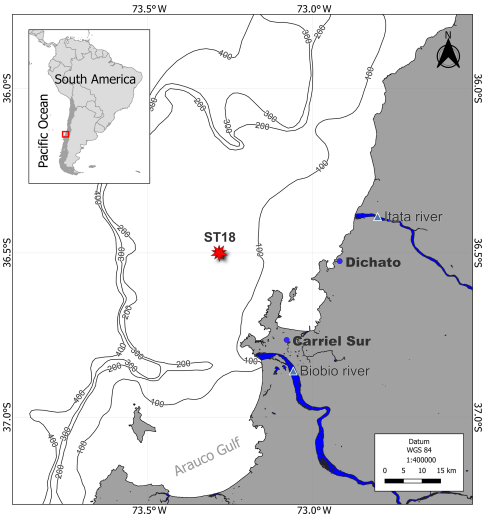

Figure 1. Time series location map (ST18) over the central Chile upwelling platform. The Itata and Biobio rivers, Carriel Sur meteorological station, and town of Dichato are indicated.

This is a time series study, from 2018 until 2021, encompassing CH_4 regeneration in different productivity phases (Table 1) according to Testa et al. (2018). In this regard, two types of experiments described in the following sections will be conducted.

2.3 Short-term experiments of CH_4 cycling from size-fractionated planktonic community enriched with organic substrates

The size fractionation of planktonic communities was conducted through a careful sequential filtration process, where 5 L of seawater was gently passed through a pre-filter of 150 µm nylon, followed by 3 µm Isopore and 0.22 µm Millipore membranes, yielding two fractions: picoplankton (< 3 µm) and femtoplankton (< 0.2 µm) communities; the last one was used as a negative control in some experiments. NC was obtained directly without filtering (Table 1).

Table 1. Summary of the experimental setup of short-term (GC vials) and long-term (microcosms) experiments with different treatments. NC: seawater with the natural plankton (control); $< 3\,\mu m$: picoplankton; $< 0.2\,\mu m$: femtoplankton (control +); $< 0.2\,\mu m + HgCl_2$: femtoplankton with $HgCl_2$ (control +); CC: picoplankton concentrate; and the addition of methylated substrates (MPn: methylphosphonic acid; TMA: trimethylamines). Different phases of the productivity period are as follows: PI – Phase I; PII – Phase II; and PIII – Phase III.

Date	Type of experiment	Setup	Plankton size (µm)	Place	Time (h)	Productivity period
December 2018	GC vials	Plankton fractionation	CN, < 3 and < 0.2	Incubator	24	High (PI)
January 2019	GC vials	Plankton fractionation	CN, < 3 and < 0.2	Incubator	24	High (PI)
March 2019	GC vials	Add: MPn	< 3	Incubator	24	Intermediate (PII)
May 2019	GC vials	Add: MPn and TMA	< 3	Incubator	24	Basal (PIII)
April 2019	Microcosms	Add: MPn and TMA	CN, < 3 and CC	Cold room	~ 60	Intermediate (PII)
September 2019	Microcosms	Add: MPn and TMA	CN, < 3 and CC	Cold room	~ 60	High (PI)

Prior to incubation, initial seawater sampling was taken for each treatment group, wherein triplicate measurements were taken of DO (125 mL), COD (60 mL), chl *a* (100 mL) and nutrients (15 mL). Subsequently, each size-fractionated sample was homogenized and swiftly transferred into 20 mL vials (108 in total, 27 per treatment). These vials were immediately sealed using rubber and aluminum caps to prevent any potential atmospheric gas contamination. The incubation of these vials took place within an FOC 225E incubator, maintained at a temperature of 13 °C and in a 12 h photoperiod (24 h). The illumination was calibrated to fall in a range of 11–11.5 $\mu mol\,m^{-2}\,s^{-1}$ using blue and neutral-density blank filters. At intervals of 4 h, three vials from each treatment (Table 1) were withdrawn and immediately poisoned with 50 µL of $HgCl_2$, and then the vials were gently agitated to ensure homogenization. Gas chromatography was employed to analyze the CH_4 content of the vials. In another set of experiments (Table 1), the picoplankton fraction was singled out to ascertain its capacity for metabolizing methylated substrates and subsequently regenerating CH_4. This involved adding MPn and TMA to the samples. The final concentration of both substrates in these treatments was maintained at 1 µM, assuming that natural concentrations in the seawater were at trace levels. Thus, these could be considered potential experiments (highly enriched). The experimental conditions remained consistent with those employed in the earlier experiment.

2.4 Long-term experiments of CH_4 cycling from size-fractionated planktonic community enriched with organic substrates

Nine microcosms were developed using a system of gas-tight polycarbonate bottles (13 L). Each microcosm contained 10 L of seawater for treatment and 3 L of headspace. They were equipped with a closed gas circuit and connected to a gas spectrometer analyzer capable of simultaneously and continuously measuring various gases, including CO_2, CH_4 and N_2O, and humidity percentage (Fig. 2). Each bottle featured a rubber cap equipped with four holes (as depicted in Fig. 2), housing a 5 mm glass capillary within each hole. These capillaries were connected to gas-tight Teflon hoses. Specifically, the first capillary extended to the middle of the headspace (1) and was linked to an accessory (16-Port Distribution Manifold A0311) of the Picarro G-2308 spectrometer for a cavity ring-down spectroscopy system (CRDS), designed for the measurement of gases in equilibrium with the aqueous phase. The second capillary was suspended within the headspace (2) and connected to a Tedlar bag (3 L) filled with N_2. This arrangement aimed to prevent imbalance when drawing water samples from the microcosm. The third capillary, also suspended in the headspace (3), was equipped with a three-way cannula and was connected to the air outlet of the Picarro G-2308 spectrometer to facilitate the recirculation of air within the headspace. This system optimization aimed to mitigate excessive headspace during spectrometer air sampling, preventing a gas–seawater phase imbalance. This hose (3) was adjustable and replaced upon measuring gas concentrations in each microcosm. The fourth glass capillary was submerged in the seawater, 3 cm from the bottom (4). It was attached to a three-way cannula, streamlining the sample extraction process.

In both April and September of 2019, a series of long-term microcosm experiments were conducted. These months were strategically chosen: the first coinciding with the transition of phytoplankton composition to nano-picoplankton (basal productivity period) and the second with diatom blooms (larger phytoplankton dominance) (high-productivity period), as highlighted in studies by Anabalón et al. (2007), Cuevas et al. (2004), and Morales and Anabalón (2012). The experiment encompassed three distinct treatments: (1) control without any methylated substrate addition in natural communities (NCs), picoplankton community ($< 3\,\mu m$) and picoplanktonic concentrated community (CC); (2) all treatments enriched with MPn; (3) and all treatments enriched with TMA (see Table 1).

The concentrated fraction of picoplankton (CC) was procured through tangential flow filtration via a 0.2 µm filter, following a procedure developed by Giovannoni et al. (1990) for harvesting greater quantities of microbial biomass and using pre-filtering steps as discussed earlier to concentrate only picoplankton ($< 3\,\mu m$). To discern whether the tangential flow

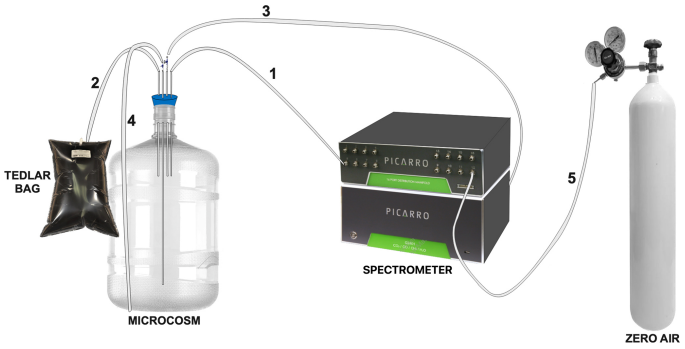

Figure 2. Assembly of the microcosm for long-term experiments (10 L). Capillary 1 is connected directly to the spectrometer. Capillary 2 is connected to a TEDLAR bag filled with N_2 (3 L). Capillary 3 is removable and connected to the outlet of the spectrometer. Capillary 4 is connected to a loose hose for water sampling, and hose 5 is connected to zero air.

filtering was effective, the abundance of cyanobacteria, picoeukaryotes and heterotrophic bacteria was measured with flow cytometry. The incubations were carried out within a controlled cold room environment, maintaining a temperature range of 12 to 13 °C, with the same illumination used in short periods over 60 h. In the initial stages, each bottle was sealed and allowed to acclimate for 6 h in darkness. Following this stage, 1 mL of MPn (10 mM stock solution) and TMA (10 mM stock solution) were introduced to each bottle, yielding a final concentration of 1 µM, matching the conditions established in prior experiments.

To prevent CH_4 residue contamination, a purge with zero air (synthetic air without CH_4 tracers) was performed (as shown in Fig. 2, line 5), ensuring accurate CH_4 concentration measurement within each microcosm and establishing a baseline. Every 4 h a cycle of CH_4 measurements was conducted continuously over 3 min, followed by a 6 min hose cleaning (used for recirculation) with zero air before connecting it to capillary 3 for subsequent measurement. It is important to note that the equipment absorbed 240 mL of air per minute of reading. Therefore, air recirculation within the microcosm, as previously mentioned, was essential. Preceding the actual experiment, the concentrations of gases measured by the spectrometer were closely monitored for 30 min, confirming that the recirculation process did not impact the measured gas concentrations.

2.5 Chemical and biological analysis

2.5.1 Dissolved methane

Once the CH_4 samples were taken, they were stored upside down at room temperature and protected from light and then analyzed through gas chromatography (GC). CH_4 (discrete samples) was determined using the phase equilibrium method (McAuliffe, 1963). In this procedure, each vial was carefully treated, with the addition of 5 mL of inert gas (helium), creating a headspace to facilitate equilibrium between the aqueous and gas phases. Subsequently, the gas phase was measured into a gas chromatography Shimadzu 17 equipped with a flame ionization detector (FID). A Restek Rt-QS-Bond column (30 m length, 0.53 mm inner diameter, 20 µm film thickness) was employed, maintained at a temperature of 30 °C with a flow of 2.6 mL min^{-1} using He as an ultrapure gas carrier.

Five-point calibration curves (linear response of the detector) were made for each monthly sample set (treatment) using a gas with a composition and concentration equivalent to that of the current atmosphere from NOAA (1863.4 ± 0.3 ppbv for CH_4) (Bullister et al., 2016) as the primary standard, as well as three standard gas mixtures (Air Liquide, USA) and zero air. In each CH_4 sample set (every treatment), standards were added at the beginning, middle and end of the measurements to corroborate the correct functioning of the detector. CH_4 measurements (triplicate) with a variation coefficient greater than 10 % were not considered.

2.5.2 Dissolved oxygen

To assess DO content, 125 mL glass flasks were used for sample collection in triplicate. These samples were immediately fixed and analyzed within 6 h of collection through the Winkler method (Carpenter, 1965). The analysis was conducted using a Dosimat 665 instrument featuring an automatic photometric endpoint detector. The detection limit for this method stood at 2 µmol L^{-1}.

2.5.3 Nutrient

Nutrient samples were collected in triplicate using a 60 mL syringe and filtered through a 0.45 µm cellulose acetate filter. The filtered content was held in 15 mL Falcon polyethylene bottles and stored at −20 °C. Analysis of these nutrient samples followed standard colorimetric techniques (Grasshoff et al., 1983) and was conducted using a SealAA3 segmented flow auto-analyzer. This analyzer featured four distinct channels, each equipped with specific modules tailored for individual nutrients.

2.5.4 Chlorophyll *a*

To quantify chl-*a* content, triplicate samples of 100 mL seawater were filtered using a GF/F filter and immediately stored at −20 °C. Analysis was performed according to the method outlined by Holm-Hansen et al. (1965). A Turner Designs 10AU fluorometer was employed for measurement, and a standard pigment served as a reference (Sigma-Aldrich C6144-1MG).

2.5.5 Dissolved organic carbon

For DOC assessment, samples were collected in triplicate using polyethylene bottles. Each 60 mL seawater sample was filtered through a GF/F filter that had been pre-treated by heating at 450 °C for 4 h. After filtration, the samples were acidified to achieve a pH range of 2–3 and stored at −20 °C. Analysis of these samples involved the infrared combustion method using a Shimadzu organic carbon analyzer (TOC-LCPH).

2.5.6 Cytometry

For picoplankton abundance, 3 mL of water was fixed with a glutaraldehyde solution (1 %) and promptly frozen (−80 °C) in liquid nitrogen for storage. Samples were analyzed with flow cytometry using an Influx Cytopeia equipped with five lasers (355, 457, 488, 532, 638 nm). Sort gates were optimized based on the autofluorescence of each group. *Synechococcus sp.* were identified based on their orange fluorescence (530/40 nm) using 488 nm blue and 532 nm green lasers, picoeukaryotes were identified by their red fluorescence (692/40 nm) using 488 nm blue laser, and bacterioplankton were detected using a combination of side scatter light (SSC) (related to cell size) and green fluorescence (530/40 nm).

2.6 Data analysis

2.6.1 Dissolved methane

Dissolved CH_4 concentration was calculated using the solubility coefficient from Wiesenburg and Guinasso (1979). The water column was divided into two layers according to density gradients: (1) well-mixed surface layer (0–20 m) and (2) subsurface layer (20–90 m) from the base of the mixed layer to the bottom, around ∼ 90 m (Farías et al., 2015); this was to interpret the vertical and temporal variability in CH_4.

CH_4 dissolved in the microcosms was measured using continuous sampling connected to the CRDS. Dry mole fractions of CH_4 were converted to concentrations of dissolved CH_4 with the Wiesenburg and Guinasso (1979) solubility coefficient by using in situ temperature and salinity. Each time in the microcosm experiment represents the average of the plateau of each measurement (around 150 and 200 measurements, approximately).

2.6.2 Methane saturation

CH_4 saturation was calculate following Eq. (1):

$$\mathrm{Sat}(\%) = \frac{[\mathrm{CH_4}]_{\text{in situ}}}{[\mathrm{CH_4}]_{\mathrm{eq}}}, \tag{1}$$

where $[CH_4]_{eq}$ was calculated using the solubility coefficient from Wiesenburg and Guinasso (1979).

2.6.3 Methane anomalies and methane hot moments

Monthly anomalies of CH_4 were estimated only in the surface layer, using the following Eq. (2):

$$\mathrm{Anomaly} = \frac{x\mathrm{CH_4} - \bar{x}\mathrm{CH_4}}{\sigma\mathrm{CH_4}}, \tag{2}$$

where $x\mathrm{CH_4}$ is the discrete value at a certain depth (surface) and time (month), $\bar{x}\mathrm{CH_4}$ is the median value for the whole (2018–2021) period at surface, and $\sigma\mathrm{CH_4}$ is the standard deviation of this dataset. CH_4 hot moments were defined as a ΔCH_4 3 times higher than the average monthly value of the anomaly ($\bar{x}\Delta\mathrm{CH_4}$) at each depth within the surface layer as Eq. (3):

$$\frac{\Delta\mathrm{CH_4}}{\bar{x}_{\Delta\mathrm{CH_4}}} > 3, \tag{3}$$

where ΔCH_4 is the disequilibrium of this gas at each depth and was estimated as Eq. (4):

$$\Delta\mathrm{CH_4} = [\mathrm{CH_4}]_{\text{in situ}} - [\mathrm{CH_4}]_{\mathrm{eq}}. \tag{4}$$

2.6.4 Inventories

Inventories of CH_4, chl a, and nutrients at the surface (SL) and illuminated layer and subsurface and dark layer (SSL) were calculate through the trapezoidal integration of concentrations of each variable at every layer: minimum three depths in each layer. The averages were taken for DOC because there were only two measurements in each layer.

2.6.5 Methane recycling rates

The net CH_4 recycling rate (net CH_4 accumulation minus CH_4 consumption) in different fractions of the phytoplankton community was calculated through a linear regression of CH_4 concentrations (Farías et al., 2009) during the incubation time (24 h), separating the light cycles (12 h of light and 12 h of darkness).

2.6.6 Methane fluxes

The daily CH_4 flux ($F = \mu mol\, m^{-2}\, d^{-1}$) across the air–sea interface was determined using the equation from Broecker and Peng (1974), modified by Wanninkhof (1992) as follows:

$$F = K_w \cdot (C_w - C^*), \quad (5)$$

where K_w ($cm\, h^{-1}$) is the transfer velocity from the surface water to the atmosphere, as a function of wind speed, temperature and salinity from the mixed layer depth (MLD), where wind speed was obtained from a meteorological station located at Carriel Sur (http://www.meteochile.gob.cl/, last access: May 2022) and MLD was calculated using the potential-density-based criterion of Kara et al. (2003). C_w ($nmol\, L^{-1}$) is the mean CH_4 concentration in the mixed layer, and C^* is the gas concentration in the mixed layer expected to be in equilibrium with the atmosphere according to Wiesenburg and Guinasso (1979). Historical atmospheric values were obtained from registers of gas hemispheric and global monthly means from the NOAA/ESRL program at NOAA (http://www.esrl.noaa.gov, last access: May 2022). More details about the calculation of CH_4 fluxes are found in Farías et al. (2021).

2.6.7 Brunt–Väisälä frequency (BVF)

The Brunt–Väisälä frequency was derived from the observed pressures, temperatures and salinities for each depth set using the TEOS-10 equation of state. This was done in Ocean Data View (ODV v5.6.4) software. Negative values indicate unstable conditions (Schlitzer, 2023).

2.7 Statical analysis

To determine significant differences between the upwelling and non-upwelling periods in both surface and subsurface layers, the non-parametric Mann–Whitney U test was used. To analyze the degree of relationship between oceanographic variables and the variability in CH_4 in the surface layer, Spearman correlations were used. Also, to identify patterns in surface and subsurface variation, a principal component analysis (PCA) was performed. In addition, the Kruskal–Wallis non-parametric statistical test was used to define significant differences between the concentrations given by the different treatments. A statistically significant value was considered $p < 0.05$.

3 Result and discussion

3.1 Oceanographic characteristics related to wind-driven coastal upwelling in central Chile

Figure 3 shows the seasonal variability in DO, stratification, chl *a*, DOC, nutrients and their ratios. Coastal areas off central Chile have a well-documented seasonality of upwelling favorable winds (Strub et al., 1998). Previous studies, based on wind forcing, have identified two distinct seasons: spring–summer (September to April) upwelling and autumn–winter (May to August) non-upwelling (Sobarzo et al., 2007). This seasonality significantly influences temperature, salinity, DO, nutrients and surface chl-*a* concentrations in response to wind-driven stress (Strub et al., 1998; Aguirre et al., 2012). Notably, although most oceanographic variables have clear seasonal patterns, a comparatively weak seasonality is observed in dissolved CH_4 (Fig. 3a).

In the subsurface layer, CH_4 concentrations range from 0.43 to 78.72 nM (mean ± SD = 23.44 ± 15.38 nM; Fig. 3a). These elevated levels could be associated with the seasonal dynamics of organic matter mineralization under hypoxic and suboxic conditions during the upwelling period (spring–summer) (Brown et al., 2014; Capelle and Tortell, 2016; Kock et al., 2008; Farías et al., 2021); however, there are no significant differences in CH_4 accumulations ($p = 0.40$) in subsurface waters during the upwelling (mean ± SD = 22.52 ± 14.34 nM) and non-upwelling (mean ± SD = 24.60 ± 16.65 nM) periods (Fig. 3a). Previously, long-term CH_4 climatology has observed similar values in surface and subsurface layers (Farías et al., 2021).

In the surface layer, there is a highly heterogeneous distribution of CH_4 concentrations, ranging from 0.14 to 41.72 nM (mean ± SD = 11.70 ± 7.79 nM). There are brief events of high CH_4 accumulations within the water column, known as "hot moments" (McClain et al., 2003; referring to disproportionate accumulations over time). CH_4 concentrations during hot moments are between 10.17 nM (390 % saturation) and 41.72 nM (1650 % saturation) and persist during upwelling and non-upwelling periods, as observed in Figs. S1 and S2 in the Supplement. Persistently high CH_4 concentrations in mixing layer depth results in substantial CH_4 effluxes, varying between 3.35 and 23.42 $\mu mol\, m^{-2}\, d^{-1}$ (mean ± SD = 10.10 ± 5.77 $\mu mol\, m^{-2}\, d^{-1}$). When effluxes are estimated and compared for upwelling and non-upwelling periods, there are not significant differences. The lack of seasonal differences in mean surface CH_4 concentrations ($p = 0.63$) and effluxes ($p = 0.23$) could indicate additional input sources, such as river discharges or local surface production. Potentially, the Itata River may contribute to CH_4, DOC and chromophoric dissolved organic matter (DOM; CDOM) discharge (Bello, 2016; Vargas et al., 2016; Rain-Franco et al., 2019), stimulating CH_4 production through aero-

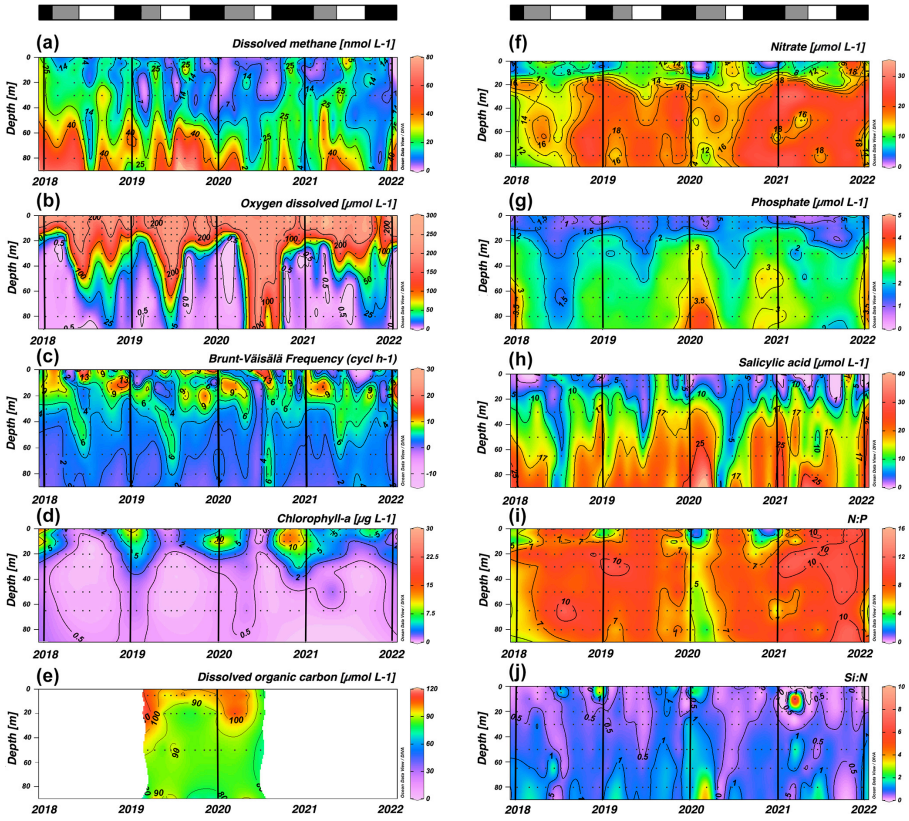

Figure 3. Time series of vertical distributions of **(a)** methane (nmol L^{-1}), **(b)** dissolved oxygen (µmol L^{-1}), **(c)** Brunt–Väisälä frequency (cycles h^{-1}), **(d)** chlorophyll *a* (µg L^{-1}), **(e)** dissolved organic carbon (no purgeable organic carbon – µM), **(f)** nitrate (µmol L^{-1}), **(g)** phosphate (µmol L^{-1}), **(h)** salicylic acid (µmol L^{-1}), N : P ratio and **(j)** Si : N ratio. Sampling was made at ST18 from January 2018 to December 2021. Black lines indicate the start of each year (January). The top bars show different periods' primary production: in black is a high-productivity period (Phase I), in gray is an intermediate-productivity period (Phase II), and in white is a low-productivity period (Phase III).

bic methanogenesis and photooxidation processes (Li et al., 2020; Zhang and Xie, 2015).

CH_4 profiles from samples are shown in Fig. S2. Specific dates present peaks in surface CH_4 over different concentrations, occasionally presenting levels exceeding those in the subsurface layer; so, it is understood that these hot moments in the surface layer are not associated with the vertical advection of CH_4-rich bottom waters.

Thus, it is considered whether hot moments result from physical processes, such as vertical and/or advection associated with upwelling and river discharge, respectively, or biological microbial processes. For the latter, hot moments might be due to in situ aerobic methanogenesis, a process related to the growth and metabolic activities of microalgae (Günthel et al., 2020; Hartmann et al., 2020; Del Valle and Karl, 2014; Bizic, 2021; Cerbin et al., 2022) and bacteria (Repeta et al., 2016; Metcalf et al., 2012; Sun et al., 2019). This type of production is suggested to be a significant reason for CH_4 fluxes in various aquatic systems, including stratified lakes (Grossart et al., 2011; Günthel et al., 2019; Wang et al., 2018) and open oceans (Damm et al., 2010; Karl et al., 2008; Repeta et al., 2016; Sosa et al., 2020; Ye et al., 2020).

Relatively high Brunt–Väisälä frequency (BVF) values (> 10 cycles h^{-1}) are observed between depths of 0 and 20 m,

particularly from September to December (Fig. 3c), whereas subsurface BVF values seem to be associated with annual patterns of thermal stratification, where upwelling from the nearly homogenous ESSW between October and April leads to high-density homogeneity and lower BVF values. During autumn and winter, elevated BVF values are observed in surface waters, probably due to discharge from the Itata River; remarkably there are notably stable values in the subsurface layer (Fig. 3c).

The upper 20 m of the water column has chl-*a* concentrations above $10\,\mu g\,L^{-1}$ (with a marked subsurface peak over different depths) (mean $\pm$ SD 6.60 ± 5.98) in September to January (spring–summer), while lower and more homogeneous values (ranging from 0.5 to $1\,\mu g\,L^{-1}$) are detected during late summer (February to April, mean $\pm$ SD 3.23 ± 2.87) and autumn and winter (May to August, mean $\pm$ SD 1.36 ± 1.91) (Fig. 3d). The study area presents typical DOC concentrations, as expected for highly productive coastal zones (Igarza et al., 2019; Vargas et al., 2013), ranging from 58.79 to 128.63 µM (mean $\pm$ SD = 90.37 ± 17.05) with peak DOC concentrations during late summer and early autumn (Fig. 3e). The surface layer shows reduced but not depleted nutrient concentrations, whereas the subsurface layer presents consistently higher nutrient concentrations (Fig. 3f–h). Within the upper 10 m depth, minimum mean NO_3^- and PO_4^{3-} concentrations occur from September to January and intermediate and higher values between February and August (Fig. 3f and g). These trends are consistent with plankton temporal dynamics (see below). In contrast, $Si(OH)_4$ exhibits higher but heterogeneous concentrations during late autumn and winter and lower values during spring and summer (Fig. 3h). This pattern reflects the high levels of $Si(OH)_4$ associated with river discharges in winter and the development of diatom blooms in spring and summer. CH_4 hot moments occur consistently throughout the year with different stratification scenarios in the water column (Fig. 3a and c) and with different chl-*a* levels (Fig. 3d), revealing a complex interaction between substrates (nutrients and DOC), microorganisms involved and environmental factors (e.g., light, nutrients, water column stability).

Three distinct periods or phases of annual productivity are considered within the study area, based on existing data of primary production, phytoplankton biomass and phytoplankton succession (i.e., changes in composition), related to other biophysical variables (Testa et al., 2018). These periods are September to January (Phase I), with high productivity and chl-*a* biomass, dominated by microplankton including large diatoms, tintinnids and dinoflagellates; from February to April (Phase II) with intermediate productivity, characterized by a shift in plankton composition biomass from larger to smaller organisms, such as flagellates; and from May to August (Phase III), with basal level productivity and relatively low chl-*a* biomass, which corresponds to a non-upwelling period, with a prevalence of pico- and nanoplankton (e.g., *Synechococcus*) including small flagellates and ciliates.

Table 2 presents inventories on CH_4, chl *a*, DOC, NO_3^-, PO_4^{3-}, $Si(OH)_4$ and inorganic nutrient ratios (N : P and Si : N) observed in these periods. The data on chl *a* indicate a marked variation, decreasing from spring to winter (Table 2).

Notably, surface data on DOC show a marginal reduction from Phase I to Phase III (Table 2). It is possible that this fluctuation in DOC accumulation and/or depletion is due to the microbial regeneration exceeding the heterotrophic bacterial consumption (Hansell and Orellana, 2021), or it is attributed to allochthonous sources from rivers (Bauer and Druffel, 1998). Nutrient distribution and concentrations in the surface layer show significant variability among phases (Fig. 3f–h) due to the varied influence by nutrient-rich upwelling events (predominantly observed in spring–summer), biological assimilation and river discharge. These variations significantly affect the N : P and Si : N ratios (Fig. 3i and j), potentially influencing phytoplankton composition. During winter (Phase III), the N : P ratio approaches the expected Redfield stoichiometry, attributed to reduced denitrification in bottom waters (Fernandez et al., 2015) and limited vertical advection towards the surface, contrasting with Phase I. Simultaneously, the Si : N ratio increases due to freshwater discharge from the Itata River (Phase III), encouraging an increase in large diatoms and subsequent $Si(OH)_4$ consumption (Phase I). Considering that hot moments occur throughout different phases and stages of primary production, as well as phytoplankton composition succession (Collado-Fabbri et al., 2011; Aldunate et al., 2018; Anabalón et al., 2007), various levels of chl *a* (see Table 2), and under different nutrient ratios and DOC concentrations (Table 2), it suggests that the conditions and processes favoring the occurrence of hot moments are variables and not entirely clear.

The correlation analysis in the water column showed no significant correlations between CH_4 and the other physicochemical variables (Fig. S3a); however nutrients such as PO_4^{3-} were significantly correlated with T (negative correlation), S (positive correlation), DO (negative correlation) and Si : N ratio (positive correlation) (Fig. S3a), which may be associated with the nutrient-rich, oxygen-poor ESSW. When the surface layer was analyzed in the three productivity periods (Fig. S3b–d), again, no correlation was observed between CH_4 and the other biogeochemical variables; however, in Phases I and II, significant correlations are observed between the nutrients and T, S and DO (negative correlations) (Fig. S3b and c), which may be associated with the upwelling during spring–summer. In Phase III (Fig. S3d), only $Si(OH)_4$ showed significant correlations with T (negative correlation), NO_3^- (positive correlation), PO_4^{3-} (positive correlation) and the Si : N ratio (positive correlation); this may be due to Si input during the rainfall period presented in the autumn–winter period. Moreover, the slight correlation (but no significant) between CH_4 and chl *a* in Phase III suggests that possibly organic matter degradation/con-

Table 2. Average inventories of biogeochemical variables: methane ($\mu mol\,m^{-2}$), chlorophyll *a* ($mg\,m^{-2}$), DOC ($\mu mol\,m^{-2}$), nitrate ($\mu mol\,m^{-2}$), phosphate ($\mu mol\,m^{-2}$), silicate ($\mu mol\,m^{-2}$), and N : P and Si : N ratios, estimated for each productivity period (mean ± SD) from 2018 to 2021. These inventories are estimated for surface layer (SL) and subsurface layer (SSL). Number of hot moments in each period are counted. Phase I: September to January. Phase II: February to April. Phase III: May to August.

Variable	Layer	Productivity periods		
		High Phase I (spring–summer)	Intermediate Phase II (summer–autumn)	Basal Phase III (autumn–winter)
CH_4	SL	265.59 ± 58.36	162.35 ± 21.44	240.54 ± 78.97
	SSL	1315.07 ± 173.69	1012.86 ± 163.23	1275.17 ± 286.38
chl *a*	SL	154.4 ± 102.31	51.32 ± 31.02	26.19 ± 21.17
DOC	SL	114.44 ± 53.94	112.88 ± 8.36	92.41 ± 11.27
	SSL	100.35 ± 46.51	96.97 ± 23.78	86.12 ± 8.95
NO_3^-	SL	260.61 ± 96.25	208.67 ± 49.51	224.65 ± 13.44
	SSL	1274.41 ± 344.24	1033.51 ± 38.5	987.6 ± 113.58
PO_4^{3-}	SL	38.08 ± 10.35	30.29 ± 3.51	28.16 ± 2.99
	SSL	170.22 ± 34.07	137.05 ± 21.57	119.38 ± 11.73
$Si(OH)_4$	SL	131.75 ± 47.07	91.65 ± 38.68	111.24 ± 37.9
	SSL	1065.32 ± 206.98	811.2 ± 225.51	678.07 ± 168.68
N : P	SL	7.69 ± 2.57	7.59 ± 2.44	8.48 ± 0.55
	SSL	9.28 ± 2.52	8.24 ± 0.92	8.46 ± 0.84
Si : N	SL	0.67 ± 0.1	0.69 ± 0.73	0.49 ± 0.15
	SSL	1.04 ± 0.08	1.01 ± 0.26	0.74 ± 0.11
Hot moments	SL	19	9	15

sumption could impact CH_4 production and that low-scale processes (order of hours or days) could mask this correlation, since there is a wide range in the composition of the phytoplankton species involved in CH_4 cycling (Klintzsch et al., 2019, 2023; Günthel et al., 2020).

We further explore the multivariate relationship between CH_4 variability and other variables by separating the data into the surface and subsurface layers by performing a PCA (Fig. S4). Although the CH_4 vector contributes minimally to the total variance in the dataset, distinct behavior is observed in both layers (Fig. S4a and b). In the surface layer, principal component 1 (PC1) shows almost no variability in CH_4 and accounts for 25 % of the total variance. PC2 contains 22.1 % of the total variance and reveals a direct relationship between CH_4 and the variables chl *a*, primary production, Si : N ratio, $Si(OH)_4$, PO_4^{3-} and NO_3^- while being negatively correlated with temperature, DO, NO_2^- and N : P ratio. When separating the dataset into phases, there are differences in variability and the components (Fig. S4c and d). Surface variability is highest in Phase I and lowest in Phase III. Phases I and II vary on both axes, while Phase III is mainly contained on PC2 (Fig. S4c). For the subsurface, the variability is similar in all phases, but the components on which the variability occurs are more differentiated. Phase III varies almost exclusively in the first dimension (the point cloud aligns along the *x* axis), while Phases I and II vary in both dimensions (the point cloud is oblique to the axes) (Fig. S4d); this may be due to the differentiation between the upwelling (Phases I and II) and non-upwelling (Phase III) periods.

So, the complexity inherent in CH_4 dynamics within the study area poses a challenge to comprehension. Consequently, both short- and long-term CH_4 cycling experiments have been conducted to enhance our understanding. These experiments specifically target size-fractioned planktonic communities combined with organic substrates. The objective is to unravel the intricate interactions and substrates that potentially influence CH_4 production. By focusing on size fractions within planktonic communities, it is possible to assess the contribution of diverse groups to CH_4 production.

3.2 Short-term CH_4 cycling within size-fractioned planktonic communities

Figure 4 shows CH_4 accumulation and depletion in plankton-fractionated experiments over a time frame, with daily incubations (12 h of light and 12 h of darkness). Initial experiments were conducted in December 2018 (Fig. 4a) and January 2019 (Fig. 4b), corresponding to a period of high productivity or Phase I (Table S1 in the Supplement) and coin-

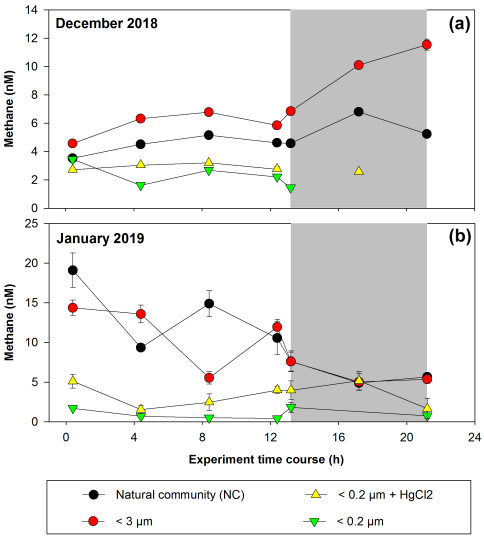

Figure 4. Time courses of dissolved methane concentration (nM) during incubations with fractionated plankton experiments (NC: natural community; < 3 µm: picoplankton and controls (< 0.2 µm)). **(a)** December 2018 and **(b)** January 2019. Photoperiod is represented in white (light) and gray (dark). Error bars represent standard deviation of triplicate samples; when error bars are not visible, they are within the area of the symbol.

ciding with strong vertical advection. The surface water exhibits cooling (∼ 12–13 °C) and elevated CH_4 levels (9.44–17.09 nM), indicative of an active upwelling period (Farías et al., 2021), aligning with other indicators of coastal upwelling (Aguirre et al., 2021).

In the treatments involving fractions $< 0.2\,\mu m$ and $< 0.2\,\mu m + HgCl_2$, which serve as negative controls, CH_4 concentrations remain relatively constant during incubation, with concentrations below 2.32 nM (Fig. 4a) and 5.51 nM (Fig. 4b), indicating biological CH_4 production (Table S2). However, abiotic CH_4 production via photooxidation of CDOM may occur (Li et al., 2020; Zhang and Xie, 2015), but this is not considered in this study. Processes such as DOM photochemical reactions (Mopper et al., 2015), which can contribute to the DOM pool at shallower depths (< 10 m) and be photooxidized to produce CH_4, are disregarded under natural conditions (Li et al., 2020; Zhang and Xie, 2015). In December, CH_4 concentrations in the NC (positive control) and < 3 µm fractions undergo slight increases under light conditions (Fig. 4a; Table S2). However, during darkness, the net CH_4 accumulation is significantly higher in the < 3 µm fraction ($p = 0.03$; Table S2). Picoplankton includes autotrophic and heterotrophic unicellular organisms in the size range of 0.2 to 2 µm. The autotrophic organisms are comprised of cyanobacteria (*Prochlorococcus* and *Synechococcus*) and diverse picoeukaryotes larger than 1 µm (Worden, 2006), while the heterotrophic organisms are primarily prokaryotes, with bacteria overwhelmingly dominating over archaea in the upper layers (Smith et al., 2013). This fraction (< 3 µm) includes several coexisting metabolic groups that depend on different energy sources such as sunlight, DOC or even a combination of the two (mixotrophy). These groups are critical for the functioning of the microbial food web and are predominantly responsible for DOC cycling (Muñoz-Marín et al., 2020; Reintjes et al., 2020) and its derivative compounds (including CH_4).

In January, the experiments show distinct results, with CH_4 levels decreasing over incubation time in both the NC and < 3 µm fractions for both photoperiods (Fig. 4b), although the rate of consumption is lower in darkness (Table S2). These differences suggest that the composition of the microbial community during the high-productivity period, as well as the quantity and quality of DOC and nutrient concentrations and their ratios (Allen et al., 2012; Spilling et al., 2019), controls CH_4 cycling. Indeed, the environmental conditions differ during sampling (Table S1); although both months are oxygenated, both vary in chl-*a* and nutrient levels, including CH_4 (Fig. 3c; Table S1).

Significant differences in CH_4 accumulation rates between the NC and < 150 µm fraction treatments (data not shown) are observed compared with the < 3 µm fraction (Table S2). Peak cycling rates occur in the < 3 µm fraction, indicating that larger microorganisms do not affect the net CH_4 accumulation and consumption (Table S2), highlighting the importance of the microbial loop in CH_4 cycling. Additionally, the observed differences between photoperiods in both fractions may suggest coupling mechanisms between autotrophic phytoplankton and heterotrophic bacterioplankton communities (León-Palmero et al., 2020; Morán et al., 2002; Repeta et al., 2016).

CH_4 consumption by methanotrophs should be considered in CH_4 cycling experiments, as aerobic CH_4 oxidation significantly reduces the net CH_4 accumulation rates (net production vs. consumption) (Mao et al., 2022). While the impact of light on methanotrophs is not widely understood (Broman et al., 2023), the existing literature suggests that methanotrophs may experience inhibition under light conditions (Dumestre et al., 1999; Morana et al., 2020). Consequently, CH_4 accumulation should be higher under these conditions. However, this does not agree with our results (for light and dark conditions), indicating that methylotrophs are more dynamic and complex than expected, making them difficult to understand through the observation of their daily cycles.

3.3 Short-term CH_4 cycling experiment from picoplankton amended with organic substrates

As the picoplankton fraction showed the highest rate of CH_4 accumulation (Fig. 4), this prompts its selection for assessing its potential for methylotrophic methanogenesis through the addition of methylated substrates (MPn and TMA) in a daily cycle. Phosphonate (MPn) and methylamine compounds (mono-, di- and trimethylamines) are dissolved methylated compounds known to stimulate CH_4 production because they have a methyl radical ($-CH_3$), a potential precursor for CH_4 formation in oxygenated environments (Karl et al., 2008; Repeta et al., 2016; Wang et al., 2021; Bižić-Ionescu et al., 2018).

These compounds are ubiquitous in various ecosystems (Lohrer et al., 2020; Sun et al., 2019), yet they have distinct metabolic origins. The MPn originates from microorganisms as Archaea *Nitrosopumilus maritimus* (Metcalf et al., 2012) and *Candidatus pelagibacter spp.* (Born et al., 2017), two of the most abundant marine microorganisms. MPn is found at very low concentrations ($\sim 0.01\,\mu M$, close to its analytical detection limit) likely due to rapid microbial turnover (Karl et al., 2008; Martínez et al., 2013; Urata et al., 2022). The methylamine compounds like the trimethylamine compounds exhibit a wide concentration range in the ocean, from nM levels in the open ocean to µM levels in sediments and near the coast (Sun et al., 2019). Environmental TMA concentrations could be higher, particularly in upwelling regions that bring the TMA from bottom waters to the surface (Gibb et al., 1999; Sun et al., 2019). In this context, the amendments performed for each substrate, 100-fold for MPn and 1000-fold for TMA, convert these experiments into potential rates.

These amendment experiments were conducted in Phase II (March 2019) and Phase III (May 2019), periods of change in phytoplankton succession (composition), biomass and abundance (Testa et al., 2018). In winter, the relative abundance of picoplankton with respect to microplankton (particularly the presence of *Synechococcus* and nitrifying archaea) increases significantly, especially photosynthetic picoeukaryotes (Collado-Fabbri et al., 2011). The time course CH_4 accumulation during incubations is illustrated in Fig. 5. We observe highly variable temporal fluctuations during these periods (March and May). A particularity is the abrupt increase in CH_4 concentration upon transitioning from light to dark cycles in March (Phase II), as well as the significant CH_4 accumulation that persists in darkness (Fig. 5a). In May (Phase III), the time course distribution of CH_4 in each treatment exhibits considerable variability. Notably, the addition of MPn results in greater accumulation in CH_4, particularly in darkness, accompanied by a pronounced increase over incubation time (Fig. 5b; Table S2). In both periods, the $< 3\,\mu m + MPn$ treatment exhibits contrasting patterns under dark conditions (Figs. 5a and 4b), decreasing in Phase II and increasing in Phase III, suggesting the importance of microbial composition. During winter (Phase III), a higher DOC concentration is found (Fig. 3e), which may lead to higher bacterial and archaeal activity that could be metabolizing DOC, including MPn under dark conditions. On the other hand, despite a coefficient of variation $< 10\,\%$, we cannot entirely discount experimental issues in the abrupt rise of the $< 3\,\mu m + MPn$ treatment at around 12 h.

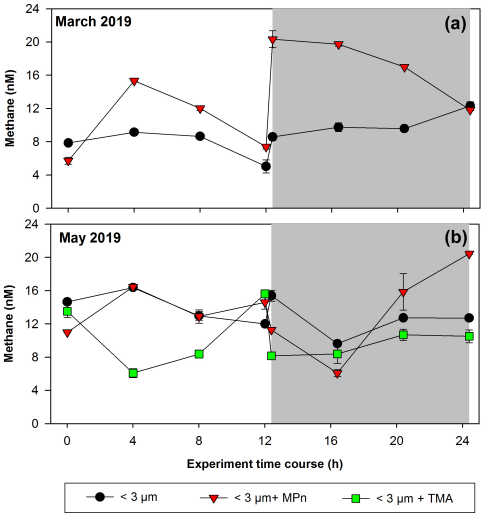

Figure 5. Time courses of dissolved methane concentration (nM) during incubations with the addition of methylated substrates (MPn: methyl phosphonic acid; TMA: trimethylamine) performed with bacterioplankton ($< 3\,\mu m$) and bacterioplankton concentrate (CC). **(a)** March 2019 and **(b)** May 2019. Photoperiod is represented in white (light) and gray (dark). Error bars represent standard deviation of triplicate samples; when error bars are not visible, they are within the area of the symbol.

Conversely, the TMA treatment does not result in any CH_4 accumulation, being lower compared to the control and MPn treatments (Fig. 5b); while TMA can be metabolized by marine bacteria (Lidbury et al., 2015; Bižić-Ionescu et al., 2018), the reduced CH_4 production in this treatment suggests an end product different than CH_4 (Sun et al., 2019). In contrast, heterotrophic picoplankton might metabolize MPn and produce CH_4, showing in situ methanogenesis via the carbon–phosphorus (C–P) lyase pathway (Karl et al., 2008).

3.4 Long-term CH_4 cycling from concentrated picoplankton amended with organic substrates

For a more comprehensive understanding, our study involves long-term microcosm experiments conducted during two distinct phases of productivity. One of these phases oc-

curs during intermediate productivity (Phase II or late summer to autumn), characterized by a notable prevalence of autotrophic small diatoms, picoeukaryotes and cyanobacteria (*Synechococcus*), in contrast to the high-productivity period (Phase I or early springtime) (Fig. S5a and d), when large diatoms are predominant (Fig. S5b and e), while heterotrophic bacterioplankton exhibits an almost constant presence in both periods (Fig. S5c and f). These temporal distributions align with well-documented phytoplankton and bacterioplankton patterns in our study area (Aldunate et al., 2018; Collado-Fabbri et al., 2011; De La Iglesia et al., 2020; Molina et al., 2020).

Briefly, Flavobacteriaceae, SAR11 subclade IA (*Candidatus Pelagibacter spp.*), SAR11 subclade 1b, gammaproteobacterial clades and SAR86 are prevalent during upwelling seasons, while during non-upwelling seasons or Phase III, SAR11 subclade II, marine Actinobacteria and unclassified Alphaproteobacteria dominate (Aldunate et al., 2018). In addition, photosynthetic picoplankton eukaryotes related to Mamiellophyceae (*Bathycoccus*, *Micromonas* and *Ostreococcus*) are predominantly observed with high significance in the surface layer during the transition period (Collado-Fabbri et al., 2011; De La Iglesia et al., 2020), whereas the abundance of heterotrophic bacteria, ranging from 0.23 to 6.50×10^6 cells mL^{-1}, is mainly concentrated in the surface during late summer and autumn, with minima in winter (Molina et al., 2020). However, in our study, the abundance of heterotrophic bacteria shows no significant differences ($p = 0.05$) in both periods (1×10^6 cells mL^{-1}) (Fig. S5c and f). This is due to the low DOC at the beginning of the upwelling period (Fig. 3e).

The CH_4 accumulations during time incubations under different treatments in Phase II are illustrated in Fig. 6. Net CH_4 cycling rates are detailed in Table S4. Variations are observed when these rates are differentiated between light and dark periods, as well as across different periods or phases of productivity (Table S4). The concentrated community (CC) results in substantial enrichments of cyanobacteria (*Synechococcus*), picoeukaryotes and heterotrophic bacteria by factors of 1.9, 1.8 and 4.6, respectively, compared to the NC and factors of 1.8, 1.8 and 6.1, respectively, in relation to the natural $< 3\,\mu m$ fraction (Fig. S5a–c). In both cases, a significant increase in bacteria is observed (Fig. S5c). The microbial abundance proportions in the NC treatment at the beginning of the experiment closely align with field observations (Collado-Fabbri et al., 2011; Anabalón et al., 2007; Morales et al., 2007; Morales and Anabalón, 2012).

Mean chl-*a* levels in the $< 3\,\mu m$ fraction are 21.7 and 4.5 times lower than in the NC and CC, respectively (Table S3). This suggests that this fraction contains phytopicoeukaryotes (e.g., coccolithophorids, cryptophytes) and picocyanobacteria (e.g., *Synechococcus*) in a lower proportion than the CC. Additionally, the CC treatment displays higher background levels of DOC and nutrients probably due to the natural diurnal mortality of picoplankton (Llabrés et al., 2011). It cannot be ruled out that the baseline is due to tangential flow filtration, although it is one of the most used methods to concentrate DOM (Benner et al., 1992), reducing the amount of membrane sorption and fouling (Minor et al., 2014).

In April (Phase II), CH_4 cycling rates consistently exhibit higher values during the dark phase, suggesting a significant involvement of heterotrophic bacterioplankton (Table S4). Additionally, these rates are notably elevated in the CC treatments, particularly in the CC + MPn (Table S4). When comparing the treatments (NC, $< 3\,\mu m$ and CC) without (controls) and with the addition of MPn and TMA (Fig. 6; Table S4), although temporal patterns are similar, significant differences between treatments ($p = 0.002$) are found with slightly higher CH_4 cycling rates in $< 3\,\mu m$ in dark conditions (Fig. 6a; Table S4). With the addition of MPn (Fig. 6b; Table S4), the CC + MPn treatment, characterized by the highest abundance of autotrophic (cyanobacteria) and heterotrophic microorganisms (Fig. S5), exhibits a significant increase in a net CH_4 accumulation in both light and dark conditions (Table S4). In addition, higher chl-*a* concentrations (Table S3) in the NC treatment may have supported greater CH_4 accumulation compared to the $< 3\,\mu m$ fraction (Fig. 6b). Regarding the TMA enrichment (Fig. 6c), both the CC and the $< 3\,\mu m$ fraction treatments respond similarly, increasing CH_4 concentration over time ($p = 3 \times 10^{-6}$; Fig. 6c) although the recycling rates were slightly higher in $< 3\,\mu m$ + TMA, suggesting that microbial abundance does not significantly affect CH_4 production with TMA or that the heterotrophic community in the CC treatment weakly metabolizes TMA (De Angelis and Lee, 1994; Bižić-Ionescu et al., 2018).

Although the metabolization of methylated substrates, such as MPn to CH_4 by various types of bacteria, has been extensively documented (Repeta et al., 2016; Del Valle and Karl, 2014; Metcalf et al., 2012; Zhao et al., 2022; Damm et al., 2010; Karl et al., 2008), this has only been reported mostly under phosphorus-starved conditions. However, this is unlikely in our study area, which experienced high PO_4^{3-} availability, even in excess compared to N (Table 2). Specifically, the expression of phosphonate C–P lyase genes could arise when P-starved (Carini et al., 2014; Taenzer et al., 2020; Sosa et al., 2019). Thus, an alternative explanation for the significant CH_4 accumulation in the CC with MPn treatment could be related to the presence of photosynthetic cyanobacteria (Bižić et al., 2020), which have adaptive strategies to fluctuating P levels (Li and Dittrich, 2019). This is further complemented by the capacity of some bacteria to degrade phosphonates in environments with a substantial background of P (Schowanek and Verstraete, 1990).

Given that *Synechococcus* dominates during the non-upwelling period (autumn–winter season) in the photic layer (Collado-Fabbri et al., 2011), it becomes plausible to consider CH_4 production mediated by this microorganism in this period. Consequently, CH_4 production pathways appear

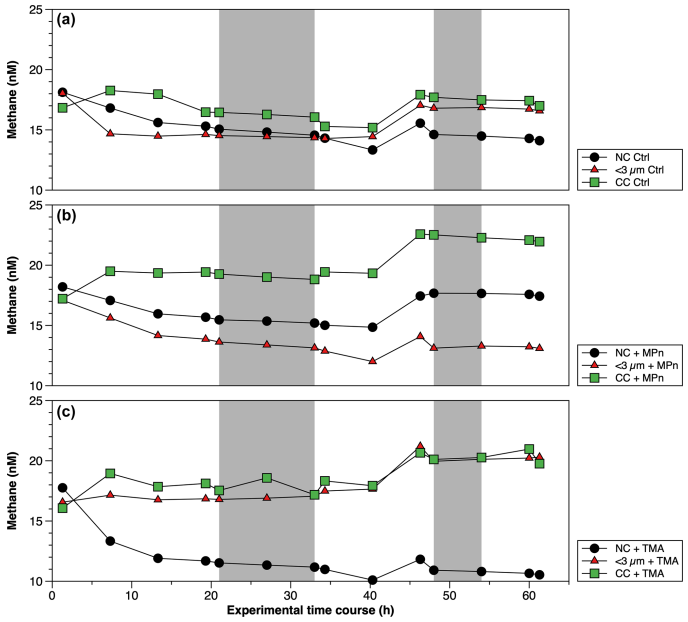

Figure 6. Time courses of dissolved methane (nM) during incubation in long-term microcosm experiments (10 L) with the addition of methylated substrates (MPn: methyl phosphonic acid; TMA: trimethylamine) performed with three planktonic communities (NC: natural community; < 3 µm: bacterioplankton; CC: community concentrate) under oxygenated conditions in April 2019. Photoperiod is represented in white (light) and gray (dark).

multifaceted, involving complex interplays between photochemical and metabolic processes. The mechanism by which cyanobacteria effectively convert fixed CO_2 to CH_4 under light conditions appears intricately linked to the photosynthetic process (Bižić et al., 2020; Klintzsch et al., 2020) as inhibitors of photosynthesis blocked CH_4 production under light conditions (Bižić et al., 2020). They suggest that distinct mechanisms might govern CH_4 production under light and dark conditions, influenced by freshly synthesized photosynthetic products in light and storage compounds during darkness.

In September (Phase I), CH_4 cycling rates exhibit substantial differences compared to those estimated for Phase II. Notably, these rates are lower in most treatments, with a reversal observed in the pattern compared to Phase II; i.e., CH_4 cycling rates during light conditions surpass those during dark conditions (Table S4). Furthermore, the CC treatments consistently demonstrate the highest rates compared to the other treatments (Table S4). Temporal CH_4 accumulation in this phase consistently demonstrates higher CH_4 levels in the CC treatment compared to the NC and < 3 µm fraction (controls) (Fig. 7a). However, a noteworthy contrast appears when considering the impact of substrate additions. Specifically, the addition of TMA in the CC treatment in this phase results in a more pronounced CH_4 production (Fig. 7c) compared to the effect of MPn (Fig. 7b), especially in dark conditions (Table S4). This pattern, the opposite of that found in Phase II, could potentially be explained by the observed decrease in *Synechococcus* abundance (Fig. S5d), which remains unresponsive to MPn, and the concurrent increase in nano- and picoeukaryotes and bacteria at the end of the experiment (Fig. S5e and f), the last of which could be conducive to the action of TMA (Bižić-Ionescu et al., 2018; De Angelis and Lee, 1994; Lidbury et al., 2015). Indeed, a marked reduction in *Synechococcus* abundance is observed (showing a 4.6-fold decrease) compared to Phase II (Fig. S5a and d), whereas nano- and picoeukaryotes experience notable abundance (3.1 to 3.7 times higher than the transition period) (Fig. S5b and e).

In this phase, the distribution proportions within the NC treatment are cyanobacteria, nano- and picoeukaryotes, and bacteria accounting for 1.1, 2.3 and 96.6, respectively. In contrast, within the CC treatment, the initial distribution proportions are higher with respect to the NC: cyanobac-

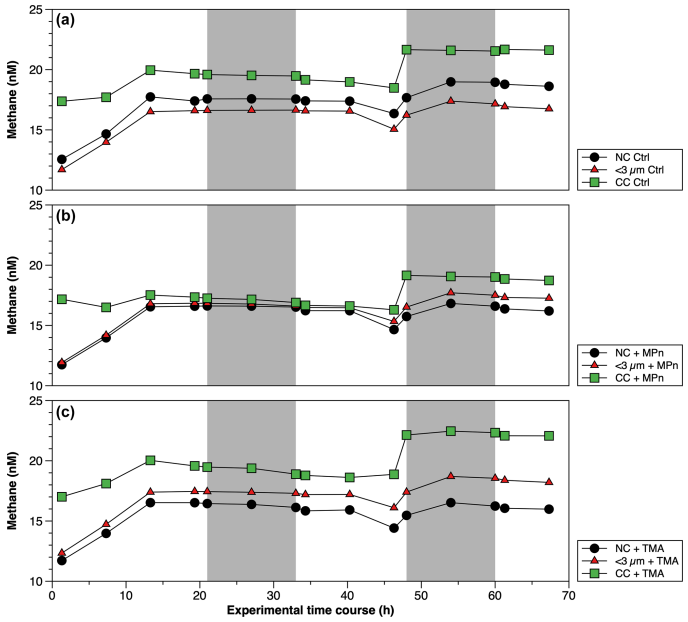

Figure 7. Time courses of dissolved methane (nM) during incubation in long-term microcosm experiments (10 L) with the addition of methylated substrates (MPn: methyl phosphonic acid; TMA: trimethylamine) performed with three planktonic communities (NC: natural community; < 3 µm: bacterioplankton; CC: community concentrate) under oxygenated conditions in September 2019. Photoperiod is represented in white (light) and gray (dark).

teria, picoeukaryotes and bacterioplankton displayed proportions 1.6, 0.6 and 2.9 times greater, respectively. This underscores the increased significance of bacteria and autotrophic picoeukaryotes during this phase, as further corroborated by chl-*a* measurements (Table S3). An intricate interplay between microbial communities and CH_4 cycling within distinct phases of productivity is schematically illustrate in Fig. 8. The prevalence of cyanobacteria, picoeukaryotes and heterotrophic bacteria varied significantly between these phases. So, this indicates that substrate utilization is related to the availability of nutrients as well as the complexity of the substrate and the composition of the heterotrophic bacterial community, potentially driving CH_4 production dynamics.

High CH_4 levels in surface water during the non-upwelling period, comparable to the upwelling period, could result from in situ CH_4 production mediated by photosynthetic *Synechococcus* or demethylation by heterotrophic bacteria (Fig. 8a). On the other hand, although the trimethylamine methyltransferase enzyme has been described as being involved in the demethylation of TMA in methanogen microorganisms (Paul et al., 2000), it cannot be ruled out that in Phase I (spring) heterotrophic bacteria dominance can metabolize TMA through an alternative pathway still unknown (Fig. 8b), nor can it be ruled out that the upwelling brings methanogens with the necessary machinery to metabolize TMA at the ocean surface.

4 Conclusions

Overall, picoplankton produced CH_4 in all experiments conducted in both light and dark conditions, although the net CH_4 production rate was higher in dark conditions. Moreover, laboratory experiments demonstrated that organic compounds such as TMA and MPn are metabolized by heterotrophic bacterioplankton, contributing to the production of oxic CH_4 in the oxygenated surface layer.

Coastal upwelling could bring with it organic amino compounds such as TMA including mono- and di-trimethylamines from sediments, which added to plankton decomposition compounds, and the change in picoplanktonic composition (bacteria and the remarkable increase in pico- and nano-eukaryotes) during the favorable upwelling period could promote CH_4 production via TMA, through a path-

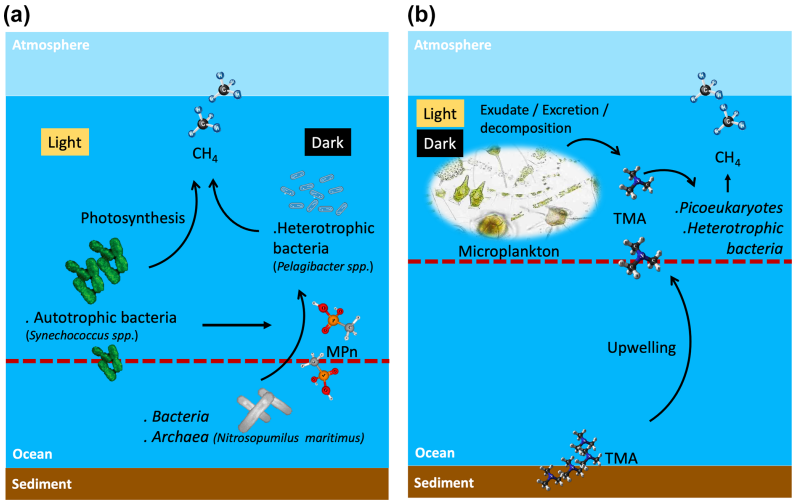

Figure 8. Suggested scheme of methane cycling mechanisms in two contrasting periods of primary production and oceanographic conditions during light and dark phases, where potential planktonic communities and methylated substrates are involved to metabolize methane in surface waters. **(a)** Phases II and III or late upwelling or non-upwelling season and **(b)** Phase I or active upwelling season. Dashed line shows the 100 µmol L^{-1} oxycline, above this line oxic methane is produced. TMA: trimethylamine; MPn: methyl phosphonic acid.

way that is still unknown, but would potentially add to CH_4 supersaturation in the oxygenated surface layer, beyond the contribution of CH_4 by advection.

Synechococcus could be responsible for CH_4 regeneration through photosynthesis. These cyanobacteria are abundant in the non-upwelling period and, together with other picoeukaryotes, maintain intermediate and basal chl-*a* levels during this period that matched with higher DOC levels and inorganic N : P ratios (compared to the upwelling period). This may stimulate heterotrophic bacteria to metabolize MPn and thus contribute to the recycling of oxic CH_4.

It is important to note that amended experiments were conducted in Phase II (March 2019) and Phase III (May 2019), periods marked by changes in the phytoplankton succession (composition), biomass and abundance in winter; the relative abundance of picoplankton with respect to microplankton (particularly the presence of *Synechococcus* and nitrifying archaea) increases significantly, especially photosynthetic picoeukaryotes.

Data availability. All raw data can be provided by the corresponding authors upon request.

Supplement. The supplement related to this article is available online at: https://doi.org/10.5194/bg-21-2029-2024-supplement.

Author contributions. SET and LF designed the experiments, and SET carried them out, performed the measurements, analyzed the data, and drafted the manuscript. LF reviewed and edited the manuscript.

Competing interests. The contact author has declared that neither of the authors has any competing interests.

Disclaimer. Publisher's note: Copernicus Publications remains neutral with regard to jurisdictional claims made in the text, published maps, institutional affiliations, or any other geographical representation in this paper. While Copernicus Publications makes every effort to include appropriate place names, the final responsibility lies with the authors.

Acknowledgements. Thanks to Gerardo Garcia for his experience and teaching in the use of laboratory equipment and his help in setting up the experiments; Karen Sanzana for nutrient analysis; and Oliver Alarcon for oxygen analysis. Both the crew of RV *Kay–Kay II* and the Dichato Marine Station of the University of Concepción provided valuable help during fieldwork, as well as all participating colleagues in the time series station (University of Concepción), who provided the core measurements. We also appreciate the work done during the COVID pandemic by Juan Faúndez.

Financial support. This research was funded by the Fondo Nacional de Desarrollo Científico y Tecnológico (FONDECYT) grant no. 1200861 and also Millennium Science Initiative Program ICM 2019-015 (SECOS) and CR2 FONDAP-CONICYT no. 1522A001.

Review statement. This paper was edited by Hermann Bange and reviewed by two anonymous referees.

References

Aguirre, C., Pizarro, Ó., Strub, P. T., Garreaud, R., and Barth, J. A.: Seasonal dynamics of the near-surface alongshore flow off central Chile, J. Geophys. Res.-Oceans, 117, C01006, https://doi.org/10.1029/2011JC007379, 2012.

Aguirre, C., Garreaud, R., Belmar, L., Farías, L., Ramajo, L., and Barrera, F.: High-frequency variability of the surface ocean properties off central Chile during the upwelling season, Front. Mar. Sci., 8, 1–19, https://doi.org/10.3389/fmars.2021.702051, 2021.

Aldunate, M., De la Iglesia, R., Bertagnolli, A. D., and Ulloa, O.: Oxygen modulates bacterial community composition in the coastal upwelling waters off central Chile, Deep-Sea Res. Pt. II, 156, 68–79, https://doi.org/10.1016/j.dsr2.2018.02.001, 2018.

Allen, L. Z., Allen, E. E., Badger, J. H., McCrow, J. P., Paulsen, I. T., Elbourne, L. D., Thiagarajan, M., Rusch, D. B., Nealson, K. H., Williamson, S. J., Venter, J. C., and Allen, A. E.: Influence of nutrients and currents on the genomic composition of microbes across an upwelling mosaic, ISME J., 6, 1403–1414, https://doi.org/10.1038/ismej.2011.201, 2012.

Anabalón, V., Morales, C. E., Escribano, R., Varas, A. M., and Varas, M. A.: The contribution of nano- and microplanktonic assemblages in the surface layer (0–30 m) under different hydrographic conditions in the upwelling area off Concepción, central Chile, Prog. Oceanogr., 75, 396–414, https://doi.org/10.1016/j.pocean.2007.08.023, 2007.

Bange, H. W., Bartell, U. H., Rapsomanikis, S., and Andreae, M. O.: Methane in the Baltic and North Seas and a reassessment of the marine emissions of methane, Global Biogeochem. Cy., 8, 465–480, 1994.

Bauer, J. and Druffel, E.: Ocean margins as a significant source of organic matter to the deep open ocean, Letter to Nature, 392, 482–485, https://doi.org/10.1038/33122, 1998.

Bello, E.: Variabilidad estacional en la descarga de metano disuelto desde un sistema estuarino a la zona marina adyacente, el caso de ríos de la zona central de chile (río Itata), Universidad de Concepción, 76 pp., http://repositorio.udec.cl/jspui/handle/11594/10347 (last access: 18 April 2024), 2016.

Belviso, S., Kim, S.-K., Rassoulzadegan, F., Krajka, B., Nguyen, B. C., Mihalopoulos, N., and Buat-Menard, P.: Production of dimethylsulfonium propionate (DMSP) and dimethylsulfide (DMS) by a microbial food web, Limnol. Oceanogr., 35, 1810–1821, https://doi.org/10.4319/lo.1990.35.8.1810, 1990.

Benner, R., Dean Pakulski, J., Mccarthy, M., Hedges, J. I., Hatcher, P. G., Benner, R., Pakulski, J. D., McCarthy, M., Hedges, J. I., Hatcher, P. G., H van Beest, B. W., Kramer, G. J., and van Santen, R. A.: Bulk chemical characteristics of dissolved organic matter in the ocean, Science, 255, 1561–1564, https://doi.org/10.1126/science.255.5051.1561, 1992.

Berg, A., Lindblad, P., and Svensson, B. H.: Cyanobacteria as a source of hydrogen for methane formation, World J. Microb. Biot., 30, 539–545, https://doi.org/10.1007/s11274-013-1463-5, 2014.

Bianchi, T. S.: The role of terrestrially derived organic carbon in the coastal ocean: A changing paradigm and the priming effect, P. Natl. Acad. Sci. USA, 108, 19473–19481, https://doi.org/10.1073/pnas.1017982108, 2011.

Bizic, M.: Phytoplankton photosynthesis: An unexplored source of biogenic methane emission from oxic environments, J. Plankton Res., 43, 822–830, https://doi.org/10.1093/plankt/fbab069, 2021.

Bižić, M., Klintzsch, T., Ionescu, D., Hindiyeh, M. Y., Günthel, M., Muro-Pastor, A. M., Eckert, W., Urich, T., Keppler, F., and Grossart, H. P.: Aquatic and terrestrial cyanobacteria produce methane, Sci. Adv., 6, 1–10, https://doi.org/10.1126/sciadv.aax5343, 2020.

Bižić-Ionescu, M., Ionescu, D., Günthel, M., Tang, K. W., and Grossart, H. P.: Oxic methane cycling: new evidence for methane formation in oxic lake water, in: Biogenesis of Hydrocarbons, Handbook of Hydrocarbon and Lipid Microbiology, edited by: Stams, A. J. M. and Souza, D. Z., Springer International Publishing AG, part of Springer Nature, 1–22, https://doi.org/10.1007/978-3-319-53114-4_10-1, 2018.

Borges, A. V. and Abril, G.: Carbon Dioxide and Methane Dynamics in Estuaries, in: Treatise on Estuarine and Coastal Science, vol. 5, edited by: Wolanski, E. and McLusky, D., Elsevier Inc. Academic Press, 119–161, https://doi.org/10.1016/B978-0-12-374711-2.00504-0, 2012.

Born, D. A., Ulrich, E. C., Ju, K. S., Peck, S. C., Van Der Donk, W. A., and Drennan, C. L.: Structural basis for methylphosphonate biosynthesis, Science, 358, 1336–1339, https://doi.org/10.1126/science.aao3435, 2017.

Broecker, W. S. and Peng, T. H.: Gas exchange rates between air and sea, Tellus, 26, 21–35, https://doi.org/10.1111/j.2153-3490.1974.tb01640.x, 1974.

Broman, E., Barua, R., Donald, D., Roth, F., Humborg, C., Norkko, A., Jilbert, T., Bonaglia, S., and Nascimento, F. J. A.: No evidence of light inhibition on aerobic methanotrophs in coastal sediments using eDNA and eRNA, Environmental DNA, 5, 766–781, https://doi.org/10.1002/edn3.441, 2023.

Brown, I. J., Torres, R., and Rees, A. P.: The origin of sub-surface source waters define the sea-air flux of methane in the Mauritanian Upwelling, NW Africa, Dynam. Atmos. Oceans, 67, 39–46, https://doi.org/10.1016/j.dynatmoce.2014.06.001, 2014.

Bullister, J. L., Wisegarver, D. P., and Wilson, S. T.: The production of methane and nitrous oxide gas standards for Scientific Committee on Ocean Research (SCOR) Working Group #143, Pacific Marine Environmental Laboratory (NOAA-PMEL) for SCOR WG 143, Seattle, WA, 1–9, https://doi.org/10.25607/OBP-24, 2016.

Capelle, D. W. and Tortell, P. D.: Factors controlling methane and nitrous-oxide variability in the southern British Columbia coastal upwelling system, Mar. Chem., 179, 56–67, https://doi.org/10.1016/j.marchem.2016.01.011, 2016.

Capone, D. G. and Hutchins, D. A.: Microbial biogeochemistry of coastal upwelling regimes in a changing ocean, Nat. Geosci., 6, 711–717, https://doi.org/10.1038/ngeo1916, 2013.

Carini, P., White, A. E., Campbell, E. O., and Giovannoni, S. J.: Methane production by phosphate-starved SAR11

chemoheterotrophic marine bacteria, Nat. Commun., 5, 1–7, https://doi.org/10.1038/ncomms5346, 2014.

Carpenter, J.: Do rats and pigeons readily acquire instrumental responses for food in the presence of free food?, Limnol. Oceanogr., 10, 141–143, https://doi.org/10.3758/BF03209628, 1965.

Carpenter, L. J., Archer, S. D., and Beale, R.: Ocean-atmosphere trace gas exchange, Chem. Soc. Rev., 41, 6473–6506, https://doi.org/10.1039/c2cs35121h, 2012.

Cerbin, S., Pérez, G., Rybak, M., Wejnerowski, Ł., Konowalczyk, A., Helmsing, N., Naus-Wiezer, S., Meima-Franke, M., Pytlak, Ł., Raaijmakers, C., Nowak, W., and Bodelier, P. L. E.: Methane-derived carbon as a driver for cyanobacterial growth, Front. Microbiol., 13, 1–16, https://doi.org/10.3389/fmicb.2022.837198, 2022.

Cicerone, R. J. and Oremland, R. S.: Biogeochemical aspects of atmospheric methane, Global Biogeochem. Cy., 2, 299–327, https://doi.org/10.1029/GB002i004p00299, 1988.

Collado-Fabbri, S., Vaulot, D., and Ulloa, O.: Structure and seasonal dynamics of the eukaryotic picophytoplankton community in a wind-driven coastal upwelling ecosystem, Limnol. Oceanogr., 56, 2334–2346, https://doi.org/10.4319/lo.2011.56.6.2334, 2011.

Cuevas, L. A., Daneri, G., Jacob, B., and Montero, P.: Microbial abundance and activity in the seasonal upwelling area off Concepción (∼ 36° S), central Chile: A comparison of upwelling and non-upwelling conditions, Deep-Sea Res. Pt. II, 51, 2427–2440, https://doi.org/10.1016/j.dsr2.2004.07.026, 2004.

Damm, E., Helmke, E., Thoms, S., Schauer, U., Nöthig, E., Bakker, K., and Kiene, R. P.: Methane production in aerobic oligotrophic surface water in the central Arctic Ocean, Biogeosciences, 7, 1099–1108, https://doi.org/10.5194/bg-7-1099-2010, 2010.

Damm, E., Beszczynska-Möller, T. A., Nöthing, E. M., and Kattner, G.: Methane excess production in oxygen-rich polar water and a model of cellular conditions for this paradox, Polar Sci., 9, 327–334, https://doi.org/10.1016/j.polar.2015.05.001, 2015.

De Angelis, M. A. and Lee, C.: Methane production during zooplankton grazing on marine phytoplankton, Limnol. Oceanogr., 39, 1298–1308, 1994.

De La Iglesia, R., Echenique-Subiabre, I., Rodríguez-Marconi, S., Espinoza, J. P., Von Dassow, P., Ulloa, O., and Trefault, N.: Distinct oxygen environments shape picoeukaryote assemblages thriving oxygen minimum zone waters off central Chile, J. Plankton Res., 42, 514–529, https://doi.org/10.1093/plankt/fbaa036, 2020.

Del Valle, D. A. and Karl, D. M.: Aerobic production of methane from dissolved water-column methylphosphonate and sinking particles in the North Pacific Subtropical Gyre, Aquat. Microb. Ecol., 73, 93–105, https://doi.org/10.3354/ame01714, 2014.

Dinasquet, J., Tiirola, M., and Azam, F.: Enrichment of bacterioplankton able to utilize one-carbon and methylated compounds in the Coastal Pacific Ocean, Front. Mar. Sci., 5, 1–13, https://doi.org/10.3389/fmars.2018.00307, 2018.

Dumestre, J. F., Guézennec, J., Galy-Lacaux, C., Delmas, R., Richard, S., and Labroue, L.: Influence of light intensity on methanotrophic bacterial activity in Petit Saut Reservoir, French Guiana, Appl. Environ. Microb., 65, 534–539, https://doi.org/10.1128/aem.65.2.534-539.1999, 1999.

Farías, L., Graco, M., and Ulloa, O.: Temporal variability of nitrogen cycling in continental-shelf sediments of the upwelling ecosystem off central Chile, Deep-Sea Res. Pt. II, 51, 2491–2505, https://doi.org/10.1016/j.dsr2.2004.07.029, 2004.

Farías, L., Fernández, C., Faúndez, J., Cornejo, M., and Alcaman, M. E.: Chemolithoautotrophic production mediating the cycling of the greenhouse gases N_2O and CH_4 in an upwelling ecosystem, Biogeosciences, 6, 3053–3069, https://doi.org/10.5194/bg-6-3053-2009, 2009.

Farías, L., Besoain, V., and García-Loyola, S.: Presence of nitrous oxide hotspots in the coastal upwelling area off central Chile: an analysis of temporal variability based on ten years of a biogeochemical time series, Environ. Res. Lett., 10, 1–13, https://doi.org/10.1088/1748-9326/10/4/044017, 2015.

Farías, L., Tenorio, S., Sanzana, K., and Faundez, J.: Temporal methane variability in the water column of an area of seasonal coastal upwelling: A study based on a 12 year time series, Prog. Oceanogr., 195, 102589, https://doi.org/10.1016/j.pocean.2021.102589, 2021.

Ferderlman, T. G., Lee, C., Pantoja, S., Harder, J., Bebout, B. M., and Fossing, H.: Sulfate reduction and methanogenesis in a *Thioploca*-dominates sediment off the coast of Chile, Geochim. Cosmochim. Ac., 61, 3065–3079, https://doi.org/10.1016/S0016-7037(97)00158-0, 1997.

Fernandez, C., González, M. L., Muñoz, C., Molina, V., and Farias, L.: Temporal and spatial variability of biological nitrogen fixation off the upwelling system of central Chile (35–38.5° S), J. Geophys. Res.-Oceans, 120, 3330–3349, https://doi.org/10.1002/2014JC010410, 2015.

Florez-Leiva, L., Damm, E., Farías, L., and Farias, L.: Methane production induced by dimethylsulfide in surface water of an upwelling ecosystem, Prog. Oceanogr., 112–113, 38–48, https://doi.org/10.1016/j.pocean.2013.03.005, 2013.

Gibb, S. W., Mantoura, R. F. C., Liss, P. S., and Barlow, R. G.: Distributions and biogeochemistries of methylamines and ammonium in the Arabian Sea, Deep-Sea Res. Pt. II, 46, 593–615, https://doi.org/10.1016/S0967-0645(98)00119-2, 1999.

Giovannoni, S. J., Delong, E. F., Schmidt, T. M., and Pace, N. R.: Tangential flow filtration and preliminary phylogenetic analysis of marine picoplankton, Appl. Environ. Microb., 56, 2572–2575, 1990.

Grasshoff, K., Ehrhardt, M., and Kremling, K.: Methods of Seawater Analysis, 2nd Edn., John Wiley & Sons, Ltd, Deerfield Beach, Florida, Verlag Chemie, 419 pp., https://doi.org/10.1002/iroh.19850700232, 1983.

Grossart, H. P., Frindte, K., Dziallas, C., Eckert, W., and Tang, K. W.: Microbial methane production in oxygenated water column of an oligotrophic lake, P. Natl. Acad. Sci. USA, 108, 19657–19661, https://doi.org/10.1073/pnas.1110716108, 2011.

Günthel, M., Donis, D., Kirillin, G., Ionescu, D., Bizic, M., McGinnis, D. F., Grossart, H. P., and Tang, K. W.: Contribution of oxic methane production to surface methane emission in lakes and its global importance, Nat. Commun., 10, 5497, https://doi.org/10.1038/s41467-019-13320-0, 2019.

Günthel, M., Klawonn, I., Woodhouse, J., Bižić, M., Ionescu, D., Ganzert, L., Kümmel, S., Nijenhuis, I., Zoccarato, L., Grossart, H. P., and Tang, K. W.: Photosynthesis-driven methane production in oxic lake water as an important contribu-

tor to methane emission, Limnol. Oceanogr., 65, 2853–2865, https://doi.org/10.1002/lno.11557, 2020.

Hahn, M. W.: Broad diversity of viable bacteria in "sterile" (0.2 µm) filtered water, Res. Microbiol., 155, 688–691, https://doi.org/10.1016/j.resmic.2004.05.003, 2004.

Hansell, D. A. and Orellana, M. V.: Dissolved organic matter in the global ocean: A primer, Gels, 7, 128, https://doi.org/10.3390/gels7030128, 2021.

Harmsen, M., van Vuuren, D. P., Bodirsky, B. L., Chateau, J., Durand-Lasserve, O., Drouet, L., Fricko, O., Fujimori, S., Gernaat, D. E. H. J., Hanaoka, T., Hilaire, J., Keramidas, K., Luderer, G., Moura, M. C. P., Sano, F., Smith, S. J., and Wada, K.: The role of methane in future climate strategies: mitigation potentials and climate impacts, Climatic Change, 163, 1409–1425, https://doi.org/10.1007/s10584-019-02437-2, 2020.

Hartmann, J. F., Günthel, M., Klintzsch, T., Kirillin, G., Grossart, H. P., Keppler, F., and Isenbeck-Schröter, M.: High spatiotemporal dynamics of methane production and emission in oxic surface water, Environ. Sci. Technol., 54, 1451–1463, https://doi.org/10.1021/acs.est.9b03182, 2020.

Holmes, E. M., Sansone, F. J., Rust, T. M., and Popp, B. N.: Methane production, consumption, and air-sea exchange in the open ocean: An evaluation based on carbon isotopic ratios, Global Biogeochem. Cy., 14, 1–10, https://doi.org/10.1029/1999GB001209, 2000.

Holm-Hansen, O., Lorenzen, C. J., Holmes, R. W., and Strickland, J. D. H.: Fluorometric determination of chlorophyll, Journal du Conseil International pour L'Exploration de la Mer, 30, 3–15, https://doi.org/10.1093/icesjms/30.1.3, 1965.

Igarza, M., Dittmar, T., Graco, M., and Niggemann, J.: Dissolved organic matter cycling in the coastal upwelling system off central Peru during an "El Niño" year, Front. Mar. Sci., 6, 1–17, https://doi.org/10.3389/fmars.2019.00198, 2019.

IPCC: Climate Change 2021 – The Physical Science Basis: Working Group I Contribution to the Sixth Assessment Report of the Intergovernmental Panel on Climate Change, Cambridge University Press, https://doi.org/10.1017/9781009157896, 2023.

Kara, A. B., Rochford, P. A., and Hurlburt, H. E.: Mixed layer depth variability over the global ocean, J. Geophys. Res.-Oceans, 108, 1–15, https://doi.org/10.1029/2000jc000736, 2003.

Karl, D. and Tilbrook, B.: Production and transport of methane in oceanic particulate organic matter, Nature, 368, 732–734, 1994.

Karl, D., Beversdorf, L., Björkman, K., Church, M., Martinez, A., and DeLong, E.: Aerobic production of methane in the sea, Nat. Geosci., 1, 473–478, https://doi.org/10.1038/ngeo234, 2008.

Klintzsch, T., Langer, G., Nehrke, G., Wieland, A., Lenhart, K., and Keppler, F.: Methane production by three widespread marine phytoplankton species: release rates, precursor compounds, and potential relevance for the environment, Biogeosciences, 16, 4129–4144, https://doi.org/10.5194/bg-16-4129-2019, 2019.

Klintzsch, T., Langer, G., Wieland, A., Geisinger, H., Lenhart, K., Nehrke, G., and Keppler, F.: Effects of temperature and light on methane production of widespread marine phytoplankton, J. Geophys. Res.-Biogeo., 125, 1–16, https://doi.org/10.1029/2020JG005793, 2020.

Klintzsch, T., Geisinger, H., Wieland, A., Langer, G., Nehrke, G., Bizic, M., Greule, M., Lenhart, K., Borsch, C., Schroll, M., and Keppler, F.: Stable carbon isotope signature of methane released from phytoplankton, Geophys. Res. Lett., 50, 1–12, https://doi.org/10.1029/2023gl103317, 2023.

Kock, A., Gebhardt, S., and Bange, H. W.: Methane emissions from the upwelling area off Mauritania (NW Africa), Biogeosciences, 5, 1119–1125, https://doi.org/10.5194/bg-5-1119-2008, 2008.

Lamontagne, R. A., Swinnerton, J. W., Linnenbom, V. J., and Smith, W. D.: Methane concentrations in various marine environments, J. Geophys. Res., 78, 5317–5324, https://doi.org/10.1029/JC078i024p05317, 1973.

Lenhart, K., Klintzsch, T., Langer, G., Nehrke, G., Bunge, M., Schnell, S., and Keppler, F.: Evidence for methane production by the marine algae *Emiliania huxleyi*, Biogeosciences, 13, 3163–3174, https://doi.org/10.5194/bg-13-3163-2016, 2016.

León-Palmero, E., Contreras-Ruiz, A., Sierra, A., Morales-Baquero, R., and Reche, I.: Dissolved CH_4 coupled to photosynthetic picoeukaryotes in oxic waters and to cumulative chlorophyll *a* in anoxic waters of reservoirs, Biogeosciences, 17, 3223–3245, https://doi.org/10.5194/bg-17-3223-2020, 2020.

Li, J. and Dittrich, M.: Dynamic polyphosphate metabolism in cyanobacteria responding to phosphorus availability, Environ. Microbiol., 21, 572–583, https://doi.org/10.1111/1462-2920.14488, 2019.

Li, Y., Fichot, C. G., Geng, L., Scarratt, M. G., and Xie, H.: The contribution of methane photoproduction to the oceanic methane paradox, Geophys. Res. Lett., 47, 1–10, https://doi.org/10.1029/2020GL088362, 2020.

Lidbury, I. D. E. A., Murrell, J. C., and Chen, Y.: Trimethylamine and trimethylamine N-oxide are supplementary energy sources for a marine heterotrophic bacterium: Implications for marine carbon and nitrogen cycling, ISME J., 9, 760–769, https://doi.org/10.1038/ismej.2014.149, 2015.

Llabrés, M., Agustí, S., and Herndl, G. J.: Diel in situ picophytoplankton cell death cycles coupled with cell division, J. Phycol., 47, 1247–1257, https://doi.org/10.1111/j.1529-8817.2011.01072.x, 2011.

Lohrer, C., Cwierz, P. P., Wirth, M. A., Schulz-Bull, D. E., and Kanwischer, M.: Methodological aspects of methylphosphonic acid analysis: Determination in river and coastal water samples, Talanta, 211, 1–8, https://doi.org/10.1016/j.talanta.2020.120724, 2020.

Lu, X., Jacob, D. J., Zhang, Y., Maasakkers, J. D., Sulprizio, M. P., Shen, L., Qu, Z., Scarpelli, T. R., Nesser, H., Yantosca, R. M., Sheng, J., Andrews, A., Parker, R. J., Boesch, H., Bloom, A. A., and Ma, S.: Global methane budget and trend, 2010–2017: complementarity of inverse analyses using in situ (GLOBALVIEWplus CH_4 ObsPack) and satellite (GOSAT) observations, Atmos. Chem. Phys., 21, 4637–4657, https://doi.org/10.5194/acp-21-4637-2021, 2021.

Ma, X., Sun, M., Lennartz, S. T., and Bange, H. W.: A decade of methane measurements at the Boknis Eck Time Series Station in Eckernförde Bay (southwestern Baltic Sea), Biogeosciences, 17, 3427–3438, https://doi.org/10.5194/bg-17-3427-2020, 2020.

Mao, S. H., Zhang, H. H., Zhuang, G. C., Li, X. J., Liu, Q., Zhou, Z., Wang, W. L., Li, C. Y., Lu, K. Y., Liu, X. T., Montgomery, A., Joye, S. B., Zhang, Y. Z., and Yang, G. P.: Aerobic oxidation of methane significantly reduces global diffusive methane emissions from shallow marine waters, Nat. Commun., 13, 7309, https://doi.org/10.1038/s41467-022-35082-y, 2022.

Martínez, A., Ventouras, L. A., Wilson, S. T., Karl, D. M., and DeLong, E. F.: Metatranscriptomic and functional metagenomic analysis of methylphosphonate utilization by marine bacteria, Front. Microbiol., 4, 340, https://doi.org/10.3389/fmicb.2013.00340, 2013.

McAuliffe, C.: Solubility in water of C1-C9 hydrocarbons, Nature, 200, 1092–1093, 1963.

McClain, M. E., Boyer, E. W., Dent, C. L., Gergel, S. E., Grimm, N. B., Groffman, P. M., Hart, S. C., Harvey, J. W., Johnston, C. A., Mayorga, E., McDowell, W. H., and Pinay, G.: Biogeochemical Hot Spots and Hot Moments at the Interface of Terrestrial and Aquatic Ecosystems, Ecosystems, 6, 301–312, https://doi.org/10.1007/s10021-003-0161-9, 2003.

Metcalf, W. W., Griffin, B. M., Cicchillo, R., Gao, J., Janga, S., Cooke, H., Circello, B., Evans, B., Martens-Habbena, W., Stahl, D., and Van Der Donk, W.: Synthesis of methylphosphonic acid by marine microbes: a source for methane in the Aerobic Ocean, Science, 337, 1104–1107, https://doi.org/10.1126/science.1219875, 2012.

Minor, E. C., Swenson, M. M., Mattson, B. M., and Oyler, A. R.: Structural characterization of dissolved organic matter: A review of current techniques for isolation and analysis, Environ. Sci.-Proc. Imp., 16, 2064–2079, https://doi.org/10.1039/c4em00062e, 2014.

Molina, V., Belmar, L., Levipan, H. A., Ramírez-Flandes, S., Anguita, C., Galán, A., Montes, I., and Ulloa, O.: Spatiotemporal distribution of key pelagic microbes in a seasonal oxygen-deficient coastal upwelling system of the Eastern South Pacific Ocean, Front. Mar. Sci., 7, 1–17, https://doi.org/10.3389/fmars.2020.561597, 2020.

Mopper, K., Kieber, D. J., and Stubbins, A.: Marine photochemistry of organic matter: processes and impacts. processes and impacts., in: Biogeochemistry of Marine Dissolved Organic Matter, edited by: Hansell, D. A. and Carlson, C. A., Elsevier Inc. Academic Press, 389–450, https://doi.org/10.1016/B978-0-12-405940-5.00008-X, 2015.

Morales, C. and Anabalón, V.: Phytoplankton biomass and microbial abundances during the spring upwelling season in the coastal area off Concepción, central-southern Chile: variability around a time series station, Prog. Oceanogr., 92–95, 81–91, https://doi.org/10.1016/j.pocean.2011.07.004, 2012.

Morales, C., González, H. E., Hormazabal, S. E., Yuras, G., Letelier, J., and Castro, L. R.: The distribution of chlorophyll-a and dominant planktonic components in the coastal transition zone off Concepción, central Chile, during different oceanographic conditions, Prog. Oceanogr., 75, 452–469, https://doi.org/10.1016/j.pocean.2007.08.026, 2007.

Morán, X. A. G., Estrada, M., Gasol, J. M., and Pedrós-Alió, C.: Dissolved primary production and the strength of phytoplankton-bacterioplankton coupling in contrasting marine regions, Microb. Ecol., 44, 217–223, https://doi.org/10.1007/s00248-002-1026-z, 2002.

Morana, C., Bouillon, S., Nolla-Ardèvol, V., Roland, F. A. E., Okello, W., Descy, J.-P., Nankabirwa, A., Nabafu, E., Springael, D., and Borges, A. V.: Methane paradox in tropical lakes? Sedimentary fluxes rather than pelagic production in oxic conditions sustain methanotrophy and emissions to the atmosphere, Biogeosciences, 17, 5209–5221, https://doi.org/10.5194/bg-17-5209-2020, 2020.

Muñoz-Marín, M. C., Gómez-Baena, G., López-Lozano, A., Moreno-Cabezuelo, J. A., Díez, J., and García-Fernández, J. M.: Mixotrophy in marine picocyanobacteria: use of organic compounds by *Prochlorococcus* and *Synechococcus*, ISME J., 14, 1065–1073, https://doi.org/10.1038/s41396-020-0603-9, 2020.

Oremland, R. S.: Methanogenic activity in plankton samples and fish intestines: A mechanism for in situ methanogenesis in oceanic surface waters, Limnol. Oceanogr., 24, 1136–1141, 1979.

Paul, L., Ferguson, D. J., and Krzycki, J. A.: The trimethylamine methyltransferase gene and multiple dimethylamine methyltransferase genes of methanosarcina barkeri contain in-frame and read-through amber codons, J. Bacteriol., 182, 2520–2529, 2000.

Rain-Franco, A., Sobarzo, M., Caparros, J., and Fernandez, C.: Variability of chromophoric dissolved organic matter in three freshwater-influenced systems along central-southern Chile, Prog. Oceanogr., 174, 154–161, https://doi.org/10.1016/j.pocean.2018.09.009, 2019.

Reeburgh, W. S.: Oceanic methane biogeochemistry, Chem. Rev., 107, 486–513, https://doi.org/10.1021/cr050362v, 2007.

Reintjes, G., Fuchs, B. M., Scharfe, M., Wiltshire, K. H., Amann, R., and Arnosti, C.: Short-term changes in polysaccharide utilization mechanisms of marine bacterioplankton during a spring phytoplankton bloom, Environ. Microbiol., 22, 1884–1900, https://doi.org/10.1111/1462-2920.14971, 2020.

Repeta, D. J., Ferrón, S., Sosa, O. A., Johnson, C. G., Repeta, L. D., Acker, M., DeLong, E. F., and Karl, D. M.: Marine methane paradox explained by bacterial degradation of dissolved organic matter, Nat. Geosci., 9, 1–7, https://doi.org/10.1038/ngeo2837, 2016.

Roth, F., Sun, X., Geibel, M. C., Prytherch, J., Brüchert, V., Bonaglia, S., Broman, E., Nascimento, F., Norkko, A., and Humborg, C.: High spatiotemporal variability of methane concentrations challenges estimates of emissions across vegetated coastal ecosystems, Glob. Change Biol., 28, 4308–4322, https://doi.org/10.1111/gcb.16177, 2022.

Saunois, M., Stavert, A. R., Poulter, B., Bousquet, P., Canadell, J. G., Jackson, R. B., Raymond, P. A., Dlugokencky, E. J., Houweling, S., Patra, P. K., Ciais, P., Arora, V. K., Bastviken, D., Bergamaschi, P., Blake, D. R., Brailsford, G., Bruhwiler, L., Carlson, K. M., Carrol, M., Castaldi, S., Chandra, N., Crevoisier, C., Crill, P. M., Covey, K., Curry, C. L., Etiope, G., Frankenberg, C., Gedney, N., Hegglin, M. I., Höglund-Isaksson, L., Hugelius, G., Ishizawa, M., Ito, A., Janssens-Maenhout, G., Jensen, K. M., Joos, F., Kleinen, T., Krummel, P. B., Langenfelds, R. L., Laruelle, G. G., Liu, L., Machida, T., Maksyutov, S., McDonald, K. C., McNorton, J., Miller, P. A., Melton, J. R., Morino, I., Müller, J., Murguia-Flores, F., Naik, V., Niwa, Y., Noce, S., O'Doherty, S., Parker, R. J., Peng, C., Peng, S., Peters, G. P., Prigent, C., Prinn, R., Ramonet, M., Regnier, P., Riley, W. J., Rosentreter, J. A., Segers, A., Simpson, I. J., Shi, H., Smith, S. J., Steele, L. P., Thornton, B. F., Tian, H., Tohjima, Y., Tubiello, F. N., Tsuruta, A., Viovy, N., Voulgarakis, A., Weber, T. S., van Weele, M., van der Werf, G. R., Weiss, R. F., Worthy, D., Wunch, D., Yin, Y., Yoshida, Y., Zhang, W., Zhang, Z., Zhao, Y., Zheng, B., Zhu, Q., Zhu, Q., and Zhuang, Q.: The Global Methane Budget 2000–2017, Earth Syst. Sci. Data, 12, 1561–1623, https://doi.org/10.5194/essd-12-1561-2020, 2020.

Schlitzer, R.: Ocean Data View, https://odv.awi.de (last access: 16 April 2024), 2023.

Schowanek, D. and Verstraete, W.: Phosphonate utilization by bacteria in the presence of alternative phosphorus sources, Biodegradation, Kluwer Academic Publishers, 1990 pp., https://doi.org/10.1007/BF00117050, 1990.

Sieburth, J., Smetacek, V., and Lenz, J.: Pelagic ecosystem structure: Heterotrophic compartments of the plankton and their relationship to plankton size fractions, Linmol. Oceanogr., 23, 1256–1263, https://doi.org/10.4319/lo.1978.23.6.1256, 1978.

Smith, M. W., Allen, L. Z., Allen, A. E., Herfort, L., and Simon, H. M.: Contrasting genomic properties of free-living and particle-attached microbial assemblages within a coastal ecosystem, Front. Microbiol., 4, 1–20, https://doi.org/10.3389/fmicb.2013.00120, 2013.

Sobarzo, M. and Djurfeldt, L.: Coastal upwelling process on a continental shelf limited by submarine canyons, Concepción, central Chile, J. Geophys. Res., 109, 1–20, https://doi.org/10.1029/2004JC002350, 2004.

Sobarzo, M., Bravo, L., Donoso, D., Garcés-Vargas, J., and Schneider, W.: Coastal upwelling and seasonal cycles that influence the water column over the continental shelf off central Chile, Prog. Oceanogr., 75, 363–382, https://doi.org/10.1016/j.pocean.2007.08.022, 2007.

Sosa, O. A., Repeta, D. J., DeLong, E. F., Ashkezari, M. D., and Karl, D. M.: Phosphate-limited ocean regions select for bacterial populations enriched in the carbon–phosphorus lyase pathway for phosphonate degradation, Environ. Microbiol., 21, 2402–2414, https://doi.org/10.1111/1462-2920.14628, 2019.

Sosa, O. A., Burrell, T. J., Wilson, S. T., Foreman, R. K., Karl, D. M., and Repeta, D. J.: Phosphonate cycling supports methane and ethylene supersaturation in the phosphate-depleted western North Atlantic Ocean, Limnol. Oceanogr., 65, 1–17, https://doi.org/10.1002/lno.11463, 2020.

Spilling, K., Camarena-Gómez, M. T., Lipsewers, T., Martinez-Varela, A., Díaz-Rosas, F., Eronen-Rasimus, E., Silva, N., von Dassow, P., and Montecino, V.: Impacts of reduced inorganic N : P ratio on three distinct plankton communities in the Humboldt upwelling system, Mar. Biol., 166, 1–17, https://doi.org/10.1007/s00227-019-3561-x, 2019.

Stefels, J. and Van Boekel, W.: Production of DMS from dissolved DMSP in axenic cultures of the marine phytoplankton species *Phaeocystis sp*, Mar. Ecol.-Prog. Ser., 97, 11–18, https://www.jstor.org/stable/24833593 (last access: 27 February 2024), 1993.

Strub, T., Mesías, J., Montecino, V., Rutllant, J., and Salinas, S.: Coastal ocean circulation off western south america, in: The global coastal ocean – regional studies and syntheses, vol. 11, edited by: Robinson, A. R. and Brink, K. H., John Wiley & Sons, Inc, NY, 273–313, 1998.

Sun, J., Steindler, L., Thrash, J. C., Halsey, K. H., Smith, D. P., Carter, A. E., Landry, Z. C., and Giovannoni, S. J.: One carbon metabolism in SAR11 pelagic marine bacteria, PLoS One, 6, 1–12, https://doi.org/10.1371/journal.pone.0023973, 2011.

Sun, J., Mausz, M. A., Chen, Y., and Giovannoni, S. J.: Microbial trimethylamine metabolism in marine environments, Environ. Microbiol., 21, 513–520, https://doi.org/10.1111/1462-2920.14461, 2019.

Taenzer, L., Carini, P. C., Masterson, A. M., Bourque, B., Gaube, J. H., and Leavitt, W. D.: Microbial Methane From Methylphosphonate Isotopically Records Source, Geophys. Res. Lett., 47, 1–9, https://doi.org/10.1029/2019GL085872, 2020.

Testa, G., Masotti, I., and Farías, L.: Temporal variability in net primary production in an upwelling area off central Chile (36° S), Front. Mar. Sci., 5, 1–17, https://doi.org/10.3389/fmars.2018.00179, 2018.

Upstill-Goddard, R. C. and Barnes, J.: Methane emissions from UK estuaries: Re-evaluating the estuarine source of tropospheric methane from Europe, Mar. Chem., 180, 14–23, https://doi.org/10.1016/j.marchem.2016.01.010, 2016.

Urata, S., Kurosawa, Y., Yamasaki, N., Yamamoto, H., Nishiwaki, N., Hongo, Y., Adachi, M., and Yamaguchi, H.: Utilization of phosphonic acid compounds by marine bacteria of the genera *Phaeobacter*, *Ruegeria*, and *Thalassospira* (α-Proteobacteria), FEMS Microbiol. Lett., 369, fnac065, https://doi.org/10.1093/femsle/fnac065, 2022.

Vargas, C. A., Martínez, R. A., Cuevas, L. A., Pavez, M. A., Cartes, C., González, H. E., Escribano, R., and Daneri, G.: The relative importance of microbial and classical food webs in a highly productive coastal upwelling area, Limnol. Oceanogr., 52, 1495–1510, https://doi.org/10.4319/lo.2007.52.4.1495, 2007.

Vargas, C. A., Arriagada, L., Sobarzo, M., Contreras, P. Y., and Saldías, G.: Bacterial production along a river-to-ocean continuum in central Chile: implications for organic matter cycling, Aquat. Microb. Ecol., 68, 195–213, https://doi.org/10.3354/ame01608, 2013.

Vargas, C. A., Contreras, P. Y., Pérez, C. A., Sobarzo, M., Saldías, G. S., and Salisbury, J.: Influences of riverine and upwelling waters on the coastal carbonate system off Central Chile and their ocean acidification implications, J. Geophys. Res.-Biogeo., 121, 1–16, https://doi.org/10.1002/2015JG003213, 2016.

Wang, Q., Dore, J. E., and McDermott, T. R.: Methylphosphonate metabolism by *Pseudomonas sp.* populations contributes to the methane oversaturation paradox in an oxic freshwater lake, Environ. Microbiol., 19, 1–41, https://doi.org/10.1111/1462-2920.13747, 2018.

Wang, Q., Alowaifeer, A., Kerner, P., Balasubramanian, N., Patterson, A., Christian, W., Tarver, A., Dore, J. E., Hatzenpichler, R., Bothner, B., and McDermott, T. R.: Aerobic bacterial methane synthesis, P. Natl. Acad. Sci. USA, 118, 1–9, https://doi.org/10.1073/pnas.2019229118, 2021.

Wanninkhof, R.: Relationship between wind speed and gas exchange over the ocean, J. Geophys. Res., 97, 7373–7382, https://doi.org/10.1029/92JC00188, 1992.

Weber, T., Wiseman, N. A., and Kock, A.: Global ocean methane emissions dominated by shallow coastal waters, Nat. Commun., 10, 1–10, https://doi.org/10.1038/s41467-019-12541-7, 2019.

Wiesenburg, D. A. and Guinasso, N. L.: Equilibrium solubilities of methane, carbon monoxide, and hydrogen in water and sea water, American Chemical Society, 24, 356–360, 1979.

Worden, A.: Picoeukaryote diversity in coastal waters of the Pacific Ocean, Aquat. Microb. Ecol., 43, 165–175, https://doi.org/10.3354/ame043165, 2006.

Xu, S., Sun, Z., Geng, W., Cao, H., Zhang, X., Zhai, B., and Wu, Z.: Advance in Numerical Simulation Research of Marine Methane Processes, Front. Earth Sci., 10, 891393, https://doi.org/10.3389/feart.2022.891393, 2022.

Ye, W. W., Wang, X. L., Zhang, X.-H., and Zhang, G.-L.: Methane production in oxic seawater of the western North Pacific and its marginal seas, Limnol. Oceanogr., 65, 1–14, https://doi.org/10.1002/lno.11457, 2020.

Zhang, Y. and Xie, H.: Photomineralization and photomethanification of dissolved organic matter in Saguenay River surface water, Biogeosciences, 12, 6823–6836, https://doi.org/10.5194/bg-12-6823-2015, 2015.

Zhao, L., Lin, L.-Z., Chen, M.-Y., Teng, W.-K., Zheng, L.-L., Peng, L., Lv, J., Brand, J. J., Hu, C.-X., Han, B.-P., Song, L.-R., and Shu, W.-S.: The widespread capability of methylphosphonate utilization in filamentous cyanobacteria and its ecological significance, Water Res., 217, 1–11, https://doi.org/10.1016/j.watres.2022.118385, 2022.

5. DISCUSIÓN

5.1. Monitoreo en el océano: desde campañas a bordo hasta tecnologías de alta frecuencia

La combinación de series temporales obtenidas mediante cruceros, boyas autónomas y sensores de alta frecuencia permitió capturar la compleja dinámica temporal del CH_4 (Grilli et al., 2018, 2020; Nicholson et al., 2018; Roth et al., 2022) en la zona costera de Chile central, integrando procesos desde escalas diarias hasta interanuales. Mientras que los cruceros permitieron dar el contexto hidrológico y biogeoquímico estacional e interanual (Farías et al., 2021b; Ma et al., 2020; Wilson et al., 2017); las observaciones continuas de la boya costera revelaron la variabilidad sinóptica y diurna del CH_4 (Roth et al., 2022), asociados a eventos de surgencia activa y relajada. Este enfoque multiescalar, poco abordado en sistemas de surgencias, permitió reducir la incertidumbre en la estimación de los flujos de este gas (ver capítulo 5.5) y evidenció la ocurrencia de "hot moments" (ver capítulo 5.3).

La disponibilidad de series de alta frecuencia mejora la parametrización de la desgasificación del CH_4 e intercambio en la interfaz mar-atmósfera, permitiendo una descripción más realista de la variabilidad de los flujos de CH_4 y su incorporación en esquemas de predicción climática a corto plazo. Al capturar eventos extremos y su recurrencia temporal, se refinan los presupuestos de CH_4 costero y se reduce la incertidumbre de las proyecciones de forzamiento radiativo global (IPCC, 2021). Esto es especialmente relevante en los EBUS, donde la alta productividad biológica y el establecimiento de la ZMO, favorecen la acumulación y emisión de GEI como CH_4.

No obstante, persisten desafíos metodológicos y tecnológicos, como la calibración cruzada entre plataformas, la corrección de deriva de los sensores a largo plazo y efectos

del biofouling sobre los sensores ópticos que pueden alterar las mediciones e introducir sesgos. Por ello se recomienda realizar campañas de inter-comparación anual, desarrollar algoritmos de auto calibración *in situ*, y establecer protocolos estándares para la integración y validación de datos de distintas fuentes (Wilson et al., 2018).

Los resultados de la serie temporal de CH_4 de alta frecuencia, fue procesada mediante una técnica de deconvolución basada en teoría inversa (Dølven et al., 2022b) que permitió corregir el tiempo de respuesta del sensor (t_{63}≈50–55 min a 4–14 °C) y resolver la variabilidad diurna y sinóptica en la zona costera. La serie corregida mostró alta concordancia con la señal original (R^2=0,98; MAE=0,8 µatm), preservando la estructura y amplitud de los eventos, y acentuó los picos de CH_4 asociados a eventos de surgencia activa sin introducir sesgos. Además, la comparación con muestras discretas *in situ* (n=18) evidenció una buena regresión lineal que reprodujo un patrón y amplitud similar (R^2=0,7), respaldando que el sensor capta variabilidad a alta frecuencia. Esto pone en evidencia que la tecnología TDLAS (Tunable Diode Laser Absorption Spectroscopy, por sus siglas en inglés) es excelente para operaciones a largo plazo debido a su alta estabilidad (Dølven et al., 2022b). Otras mediciones realizadas con sensores se han realizado en lagos (Grilli et al., 2020), en zonas de seeps marinos (Di et al., 2014; Dølven et al., 2022b; Jansson et al., 2019; Padilla et al., 2025; Schmidt et al., 2013), cerca de glaciares (Lamarche-Gagnon et al., 2019), logrando capturar una alta variabilidad, no obstante, estas tecnologías aún siguen en desarrollo (Padilla et al., 2025), debido a la concentración tan baja en el océano (del orden de nM) y al método empleado, como la difusión a través de una membrana (Boulart et al., 2010), teniendo en cuenta el tiempo de respuesta del sensor, ya que depende de ello si se necesita o no la corrección de la serie (Dølven et al., 2022b; Padilla et al., 2025).

5.2. Variación estacional e interanual del CH_4 disuelto en la plataforma continental de Chile central.

El contenido de CH_4 y su distribución vertical en la columna de agua de CH_4 viene determinado por una serie de procesos biológicos que controlan su producción (metanogénesis) y consumo (metanotrofía), así como de procesos fisios como la difusión, transporte (advección vertical y lateral) y su intercambio con la atmósfera (Reeburgh, 2007).

La plataforma continental de Chile central es una reconocida área de surgencia costera forzada por vientos a lo largos e la costa que imprimen una marcada estacionalidad (Letelier et al., 2009; Pinochet et al., 2019; Sobarzo et al., 2007). En general, vientos del S y del SO predominan en primavera-verano durante el 64-73% del año (estrés de viento promedio de 4.03 N m^2), generando un transporte Ekman neto costas afuera compensado por el ascenso superficiales/fondo de origen ecuatoriales (AESS), bajas en oxígeno y aguas ricas en nutrientes y GEI (CO_2, N_2O y CH_4). Eso contrasta con el predominio de vientos N y NO en el periodo otoño-invierno durante el 26-36% del año (estrés del viento promedio de 0.89 N m^2), conduciendo un hundimiento de aguas superficiales de origen subantártico (ASAA), oxigenadas y con pobreza relativa de nutrientes y GEI.

Estas respuestas son coherentes con el forzamiento atmosférico-oceánico regional controlado principalmente por el movimiento del anticiclón (Strub et al., 1998), que modula estacionalmente la estructura térmica y salina de la columna de agua (Escribano et al., 2004; Sobarzo et al., 2007) y las variables biogeoquímicas como el oxígeno (De La Maza and Farías, 2023) y la clorofila (Morales and Anabalón, 2012; Testa et al., 2018); estas últimas fundamentales para reciclaje de CH_4. No obstante, el contenido (inventarios) de CH_4 no exhibió un ciclo estacional robusto en 12 años de monitoreo. Esto sugiere que, a diferencia de T, S, O_2 y Chl-a, la señal de CH_4 está controlada por balances y/o

mecanismos diferentes a los que operan para las variables biogeoquímicas mencionadas, incluso para otros gases como el N_2O (Farías et al., 2015) y el CO_2 (Aguirre et al., 2021).

Los mecanismos o procesos que podrían estar actuando con distintos grados de ponderación a lo largo de un ciclo anual y que de cierta manera se reflejan en perfiles verticales típicos observados (Figura 5, manuscrito 1) son:

- Una señal estacional debido a la mineralización anaeróbica de la materia orgánica en sedimentos que conlleva a la producción de CH_4 y su acumulación en aguas de fondo a niveles de 100 nM (Farías et al., 2021b). El origen bentónico dominante debido a metanogénesis anaeróbica ya ha sido medido en los sedimentos de plataforma frente a Chile central (Ferderlman et al., 1997) por debajo de la zona de desnitrificación y sulfato reducción (diágenesis temprana). Estos procesos están modulados por la intensidad de surgencia y la estratificación que condicionan la producción primaria y la ventilación, y está ampliamente aceptado que los sedimentos situados bajo las zonas de surgencia reciben un mayor aporte de MO a través de la sedimentación (Hebbeln et al., 2000) y altas concentraciones de C y N orgánico (Summerhayes, 1983), por lo que desempeñan un papel en los ciclos globales de C y nutrientes (Walsh, 1991). Sin embargo, este estudio no pudo determinar si el CH_4 acumulado en el agua del fondo procede de la degradación aeróbica (metanogénesis anaeróbica) de la materia orgánica en el sedimento o aquella acumulada en aguas de fondo. (Martens and Klump, 1980).

- Un perfil típico de distribución típica de CH_4 en el océano costero, donde el CH_4 aumenta con la profundidad (perfil tipo 1), producto de una intensa producción bentónica y su distribución por mecanismos de difusión-advección. Se observó un claro aumento de las concentraciones de CH_4 en la capa de fondo, especialmente muy marcado durante el verano tardío al final del periodo de surgencia costera

(febrero y marzo), con una diferencia de hasta 18 veces más en esta capa en comparación con la capa superficial. Las concentraciones elevadas de CH_4 en las aguas del fondo de la plataforma continentales han sido observadas en otras áreas de surgencia como California (Capelle and Tortell, 2016) y Benguela (Sabbaghzadeh et al., 2024).

- La acumulación de CH_4 en aguas subsuperficiales, por debajo de la capa de mezcla, también es recurrente en la zona de estudio (Figura 5, manuscrito 1). Este patrón fue descrito tempranamente en aguas abiertas por Scranton & Brewer (1977) y se ha explicado por diversos procesos, principalmente la acumulación de materia orgánica en picnoclinas (Panagiota-Myrsini et al., 2017), que favorece la formación de CH_4 en micro zonas anaeróbicas dentro de partículas en suspensión y en hundimiento (De Angelis and Lee, 1994; Holmes et al., 2000; Karl and Tilbrook, 1994), así como en el tracto intestinal de copépodos (De Angelis and Lee, 1994). En este sentido, el máximo superficial de CH_4 coincide con la máxima estratificación de la columna de agua inferida a través de la frecuencia de Brunt–Väisälä; este índice mostró sus valores máximos entre 10 y 25 m de profundidad, rangos que coinciden con la termoclina y la oxiclina**,** junto con la base de la capa fótica. Por tanto, varios de los metabolismos implicados en la producción de CH_4 podrían localizarse en esta capa.

- Los máximos superficiales intermitentes de CH_4 observados en el área de estudio (perfil típico II) se explican por procesos pelágicos rápidos (producción biogénica a escalas de horas–días) asociados al reciclaje de compuestos metilados generados por el fito- y bacterioplancton (Capelle and Tortell, 2016; Florez-Leiva et al., 2013). Estos procesos pueden superar temporalmente la mezcla vertical y la advección, como se ha descrito para sistemas de surgencia y márgenes productivos. En consecuencia, los máximos de CH_4 en la capa superficial reflejan

el balance neto entre producción local y consumo (metanotrofía)**,** operando a escalas más cortas que la mezcla física y favoreciendo la acumulación local (Burke et al., 1983; Conrad and Wolfgang, 1988; Karl and Tilbrook, 1994). En ambos periodos (favorable y no favorable a la surgencia) es plausible una fuente pelágica (formación *in situ*) sostenida por el reciclaje biogeoquímico mediado por la actividad microbiana asociada la degradación de compuestos metilados o directamente por cianobacterias (y otros productores primarios) con señal acoplada a la productividad (luz/oscuro), mecanismos se discuten con mayor detalle en el capítulo 5.4. Por otro lado, aportes laterales desde plumas costeras/reforzadas por descarga continentales de esteros o emisarios urbanos pueden sostener la sobresaturación superficial particularmente durante el periodo no favorable a la surgencia (en otoño – invierno) asociado a una alta precipitación y caudal de ríos y esteros donde la descarga de CH_4 es alta tal como lo observado en el rio Itata (Bello, 2016).

Todos estos procesos descritos son coherentes con la alta heterogeneidad observada en numerosos ecosistemas (Capelle and Tortell, 2016; Kock et al., 2008; Sabbaghzadeh et al., 2024), la cual también es consistente con heterogeneidades espaciales (Farías et al., 2021a; Jakobs et al., 2014).

Es conocido que ENSO fase El Niño irrumpe la estacionalidad de la columna de agua (cambios en masas de agua, OD y nutrientes) en diversos ecosistemas. El ENSO, su fase cálida (El Niño) cambia la dinámica física, química y biológica del Pacífico Sur oriental (Escribano et al., 2004; Graco et al., 2007; Gutiérrez et al., 2008): Por ejemplo, las aguas costeras frente a Perú bajo condiciones El Niño, (i) aumenta de la temperatura superficial del mar y la isoterma de 15°C se profundiza en la columna de agua, (ii) cambia la distribución de la masa de agua, dominando en la superficie Agua Subtropical Superficial, (iii) la producción primaria disminuye debido a una disminución en el

suministro de nutrientes a las aguas superficiales y, iv) el límite superior de la frontera de la OMZ, por lo general menos profundo, se profundiza a profundidades mayores que 100 m. En la zona central de Chile se ha observado cambios en la oxigenación (De La Maza and Farías, 2023) y cambios en la produtividad (Testa et al., 2018), en los componentes químicos y biológicos (Escribano et al., 2004).

El contenido de CH_4 en la columna de agua **(**superficie–fondo) mostró diferencias significativas entre años ($p = 0.0$). Los veranos 2009/10 y 2014/15 no mostraron acumulación de CH_4 en el fondo, mientras que en 2016/17 hubo acumulación en toda la columna; estos años mostraron aguas más salinas, cálidas y oxigenadas, indicando condiciones hidrográficas anómalas que se vinculan la variabilidad con eventos ENSP (2006/07, 2009/10, 2014, 2015/16 (El Niño Godzilla), 2017 **(**El Niño costero).

Las diferencias en la respuesta podrían depender de la génesis (región en el Pacífico ecuatorial) y la diversidad de los eventos El Niño (Cai et al., 2020; Capotondi et al., 2015); los diferentes tipos de respuestas o manifestaciones en la distribución vertical de las variables biogeoquímicas podrían depender de la intensidad señales (fuertes, moderadas o débiles) a través del Pacífico Sur oriental. Es posible que las aguas costeras de Chile central respondan de manera diferente a las de Perú y el norte de Chile debido a la tele conexión oceánica respecto a Chile centro-sur; esta última puede ser considerada como la región más austral donde la señal de ondas Kelvin puede llegar más alterada y las condiciones oceanográficas e hidrográficas también son diferentes. Además, la región centro-sur de Chile está experimentando una intensificación de la surgencia costera asociada principalmente a los cambios del Anticiclón del Pacífico Sur, que a su vez están parcialmente controlados por procesos similares al ENSO (Aguirre et al., 2018; Pinochet et al., 2019; Winckler, 2020).

5.3. Variación a corto plazo del CH_4 disuelto en un periodo de surgencia de costera

Las observaciones horarias obtenidas durante la temporada de surgencia (sept 2024-feb 2025) registraron variaciones de saturaciones superficiales de CH_4 entre 178% y 4555%, y revelaron una gran coherencia sinóptica entre estrés del viento, la temperatura, la salinidad y el CH_4 superficial (Fig.1, capítulo 2). El análisis de espectral (Fig. 2, capítulo 2) mostró que el 40,3 % de la varianza del CH_4 se produjo en el intervalo de 3 a 10 días, frente al 2,5 % a las 24 h, con un componente de baja frecuencia (>10 días) que explica el 52,1 % (tendencia intra estacional).

La variabilidad sinóptica asociada a eventos activos y relajados de surgencia ha sido extensivamente descrita tanto en Chile central (Aguirre et al., 2021; Garreaud et al., 2011; Sobarzo et al., 2022), como en otras zonas de surgencia costera como la corriente de California (Send et al., 1987) y Benguela (Bailey and Chapman, 1991) y se caracteriza por pulsos de intensidad de viento a lo largo de la costa seguido por un debilitamiento o inversión de vientos, entre 2 -9 y 14 días, respectivamente. Esta dinámica tiene grandes implicancias en la ecología y la biogeoquímica del fitoplancton y el bacterioplancton (Cuevas et al., 2004; Daneri et al., 2000; Montero et al., 2007; Morales and Anabalón, 2012).

Respecto a la variabilidad sinóptica de metano, aunque muy poco descrita debido a la dificultad tecnológica para medirla (sensores), evidencia peaks y valles con una amplitud mayor a la previamente descrita para la zona (4,8 a 129 nM), por ejemplo, Monteiro et al. (2006) describe la variabilidad a escala sinóptica (“event-scale”, días) del CH_4 junto con el O_2 en el margen de Benguela, a partir de una serie horaria de un año en la capa de fondo, poniendo en evidencia que máximo de CH_4 co-ocurren con la transición a hipoxia/anoxia y están modulados por forzamientos físicos (intrusiones/cambios de masas de agua y vientos).

Los análisis compuestos (Fig. 3, capítulo 2) indican respuestas rápidas en la salinidad (<12 h) y la temperatura (12-24 h) tras el inicio de la surgencia, seguidas de un aumento del CH_4 a las ~32 h, lo que concuerda con ascenso de aguas de fondo densas, salinas, pobre en O_2 y rica en CH_4 en la bahía, asociado a AESS. Por el contrario, durante los eventos de relajación o downwelling, predominan un rápido calentamiento superficial y disminución de la salinidad después de ~30 h, lo que indica una respuesta de circulación interna dentro de la bahía (Largier, 2020b). Aunque los estuarios aledaños a la bahía pueden aportar agua dulce rica en CH_4 (Rocher-Ros et al., 2023a), como los medidos en el estuario de Dichato (45-1089 nM, datos no publicados), en este estudio no se encontró una relación clara a escala de eventos, lo que sugiere que el afloramiento domina la dinámica de la bahía (Sobarzo et al., 2022). Por lo tanto, la coherencia sinóptica entre el CH_4, el viento, la temperatura y la salinidad indica un fuerte acoplamiento con la advección vertical de aguas ricas en CH_4 y pobres en O_2, durante diferentes fases e intensidades de los eventos de afloramiento en la bahía de Coliumo.

El ciclo diurno del CH_4 fue pequeño. (anomalías promedio de ~2 nM) y probablemente reflejen los efectos contra restantes del calentamiento diurno y la brisa marina. No se pudo discernir si los ciclos diurnos de la actividad microbiana influyen sobre lo variabilidad observada. Es conocido que la actividad microbiana puede regir un comportamiento de producción y consumo a lo largo del día (Klintzsch et al., 2020; Orion Jedrysek, 1995) y como se observó en los resultados experimentales de esta tesis (capítulo 4).

Además, señales diarias concurrentes pueden interferir o cancelarse: (i) la marea barotrópica y baroclínica (M2/S2; K1/O1) y las mareas internas inyectan potencia a 12–25 h y desfases locales; (ii) la brisa marina modula los vientos y la mezcla superficial, con máximos vespertinos que aumentan la ventilación y la pérdida de CH_4, mientras el enfriamiento y vientos débiles nocturnos favorecen leves acumulaciones; (iii) aportes y

resuspensión antrópica/litoral como descarga de esteros, contaminación por efluentes y mareas verdes añaden ruido no coherente al ciclo diurno. Respecto a lo último, la proliferación de algas verdes (*Ulva sp*.) en el intermareal de la Bahía de Coliumo (Navarrete et al., 2025) podría favorecer la producción de CH_4 al aportar materia orgánica por descomposición, especialmente bajo eventos de hipoxia (Hernández-Miranda et al., 2012, 2017). Al respecto hay reportes de producción de CH_4 por descomposición de macroalgas (Björk et al., n.d.; Hall et al., 2025). Además, los esteros de Dichato y Coliumo actúan como fuentes puntuales de CH_4 hacia la bahía, con concentraciones de hasta 1089 nM (datos no publicados), esto le puede entregar un ruido adicional a la variabilidad local. Esto ha sido observado también en otras zonas costeras al sur de California (Castro-Morales et al., 2014).

El resultado es una amplitud diaria no significativa, donde la circulación forzada por vientos y topografía confiere tiempos de residencia y de mezcla que promedian señales de 24 h, superpuesto a mareas/ondas internas (Sobarzo et al., 2010) mientras la banda sinóptica (3–10 días) domina la variabilidad por el paso de bajas costeras, jets, corrientes de mareas internas y otros forzantes meteorológicos (Aguirre et al., 2010; Garreaud et al., 2002; Garreaud and Rutllant, 2003; Muñoz and Garreaud, 2005; Sobarzo et al., 2022) en Chile central. En conjunto, pueden reducir la relación señal/ruido del ciclo diario de CH_4 frente a la variabilidad sinóptica e inter estacional de mayor energía.

Finalmente, la variación de corto plazo se inserta en una variabilidad intraestacioal de un evento de surgencia costera que ocurre un 64% del año. El inicio de la surgencia que procede a un periodo de transición (agosto/septiembre) donde predomina vientos no favorable a la surgencia, ocasionando mezcla en la columna de agua y una distribución de CH_4 más homogéneas (Farías et al., 2021). El periodo de activación o inicio de la surgencia (septiembre a Diciembre) se caracteriza por intensos vientos favorables a la surgencia que se intercalan con vientos del norte y dan lugar a procesos de hundimiento y

fuertes precipitaciones y descargas de ríos y esteros, esto genera una gran amplificación en los máximos y mínimos de CH_4. Los mínimos de CH_4 se registraron cuando predominan los vientos de N (downnelling) asociado a bajas de presión y precipitaciones, que mezclan y diluyen el CH_4 en la superficie con aguas subantárticas pobres en CH_4 (Farías et al., 2021a). En el periodo maduro de la surgencia (enero a marzo), se caracteriza por una mayor estabilidad de los vientos del S, con menor amplitud. Este patrón, podría indicar que la surgencia sostenida promueve una mayor difusión de CH_4 en la superficie, pero sin agotar completamente el suministro subsuperficial de CH_4 hacia la superficie.

5.4. Procesos biogeoquímicos e interacciones microbianas en la capa superficial oxigenada

En la capa superficial, existe una distribución muy heterogénea de las concentraciones de CH_4 que da lugar a breves episodios de elevadas acumulaciones de CH_4 en la columna de agua, conocidos como "hot moments", que son acumulaciones desproporcionadas a lo largo del tiempo (McClain et al., 2003). Las concentraciones de CH_4 durante los "hot moments" fueron entre 10,17 nM (390 % de saturación) y 41,72 nM (1650 % de saturación) y persisten durante los periodos de surgencia y no surgencia (Fig. S1 y S2, capítulo 4).

Los perfiles de CH_4 en fechas específicas evidenciaron peaks de CH_4 superficial con diferentes concentraciones, que en ocasiones superan los niveles de la capa subsuperficial; esto sugiere que los "hot moments" en la capa superficial no están asociados con la advección vertical de aguas profundas ricas en CH_4, sino son el resultado de la descarga fluvial o procesos microbianos.

En síntesis, los avances que han permitido vislumbrar la paradoja del CH_4 se resumen en:

i) interacciones microbianas que permiten la producción y uso de compuestos orgánicos disueltos que liberan CH_4 como subproducto por desmetilación de compuestos metilados unidos a un fósforo (Carini et al., 2014; Repeta et al., 2016; Sosa et al., 2019, 2020); azufre (Althoff et al., 2014; Damm et al., 2015; Florez-Leiva et al., 2013; Lenhart et al., 2016) y nitrógeno (De Angelis and Lee, 1994; Bižić et al., 2020; Bižić-Ionescu et al., 2018), como el ácido metilfosfónico (MPn) metilaminas, metioninas vía escisión entre los enlaces C–P, C-N, C-S mediante enzimas liasas. Investigaciones iniciales (Karl and Tilbrook, 1994; Metcalf et al., 2012; Repeta et al., 2016) han sido complementadas por avances genómicos e isotopicas (Klintzsch et al., 2023; Lenhart et al., 2016) y han dilucidado rutas más complejas como radicales metilo inducido por ROS ((Ernst et al., 2022)

ii) Producción directa mediante la fotosíntesis (marinas y de agua dulce) (Bižić et al., 2020; Klintzsch et al., 2020; León-Palmero et al., 2020; Zheng et al., 2017); potencialmente relevante durante floraciones algales, dado principalmente por microalgas (Bizic, 2021; Cerbin et al., 2022; Günthel et al., 2020; Hartmann et al., 2020; Del Valle and Karl, 2014), cianobacterias fotosisnteticas (Berg et al., 2014; Bižić et al., 2020; Cerbin et al., 2022; Fazi et al., 2021) y picoeucariontes (León-Palmero et al., 2020). Producción directa en condiciones de oscuridad dado por cianobacterias (heterotrofia) también se ha reportado (Bižić et al., 2020; Klintzsch et al., 2020).

iii) Foto producción abiótica desde CDOM/DOM por radiación solar UV–visible (fotooxidación); suele ser menor que las vías microbianas, pero puede

contribuir y competir con la oxidación metanotrófica en la capa superficial (Li et al., 2020).

En la presente tesis se presentan evidencias de una metanogénesis metilotrófica en la siguiente sección. Por otro lado, se observó que los "hot moments" se producen de forma constante a lo largo del años, bajo diferentes escenarios de estratificación en la columna de agua, en fases de la producción primaria, diferentes estados de la sucesión fitoplanctónica (Collado-Fabbri et al., 2011; Aldunate et al., 2018; Anabalón et al., 2007), diferentes niveles de clorofila-a y diferentes proporciones de nutrientes y concentraciones de DOC (tabla 2), lo que revela una compleja interacción entre los sustratos (nutrientes y DOC), los microorganismos implicados y factores ambientales (por ejemplo, la luz, los nutrientes y la estabilidad de la columna de agua).

5.4. Mecanismos microbianos de regeneración de CH_4 en la superficie del océano, basados en experimentos controlados de laboratorio.

Durante la fase de alta productividad estival (diciembre–enero), las incubaciones en viales GC mostraron fluctuaciones de CH_4 (acumulación y consumo) en la comunidad natural, especialmente, en la fracción <3 µm (picoplancton). Los controles negativos (<0,2 µm y <0,2 µm + $HgCl_2$) se mantuvieron constantes (≤2,32 nM en diciembre y ≤5,51 nM en enero), lo que confirma un origen biológico del reciclaje de CH_4 en estas incubaciones (Tenorio and Farías, 2024), por lo tanto, se desestima procesos abióticos abióticas asociados a la fotooxidación de CDOM (Li et al., 2020), aunque la proporción relativa de esta fuente aún está en discusión.

La tasa de acumulación o consumo neto CH_4 fueron muy variables entre -0,04 y 0,46 nmol L^{-1} h^{-1}, influidas por el fotoperiodo (luz y oscuridad). Dependiendo del mes de

estudio la acumulación neta tendió a ser mayor en oscuridad para la fracción <3 µm ($p = 0.03$) en diciembre (fase I), mientras que en enero predominó el consumo neto tanto en la comunidad natural como en la fracción <3 µm, en ambos fotoperíodos. Los resultados no son concluyentes pero las diferencias sugieren que la composición microbiana y la cantidad/calidad del DOC (y sus relaciones estequiométricas) controlan el reciclaje de CH_4 (Allen et al., 2012; Spilling et al., 2019).El efecto del fotoperíodo no permitió explorar el efecto una mayor acumulación bajo luz por inhibición foto-fisiológica de metanotrofos (Dumestre et al., 1999; Murase and Sugimoto, 2005), ya que los ensayos mostraron respuestas mixtas luz/oscuridad, lo que sugiere que el balance producción–oxidación es altamente dinámico y depende del estado y composición de la comunidad microbiana y de la disponibilidad de sustratos (Tenorio and Farías, 2024). Este matiz coincide con trabajos que reportan inhibición, pero también escenarios sin un efecto claro de la luz sobre la metanotrofía, según el hábitat y la comunidad (Broman et al., 2023).

El predominio de la fracción <3 µm en las tasas netas del reciclaje de CH_4 (Fig. 5, capítulo 4) indica que el picoplancton (cianobacterias, picoeucariotas y bacterias heterótrofas) sostiene gran parte del reciclaje rápido de sustratos que permite la producción/consumo de CH_4 en un periodo corto de 24 h (Muñoz-Marín et al., 2020; Reintjes et al., 2020; Smith et al., 2013; Tenorio and Farías, 2024; Worden, 2006). Este resultado es coherente con el acoplamiento fito-bacteriano descrito para la zona de surgencia de Chile central, donde las bacterias canalizan una fracción relevante de la productividad primaria y liberan DOM como parte de la intensificación de la exudación**,** senescencia **y** pastoreo (Cuevas et al., 2004; Montero et al., 2007; Strom et al., 1997; Troncoso et al., 2003). Esos procesos bacterianos pueden estimular las rutas metilotróficas de metanogénesis (León-Palmero et al., 2020; Morán et al., 2002; Repeta et al., 2016).

La sobresaturación superficial observada durante periodos de diferente estados de sucesión fitoplanctónica, concentración de nutrientes y COD y la expuesta variabilidad

del CH_4 a lo largo de un día (esprimentos en viales), respaldan la metanogénesis metilotrófica en aguas oxigenadas debido a la disponibilidad y el reciclaje rápido de compuestos metilados (e.g. MPn y metil aminas como la TMA) (Bižić-Ionescu et al., 2018; Karl et al., 2008; Klintzsch et al., 2019, 2020; Repeta et al., 2016; Tenorio and Farías, 2024). Además, la literatura reciente muestra que microalgas y cianobacterias pueden producir CH_4 bajo diversas combinaciones de luz/temperatura (Klintzsch et al., 2020; Lenhart et al., 2016) y que el acoplamiento con la fijación de N_2 vía nitrogenasas puede generar CH_4 (directa o indirectamente) modulando la señal en la superficie (Berg et al., 2014; Zheng et al., 2017). Dicho mecanismo toma relevancia en periodos de otoño-invierno cuando la comunidad picoplanctónica de cianobacterias tienes una mayor abundancia relativa (Testa et al., 2018).

Para una comprensión más amplia, realizamos experimentos de microcosmos de medición continua cada 4 horas durante 3 días en dos fases de la productividad anual (sensu Testa et al, 2018): Fase II (fin de verano, inicios de otoño, productividad intermedia), donde predominan diatomeas pequeñas autótrofas, picoeucariotas y cianobacterias predominantes, (*Synechococcus*) (Collado-Fabbri et al., 2011); y Fase I (inicios de primavera, alta productividad), con predominio de diatomeas grandes (Anabalón et al., 2007). Nuestros resultados evidencian la predominancia de *Synechococcus sp*. En la Fase II, las concentraciones de bacterias heterótrofas fueron similares en ambas fases. Estos patrones concuerdan con lo documentado para el área de estudio (Alarcón, 2008; Aldunate et al., 2018; Collado-Fabbri et al., 2011; De La Iglesia et al., 2020; Molina et al., 2020).

Durante la fase II (abril, periodo de no surgencia**)**, las tasas de reciclaje de CH_4 fueron más altas durante la oscuridad, y acumuló CH_4 a tasas 5,4 veces superiores a las observadas durante el periodo con luz indicando una fuerte participación del bacterioplancton heterótrofo (Tabla S4, capítulo 4). En esta fase, el tratamiento de

comunidad concentrada (CC); con incrementos sustanciales en cianobacterias (*Synechococcus*, ×1.9), picoeucariotas (×1.8) y bacterias heterótrofas (×4.6) respecto a la comunidad natural (NC); mostro tasas de CH_4 notablemente mayores, especialmente en CC + MPn. La adición de MPn potenció la acumulación de CH_4 tanto en luz como oscuridad, sugiriendo una vía metilotrófica activa, en una comunidad dominada por *Synechococcus* y bacterias heterótrofas (Bižić et al., 2020). Aunque la conversión de MPn a CH_4 se ha asociado típicamente a condiciones de limitación por fósforo (Karl et al., 2008; Metcalf et al., 2012; Repeta et al., 2016), en este estudio no se evidenció ninguna limitación. Por tanto, la producción de CH_4 podría deberse a estrategias adaptativas de cianobacterias fotosintéticas frente a fluctuaciones en P (Li and Dittrich, 2019). o a la actividad de bacterias capaces de degradar fosfonatos en ambientes ricos en P (Schowanek and Verstraete, 1990).

El tratamiento con TMA también estimuló la acumulación de CH_4, pero en una menor magnitud y sin diferencias significativas entre las fracciones <3 μm y CC, lo que sugiere que la abundancia microbiana no determina necesariamente la capacidad de metabolizar TMA, posiblemente debido a una baja eficiencia en la comunidad heterotrófica concentrada para metabolizar este compuesto (De Angelis and Lee, 1994; Bižić-Ionescu et al., 2018). En conjunto, los resultados de la Fase II apoyan un mecanismo aeróbico de metanogénesis metilotrófica asociado al bacterioplancton (o picoplancton) bajo condiciones de oscuridad, alimentado por el reciclaje rápido de materia orgánica y compuestos metilados.

En contraste, durante la Fase I (septiembre, inicios de la surgencia activa)**,** las tasas de ciclado de CH_4 disminuyeron y el patrón se invirtió, siendo más altas bajo condiciones de luz. En esta fase, el tratamiento CC mantuvo las tasas más elevadas, pero la producción de CH_4 se asoció principalmente a TMA, especialmente en oscuridad, a diferencia del efecto dominante del MPn en la fase II. Esta inversión coincide con una reducción drástica

de *Synechococcus* (x−4.6) y un aumento de nano- y picoeucariotas (x3–4)**,** así como de bacterias heterótrofas, lo que indica una reconfiguración de la comunidad microbiana que favorece rutas alternativas de producción de CH_4. El metabolismo de TMA podría involucrar enzimas metiltransferasas o vías bacterianas aún no descritas (Lidbury et al., 2015; Paul et al., 2000), o incluso la llegada de microorganismos metanogénicos transportados por la surgencia.

En síntesis, los experimentos con distinto tiempo de incubación evidenciaron vías de metanogénesis metilotrófica en aguas oxigenadas, sustentados por la disponibilidad y rápida renovación de compuestos metilados (Bižić-Ionescu et al., 2018; Karl et al., 2008; Klintzsch et al., 2019, 2020; Repeta et al., 2016). Adicionalmente, la producción directa de CH_4 por microalgas y cianobacterias mediante la fotosíntesis (Klintzsch et al., 2020; Lenhart et al., 2016)(Lenhart et al., 2016; Klintzsch et al., 2020), y fijación de N_2 mediada por nitrogenasas asociadas a Fe (Berg et al., 2014; Fixen et al., 2016; Zheng et al., 2018), podrían contribuir a la sobresaturación superficial de CH_4 detectada (Tenorio y Farías, 2024). Esto ponen en evidencia que dos mecanismos (Fig. 6) estarían actuando en el área de surgencia de Chile central.

Por lo tanto, la integración de observaciones experimentales refuerza que las rutas aeróbicas del CH_4 constituyen un proceso clave para entender la dinámica de gases de efecto invernadero en sistemas de surgencia estacional, y que deben incorporarse en los modelos de intercambio mar-atmósfera para reducir la incertidumbre de las emisiones costeras.

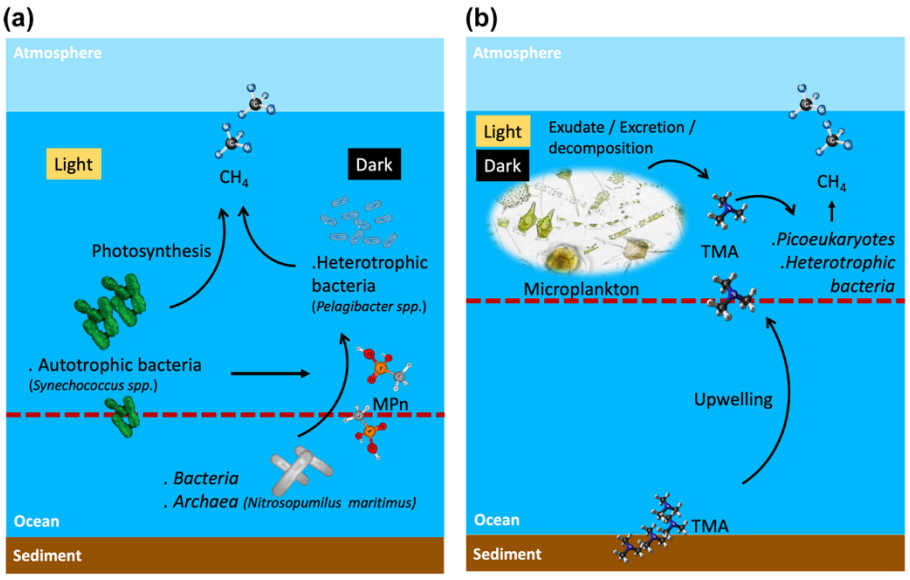

Figura 6. Esquema sugerido de los mecanismos de producción óxica en el ciclo del metano en dos períodos contrastantes de producción primaria y condiciones oceanográficas durante las fases de luz y oscuridad, en los que participan comunidades planctónicas potenciales y sustratos metilados para metabolizar el metano en las aguas superficiales. (a) Fases II y III o final de la surgencia o durante el periodo de no surgencia y (b) Fase I o periodo de surgencia. La línea discontinua muestra la oxiclina de 100 $\mu molL^{-1}$, por encima de esta línea se produce metano óxico. TMA: trimetilamina; MPn: ácido metilfosfónico.

5.5. Intercambio de CH_4 en la interfaz océano-atmósfera en plataforma continental bahía semicerrada de Chile central

5.5.1. Plataforma continental

Las estimaciones de los flujos diarios de CH_4 en la estación 18, una zona representativa de una plataforma continental sujeta a surgencia costera, fluctuaron entre 1,27 y 47,02 con valores medios 10,94 μmol m^{-2} d^{-1} (DS: 7,5 μmol m^{-2} d^{-1}). Los flujos diarios fueron medidos a partir de una serie mensual de 12 años de observación usando la parametrización de Wanninkhof, (1992) ampliamente usada y comparada con otras (Jacobs et al., 2021; Kock et al., 2008; Ma et al., 2020; Morgan et al., 2019), indicando que es la que mejor se ajusta a los regímenes de viento del área de estudio (Farias et al., 2021). La velocidad del viento fue obtenida desde estaciones meteorológicas cercanas, y aunque existe un efecto de fricción, es la que mejor representa la dinámica del área, por sobre vientos satelitales o datos reanálisis.

Relativo a la estacionalidad, aunque los flujos son mayores en periodos de surgencia ($\bar{x}$ ± DS = 12,29 ± 7,91 μmol m^{-2}), no se registraron diferencias significativas entre este y el periodo no favorable a la surgencia ($\bar{x}$ ± DS = 8,51 ± 5,99 μmol m^{-2}). Aunque, los vientos favorables a la surgencia ejercen un papel general de desgasificación (Ho et al., 2011; Sweeney et al., 2007); el contenido de metano en la capa de mezcla no muestra una variación estacional significativa, indicando que ambos componentes (el gradiente y la velocidad de transferencia juegan un papel importante en la tasa de intercambio.

Las tasas de intercambio son mayores que otras medidas en áreas costeras sujetas a surgencia (Tabla 5) como la costa de Canadá (Capelle and Tortell, 2016), el mar Arábigo (Bange et al., 1998), el Mar Báltico (Bange et al., 2010) o Mauritania (Brown et al., 2014),

aunque la definición temporal en estos estudios es limitada y no incluye largas series de tiempo como en el Mar Báltico, donde los flujos son 16,2 veces mayores, debido a la hipoxia/anoxia y a fuertes fuentes bentónicas.

Tabla 5. Flujos de metano hacia la atmósfera en diferentes sistemas de surgencia.

Localización	Concentración de CH_4 en la capa superficial		Flujos de CH_4 hacia la atmósfera		Referencias
	nM	% Sat	Flujos diarios ($\mu mol\ m^{-2}\ d^{-1}$)	Emision anual por área ($Gg\ CH_4\ año^{-1}$)	
Atlántico Nor-oriental subtropical (Océano abierto)	3,52	-	0,11	-	Scranton y Brewer (1976)
Mar Arábigo					
Surgencia costera (SC)	2,25 ± 0,10	116 ± 8	1,37 - 2,33	0,50 - 0,90	Bange et al. (1988)
Océano abierto (OA)	-	113 ± 5	1,06 - 1,87	1,00 - 1,80	
Pacífico Norte oriental subtropical					Sansone et al. (2001)
Giro	2,84	-	3,00	-	
SC	3,51	-	0,77	-	
Bahía de Benguela (BB)					
Sur BB	32,73	-	-9,98 – 0,35	-	Berner et al. (2003)
Centro BB	26,00 - 100,00	-	-24,57 – 27,53	-	
Norte BB	13,50 - 120,00	-	145,00 – 39,00	-	
Atlántio Nororiental tropical (Surgencia Mauritania)	2,10 – 5,50	-	26,15 – 45,67	1,60 - 2,90	Kock et al. (2008)
Serie de Tiempo, estación Boknis Eck (BE) (Bahía Eckernförde, mar Báltico)	6,60 - 235,00	1785 - 8340	6,20 - 14,70	-	Bange (2010)

Central Chile upwelling system	3,08 - 16,00	125 - 550	11 – 115	-	Flores-Leiva et al. (2013)
Surgencia al norte de los 20°N (Mauritania), NO de África	2,20 ± 0,30	101,70 ± 14,00	10,17 ± 8,51	0,77 ± 0,64	Browm et al 2014
Sur de la isla de Gotland (Mar Báltico)	5,10	137%	-		Schneider et al 2014
Surgencia de la Columbia Británica: Costa Oeste de la Isla de Vancouver	6,70 - 9,50	-	2,5 a 34,1	-	Capelle et al., 2016
Zona costera Belga					
Near shore (NS)	670	-	345,24	-	Borges et al 2017
Off shore	4	-	76,72	-	
Estación ALOHA en el giro subtropical del Pacífico norte	2,00 – 2,30	99,00 - 105,00	-0,2 - 1,5	-	Wilson et al., 2017
Suroeste del Mar Báltico	187,20 – 217,80	129 - 5563	0,3-746,3	-	Ma et al 2020
Mar Arabigo Mangalore Kochi	 12 35,5	 101 - 6435 101 – 7456	0,03 - 170	3,2	Sudheesh et al., 2020
Surgencia costera de Chile central	1,75 – 54,64	6,97 – 1508,95	1,27 – 47,02	1 – 4	Este estudio

La variabilidad interanual de los flujos de CH_4, comparando periodos estacionales (primavera-verano vs otoño-invierno) no parece estar asociada con cambios en el estrés del viento favorable a la surgencia costera, por lo que estos pueden deberse a algunas condiciones biogeoquímicas e hidrográficas en la columna de agua remotamente advectada desde la zona ecuatorial asociados a eventos ENSO (Fig. 3).

En cuanto a la variabilidad interanual de los flujos de CH_4, el flujo más alto se observó durante EN 2015/16 y el flujo más bajo durante el EN 2009/10. Estas diferencias parecen estar asociadas con el tipo de eventos El Niño. La variabilidad del flujo de CH_4 no parece estar asociada con cambios en el estrés favorable a la surgencia por lo que estos pueden deberse a condiciones biogeoquímicas e hidrográficas en la columna de agua remotamente advectada. Durante el otoño-invierno de 2009, 2011, 2012 y 2015, los flujos de CH_4 son mayores o similares a los estimados en primavera-verano. Esto es un patrón diferente al observado habitualmente, donde el flujo medio de CH_4 en primavera-verano supera entre 1,4 y 2,7 veces el estimado en otoño-invierno. Aun así, la variabilidad interanual del flujo de CH_4 permanece sin resolverse y es más probable que esté asociada a las condiciones oceanográficas y a las variaciones en las masas de agua advectadas y/o a la escorrentía continental. Sabiendo que los eventos El Niño aumentan las precipitaciones, los niveles de CH_4 podrían proceder de la descarga de los ríos y de la escorrentía continental (Rao and Sarma, 2017; Rocher-Ros et al., 2023b), como la influencia de la pluma de río Itata (Saldías et al., 2012; Testa et al., 2018). No obstante, en la última década de mega sequía (Garreaud et al., 2019) ya casi no hay plumas estacionales sino eventos episodios de alta descarga debido a ríos atmosféricos (Garreaud et al., 2024). Sabiendo que los eventos EN aumentan las precipitaciones, los niveles de CH_4 podrían proceder de la descarga de los ríos y de la escorrentía continental (Roa et al., 2017; Rocher-Ros et al., 2023), como ocurrió en 2015-2016, no obstante, esto no ocurrió en EN del 2009-2010. Por ello son necesarios más esfuerzos para comprender mejor los mecanismos biogeoquímicos y físicos relacionados (por ejemplo, ENSO, Oscilación Decadal del Pacífico PDO y otras tele-conexiones climáticas).

5.5.2. Bahia Coliumo

En un periodo de surgencia costera (septiembre 2024 – febrero 2025), los flujos de CH_4 hacia la atmósfera en la bahía de Coliumo, medidos en forma horaria a partir de un sensor calibrado y validado, fluctuaron entre 0 y 10,7 μmol m^{-2} h^{-1} ($\bar{x}$ ± DS = 0,79 ± 1,24 μmol m^{-2} h^{-1}), correspondientes a 1,6 y 94 μmol m^{-2} d^{-1} ($\bar{x}$ ± DS = 18,8 ± 16,29). Estos flujos fueron estimados a partir de la estación meteorológica de Dichato, que representa bien el régimen local de vientos de la bahía (Calliari and Alfaro, 1997), usando la misma parametrización que en la estación 18 (Wanninkhof, 1992).

La variabilidad intra estacional estuvo dominada por la progresión de las estaciones y fue especialmente evidente en las anomalías del estrés del viento, la temperatura (Fig. 1, capítulo 2), cambios graduales en la amplitud de la variabilidad sinóptica (3-10 d) y en la duración de los eventos de afloramiento activos (Fig. 2-3). Esto permitió tener mayor frecuencia de anomalías positivas de CH_4 durante el verano. Esta evolución está impulsada por la migración hacia el polo del anticiclón del Pacífico sudoriental (SPA), que comienza en primavera (septiembre) y refuerza los vientos costeros hacia el ecuador (sur), favorables para el afloramiento; las bajas costeras intermitentes modulan estos vientos, especialmente en primavera hasta que el SPA se estabiliza en verano (Strub et al., 2013). En conjunto, estos procesos indican que la bahía de Coliumo actúa como un punto caliente biogeoquímico dinámico, donde los forzamientos físicos y los procesos microbianos mantienen conjuntamente un CH_4 disuelto localmente elevado en relación con la plataforma adyacente. Así, la variabilidad intra estacional establece el fondo, y la variabilidad sinóptica (3-10 d) y diaria (~24 h) modula aún más las concentraciones de CH_4 y los procesos que controlan su ciclo.

En la escala sinóptica, durante los eventos activos de surgencia los flujos diarios fluctuaron entre 1,7 y 93,89 μmol m^{-2} d^{-1} ($\bar{x}$ ± DS = 25,38 ± 17,74 μmol m^{-2} d^{-1}), durante

los periodos relajados variaron entre 1,58 y 51,2 μmol m^{-2} d^{-1}, ($\bar{x}$ ± DS = 9,156 ± 9,58 μmol m^{-2} d^{-1}), mientras en periodos de downwelling fueron de 2,42 y 34,99 μmol m^{-2} d^{-1}, ($\bar{x}$ ± DS = 10,15 ± 6,44 μmol m^{-2} d^{-1}). Evidenciando que, durante los eventos activos, la advección de aguas de fondo y la trasferencia dada por el viento son factores que gatillan flujos positivos hacia la atmósfera.

Más allá del mecanismo de control atmosférico (viento), en las bahías costeras poco profundas (Morgan et al., 2019; Weber et al., 2019), el control físico (mareas) es importante, a través del bombeo de sedimentos y la mezcla/turbulencia que añaden a la dinámica diaria del gas de efecto invernadero (De Groot et al., 2023; Sturm et al., 2017). Durante la marea baja, el gradiente de presión impulsa el bombeo de aguas intersticiales ricas en CH_4 desde los sedimentos hacia la columna de agua, lo que provoca peaks en la concentración y los flujos de CH_4 (Sturm et al., 2017). Por el contrario, en marea alta el aumento de la profundidad inhibe la liberación de burbujas del sedimento debido al aumento de la presión hidrostática (Borges and Abril, 2012), sin embargo, intensifica la mezcla turbulenta en la superficie y acelera el venteo de CH_4 dando lugar a altos flujos de metano a la atmósfera, con concentraciones más diluidas en la columna de agua a pesar de la baja actividad metanotrófica (De Groot et al., 2023).

Los eventos de precipitación observados solo al inicio de la surgencia costera no muestran señales esperadas debido a descargas continentales. El aporte continental ha sido descrito por aumentar el contenido de metano en la capa superficial y por ende favorece los flujos de CH_4 al incorporar aguas ricas en metano (Bello, 2016; Rocher-Ros et al., 2023b; Upstill-goddard and Barnes, 2016). Este proceso podría ser importante en una bahía semicerrada como Coliumo, influido por los esteros Coliumo y Dichato y el río Pingueral, todos con impacto antropogénico (Inostroza et al., 2024). La falta de relación puede deberse a la mínima descarga de agua dulce de esos esteros, al rápido intercambio de la había con la zona adyacente (Valle-Levinson et al., 2003) o a la dilución producida

en el trayecto como ocurren en la bahía sur de Alemania (Bussmann et al., 2021), no obstante este proceso requiere mejor estudio temporal y espacial del CH_4 así como la influencia de plumas de ríos adyacentes, ya que se ha evidenciado dilución pero con peacks heterogéneas distribuidos espacialmente (Bussmann et al., 2021).

En relación con el ciclo diario del CH_4 (0-23h), los flujos fluctuaron entre 0 y 10,7 μmol m^{-2} h^{-1}, ($\bar{x} \pm DS = 0,65 \pm 0,82$ μmol m^{-2} h^{-1}), los valores más bajos coincidieron con valores de vientos calmos (media ~1 m/s) con dirección hacia el N y bajas temperaturas, durante la noche (Fig. 5). periodo en el que la mezcla superficial es mínima, y el gradiente de concentración de CH_4 se mantiene relativamente alto y estable. Los valores más altos coinciden tras la máxima radiación durante la tarde, lo que permite el aumento de la temperatura del agua y por tanto una desgasificación (menor solubilidad de los gases); sumado al refuerzo de los vientos que rompen la capa de mezcla y permiten un mayor intercambio en la interfase mar-atmósfera. La sobresaturación de metano, persistente a lo largo del día, pone de relieve la importancia de la brisa marina, donde los ciclos locales del viento modulan la calma y la mezcla diarias (Aguirre et al., 2021; Muñoz, 2008).

5.6. Emisiones de metano a la atmosfera por ecosistemas costeros

Las zonas costeras someras, en promedio son un aporte neto de CH_4 hacia la atmósfera y dominan el presupuesto global marino (Borges et al., 2016; Resplandy et al., 2024; Weber et al., 2019). En este sentido, respecto a la plataforma continental de Chile central, representada por la ST18, los flujos promedios variaron entre 1,27 y 47,02 μmol m^{-2} d^{-1}; estos son relativamente altos comparado con la surgencia de la costa oeste de Canadá (Capelle and Tortell, 2016), Mar Arábigo (Bange et al., 1998), el mar Báltico (Bange et al., 2010), y el NO de Mauritania (Brown et al., 2014). Para este último Kock et al. (2008), reportó flujos mayores, debido a la magnitud del viento que fue 13,3 mayor

que el reportado por Brown et al. (2014). También, se resalta los altos flujos reportados por Florez-Leiva et al. (2013) para esta zona de estudio (Tabla 5.1), esto se debe a magnitudes de vientos mayores (3,5 a 15,6 m s^{-1}) que los encontrados en este estudio (0,64 a 13,38 m s^{-1}).

Considerando el ciclo anual de flujos de CH_4, calculados a través de los promedios ponderados durante los periodos de surgencia (64%) y no surgencia (36%) (Farías et al., 2021b), y superficie representativa de la plataforma continental de Chile central equivalente a 41 150 km^2 (*sensu* Farías et al., 2015), se estima un flujo entre ~ 1 y 4 Gg y^{-1} para el área de estudio. Esta estimación podría ser mayor si se considerara que la zona también tiene fluctuaciones sinópticas (Aguirre et al., 2019, 2021; Sobarzo et al., 2022) que no son registrados con un mensual, sumado a fuertes ráfagas de vientos que no son consideradas en el cálculo del flujo porque no coinciden con la fecha de muestreo como ocurrió con Florez-Leiva et al. (2013), Brown et al. (2014) y Kock et al. (2008).

Dado que la plataforma continental frente a Concepción representa sólo el 3,5% del área global de afloramiento costero (EPA, 2010), esta zona se convierte en un verdadero hot spot para la emisión de CH_4, representando entre el 1,7 al 13% de la emisión global para las regiones de afloramiento, que varían de 0,02 a 1,5 Tg C $año^{-1}$ (Bakker et al., 2014; Denman et al., 2007; Hamdan and Wickland, 2016).

Respecto a la bahía Coliumo ubicada en la misma latitud, pero con una circulación semi cerrada y considerando un área de 4,76 km^2, contribuye anualmente con aproximadamente 0,5 Mg CH_4 y^{-1}, con flujos promedio que varían entre 1,8 y 94 μmol m^{-2} d^{-1}. Esto significa que los ambientes someros de pequeña superficie pueden contribuir con el doble de emisiones al día. No obstante, dada el área de la plataforma continental y el valor que representa solo un punto (ST18), podría estar sesgando o trasponiendo valores no representativos.

Cuando comparamos los flujos ponderados por m^2 entre la bahía (isóbata de 10m) y la plataforma adyacente (ST18, isóbata de 90m), observamos un marcado gradiente costa-océano; en 10m el flujo medio ponderado es 18,84 μmol m^{-2} d^{-1}, mientras que en 90m es 10,9 μmol m^{-2} d^{-1}. Así el flujo en 10m es ~1,7 veces mayor que en 90 m, consistente con un descenso casi exponencial de CH_4 hacia mar abierto, ya sea por procesos de dilución oxidación o menor aporte bentónico por el aumento de la profundidad (Sansone et al., 2001; Weber et al., 2019), ver Tabla 5. Por otro lado, al integrar sobre el área, la plataforma domina su extensión (41150 km^2 vs 4,76 km^2), la bahía de Coliumo actúa como un hot spot que exhibe altas tasas de flujos por unidad de superficie, pero el inventario regional de emisiones de CH_4 está dado por la plataforma continental.

Además, eventos extremos durante primavera-verano (flujos diarios >40 mol m^{-2} d^{-1}), capturados con la serie de alta frecuencia pueden contribuir hasta con un ~11.05 % de las emisiones de la Bahía de Coliumo. Estos eventos a menudo se enmascaran por la toma de mediciones discretas y pone en relieve cómo las observaciones de alta frecuencia en la Bahía de Coliumo, un sistema costero poco profundo, rico en nutrientes y físicamente dinámico, permite capturar verdaderos hot moments de CH_4. Estos pequeños sistemas son comparables con otras bahías sujetas a surgencia costera como la bahía de Tomales en la corriente de California (Sansone y Smith, 1998) y Ría de Vigo (España) en la corriente de Canarias (Kitidis et al., 2007).

5.7. Incertidumbre y mejora de las estimaciones locales regionales y globales

Amplios rangos de emisiones oceánicas han sido reportados, variando desde 4 a 45 Tg CH_4 $año^{-1}$ (Bates et al., 1996; Rhee et al., 2009; Wuebbles & Hayhoe, 2002), hasta valores más acotados entre 6 y 20 Tg CH_4 $año^{-1}$ (Saunois et al., 2025). Esto es debido a (i) escalamientos bottom-up con pocos datos, (ii) por cobertura espacial para una alta

heterogeneidad espacial del océano (hot spot, gradiente costa-océano), (iii) poca cobertura temporal para una alta variabilidad temporal (procesos sinópticos, diurnos, hot moments) que pasan desapercibidos con muestreos discretos de baja frecuencia (Saunois et al., 2016a, 2020, 2025) y la dependencia del tiempo para navegar en condiciones óptimas, y (iv) limitaciones en el desarrollo de tecnologías para la medición de este gas, así como el acceso de los mismo (costo/mantenimiento).

En relación a la serie mensual, la comparación de bloques de promedios interanuales y estacionales, mostraron que la variabilidad interanual (CV ~33%) es menor que la variabilidad estacional (CV~55%), esto sugiere que la escala estacional podría mostrar eventos no capturados por la frecuencia mensual. Por el contrario, la media interanual, al integrar todas las estaciones, suaviza la señal (bajo CV), pero al depender del número de años y de eventos climáticos como el ENSO, aumentan la dispersión, esto es demostrado por la mayor incertidumbre presentada en esta escala IC_95 = 17%, en comparación con la escala estacional.

Por otro lado, la serie de alta frecuencia permitió hacer escalamientos más cortos de 1, 3, 7,15 a 30 días, se observó que los bloques mantenían el promedio en todas las ventanas, esto es esperable dado el re-muestreo en la misma serie, mientras que mínimos y máximos se contraen fuertemente al aumentar la ventana y el CV disminuye desde ~86% a 1 día hasta ~47% en los bloques de 30d. lo que sugiere que ventanas más amplias (e.g. 30d) suavizan los peaks y disminuye a variabilidad relativa que puede estar dada por eventos de corta duración como hot moments. Esto es coherente con el estimador de incertidumbre que es mayor (IC_95 = 34,4%) en la ventana más amplia.

Esta evaluación multiescala, refleja claramente que la serie mensual y de alta frecuencia, aun cuando ambas explican la dinámica de un ambiente similar, la capacidad de observación de procesos difiere sustantivamente (Dickey, 1991).

Adicionalmente, análisis de sensibilidad a diferentes vientos y parametrizaciones (Kw) se realizaron para comparar, cómo influye en el resultado de las emisiones. La comparación entre vientos de las estaciones meteorológicas de Dichato y Carriel Sur y Re-análisis (ERA5), evidenciaron flujos 1,6 y 2,1 veces mayor para Carriel Sur y ERA5 en comparación con los flujos de Dichato. Esto confirma que el viento es el principal gatillante de los flujos CH_4 en la interfaz mar-atmósfera. Por ello, los flujos para la bahía de Coliumo se calcularon con los vientos de la estación de Dichato, debido a su localización, menos 1km de la boya (Calliari y Alfaro, 1997), están influenciados por la morfología de la zona (Largier, 2020b; Valle-Levinson et al., 2003; Varvayanni et al., 1993) y representan el 75% de la varianza para la zona, ajustándose perfectamente con la localización de la bahía, hacia el ecuador.

También, se compararon las diferentes parametrizaciones de los coeficientes de transferencia (Kw). Las parametrizaciones de W92, Nightingale et al. 2000 y Ho et al. 2006 mostraron una mayor coherencia en cuanto a los resultados del flujo, especialmente con vientos inferiores a 6 m/s. Sin embargo, W92, ampliamente utilizado en los balances de metano, sobreestima los flujos en comparación con los anteriores, especialmente cuando el viento aumenta (>4 m/s). Las parametrizaciones de Liss y Merlivat 1989, seguidas de W99, fueron las más conservadoras, especialmente con vientos calmos (~3 m/s). Ho et al., 2006, mostró coherencia con W92 y N2000 con vientos menores a 6 m/s, pero con vientos superiores a estos se sitúa en un valor intermedio entre ambos y puede captar mejor las ráfagas de viento que se producen dentro de la bahía, sin sobreestimarlas como hace W92 ni subestimarlas como hace Nightingale et al., 2000. No obstante, para fines comparativos de ambas series, se utilizó la parametrización de W92.

CONTRASTACIÓN DE HIPÓTESIS

HIPÓTESIS 1: Existe una variabilidad diaria en las concentraciones de CH_4 superficial, asociada a forzantes físicos (ej. radiación solar, temperatura, brisa marina) que modulan la ventilación y el intercambio en la interfaz mar-atmósfera y procesos biológicos dependientes de la luz que regulan la producción y oxidación de este gas.

Esta hipótesis es rechazada dado que no se observaron variaciones significativas de CH_4 en la escala diurna, por el contrario, la concentración neta diaria durante el periodo de surgencia diluyó los promedios diarios, especialmente durante el desarrollo de la surgencia, de noviembre a febrero. Aunque las anomalías, evidenciaron una marcada variabilidad diaria, con anomalías positivas durante la noche, asociada a vientos calmos y bajas temperaturas, y anomalías negativas durante el día debido a un aumento en el viento y la temperatura; este patrón se vuelve inverso hacia el final de la surgencia (febrero, anomalías diurnas mensuales), esto sugiere que los procesos que controlan la variabilidad de CH_4 a escala diurna en bahías costeras son más complejos y están influenciados por eventos puntuales como la dirección (del N) e intensidad de los vientos como se ve al inicio de la surgencia (septiembre y octubre). Esta inversión también se puede atribuir a cambios en la composición fitoplanctónica que ocurre en la transición del periodo de surgencia y no surgencia, donde se ve favorecido por el picoplancton, que puede producir CH_4, tanto en condiciones de luz y oscuridad. A esto último, se le suman los resultados de experimentos donde hubo una mayor producción de CH_4 en condiciones de oscuridad. Otro factor importante para considerar es la ubicación de la estación de la boya costera que enmascara procesos oceanográficos con procesos locales de la zona costera.

HIPÓTESIS 2: Existe una variabilidad sinóptica (2–10 días) significativa del CH_4 superficial, mayor que la estacional, impulsada por la alternancia de viento que modulan los períodos activos y relajados de surgencia.

Esta hipótesis es aceptada, la escala sinóptica los datos de alta frecuencia evidenciaron que las mayores concentraciones de CH_4 fueron en los periodos activos de la surgencia, lo que sugiere que la dinámica del CH_4 en la bahía sujeta a surgencia costera, está dominado por procesos físicos (ej. la advección de aguas subsuperficiales ricas en CH_4 como las AESS o la re-suspensión de sedimentos) que por la producción local mediada por el bacterioplancton. Por el contrario, durante periodos de relajación o downwelling, las concentraciones de CH_4 fueron bajos, asociados principalmente a bajas de presión y dilución/mezcla con ASSA. Esto confirma confirma la influencia de los procesos físicos sobre los procesos biológicos, especialmente en zonas costeras sujetas a surgencia altamente dinámicas.

6. CONCLUSIONES

- La serie mensual de doce años en la plataforma continental de Chile central mostró una fluctuación amplia del CH_4 (1,75 y 100,86 nmol L-1), con saturaciones entre 67,11 % y el 3965 % y con mayores concentraciones en el fondo, durante el periodo favorable a la surgencia. También, se observó una sobresaturación constante de CH_4 en la superficie (>120 %), con una estacionalidad débil y una variabilidad interanual asociada al ENOS (mínimo en 2009/10 y máximos en 2015/16). La difusión-advección vertical dominó el 54% de los perfiles, indicando un acoplamiento entre procesos bentónicos y pelágicos que sostienen la sobresaturación permanente.

- La serie de alta frecuencia (horaria) mostró una variabilidad sinóptica del CH_4 superficial, asociado a eventos activos y relajados de la surgencia, con altas concentraciones en el periodo activo y bajas en los periodos relajados (ej. Eventos inactivos y downwelling). La variabilidad diaria del CH_4 no fue significativa.

- La comparación entre la serie mensual y horaria evidenció que el muestreo a baja frecuencia (mensual) subestima significativamente el contenido y flujos de CH_4 hacia la atmósfera, lo que introduce un sesgo sistemático en las estimaciones. Durante la temporada de surgencia (primavera-verano), los flujos de CH_4 en la plataforma interior (bahía) en promedio ($x \pm DS = 18,8 \pm 16,3$ µmol m^{-2} d^{-1}), son el doble de los flujos estimados en la plataforma exterior (ST18; $x \pm DS = 12,6 \pm 4$ µmol m^{-2} d^{-1}). Aun considerando que la ST8 probablemente está subestimado y que la serie de la bahía es corta (no capta la variabilidad anual), la diferencia es robusta. Esto se explica por la poca profundidad (~10 m), su cercanía con el sedimento y el proceso advectivo de surgencia. Por lo tanto, el monitoreo a alta

frecuencia es esencial para caracterizar eventos extremos y “hot moments” impulsados por el viento y la advección (surgencia).

- Los experimentos en laboratorio demostraron que el CH_4 superficial se genera biológicamente en condiciones óxicas y es dominado por el picoplancton (<3 μm), tanto en condiciones de luz como de oscuridad, pero con mayores tasas en oscuridad. En el periodo no favorable a la surgencia (otoño-invierno) *Synechococcus sp.*, podría ser responsable de la regeneración de CH_4 a través de la fotosíntesis, además, niveles de DOC y relaciones N:P inorgánicas podrían estimular a las bacterias heterótrofas a metabolizar MPn y contribuir al reciclaje de CH_4 óxico. En el periodo favorable a la surgencia (primavera-verano), la advección de aguas subsuperficiales enriquecidas en compuestos metilados (TMA y derivados) y el cambio en la estructura del picoplancton (mayor abundancia de bacterias y pico y nano-eucariotas) durante la surgencia, sugieren la producción de CH_4 a través de la TMA, proceso aún desconocido, que contribuyen a la sobresaturación de CH_4 persistente en la capa superficial oxigenada.

7. REFERENCIAS

Aguirre, C., Pizarro, O., and Sobarzo, M.: Observations of semidiurnal internal tidal currents off central Chile (36.6°S), Cont Shelf Res, 30, 1562–1574, https://doi.org/10.1016/j.csr.2010.06.003, 2010.

Aguirre, C., García-Loyola, S., Testa, G., Silva, Di., and Farías, L.: Insight into anthropogenic forcing on coastal upwelling off south-central Chile, Elementa, 6, 1–13, https://doi.org/10.1525/elementa.314, 2018.

Aguirre, C., Rojas, M., Garreaud, R. D., and Rahn, D. A.: Role of synoptic activity on projected changes in upwelling-favourable winds at the ocean's eastern boundaries, NPJ Clim Atmos Sci, 2, https://doi.org/10.1038/s41612-019-0101-9, 2019.

Aguirre, C., Garreaud, R., Belmar, L., Farías, L., Ramajo, L., and Barrera, F.: High-frequency variability of the surface ocean properties off central Chile during the upwelling season, Front Mar Sci, 8, 1–19, https://doi.org/10.3389/fmars.2021.702051, 2021.

Ahumada, R. and Chuecas, L.: Algunas características hidrográficas de Bahía de Concepción (36° 40'S; 73° 02'W) y áreas adyacentes, Gayana Miscelanea, 8, 1–56, 1979.

Alarcón, G.: Variabilidad estacional de la comunidad picoplantónica en la zona de surgencia altamente productiva, Magíster, Universidad de Concepción, 192 pp., 2008.

Aldunate, M., De la Iglesia, R., Bertagnolli, A. D., and Ulloa, O.: Oxygen modulates bacterial community composition in the coastal upwelling waters off central Chile, Deep Sea Research Part II Topical Studies in Oceanography, 156, 68–79, https://doi.org/10.1016/j.dsr2.2018.02.001, 2018.

Allen, L. Z., Allen, E. E., Badger, J. H., McCrow, J. P., Paulsen, I. T., Elbourne, L. D., Thiagarajan, M., Rusch, D. B., Nealson, K. H., Williamson, S. J., Venter, J. C., and Allen, A. E.: Influence of nutrients and currents on the genomic composition of microbes across an upwelling mosaic, ISME Journal, 6, 1403–1414, https://doi.org/10.1038/ismej.2011.201, 2012.

Althoff, F., Benzing, K., Comba, P., McRoberts, C., Boyd, D. R., Greiner, S., and Keppler, F.: Abiotic methanogenesis from organosulphur compounds under ambient conditions, Nat Commun, 5, https://doi.org/10.1038/ncomms5205, 2014.

Anabalón, V., Morales, C. E., Escribano, R., Varas, A. M., and Varas, M. A.: The contribution of nano- and micro-planktonic assemblages in the surface layer (0-30 m) under different hydrographic conditions in the upwelling area off Concepción, central Chile, Prog Oceanogr, 75, 396–414, https://doi.org/10.1016/j.pocean.2007.08.023, 2007.

Ancapichun, S. and Garcés-Vargas, J.: Variability of the Southeast Pacific Subtropical Anticyclone and its impact on sea surface temperature off north-central Chile, Cienc Mar, 41, 1–20, https://doi.org/10.7773/cm.v41i1.2338, 2015.

De Angelis, M. A. and Lee, C.: Methane production during zooplankton grazing on marine phytoplankton, Limnol. Oceanogr., 39, 1298–1308, 1994.

Atkinsont, L. P. and Richards, F. A.: The occurrence and distribution of methane in the marine environment*, 673 pp., 1967.

Bailey, G. and Chapman, P.: Short-term variability during an anchor station study in the southern Benguela upwelling system: Chemical and physical oceanography, 37 pp., 1991.

Bakker, D., Bange, H., Gruber, N., Johannessen, T., Upstill-Goddard, R. C., Borges, A., Delille, B., Löscher, C., Naqvi, S., Omar, A., and Santana-Casiano, J.: Air–sea interactions of natural long-lived greenhouse gases (CO2, N2O, CH4) in a changing climate, in: Ocean-Atmosphere Interactions of Gases and Particles, edited by: Liss, P. S. and Johnson, M. T., Springer, 113–169, https://doi.org/https://doi.org/10.1007/978-3-642-25643-1_3, 2014.

Bakun, A.: Coastal upwelling indices, west coast of North America, 1946-71, NOAA Technical Report NMFS SSRF-671, 1973.

Bange, H. W., Bartell, U. H., Rapsomanikis, S., and Andreae, M. O.: Methane in the Baltic and North Seas and a reassessment of the marine emissions of methane, Global Biogeochem Cycles, 8, 465–480, 1994.

Bange, H. W., Ramesh, R., Rapsomanikis, S., and Andreae, M. O.: Methane in surface waters of the Arabian Sea, Geophys Res Lett, 25, 3547–3550, 1998.

Bange, H. W., Bergmann, K., Hansen, H. P., Kock, A., Koppe, R., Malien, F., and Ostrau, C.: Dissolved methane during hypoxic events at the Boknis Eck time series station (Eckernförde Bay, SW Baltic Sea), Biogeosciences, 7, 1279–1284, https://doi.org/10.5194/bg-7-1279-2010, 2010.

Bates, T. S., Kelly, K. C., Johnson, J. E., and Gammon, R. H.: A reevaluation of the open ocean source of methane to the atmosphere, Journal of Geophysical Research Atmospheres, 101, 6953–6961, https://doi.org/10.1029/95JD03348, 1996.

Bello, E.: Variabilidad estacional en la descarga de metano disuelto desde un sistema estuarino a la zona marina adyacente, el caso de ríos de la zona central de chile (río Itata), Universidad de Concepción, 76 pp., 2016.

Benway, H. M., Lorenzoni, L., White, A. E., Fiedler, B., Levine, N. M., Nicholson, D. P., DeGrandpre, M. D., Sosik, H. M., Church, M. J., O'Brien, T. D., Leinen, M., Weller, R. A., Karl, D. M., Henson, S. A., and Letelier, R. M.: Ocean time series observations of changing marine ecosystems: An era of integration, synthesis, and societal applications, https://doi.org/10.3389/fmars.2019.00393, 2019.

Berg, A., Lindblad, P., and Svensson, B. H.: Cyanobacteria as a source of hydrogen for methane formation, World J Microbiol Biotechnol, 30, 539–545, https://doi.org/10.1007/s11274-013-1463-5, 2014.

Berner, U., Poggenburg, J., Faber, E., Quadfasel, D., and Frische, A.: Methane in ocean waters of the Bay of Bengal: Its sources and exchange with the atmosphere, Deep Sea Res 2 Top Stud Oceanogr, 50, 925–950, https://doi.org/10.1016/S0967-0645(02)00613-6, 2003.

Bizic, M.: Phytoplankton photosynthesis: An unexplored source of biogenic methane emission from oxic environments, J Plankton Res, 43, 822–830, https://doi.org/10.1093/plankt/fbab069, 2021.

Bižić, M., Klintzsch, T., Ionescu, D., Hindiyeh, M. Y., Günthel, M., Muro-Pastor, A. M., Eckert, W., Urich, T., Keppler, F., and Grossart, H. P.: Aquatic and terrestrial cyanobacteria produce methane, Sci Adv, 6, 1–10, https://doi.org/10.1126/sciadv.aax5343, 2020.

Bižić-Ionescu, M., Ionescu, D., Günthel, M., Tang, K. W., and Grossart, H. P.: Oxic methane cycling: new evidence for methane formation in oxic lake water, in: Biogenesis of Hydrocarbons, Handbook of Hydrocarbon and Lipid Microbiology, edited by: Stams, A. J. M. and Souza, D. Z., Springer International Publishing AG, part of Springer Nature, 1–22, https://doi.org/https://doi.org/10.1007/978-3-319-53114-4_10-1, 2018.

Björk, M., Rosenqvist, G., Gröndahl, F., and Bonaglia, S.: Methane emissions from macrophyte beach wrack on Baltic seashores, Ambio, 52, 171–1, https://doi.org/10.1007/s13280, 2023.

Borges, A. V. and Abril, G.: Carbon Dioxide and Methane Dynamics in Estuaries, in: Treatise on Estuarine and Coastal Science, vol. 5, edited by: Wolanski, E. and McLusky, D., Elsevier Inc. Academic Press, 119–161, https://doi.org/10.1016/B978-0-12-374711-2.00504-0, 2012.

Borges, A. V., Champenois, W., Gypens, N., Delille, B., and Harlay, J.: Massive marine methane emissions from near-shore shallow coastal areas, Sci Rep, 6, 1–8, https://doi.org/10.1038/srep27908, 2016.

Borges, A. V., Speeckaert, G., Champenois, W., Scranton, M. I., and Gypens, N.: Productivity and Temperature as Drivers of Seasonal and Spatial Variations of Dissolved Methane in the Southern Bight of the North Sea, Ecosystems, 21, 583–599, https://doi.org/10.1007/s10021-017-0171-7, 2017.

Boulart, C., Connelly, D. P., and Mowlem, M. C.: Sensors and technologies for in situ dissolved methane measurements and their evaluation using Technology Readiness Levels, TrAC - Trends in Analytical Chemistry, 29, 186–195, https://doi.org/10.1016/j.trac.2009.12.001, 2010.

Broman, E., Barua, R., Donald, D., Roth, F., Humborg, C., Norkko, A., Jilbert, T., Bonaglia, S., and Nascimento, F. J. A.: No evidence of light inhibition on aerobic methanotrophs in coastal sediments using eDNA and eRNA, Environmental DNA, 5, 766–781, https://doi.org/10.1002/edn3.441, 2023.

Brown, I. J., Torres, R., and Rees, A. P.: The origin of sub-surface source waters define the sea-air flux of methane in the Mauritanian Upwelling, NW Africa, Dynamics of Atmospheres and Oceans, 67, 39–46, https://doi.org/10.1016/j.dynatmoce.2014.06.001, 2014.

Burke, R. A., Reid, D. F., Brooks, J. M., and Lavoie, D. M.: Upper water column methane geochemistry in the eastern tropical North Pacific, American Society of Limnology and Oceanography, 28, 19–32, https://doi.org/10.4319/lo.1983.28.1.0019, 1983.

Bussmann, I., Brix, H., Flöser, G., Ködel, U., and Fischer, P.: Detailed Patterns of Methane Distribution in the German Bight, Front Mar Sci, 8, https://doi.org/10.3389/fmars.2021.728308, 2021.

Cai, W., McPhaden, M. J., Grimm, A. M., Rodrigues, R. R., Taschetto, A. S., Garreaud, R. D., Dewitte, B., Poveda, G., Ham, Y.-G., Santoso, A., Ng, B., Anderson, W., Wang, G., Geng, T., Jo, H.-S., Marengo, J. A., Alves, L. M., Osman, M., Li, S., Wu, L., Karamperidou, C., Takahashi, K., and Vera, C.: Climate impacts of the El Niño-Southern Oscillation on South America, Nat Rev Earth Environ, 1, 215–231, https://doi.org/10.1038/s43017-020-0040-3, 2020.

Calliari, D. and Alfaro, E.: UN MODELO DE ESTIMACION DE VIENTO PARA BAHIA COLIUMO, CHILE CENTRAL A WIND ESTIMATION MODEL FOR COLIUMO BAY, CENTRAL CHILE, Gayana Oceanol, 5, 87–93, 1997.

Campos, D. and Rondanelli, R.: ENSO-Related Precipitation Variability in Central Chile: The Role of Large Scale Moisture Transport, Journal of Geophysical Research: Atmospheres, 128, https://doi.org/10.1029/2023JD038671, 2023.

Capelle, D. W. and Tortell, P. D.: Factors controlling methane and nitrous-oxide variability in the southern British Columbia coastal upwelling system, Mar Chem, 179, 56–67, https://doi.org/10.1016/j.marchem.2016.01.011, 2016.

Capotondi, A., Wittenberg, A. T., Newman, M., Di Lorenzo, E., Yu, J.-Y., Braconnot, P., Cole, J., Dewitte, B., Giese, B., Guilyardi, E., Jin, F.-F., Karnauskas, K., Kirtman, B., Lee, T., Schneider, N., Xue, Y., and Yeh, S.-W.: Understanding enso diversity, Bull Am Meteorol Soc, 96, 921–938, https://doi.org/10.1175/BAMS-D-13-00117.1, 2015.

Carini, P., White, A. E., Campbell, E. O., and Giovannoni, S. J.: Methane production by phosphate-starved SAR11 chemoheterotrophic marine bacteria, Nat Commun, 5, 1–7, https://doi.org/10.1038/ncomms5346, 2014.

Carpenter, J.: Do rats and pigeons readily acquire instrumental responses for food in the presence of free food?, Limnol Oceanogr, 10, 141–143, https://doi.org/10.3758/BF03209628, 1965.

Castro-Morales, K., Macías-Zamora, J. V., Canino-Herrera, S. R., and Burke, R. A.: Dissolved methane concentration and flux in the coastal zone of the Southern California Bight-Mexican sector: Possible influence of wastewater, Estuar Coast Shelf Sci, 144, 65–74, https://doi.org/10.1016/j.ecss.2014.04.017, 2014.

Cerbin, S., Pérez, G., Rybak, M., Wejnerowski, Ł., Konowalczyk, A., Helmsing, N., Naus-Wiezer, S., Meima-Franke, M., Pytlak, Ł., Raaijmakers, C., Nowak, W., and Bodelier, P. L. E.: Methane-derived carbon as a driver for cyanobacterial growth, Front Microbiol, 13, 1–16, https://doi.org/10.3389/fmicb.2022.837198, 2022.

Chavez, F. P., Bertrand, A., Guevara-Carrasco, R., Soler, P., and Csirke, J.: The northern Humboldt Current System: Brief history, present status and a view towards the future, https://doi.org/10.1016/j.pocean.2008.10.012, October 2008.

Collado-Fabbri, S., Vaulot, D., and Ulloa, O.: Structure and seasonal dynamics of the eukaryotic picophytoplankton community in a wind-driven coastal upwelling ecosystem, Limnol. Oceanogr., 56, 2334–2346, https://doi.org/10.4319/lo.2011.56.6.2334, 2011.

Conrad, R. and Wolfgang, S.: Methane and hydrogen in seawater (Atlantic Ocean), Deep Sea Research Part A, Oceanographic Research Papers, 35, 1903–1917, https://doi.org/10.1016/0198-0149(88)90116-1, 1988.

Cuevas, L. A., Daneri, G., Jacob, B., and Montero, P.: Microbial abundance and activity in the seasonal upwelling area off Concepción (~36°S), central Chile: A comparison of upwelling and non-upwelling conditions, Deep Sea Res 2 Top Stud Oceanogr, 51, 2427–2440, https://doi.org/10.1016/j.dsr2.2004.07.026, 2004.

Damm, E., Beszczynska-Möller, T. A., Nöthing, E. M., and Kattner, G.: Methane excess production in oxygen-rich polar water and a model of cellular conditions for this paradox, Polar Sci, 9, 327–334, https://doi.org/10.1016/j.polar.2015.05.001, 2015.

Daneri, G., Dellarossa, V., Quiñones, R., Jacob, B., Montero, P., and Ulloa, O.: Primary production and community respiration in the Humboldt Current System off Chile and associated oceanic areas, Mar Ecol Prog Ser, 197, 41–49, https://doi.org/10.3354/meps197041, 2000.

Daneri, G., Lizárraga, L., Montero, P., González, H. E., and Tapia, F. J.: Wind forcing and short-term variability of phytoplankton and heterotrophic bacterioplankton in the coastal zone of the Concepción upwelling system (Central Chile), Prog Oceanogr, 92–95, 92–96, https://doi.org/10.1016/j.pocean.2011.07.013, 2012.

Deng, Z. and Zhao, Y.: Impact of tidal mixing on water mass properties and circulation in the Bohai Sea: A typhoon case, Journal of Marine Systems, 206, https://doi.org/10.1016/j.jmarsys.2020.103338, 2020.

Denman, K., Brasseur, G., Chidthaisong, A., Ciais, P., Cox, P., Dickinson, R., Hauglustaine, D., Heinze, C., Holland, E., Jacob, D., Lohman, U., Ramachandran, S., Da Silva Dias, P., Wofsy, S., and Zhang, X.: Couplings between changes in the climate system and biogeochemistry, in: Climate change 2007: The physical science basis. contribution of working group I to the fourth assessment report of the intergovermental panel on climate change, edited by: Solomon, S., Qin, D., Manning, M., Chen, Z.,

Marquis, M., Averyt, K., Tignor, M., and Miller, H., Cambridge University Press, Cambridge/ New York, 499–587, https://doi.org/10.1021/acs.bioconjchem.6b00417, 2007.

Di, P., Feng, D., and Chen, D.: In-situ and on-line measurement of gas flux at a hydrocarbon seep from the northern South China Sea, Cont Shelf Res, 81, 80–87, https://doi.org/10.1016/j.csr.2014.04.001, 2014.

Dickey, T. D.: The emergence of concurrent high-resolution physical and bio-optical measurements in the upper ocean and their applications, https://doi.org/10.1029/91RG00578, 1991.

Dølven, K. O., Ferré, B., Silyakova, A., Jansson, P., Linke, P., and Moser, M.: Autonomous methane seep site monitoring offshore western Svalbard: Hourly to seasonal variability and associated oceanographic parameters, Ocean Science, 18, 233–254, https://doi.org/10.5194/os-18-233-2022, 2022a.

Dølven, K. O., Vierinen, J., Grilli, R., Triest, J., and Ferré, B.: Response time correction of slow-response sensor data by deconvolution of the growth-law equation, Geoscientific Instrumentation, Methods and Data Systems, 11, 293–306, https://doi.org/10.5194/gi-11-293-2022, 2022b.

Dumestre, J. F., Guézennec, J., Galy-Lacaux, C., Delmas, R., Richard, S., and Labroue, L.: Influence of light intensity on methanotrophic bacterial activity in Petit Saut Reservoir, French Guiana, Appl Environ Microbiol, 65, 534–539, https://doi.org/10.1128/aem.65.2.534-539.1999, 1999.

EPA: Methane and Nitrous Oxide emissions from natural sources, U.S. Environmental Protection Agency, Washington D.C. USA, 194 pp., 2010.

Ernst, L., Steinfeld, B., Barayeu, U., Klintzsch, T., Kurth, M., Grimm, D., Dick, T. P., Rebelein, J. G., Bischofs, I. B., and Keppler, F.: Methane formation driven by reactive oxygen species across all living organisms, Nature, 603, 482–487, https://doi.org/10.1038/s41586-022-04511-9, 2022.

Escribano, R., Daneri, G., Farías, L., Gallardo, V. A., González, H. E., Gutiérrez, D., Lange, C. B., Morales, C. E., Pizarro, O., Ulloa, O., and Braun, M.: Biological and chemical consequences of the 1997-1998 El Niño in the Chilean coastal upwelling system: A synthesis, Deep Sea Res 2 Top Stud Oceanogr, 51, 2389–2411, https://doi.org/10.1016/j.dsr2.2004.08.011, 2004.

Farías, L., Fernández, C., Faúndez, J., Cornejo, M., and Alcaman, M. E.: Chemolithoautotrophic production mediating the cycling of the greenhouse gases N2O and CH4 in an upwelling ecosystem, Biogeosciences, 6, 3053–3069, https://doi.org/https://doi.org/10.5194/bg-6-3053-2009, 2009.

Farías, L., Besoain, V., and García-Loyola, S.: Presence of nitrous oxide hotspots in the coastal upwelling area off central Chile: an analysis of temporal variability based on ten years of a biogeochemical time series, Environmental Research Letters, 10, 1–13, https://doi.org/10.1088/1748-9326/10/4/044017, 2015.

Farías, L., Troncoso, M., Sanzana, K., Verdugo, J., and Masotti, I.: Spatial distribution of dissolved methane over extreme oceanographic gradients in the Subtropical Eastern South Pacific (17° to 37°S), J Geophys Res Oceans, 126, https://doi.org/10.1029/2020JC016925, 2021a.

Farías, L., Tenorio, S., Sanzana, K., and Faundez, J.: Temporal methane variability in the water column of an area of seasonal coastal upwelling: A study based on a 12 year time series, Prog Oceanogr, 195, https://doi.org/10.1016/j.pocean.2021.102589, 2021b.

Fazi, S., Amalfitano, S., Venturi, S., Pacini, N., Vazquez, E., Olaka, L. A., Tassi, F., Crognale, S., Herzsprung, P., Lechtenfeld, O. J., Cabassi, J., Capecchiacci, F., Rossetti, S., Yakimov, M. M., Vaselli, O., Harper, D. M., and Butturini, A.: High concentrations of dissolved biogenic methane

associated with cyanobacterial blooms in East African lake surface water, Commun Biol, 4, 1–12, https://doi.org/10.1038/s42003-021-02365-x, 2021.

Fenibo, E. O., Selvarajan, R., Wang, H., Wang, Y., and Abia, A. L. K.: Untapped talents: insight into the ecological significance of methanotrophs and its prospects, https://doi.org/10.1016/j.scitotenv.2023.166145, 10 December 2023.

Ferderlman, T. G., Lee, C., Pantoja, S., Harder, J., Bebout, B. M., and Fossing, H.: Sulfate reduction and methanogenesis in a Thioploca-dominates sediment off the coast of Chile, Geochim Cosmochim Acta, 61, 3065–3079, https://doi.org/https://doi.org/10.1016/S0016-7037(97)00158-0, 1997.

Floodgate, G. D. and Juddt, A. G.: The origins of shallow gas, Continental Shelf Research, 1145–1156 pp., 1992.

Florez-Leiva, L., Damm, E., Farías, L., and Farias, L.: Methane production induced by dimethylsulfide in surface water of an upwelling ecosystem, Prog Oceanogr, 112–113, 38–48, https://doi.org/10.1016/j.pocean.2013.03.005, 2013.

Folberth, G. A., Jones, C. D., O'Connor, F. M., Gedney, N., Griffiths, P. T., and Wiltshire, A. J.: Drivers of persistent changes in the global methane cycle under aggressive mitigation action, NPJ Clim Atmos Sci, 8, https://doi.org/10.1038/s41612-024-00867-z, 2025.

Garcia-Santos, Y., Narváez, D. A., Jacques-Coper, M., Saldías, G. S., Bozkurt, D., and Alessio, B. M.: Dominant Wind Patterns Under the Influence of Atmospheric Rivers: Implications for Coastal Upwelling off Central-Southern Chile, J Geophys Res Oceans, 130, https://doi.org/10.1029/2024JC021444, 2025.

Garreaud, R. D. and Rutllant, J.: Coastal Lows along the Subtropical West Coast of South America: Numerical Simulation of a Typical Case, 2003.

Garreaud, R. D., Rutllant, J. A., and Fuenzalida, H.: Coastal Lows along the Subtropical West Coast of South America: Mean Structure and Evolution, American Meteorological Society, 130, 75–88, https://doi.org/https://doi.org/10.1175/1520-0493(2002)130<0075:CLATSW>2.0.CO;2, 2002.

Garreaud, R. D., Rutllant, J. A., Muñoz, R. C., Rahn, D. A., Ramos, M., and Figueroa, D.: VOCALS-CUpEx: The Chilean Upwelling Experiment, Atmos Chem Phys, 11, 2015–2029, https://doi.org/10.5194/acp-11-2015-2011, 2011.

Garreaud, R. D., Boisier, J. P., Rondanelli, R., Montecinos, A., Sepúlveda, H. H., and Veloso-Aguila, D.: The Central Chile Mega Drought (2010–2018): A climate dynamics perspective, International Journal of Climatology, 40, 421–439, https://doi.org/10.1002/joc.6219, 2019.

Garreaud, R. D., Jacques-Coper, M., Marín, J. C., and Narváez, D. A.: Atmospheric Rivers in South-Central Chile: Zonal and Tilted Events, Atmosphere (Basel), 15, https://doi.org/10.3390/atmos15040406, 2024.

Graco, M., Ledesma, J., Flores, G., and Girón, M.: Nutrients, oxygen and biogeochemical processes in the Humboldt upwelling current system off Peru Nutrientes , oxígeno y procesos biogeoquímicos en el sistema de surgencias de la corriente de Humboldt frente a Perú, Rev. peru. biol, 14, 117–128, 2007.

Graco, M. I., Purca, S., Dewitte, B., Castro, C. G., Morón, O., Ledesma, J., Flores, G., and Gutiérrez, D.: The OMZ and nutrient features as a signature of interannual and low-frequency variability in the Peruvian upwelling system, Biogeosciences, 14, 4601–4617, https://doi.org/10.5194/bg-14-4601-2017, 2017.

Grasshoff, K., Ehrhardt, M., and Kremling, K.: Methods of Seawater Analysis. Second, Second, Re., John Wiley & Sons, Ltd, Deerfield Beach, Florida: Verlag Chemie, 419 pp., https://doi.org/10.1002/iroh.19850700232, 1983.

Grilli, R., Triest, J., Chappellaz, J., Calzas, M., Desbois, T., Jansson, P., Guillerm, C., Ferré, B., Lechevallier, L., Ledoux, V., and Romanini, D.: Sub-Ocean: Subsea Dissolved Methane Measurements Using an Embedded Laser Spectrometer Technology, Environ Sci Technol, 52, 10543–10551, https://doi.org/10.1021/acs.est.7b06171, 2018.

Grilli, R., Darchambeau, F., Chappellaz, J., Mugisha, A., Triest, J., and Umutoni, A.: Continuous in situ measurement of dissolved methane in Lake Kivu using a membrane inlet laser spectrometer, Geoscientific Instrumentation, Methods and Data Systems, 9, 141–151, https://doi.org/10.5194/gi-9-141-2020, 2020.

De Groot, T. R., Mol, A. M., Mesdag, K., Ramond, P., Ndhlovu, R., Engelmann, J. C., Röckmann, T., and Niemann, H.: Diel and seasonal methane dynamics in the shallow and turbulent Wadden Sea, Biogeosciences, 20, 3857–3872, https://doi.org/10.5194/bg-20-3857-2023, 2023.

Günthel, M., Klawonn, I., Woodhouse, J., Bižić, M., Ionescu, D., Ganzert, L., Kümmel, S., Nijenhuis, I., Zoccarato, L., Grossart, H. P., and Tang, K. W.: Photosynthesis-driven methane production in oxic lake water as an important contributor to methane emission, Limnol Oceanogr, 1–13, https://doi.org/10.1002/lno.11557, 2020.

Gutiérrez, D., Enríquez, E., Purca, S., Quipúzcoa, L., Marquina, R., Flores, G., and Graco, M.: Oxygenation episodes on the continental shelf of central Peru: Remote forcing and benthic ecosystem response, Prog Oceanogr, 79, 177–189, https://doi.org/10.1016/j.pocean.2008.10.025, 2008.

Hall, N., Wong, W. W., Lappan, R., Ricci, F., Jeppe, K. J., Glud, R. N., Kawaichi, S., Rotaru, A. E., Greening, C., and Cook, P. L. M.: Coastal methane emissions driven by aerotolerant methanogens using seaweed and seagrass metabolites, Nat Geosci, 18, 854–861, https://doi.org/10.1038/s41561-025-01768-3, 2025.

Hamdan, L. J. and Wickland, K. P.: Methane emissions from oceans, coasts, and freshwater habitats: New perspectives and feedbacks on climate, Limnol Oceanogr, 61, S3–S12, https://doi.org/10.1002/lno.10449, 2016.

Harmsen, M., van Vuuren, D. P., Bodirsky, B. L., Chateau, J., Durand-Lasserve, O., Drouet, L., Fricko, O., Fujimori, S., Gernaat, D. E. H. J., Hanaoka, T., Hilaire, J., Keramidas, K., Luderer, G., Moura, M. C. P., Sano, F., Smith, S. J., and Wada, K.: The role of methane in future climate strategies: mitigation potentials and climate impacts, Clim Change, 163, 1409–1425, https://doi.org/10.1007/s10584-019-02437-2, 2020.

Hartmann, J. F., Günthel, M., Klintzsch, T., Kirillin, G., Grossart, H. P., Keppler, F., and Isenbeck-Schröter, M.: High spatiotemporal dynamics of methane production and emission in oxic surface water, Environ Sci Technol, 54, 1451–1463, https://doi.org/10.1021/acs.est.9b03182, 2020.

Hebbeln, D., Marchant, M., Freudenthal, T., and Wefer, G.: Surface sediment distribution along the Chilean continental slope related to upwelling and productivity, Mar Geol, 164, 119–137, https://doi.org/10.1016/S0025-3227(99)00129-2, 2000.

Hernández-Miranda, E., Veas, R., Labra, F. A., Salamanca, M., and Quiñones, R. A.: Response of the epibenthic macrofaunal community to a strong upwelling-driven hypoxic event in a shallow bay of the southern Humboldt Current System, Mar Environ Res, 79, 16–28, https://doi.org/10.1016/j.marenvres.2012.04.004, 2012.

Hernández-Miranda, E., Veas, R., Anabalón, V., and Quiñones, R. A.: Short-term alteration of biotic and abiotic components of the pelagic system in a shallow bay produced by a strong natural hypoxia event, PLoS One, 12, https://doi.org/10.1371/journal.pone.0179023, 2017.

Herrera-Becerril, C. A., Sanchez-Cabeza, J. A., Álvarez Sánchez, L. F., Lara-Cera, A. R., Ruiz-Fernández, A. C., Cardoso-Mohedano, J. G., Machain-Castillo, M. L., and Colas, F.: Statistical identification of coastal hypoxia events controlled by wind-induced upwelling, Cont Shelf Res, 233, https://doi.org/10.1016/j.csr.2021.104634, 2022.

Ho, D. T., Wanninkhof, R., Schlosser, P., Ullman, D. S., Hebert, D., and Sullivan, K. F.: Toward a universal relationship between wind speed and gas exchange: Gas transfer velocities measured with 3He/SF6 during the Southern Ocean Gas Exchange Experiment, J Geophys Res Oceans, 116, https://doi.org/10.1029/2010JC006854, 2011.

Holmes, E. M., Sansone, F. J., Rust, T. M., and Popp, B. N.: Methane production, consumption, and air-sea exchange in the open ocean: An evaluation based on carbon isotopic ratios, Global Biogeochem Cycles, 14, 1–10, https://doi.org/10.1029/1999GB001209, 2000.

Holm-Hansen, O., Lorenzen, C. J., Holmes, R. W., and Strickland, J. D. H.: Fluorometric determination of chlorophyll, Journal du Conseil International pour L'Exploration de la Mer, 30, 3–15, https://doi.org/10.1093/icesjms/30.1.3, 1965.

Inostroza, P. A., Soriano, Y., Carmona, E., Krauss, M., Brack, W., Backhaus, T., and Quiñones, R. A.: Preliminary dataset of emerging contaminants in surface water, bottom water, porewater, and sediment: Urban and aquaculture impacts in Coliumo bay and Caucahue Channel in the central and southern coast of Chile, Data Brief, 55, https://doi.org/10.1016/j.dib.2024.110593, 2024.

IPCC: Climate change 2021: the physical science basis. Working Group I contribution to the IPCC sixth assessment report, Cambridge University Press, 35–144 pp., https://doi.org/https://doi.org/10.1017/9781009157896, 2021.

Jacobs, E., Bittig, H. C., Gräwe, U., Graves, C. A., Glockzin, M., Müller, J. D., Schneider, B., and Rehder, G.: Upwelling-induced trace gas dynamics in the Baltic Sea inferred from 8 years of autonomous measurements on a ship of opportunity, Biogeosciences, 18, 2679–2709, https://doi.org/10.5194/bg-18-2679-2021, 2021.

Jakobs, G., Holtermann, P., Berndmeyer, C., Rehder, G., Blumenberg, M., Jost, G., Nausch, G., and Schmale, O.: Seasonal and spatial methane dynamics in the water column of the central Baltic Sea (Gotland Sea), Cont Shelf Res, 91, 12–25, https://doi.org/10.1016/j.csr.2014.07.005, 2014.

Jansson, P., Triest, J., Grilli, R., Ferré, B., Silyakova, A., Mienert, J., and Chappellaz, J.: High-resolution underwater laser spectrometer sensing provides new insights into methane distribution at an Arctic seepage site, Ocean Science, 15, 1055–1069, https://doi.org/10.5194/os-15-1055-2019, 2019.

Karl, D. and Tilbrook, B.: Production and transport of methane in oceanic particulate organic matter, Nature, 368, 732–734, https://doi.org/https://doi.org/10.1038/368732a0, 1994.

Karl, D., Beversdorf, L., Björkman, K., Church, M., Martinez, A., and DeLong, E.: Aerobic production of methane in the sea, Nat Geosci, 1, 473–478, https://doi.org/10.1038/ngeo234, 2008.

Kirschke, S., Bousquet, P., Ciais, P., Saunois, M., Canadell, J. G., Dlugokencky, E. J., Bergamaschi, P., Bergmann, D., Blake, D. R., Bruhwiler, L., Cameron-Smith, P., Castaldi, S., Chevallier, F., Feng, L., Fraser, A., Heimann, M., Hodson, E. L., Houweling, S., Josse, B., Fraser, P. J., Krummel, P. B., Lamarque, J. F., Langenfelds, R. L., Le Quéré, C., Naik, V., O'doherty, S., Palmer, P. I., Pison, I., Plummer, D., Poulter, B., Prinn, R. G., Rigby, M., Ringeval, B., Santini, M., Schmidt, M., Shindell,

D. T., Simpson, I. J., Spahni, R., Steele, L. P., Strode, S. A., Sudo, K., Szopa, S., Van Der Werf, G. R., Voulgarakis, A., Van Weele, M., Weiss, R. F., Williams, J. E., and Zeng, G.: Three decades of global methane sources and sinks, https://doi.org/10.1038/ngeo1955, October 2013.

Klintzsch, T., Langer, G., Nehrke, G., Wieland, A., Lenhart, K., and Keppler, F.: Methane production by three widespread marine phytoplankton species: release rates, precursor compounds, and relevance for the environment, Biogeosciences, 16, 4129–4144, https://doi.org/https://doi.org/10.5194/bg-16-4129-2019, 2019.

Klintzsch, T., Langer, G., Wieland, A., Geisinger, H., Lenhart, K., Nehrke, G., and Keppler, F.: Effects of temperature and light on methane production of widespread marine phytoplankton, J Geophys Res Biogeosci, 125, 1–16, https://doi.org/10.1029/2020JG005793, 2020.

Klintzsch, T., Geisinger, H., Wieland, A., Langer, G., Nehrke, G., Bizic, M., Greule, M., Lenhart, K., Borsch, C., Schroll, M., and Keppler, F.: Stable carbon isotope signature of methane released from phytoplankton, Geophys Res Lett, 50, 1–12, https://doi.org/10.1029/2023gl103317, 2023.

Kock, A., Gebhardt, S., and Bange, H. W. W.: Methane emissions from the upwelling area off Mauritania (NW Africa), Biogeosciences, 5, 1119–1125, https://doi.org/10.5194/bg-5-1119-2008, 2008.

Kraus, E. B.: Atmosphere-ocean interaction, in: An introduction to marine biogeochemistry, edited by: Libes, S. 1992, Oxford Univ. Press, New York, 734, 1972.

De La Iglesia, R., Echenique-Subiabre, I., Rodríguez-Marconi, S., Espinoza, J. P., Von Dassow, P., Ulloa, O., and Trefault, N.: Distinct oxygen environments shape picoeukaryote assemblages thriving oxygen minimum zone waters off central Chile, J Plankton Res, 42, 514–529, https://doi.org/10.1093/plankt/fbaa036, 2020.

De La Maza, L. and Farías, L.: The intensification of coastal hypoxia off central Chile: Long term and high frequency variability, Front Earth Sci (Lausanne), 10, https://doi.org/10.3389/feart.2022.929271, 2023.

Lamarche-Gagnon, G., Wadham, J. L., Sherwood Lollar, B., Arndt, S., Fietzek, P., Beaton, A. D., Tedstone, A. J., Telling, J., Bagshaw, E. A., Hawkings, J. R., Kohler, T. J., Zarsky, J. D., Mowlem, M. C., Anesio, A. M., and Stibal, M.: Greenland melt drives continuous export of methane from the ice-sheet bed, Nature, 565, 73–77, https://doi.org/10.1038/s41586-018-0800-0, 2019.

Lamontagne, R. A., Swinnerton, J. W., Linnenbom, V. J., and Smith, W. D.: Methane concentrations in various marine environments, J Geophys Res, 78, 5317–5324, https://doi.org/10.1029/JC078i024p05317, 1973.

Largier, J. L.: Upwelling Bays: How Coastal Upwelling Controls Circulation, Habitat, and Productivity in Bays, Ann Rev Mar Sci, https://doi.org/https://doi.org/10.1146/annurev-marine-010419-011020, 2020a.

Largier, J. L.: Upwelling Bays: How Coastal Upwelling Controls Circulation, Habitat, and Productivity in Bays, Ann Rev Mar Sci, https://doi.org/https://doi.org/10.1146/annurev-marine-010419-011020, 2020b.

Lenhart, K., Klintzsch, T., Langer, G., Nehrke, G., Bunge, M., Schnell, S., and Keppler, F.: Evidence for methane production by the marine algae Emiliania huxleyi, Biogeosciences, 13, 3163–3174, https://doi.org/10.5194/bg-13-3163-2016, 2016.

León-Palmero, E., Contreras-Ruiz, A., Sierra, A., Morales-Baquero, R., and Reche, I.: Dissolved CH4 coupled to photosynthetic picoeukaryotes in oxic waters and to cumulative chlorophyll a in anoxic waters of reservoirs, Biogeosciences, 17, 1–23, https://doi.org/10.5194/bg-17-3223-2020, 2020.

Letelier, J., Pizarro, O., and Nuñez, S.: Seasonal variability of coastal upwelling and the upwelling front off central Chile, J Geophys Res Oceans, 114, https://doi.org/10.1029/2008JC005171, 2009.

Li, J. and Dittrich, M.: Dynamic polyphosphate metabolism in cyanobacteria responding to phosphorus availability, Environ Microbiol, 21, 572–583, https://doi.org/10.1111/1462-2920.14488, 2019.

Li, Y., Fichot, C. G., Geng, L., Scarratt, M. G., and Xie, H.: The contribution of methane photoproduction to the oceanic methane paradox, Geophys Res Lett, 47, 1–10, https://doi.org/10.1029/2020GL088362, 2020.

Lidbury, I. D. E. A., Murrell, J. C., and Chen, Y.: Trimethylamine and trimethylamine N-oxide are supplementary energy sources for a marine heterotrophic bacterium: Implications for marine carbon and nitrogen cycling, ISME Journal, 9, 760–769, https://doi.org/10.1038/ismej.2014.149, 2015.

Liu, Y. and Whitman, W. B.: Metabolic, phylogenetic, and ecological diversity of the Methanogenic Archaea, Ann N Y Acad Sci, 1125, 171–189, https://doi.org/10.1196/annals.1419.019, 2008.

Liu, Z.: Taylor diagram class , https://la.mathworks.com/matlabcentral/fileexchange/130889-taylor-diagram-class, 2025.

Lohrer, C., Cwierz, P. P., Wirth, M. A., Schulz-Bull, D. E., and Kanwischer, M.: Methodological aspects of methylphosphonic acid analysis: Determination in river and coastal water samples, Talanta, 211, 1–8, https://doi.org/10.1016/j.talanta.2020.120724, 2020.

Ma, X., Sun, M., Lennartz, S. T., and Bange, H. W.: A decade of methane measurements at the Boknis Eck Time-series Station in the Eckernförde Bay (Southwestern Baltic Sea), Biogeosciences Discussions, 2020, 1–22, https://doi.org/https://doi.org/10.5194/bg-17-3427-2020, 2020.

Mao, S. H., Zhang, H. H., Zhuang, G. C., Li, X. J., Liu, Q., Zhou, Z., Wang, W. L., Li, C. Y., Lu, K. Y., Liu, X. T., Montgomery, A., Joye, S. B., Zhang, Y. Z., and Yang, G. P.: Aerobic oxidation of methane significantly reduces global diffusive methane emissions from shallow marine waters, Nat Commun, 13, https://doi.org/10.1038/s41467-022-35082-y, 2022.

Mao, S. H., Wang, J. Y., Joye, S., and Zhuang, G. C.: Marine methane paradox: Enigmatic production of methane in oxygenated waters, https://doi.org/10.59717/j.xinn-geo.2024.100071, 12 June 2024.

Martens, C. S. and Klump, V. J.: Biogeochemical cycling in an organic-rich coastal marine basin-I. Methane sediment-water exchange processes, Geochim Cosmochim Acta, 44, 471–490, https://doi.org/10.1016/0016-7037(80)90045-9, 1980.

Masotti, I., Aparicio-Rizzo, P., Yevenes, M. A., Garreaud, R., Belmar, L., and Farías, L.: The influence of river discharge on nutrient export and phytoplankton biomass off the Central Chile Coast (33°-37°S): Seasonal cycle and interannual variability, Front Mar Sci, 5, https://doi.org/10.3389/fmars.2018.00423, 2018.

McClain, M. E., Boyer, E. W., Dent, C. L., Gergel, S. E., Grimm, N. B., Groffman, P. M., Hart, S. C., Harvey, J. W., Johnston, C. A., Mayorga, E., McDowell, W. H., and Pinay, G.: Biogeochemical Hot Spots and Hot Moments at the Interface of Terrestrial and Aquatic Ecosystems, https://doi.org/10.1007/s10021-003-0161-9, June 2003.

Mcmanus, G. B. and Peterson, W. T.: Bacterioplankton production in the nearshore zone during upwelling off central Chile, Source: Marine Ecology Progress Series, 11–17 pp., 1988.

Merma-Mora, L., Colas, F., Cardich, J., Sánchez, S., Flores, E., Lorenzo, A., Aguirre-Velarde, A., Correa, D., and Gutiérrez, D.: Bottom-water hypoxia in the Paracas Bay (Peru, 13.8°S) associated with seasonal and synoptic time scale variability of winds and water stratification, Journal of Marine Systems, 241, https://doi.org/10.1016/j.jmarsys.2023.103918, 2024.

Metcalf, W. W., Griffin, B. M., Cicchillo, R., Gao, J., Janga, S., Cooke, H., Circello, B., Evans, B., Martens-Habbena, W., Stahl, D., and Van Der Donk, W.: Synthesis of methylphosphonic acid by marine microbes: a source for methane in the Aerobic Ocean, Science (1979), 337, 1104–1107, https://doi.org/10.1126/science.1219875, 2012.

Molina, V., Belmar, L., Levipan, H. A., Ramírez-Flandes, S., Anguita, C., Galán, A., Montes, I., and Ulloa, O.: Spatiotemporal distribution of key pelagic microbes in a seasonal oxygen-deficient coastal upwelling system of the Eastern South Pacific Ocean, Front Mar Sci, 7, 1–17, https://doi.org/10.3389/fmars.2020.561597, 2020.

Montecino, V. and Lange, C. B.: The Humboldt Current System: Ecosystem components and processes, fisheries, and sediment studies, Prog Oceanogr, 83, 65–79, https://doi.org/10.1016/j.pocean.2009.07.041, 2009.

Montecinos, A., Kurgansky, M. V., Muñoz, C., and Takahashi, K.: Non-ENSO interannual rainfall variability in central Chile during austral winter, Theor Appl Climatol, 106, 557–568, https://doi.org/10.1007/s00704-011-0457-1, 2011.

Montero, P., Daneri, G., Cuevas, A., González, H. E., Jacob, B., Lizárraga, L., and Menschel, E.: Productivity cycles in the coastal upwelling area off Concepción: The importance of diatoms and bacterioplankton in the organic carbon flux, Prog Oceanogr, 75, 518–530, https://doi.org/10.1016/j.pocean.2007.08.013, 2007.

Montes, T., Guerrero-Feijóo, E., Moreira-Coello, V., Bode, A., Ruiz-Villarreal, M., Mouriño-Carballido, B., and Varela, M. M.: Vertical zonation of bacterial assemblages attributed to physical stratification during the summer relaxation of the coastal upwelling off Galicia (NW Spain), Estuar Coast Shelf Sci, 245, https://doi.org/10.1016/j.ecss.2020.106791, 2020.

Morales, C. and Anabalón, V.: Phytoplankton biomass and microbial abundances during the spring upwelling season in the coastal area off Concepción , central-southern Chile : variability around a time series station, Prog Oceanogr, 92–95, 81–91, https://doi.org/10.1016/j.pocean.2011.07.004, 2012.

Morán, X. A. G., Estrada, M., Gasol, J. M., and Pedrós-Alió, C.: Dissolved primary production and the strength of phytoplankton-bacterioplankton coupling in contrasting marine regions, Microb Ecol, 44, 217–223, https://doi.org/10.1007/s00248-002-1026-z, 2002.

Morgan, E. J., Lavric, J. V., Arévalo-Martínez, D. L., Bange, H. W., Steinhoff, T., Seifert, T., and Heimann, M.: Air-sea fluxes of greenhouse gases and oxygen in the northern Benguela Current region during upwelling events, Biogeosciences, 16, 4065–4084, https://doi.org/10.5194/bg-16-4065-2019, 2019.

Muñoz, R. C.: Diurnal cycle of surface winds over the subtropical southeast Pacific, Journal of Geophysical Research Atmospheres, 113, https://doi.org/10.1029/2008JD009957, 2008.

Muñoz, R. C. and Garreaud, R. D.: Dynamics of the Low-Level Jet off the West Coast of Subtropical South America, American Meteorological Society, 3661–3677, https://doi.org/https://doi.org/10.1175/MWR3074.1, 2005.

Muñoz-Marín, M. C., Gómez-Baena, G., López-Lozano, A., Moreno-Cabezuelo, J. A., Díez, J., and García-Fernández, J. M.: Mixotrophy in marine picocyanobacteria: use of organic compounds by Prochlorococcus and Synechococcus, https://doi.org/10.1038/s41396-020-0603-9, 1 May 2020.

Murase, J. and Sugimoto, A.: Inhibitory effect of light on methane oxidation in the pelagic water column of a mesotrophic lake (Lake Biwa, Japan), Limnol Oceanogr, 50, 1339–1343, https://doi.org/10.4319/lo.2005.50.4.1339, 2005.

Navarrete, S. A., González, A. E., Faúndez, J., Contreras-Porcia, L., Núñez, A., Rivas, J., Chacano, S., Farías, L., Saldías, G. S., and Tapia, F. J.: Growth rates and response to nutrient variability in the green tide forming alga Ulva stenophylloides from Algarrobo Bay, Chile, Mar Environ Res, 210, https://doi.org/10.1016/j.marenvres.2025.107338, 2025.

Nelson, C. Scott.: Wind stress and wind stress curl over the California current, 1–87, https://doi.org/10.5962/bhl.title.60783, 1977.

Neveux, J., Dupouy, C., Blanchot, J., Le Bouteiller, A., Landry, M. R., and Brown, S. L.: Diel dynamics of chlorophylls in high-nutrient, low-chlorophyll waters of the equatorial Pacific (180°): Interactions of growth, grazing, physiological responses, and mixing, J Geophys Res Oceans, 108, https://doi.org/10.1029/2000jc000747, 2003.

Nicholson, D. P., Michel, A. P. M., Wankel, S. D., Manganini, K., Sugrue, R. A., Sandwith, Z. O., and Monk, S. A.: Rapid Mapping of Dissolved Methane and Carbon Dioxide in Coastal Ecosystems Using the ChemYak Autonomous Surface Vehicle, Environ Sci Technol, 52, 13314–13324, https://doi.org/10.1021/acs.est.8b04190, 2018.

Oremland, R. S.: Methanogenic activity in plankton samples and fish intestines: A mechanism for in situ methanogenesis in oceanic surface waters, Limnol. Oceanogr., 24, 1136–1141, 1979.

Orion Jedrysek, M.: Carbon isotope evidence for diurnal variations in methanogenesis in freshwater lake sediments, Geochimica et Cosmochimica Acta, 557–561 pp., 1995.

Padilla, A. M., Pardis, W., Kapit, J., Bjorklund, T. A., Ward, N. D., Fornari, D. J., Hautala, S., Waite, W. F., Johnson, H. P., and Michel, A. P. M.: Spatial mapping of dissolved methane using an in situ sensor in Puget Sound, Limnol Oceanogr Methods, https://doi.org/10.1002/lom3.10717, 2025.

Paduan, J. D., Cook, M. S., and Tapia, V. M.: Patterns of upwelling and relaxation around Monterey Bay based on long-term observations of surface currents from high frequency radar, Deep Sea Res 2 Top Stud Oceanogr, 151, 129–136, https://doi.org/10.1016/j.dsr2.2016.10.007, 2018.

Panagiota-Myrsini, C., Shelley, F., Pritchard, W. J., Maanoja, S. T., and Trimmer, M.: Origin and fate of methane in the Eastern Tropical North Pacific oxygen minimum zone, ISME Journal, 11, 1386–1399, https://doi.org/10.1038/ismej.2017.6, 2017.

Paul, L., Ferguson, D. J., and Krzycki, J. A.: The trimethylamine methyltransferase gene and multiple dimethylamine methyltransferase genes of methanosarcina barkeri contain in-frame and read-through amber codons, J Bacteriol, 182, 2520–2529, https://doi.org/0021-9193/00/$04.00⩽0, 2000.

Pérez-Santos, I., Garcés-Vargas, J., Schneider, W., Ross, L., Parra, S., and Valle-Levinson, A.: Double-diffusive layering and mixing in Patagonian fjords, Prog Oceanogr, 129, 35–49, https://doi.org/10.1016/j.pocean.2014.03.012, 2014.

Pinochet, A., Garcés-Vargas, J., Lara, C., and Olguín, F.: Seasonal variability of upwelling off Central-Southern Chile, Remote Sens (Basel), 11, https://doi.org/10.3390/rs11151737, 2019.

Rao, G. D. and Sarma, V. V. S. S.: Influence of river discharge on the distribution and flux of methane in the coastal Bay of Bengal, Mar Chem, 197, 1–10, https://doi.org/10.1016/j.marchem.2017.11.002, 2017.

Reeburgh, W. S.: Oceanic methane biogeochemistry, American Chemical Society, 107, 486–513, https://doi.org/10.1021/cr050362v, 2007.

Reintjes, G., Fuchs, B. M., Scharfe, M., Wiltshire, K. H., Amann, R., and Arnosti, C.: Short-term changes in polysaccharide utilization mechanisms of marine bacterioplankton during a spring phytoplankton bloom, Environ Microbiol, 22, 1884–1900, https://doi.org/10.1111/1462-2920.14971, 2020.

Repeta, D. J., Ferrón, S., Sosa, O. A., Johnson, C. G., Repeta, L. D., Acker, M., DeLong, E. F., and Karl, D. M.: Marine methane paradox explained by bacterial degradation of dissolved organic matter, Nat Geosci, 9, 1–7, https://doi.org/10.1038/ngeo2837, 2016.

Resplandy, L., Hogikyan, A., Müller, J. D., Najjar, R. G., Bange, H. W., Bianchi, D., Weber, T., Cai, W. J., Doney, S. C., Fennel, K., Gehlen, M., Hauck, J., Lacroix, F., Landschützer, P., Le Quéré, C., Roobaert, A., Schwinger, J., Berthet, S., Bopp, L., Chau, T. T. T., Dai, M., Gruber, N., Ilyina, T., Kock, A., Manizza, M., Lachkar, Z., Laruelle, G. G., Liao, E., Lima, I. D., Nissen, C., Rödenbeck, C., Séférian, R., Toyama, K., Tsujino, H., and Regnier, P.: A Synthesis of Global Coastal Ocean Greenhouse Gas Fluxes, Global Biogeochem Cycles, 38, https://doi.org/10.1029/2023GB007803, 2024.

Rhee, T. S., Kettle, A. J., and Andreae, M. O.: Methane and nitrous oxide emissions from the ocean: A reassessment using basin-wide observations in the Atlantic, Journal of Geophysical Research Atmospheres, 114, 1–20, https://doi.org/10.1029/2008JD011662, 2009.

Robertson, R., Dong, J., and Hartlipp, P.: Diurnal Critical Latitude and the Latitude Dependence of Internal Tides, Internal Waves, and Mixing Based on Barcoo Seamount, J Geophys Res Oceans, 122, 7838–7866, https://doi.org/10.1002/2016JC012591, 2017.

Rocher-Ros, G., Stanley, E. H., Loken, L. C., Casson, N. J., Raymond, P. A., Liu, S., Amatulli, G., and Sponseller, R. A.: Global methane emissions from rivers and streams, Nature, 621, 530–535, https://doi.org/10.1038/s41586-023-06344-6, 2023a.

Rocher-Ros, G., Stanley, E. H., Loken, L. C., Casson, N. J., Raymond, P. A., Liu, S., Amatulli, G., and Sponseller, R. A.: Global methane emissions from rivers and streams, Nature, 621, 530–535, https://doi.org/10.1038/s41586-023-06344-6, 2023b.

Rosentreter, J. A., Maher, D. T., Erler, D. V, Murray, R. H., and Eyre, B. D.: Methane emissions partially offset " blue carbon " burial in mangroves, Sci Adv, 4, 1–11, 2018.

Rosentreter, J. A., Borges, A. V., Deemer, B. R., Holgerson, M. A., Liu, S., Song, C., Melack, J., Raymond, P. A., Duarte, C. M., Allen, G. H., Olefeldt, D., Poulter, B., Battin, T. I., and Eyre, B. D.: Half of global methane emissions come from highly variable aquatic ecosystem sources, Nat Geosci, 14, 225–230, https://doi.org/10.1038/s41561-021-00715-2, 2021.

Roth, F., Sun, X., Geibel, M. C., Prytherch, J., Brüchert, V., Bonaglia, S., Broman, E., Nascimento, F., Norkko, A., and Humborg, C.: High spatiotemporal variability of methane concentrations challenges estimates of emissions across vegetated coastal ecosystems, Glob Chang Biol, https://doi.org/10.1111/gcb.16177, 2022.

Sabbaghzadeh, B., Arévalo-Martínez, D. L., Mohrholz, V., Cotovicz Jr, L. C., Otto, S., Dangl, M., Glockzin, M., and Rehder, G.: Unveiling Profound Seasonal and Spatial Dynamics of Greenhouse Gases (CO2,

CH4, N2O) in the Northern Benguela Upwelling System, ESS Open Archive, https://doi.org/10.22541/essoar.171078509.96167780/v1, 2024.

Saldías, G. S., Sobarzo, M., Largier, J., Moffat, C., and Letelier, R.: Seasonal variability of turbid river plumes off central Chile based on high-resolution MODIS imagery, Remote Sens Environ, 123, 220–233, https://doi.org/10.1016/j.rse.2012.03.010, 2012.

Sansone, F. J., Popp, B. N., Gasc, A., Graham, A. W., and Rust, T. M.: Highly elevated methane in the Eastern tropical North Pacific and associated isotopically enriched fluxes to the atmosphere, Geophys Res Lett, 28, 4567–4570, https://doi.org/10.1029/2001GL013460, 2001.

Sarmiento, J. L. and Gruber, N.: Air-Sea Interface, in: Ocean Biogeochemical Dynamics, Princeton University Press, Princeton, New Jersey, 503, https://doi.org/10.2307/j.ctt3fgxqx, 2006.

Saunois, M., Bousquet, P., Poulter, B., Peregon, A., Ciais, P., Canadell, J. G., Dlugokencky, E. J., Etiope, G., Bastviken, D., Houweling, S., Janssens-Maenhout, G., Tubiello, F. N., Castaldi, S., Jackson, R. B., Alexe, M., Arora, V. K., Beerling, D. J., Bergamaschi, P., Blake, D. R., Brailsford, G., Brovkin, V., Bruhwiler, L., Crevoisier, C., Crill, P., Covey, K., Curry, C., Frankenberg, C., Gedney, N., Höglund-Isaksson, L., Ishizawa, M., Ito, A., Joos, F., Kim, H. S., Kleinen, T., Krummel, P., Lamarque, J. F., Langenfelds, R., Locatelli, R., Machida, T., Maksyutov, S., McDonald, K. C., Marshall, J., Melton, J. R., Morino, I., Naik, V., O'Doherty, S., Parmentier, F. J. W., Patra, P. K., Peng, C., Peng, S., Peters, G. P., Pison, I., Prigent, C., Prinn, R., Ramonet, M., Riley, W. J., Saito, M., Santini, M., Schroeder, R., Simpson, I. J., Spahni, R., Steele, P., Takizawa, A., Thornton, B. F., Tian, H., Tohjima, Y., Viovy, N., Voulgarakis, A., Van Weele, M., Van Der Werf, G. R., Weiss, R., Wiedinmyer, C., Wilton, D. J., Wiltshire, A., Worthy, D., Wunch, D., Xu, X., Yoshida, Y., Zhang, B., Zhang, Z., and Zhu, Q.: The global methane budget 2000-2012, Earth Syst Sci Data, 8, 697–751, https://doi.org/10.5194/essd-8-697-2016, 2016a.

Saunois, M., Jackson, R. B., Bousquet, P., Poulter, B., and Canadell, J. G.: The growing role of methane in anthropogenic climate change, https://doi.org/10.1088/1748-9326/11/12/120207, 12 December 2016b.

Saunois, M., Stavert, A. R., Poulter, B., Bousquet, P., Canadell, J. G., Jackson, R. B., Raymond, P. A., Dlugokencky, E. J., and Houweling, S.: The global methane budget 2000 – 2017, Earth Syst Sci Data, 12, 1561–1623, https://doi.org/10.5194/essd-12-1561-2020, 2020.

Saunois, M., Martinez, A., Poulter, B., Zhang, Z., Raymond, P. A., Regnier, P., Canadell, J. G., Jackson, R. B., Patra, P. K., Bousquet, P., Ciais, P., Dlugokencky, E. J., Lan, X., Allen, G. H., Bastviken, D., Beerling, D. J., Belikov, D. A., Blake, D. R., Castaldi, S., Crippa, M., Deemer, B. R., Dennison, F., Etiope, G., Gedney, N., Höglund-Isaksson, L., Holgerson, M. A., Hopcroft, P. O., Hugelius, G., Ito, A., Jain, A. K., Janardanan, R., Johnson, M. S., Kleinen, T., Krummel, P. B., Lauerwald, R., Li, T., Liu, X., McDonald, K. C., Melton, J. R., Mühle, J., Müller, J., Murguia-Flores, F., Niwa, Y., Noce, S., Pan, S., Parker, R. J., Peng, C., Ramonet, M., Riley, W. J., Rocher-Ros, G., Rosentreter, J. A., Sasakawa, M., Segers, A., Smith, S. J., Stanley, E. H., Thanwerdas, J., Tian, H., Tsuruta, A., Tubiello, F. N., Weber, T. S., van der Werf, G. R., Worthy, D. E. J., Xi, Y., Yoshida, Y., Zhang, W., Zheng, B., Zhu, Q., Zhu, Q., and Zhuang, Q.: Global Methane Budget 2000–2020, Earth Syst Sci Data, 17, 1873–1958, https://doi.org/10.5194/essd-17-1873-2025, 2025.

Schmidt, M., Linke, P., and Esser, D.: Recent Development in IR Sensor Technology for Monitoring Subsea Methane Discharge, Mar Technol Soc J, 47, 27–36, 2013.

Schowanek, D. and Verstraete, W.: Phosphonate utilization by bacteria in the presence of alternative phosphorus sources, Biodegradation, Kluwer Academic Publishers, 1990 pp., https://doi.org/10.1007/BF00117050, 1990.

Scranton, M. I. and Brewer, P. G.: Occurrence of methane in the near-surface waters of the western subtropical North-Atlantic, Deep-Sea Research, 24, 127–138, https://doi.org/10.1016/0146-6291(77)90548-3, 1977.

Send, U., Beardsley, R. C., and Winant, C. D.: Relaxation from upwelling in the coastal ocean dynamics experiment, J Geophys Res Oceans, 92, 1683–1698, https://doi.org/10.1029/JC092iC02p01683, 1987.

Shaffer, G., Hormazabal, S., Pizarro, O., and Salinas, S.: Seasonal and interannual variability of currents and temperature off central Chile, J Geophys Res Oceans, 104, 29951–29961, https://doi.org/10.1029/1999jc900253, 1999.

Silva, N., Rojas, N., and Fedele, A.: Water masses in the Humboldt Current System: properties, distribution, and the nitrate deficit as a chemical water mass tracer for Equatorial Subsurface Water off Chile, Deep Sea Research Part II: Topical Studies in Oceanography, 56, 1004–1020, https://doi.org/10.1016/j.dsr2.2008.12.013, 2009.

Smith, M. W., Allen, L. Z., Allen, A. E., Herfort, L., and Simon, H. M.: Contrasting genomic properties of free-living and particle-attached microbial assemblages within a coastal ecosystem, Front Microbiol, 4, 1–20, https://doi.org/10.3389/fmicb.2013.00120, 2013.

Sobarzo, M. and Djurfeldt, L.: Coastal upwelling process on a continental shelf limited by submarine canyons, Concepción, central Chile, J Geophys Res, 109, 1–20, https://doi.org/10.1029/2004JC002350, 2004.

Sobarzo, M., Figueroa, M., and Djurfeldt, L.: Upwelling of subsurface water into the rim of the Biobio submarine canyon as a response to surface winds, Cont Shelf Res, 21, 279–299, https://doi.org/10.1016/S0278-4343(00)00082-0, 2001.

Sobarzo, M., Bravo, L., Donoso, D., Garcés-Vargas, J., and Schneider, W.: Coastal upwelling and seasonal cycles that influence the water column over the continental shelf off central Chile, Prog Oceanogr, 75, 363–382, https://doi.org/10.1016/j.pocean.2007.08.022, 2007.

Sobarzo, M., Bravo, L., and Moffat, C.: Diurnal-period, wind-forced ocean variability on the inner shelf off Concepción, Chile, Cont Shelf Res, 30, 2043–2056, https://doi.org/10.1016/j.csr.2010.10.004, 2010.

Sobarzo, M., Soto-Riquelme, C., Flores, R. P., and Saldías, G. S.: Synoptic Flow Variability in a River-Influenced Inner Shelf off Central Chile, J Mar Sci Eng, 10, https://doi.org/10.3390/jmse10040501, 2022.

Sosa, O. A., Repeta, D. J., DeLong, E. F., Ashkezari, M. D., and Karl, D. M.: Phosphate-limited ocean regions select for bacterial populations enriched in the carbon–phosphorus lyase pathway for phosphonate degradation, Environ Microbiol, 21, 2402–2414, https://doi.org/10.1111/1462-2920.14628, 2019.

Sosa, O. A., Burrell, T. J., Wilson, S. T., Foreman, R. K., Karl, D. M., and Repeta, D. J.: Phosphonate cycling supports methane and ethylene supersaturation in the phosphate-depleted western North Atlantic Ocean, Limnol Oceanogr, 1–17, https://doi.org/10.1002/lno.11463, 2020.

Spilling, K., Camarena-Gómez, M. T., Lipsewers, T., Martinez-Varela, A., Díaz-Rosas, F., Eronen-Rasimus, E., Silva, N., von Dassow, P., and Montecino, V.: Impacts of reduced inorganic N:P ratio

on three distinct plankton communities in the Humboldt upwelling system, Mar Biol, 166, 1–17, https://doi.org/10.1007/s00227-019-3561-x, 2019.

Stolper, D. A., Lawson, M., Davis, C. L., Ferreira, A. A., Santos Neto, E. V., Ellis, G. S., Lewan, M. D., Martini, A. M., Tang, Y., Schoell, M., Sessions, A. L., and Eiler, J. M.: Formation temperatures of thermogenic and biogenic methane, Science (1979), 344, 1500–1503, 2014.

Strom, S. L., Benner, R., Ziegler, S., and Dagg, M. J.: Planktonic grazers are a potentially important source of marine dissolved organic carbon, Limnol Oceanogr, 42, 1364–1374, https://doi.org/10.4319/lo.1997.42.6.1364, 1997.

Strub, T., Mesías, J., Montecino, V., Rutllant, J., and Salinas, S.: Coastal ocean circulation off western south america, in: The global coastal ocean - regional studies and syntheses, vol. 11, edited by: Robinson, A. R. and Brink, K. H., John Wiley & Sons, Inc, NY, 273–313, 1998.

Strub, T., Combes, V., Shillington, F. A., and Pizarro, O.: Currents and processes along the eastern boundaries, in: International Geophysics, vol. 103, Academic Press, 339–384, https://doi.org/10.1016/B978-0-12-391851-2.00014-3, 2013.

Sturm, K., Werner, U., Grinham, A., and Yuan, Z.: Tidal variability in methane and nitrous oxide emissions along a subtropical estuarine gradient, Estuar Coast Shelf Sci, 192, 159–169, https://doi.org/10.1016/j.ecss.2017.04.027, 2017.

Sudheesh, V., Gupta, G. V. M., and Naqvi, W. A.: Massive Methane Loss During Seasonal Hypoxia / Anoxia in the Nearshore Massive Methane Loss During Seasonal Hypoxia/Anoxia in the Nearshore Waters of Southeastern Arabian Sea, Front Mar Sci, 7, 1–13, https://doi.org/10.3389/fmars.2020.00324, 2020.

Summerhayes, C. P.: Sedimentation of organic matter in upwelling regimes, in: Coastal upwelling, its sediment record. Part B: Sedimentary records of ancient coastal upwelling, edited by: Thiede, J. and Suess, E., Plenum, New York, 29–72, 1983.

Sun, J., Steindler, L., Thrash, J. C., Halsey, K. H., Smith, D. P., Carter, A. E., Landry, Z. C., and Giovannoni, S. J.: One carbon metabolism in SAR11 pelagic marine bacteria, PLoS One, 6, 1–12, https://doi.org/10.1371/journal.pone.0023973, 2011.

Sweeney, C., Gloor, E., Jacobson, A. R., Key, R. M., McKinley, G., Sarmiento, J. L., and Wanninkhof, R.: Constraining global air-sea gas exchange for CO2 with recent bomb 14C measurements, Global Biogeochem Cycles, 21, 1–10, https://doi.org/10.1029/2006GB002784, 2007.

Tenorio, S. E. and Farías, L.: Picoplanktonic methane production in eutrophic surface waters, Biogeosciences, 21, 2029–2050, https://doi.org/10.5194/bg-21-2029-2024, 2024.

Testa, G., Masotti, I., and Farías, L.: Temporal variability in net primary production in an upwelling area off central Chile (36°S), Front Mar Sci, 5, 1–17, https://doi.org/10.3389/fmars.2018.00179, 2018.

Torrence, C. and Compo, G. P.: A Practical Guide to Wavelet Analysis, Bull Am Meteorol Soc, 79, 61–78, https://doi.org/https://doi.org/10.1175/1520-0477(1998)079<0061:APGTWA>2.0.CO;2, 1998.

Trautman, N. and Walter, R. K.: Seasonal variability of upwelling and downwelling surface current patterns in a small coastal embayment, Cont Shelf Res, 226, https://doi.org/10.1016/j.csr.2021.104490, 2021.

Troncoso, A., Daneri, G., Cuevas, L. A., Jacob, B., and Montero, P.: Bacterial carbon flow in the Humboldt Current System off Chile, Mar Ecol Prog Ser, 250, 1–12, https://doi.org/10.3354/meps250001, 2003.

Upstill-goddard, R. C. and Barnes, J.: Methane emissions from UK estuaries : Re-evaluating the estuarine source of tropospheric methane from Europe, 180, 14–23, https://doi.org/10.1016/j.marchem.2016.01.010, 2016.

Upstill-goddard, R. C., Barnes, J., Frost, T., Punshon, S., and Owens, N. J. P.: Methane in the southern North Sea : Low-salinity inputs , estuarine removal , and atmospheric flux, 14, 1205–1217, 2000.

Valdés, L., Lavín, A., Fernández de Puelles, M. L. L., Varela, M., Anadón, R., Miranda, A., Camiñas, J., and Mas, J.: Spanish ocean observation system. IEO core project: Studies on time series of oceanographic data, in: Opertional Oceanography, vol. 66, edited by: Flemming, N. C., Vallerga, S., Pinardi, N., Behrens, H. W. A., Manzella, G., Prandle, D., and Stel, J. H., Elsevier Science, 99–105, https://doi.org/https://doi.org/10.1016/S0422-9894(02)80014-9, 2002.

Valdés, L., Bode, A., Latasa, M., Nogueira, E., Somavilla, R., Varela, M. M., González-Pola, C., and Casas, G.: Three decades of continuous ocean observations in North Atlantic Spanish waters: The RADIALES time series project, context, achievements and challenges, https://doi.org/10.1016/j.pocean.2021.102671, 1 November 2021.

Del Valle, D. A. and Karl, D. M.: Aerobic production of methane from dissolved water-column methylphosphonate and sinking particles in the North Pacific Subtropical Gyre, Aquatic Microbial Ecology, 73, 93–105, https://doi.org/10.3354/ame01714, 2014.

Valle-Levinson, A., Atkinson, L. P., Figueroa, D., and Castro, L.: Flow induced by upwelling winds in an equatorward facing bay: Gulf of Arauco, Chile, J Geophys Res Oceans, 108, https://doi.org/10.1029/2001jc001272, 2003.

Vargas, C. A., Martínez, R. A., Cuevas, L. A., Pavez, M. A., Cartes, C., González, H. E., Escribano, R., and Daneri, G.: The relative importance of microbial and classical food webs in a highly productive coastal upwelling area, Limnol Oceanogr, 52, 1495–1510, https://doi.org/10.4319/lo.2007.52.4.1495, 2007.

Varvayanni, M., Helmis, C. G., Amanatidis, G. T., Asimakopoulos, O. N., Bartzis, J. G., Soilemes, A., Papadopoulos, K. H., and Kambezidis, H. D.: Effects of Onshore and Offshore Topography on Sea Breeze Circulation: An Observational Study at Eastern Attica, Greece, PAGEOPH, 1993.

Vogel, R. M. and Shallcross, A. L.: The moving blocks bootstrap versus parametric time series models, Water Resour Res, 32, 1875–1882, https://doi.org/10.1029/96WR00928, 1996.

Wäge, J., Schmale, O., and Labrenz, M.: Quantification of methanogenic Archaea within Baltic Sea copepod faecal pellets, Mar Biol, 167, https://doi.org/10.1007/s00227-020-03759-x, 2020.

Wallmann, K., Pinero, E., Burwicz, E., Haeckel, M., Hensen, C., Dale, A., and Ruepke, L.: The global inventory of methane hydrate in marine sediments: A theoretical approach, https://doi.org/10.3390/en5072449, 2012.

Walsh, J. J.: Importance of continental margins in the marine biogeochemical cycling of carbon and nitrogen, Nature, 350, 53–55, 1991.

Wanninkhof, R.: Relationship between wind speed and gas exchange over the ocean, J Geophys Res, 97, 7373–7382, https://doi.org/10.1029/92JC00188, 1992.

Weber, T., Wiseman, N. A., and Kock, A.: Global ocean methane emissions dominated by shallow coastal waters, Nat Commun, 10, 1–10, https://doi.org/10.1038/s41467-019-12541-7, 2019.

Weller, D. I., Law, C. S., Marriner, A., Nodder, S. D., Chang, F. H., Stephens, J. A., Wilhelm, S. W., Boyd, P. W., and Sutton, P. J. H.: Progress in Oceanography Temporal variation of dissolved methane in a subtropical mesoscale eddy during a phytoplankton bloom in the southwest Pacific Ocean, Prog Oceanogr, 116, 193–206, https://doi.org/10.1016/j.pocean.2013.07.008, 2013.

Wiesenburg, D. A. and Guinasso, N. L.: Equilibrium solubilities of methane, carbon monoxide, and hydrogen in water and sea water, American Chemical Society, 24, 356–360, https://doi.org/https://doi.org/10.1021/je60083a006, 1979.

Wilson, S. T., Ferrón, S., and Karl, D. M.: Interannual Variability of Methane and Nitrous Oxide in the North Pacific Subtropical Gyre, Geophys Res Lett, 44, 9885–9892, https://doi.org/10.1002/2017GL074458, 2017.

Wilson, S. T., Bange, H. W., Arévalo-Martínez, D. L., Barnes, J., Borges, A. V., Brown, I., Bullister, J. L., Burgos, M., Capelle, D. W., Casso, M., De La Paz, M., Farías, L., Fenwick, L., Ferrón, S., Garcia, G., Glockzin, M., Karl, D. M., Kock, A., Laperriere, S., Law, C. S., Manning, C. C., Marriner, A., Myllykangas, J. P., Pohlman, J. W., Rees, A. P., Santoro, A. E., Tortell, P. D., Upstill-Goddard, R. C., Wisegarver, D. P., Zhang, G. L., and Rehder, G.: An intercomparison of oceanic methane and nitrous oxide measurements, Biogeosciences, 15, 5891–5907, https://doi.org/10.5194/bg-15-5891-2018, 2018.

Wilson, S. T., Al-Haj, A. N., Bourbonnais, A., Frey, C., Fulweiler, R. W., Kessler, J. D., Marchant, H. K., Milucka, J., Ray, N. E., Suntharalingham, P., Thornton, B. F., Upstill-Goddard, R. C., Weber, T. S., Arévalo-Martínez, D. L., Bange, H. W., Benway, H. M., Bianchi, D., Borges, A. V., Chang, B. X., Crill, P. M., Del Valle, D. A., Fariás, L., Joye, S. B., Kock, A., Labidi, J., Manning, C. C., Pohlman, J. W., Rehder, G., Sparrow, K. J., Tortell, P. D., Treude, T., Valentine, D. L., Ward, B. B., Yang, S., and Yurganov, L. N.: Ideas and perspectives: A strategic assessment of methane and nitrous oxide measurements in the marine environment, Biogeosciences, 17, 5809–5828, https://doi.org/10.5194/bg-17-5809-2020, 2020.

Winckler, P.: Towards a multi-hazard analysis of infrastructure in a seismic coast subjected to climate change, with a focus on the Chilean coastline, Proceedings of the 8th IAHR International Symposium on Hydraulic Structures, ISHS 2020, https://doi.org/10.14264/uql.2020.517, 2020.

Worden, A.: Picoeukaryote diversity in coastal waters of the Pacific Ocean, Aquatic microbial ecology, 43, 165–175, https://doi.org/doi:10.3354/ame043165, 2006.

Wuebbles, D. J. and Hayhoe, K.: Atmospheric methane and global change, Elsevier Science, 57, 177–210, https://doi.org/10.1016/S0012-8252(01)00062-9, 2002.

Zhao, P., Ouyang, L., Shen, A., and Wang, Y.: The cell cycle of phytoplankton: A review, J World Aquac Soc, https://doi.org/10.1111/jwas.12916, 2022.

Zheng, Y., Harris, D. F., Yu, Z., Fu, Y., Poudel, S., Ledbetter, R. N., Fixen, K. R., Yang, Z. Y., Boyd, E. S., Lidstrom, M. E., Seefeldt, L. C., and Harwood, C. S.: A pathway for biological methane production using bacterial iron-only nitrogenase, Nat Microbiol, 3, 281–286, https://doi.org/10.1038/s41564-017-0091-5, 2017.

Zhu, Y. and Newell, R. E.: A Proposed Algorithm for Moisture Fluxes from Atmospheric Rivers, 1998.